MODELLING ANTARCTIC ICE SHELF-OCEAN INTERACTION AT HIGH-RESOLUTION

by

Ole Richter, M.Sc, B.Sc.

Submitted in fulfilment of the requirements
for the Degree of Doctor of Philosophy

Institute for Marine and Antarctic Studies
Antarctic Gateway Partnership
University of Tasmania
December 2020

This thesis contains no material which has been accepted for a degree or diploma by the University or any other institution, except by way of background information and duly acknowledged in the thesis, and to the best of my knowledge and belief no material previously published or written by another person except where due acknowledgement is made in the text of the thesis, nor does the thesis contain any material that infringes copyright.

Signed:
Ole Richter

Date: 09.04.2020

Signed:
Ole Richter

Date: 09.04.2020

STATEMENT ON CO-AUTHORSHIP

The following people and institutions contributed to the publication of work undertaken as part of this thesis:

Candidate	Ole Richter (OR) - Institute for Marine and Antarctic Studies
Co-Author 1	Ben K. Galton-Fenzi (BKG-F) - Australian Antarctic Division
Co-Author 2	David E. Gwyther (DEG) - Institute for Marine and Antarctic Studies
Co-Author 3	Matt A. King (MAK) - School of Technology, Environments and Design
Co-Author 4	Kaitlin A. Naughten (KAN) - British Antarctic Survey

Contribution of work by co-authors for each paper:

Paper 1 (Chapter 2): Richter, O., Gwyther, E. D., Galton-Fenzi, B. K., Naughten, K. A. The Whole Antarctic Ocean Model (WAOM v1.0): Development and Evaluation. Manuscript in preparation.

Conceived and designed experiments:	OR (80 %), BKG-F (20 %)
Performed the experiments:	OR (100 %)
Analysed the data:	OR (80 %), BKG-F (10 %), DEG (10 %)
Contributed analysis tools:	OR (80 %), DEG (10 %), KAN (10 %)
Wrote the manuscript:	OR (80 %), DEG (20 %)

Paper 2 (Chapter 3): Richter, O., Galton-Fenzi, B. K., Gwyther, E. D., Naughten, A. K., King, A. M. Antarctic ice shelves lose most of their mass from shallow depths. Manuscript in preparation.

Conceived and designed experiments:	OR (80 %), BKG-F (20 %)
Performed the experiments:	OR (100 %)
Analysed the data:	OR (80 %), BKG-F (10 %), DEG (10 %)
Contributed analysis tools:	OR (80 %), DEG (10 %), KAN (10 %)
Wrote the manuscript:	OR (70 %), BKG-F (5 %), DEG (10 %), MAK (10 %), KAN (5 %)

Paper 3 (Chapter 4): Richter, O., Gwyther, E. D., King, A. M., Galton-Fenzi, B. K., Tidal modulation of Antarctic ice shelf melting. Manuscript in preparation.

Conceived and designed experiments:	OR (70 %), BKG-F (10 %), DEG (10 %), MAK (10 %)
Performed the experiments:	OR (100 %)
Analysed the data:	OR (80 %), BKG-F (10 %), DEG (10 %)
Contributed analysis tools:	OR (90 %), DEG (10 %)
Wrote the manuscript:	OR (80 %), DEG (10 %), MAK (10 %)

We, the undersigned, endorse the above stated contribution of work undertaken for each of the published (or submitted) peer-reviewed manuscripts contributing to this thesis:

Signed :			
Date:	09.04.2020	09.04.2020	26.04.2020
	Ole Richter Candidate School of Technology, Environments and Design University of Tasmania	Prof Matt A. King Primary Supervisor School of Technology, Environments and Design University of Tasmania	Prof Elaine Stratford Head of School School of Technology, Environments and Design University of Tasmania

ABSTRACT

Understanding the processes involved in basal melting of Antarctic ice shelves is important to quantify the rate at which Antarctica will lose mass in the future. We implement a state-of-the-art ocean model to derive a new estimate of continent-wide ice shelf basal melting at 2 km horizontal resolution, then explore the underlying oceanic mechanisms.

A new circum-Antarctic ice shelf-ocean model is developed, which is based on the Regional Ocean Modeling System (ROMS). Improvements over previous models of this scale are the inclusion of tides at a horizontal resolution of 2 km that is sufficient to resolve critical onshelf heat transport by bathymetric troughs and eddies. For this study we choose to run the model with conditions from the year 2007 to represent nominal present day climate. Results agree with available observations of tides, ocean state and ice shelf-ocean interaction, giving us confidence in modelled mass loss estimates.

We estimate a total basal mass loss of 1207 Gt/yr of which 79 % comes from ice shallower than 400 m deep. Ice shallower than 200 m deep contributes 33 % to the total mass loss and this ice is often confined to the ice front, areas which are not resolved by methods using satellite data. Modelled melting at depths shallower than 200 m triples in summer, when solar heated surface waters advect under the ice. These results suggest that changes in the surface ocean will need to be considered when constraining the future Antarctic mass loss and not only deep warm water intrusions.

Further, we estimate the impact of tides on Antarctic ice shelf melting and the continental shelf ocean using a downscaled version of the model with 4 km horizontal resolution. Tides contribute 57 Gt/yr (4 %) to the continent-wide ice shelf basal mass loss, while continental shelf temperatures are reduced by tidal exchange, on average by about 0.04 °C. This indicates that tides act to increase the efficiency at which ocean heat is converted to melting. Regional variations are larger, with melt rate modulations exceeding 500 % and temperatures changing by more than 0.5 °C. In particular, tides tend to heat the Weddell Sea continental shelf with warm waters reaching under the Ronne Ice Shelf and increasing its area-averaged basal melt rate by 150 %.

Finally, we explore the tidal processes that cause variations in melting using singular spectrum analysis over periods of up to one month. At most places along the ice base, friction velocity varies at tidal timescales (one day or faster), while thermal driving changes at rates slower than one day. In some key regions under the large cold-water ice shelves, however, thermal driving varies faster than friction velocity and this can not be explained by tidal modulations in boundary layer exchange rates alone. These results show that large scale ocean models aiming to predict accurate ice shelf melt rates will need to explicitly resolve tides.

This thesis shows that kilometre-scale processes on the Antarctic continental shelf that are related to the surface ocean and tides exert large controls on the mass balance of the Antarctic Ice Sheet. Global circulation models that aim to provide projections of future climate, will need to capture these processes in order to accurately predict sea level rise resulting from changes in Antarctic basal mass loss.

ACKNOWLEDGEMENTS

This thesis was supported by scholarships from the University of Tasmania and the Australian Research Council's Special Research Initiative for Antarctic Gateway Partnership (Project ID SR140300001). Further assistance and resources have been provided by the National Computational Infrastructure (NCI), which is supported by the Australian Government.

I would like to thank my supervisors Matt King, Ben Galton-Fenzi and David Gwyther for their support and guidance throughout this project - professionally and in regards to my personal development. I would also like acknowledge Kaitlin Naughten for her valuable advice in regards to model development (Chapter 2) and Richard Coleman for providing me with additional feedback on the ideas presented in Chapter 3 and 4. Finally, I would like to express my gratitude to my partner, Tina Jahnel, for her emotional support.

Contents

List of Tables

List of Figures

Chapter 1

Introduction

1.1 Antarctica in a Changing Climate

The Antarctic Ice Sheet is the largest single mass of ice on earth with a volume of 27 million km^3. If all of this ice would be discharged into the ocean, Global Mean Sea Level (GMSL) would rise by 58 m (Fretwell et al., 2013). Paleo reconstructions of GMSL imply that the Antarctic Ice Sheet is not static, but rather grows and shrinks in accordance with climate (see schematic in Fig. 1.1; Dutton et al., 2015). During periods over the last several million years, when atmospheric carbon dioxide concentrations and global mean temperatures have been comparable to today, sea levels were tens of metres higher, with the Antarctic Ice Sheet indicated as the main contributor (e.g. Rovere et al., 2014; DeConto and Pollard, 2016). In accordance with the paleo record, observations of the present state show that the Antarctic Ice Sheet is losing mass and that the mass loss rate is accelerating (see Fig. 1.2; Shepherd et al., 2018).

There are large uncertainties in sea level rise projections. Under its lowest emission scenario (RCP2.6), the IPCC predicts that GMSL in 2100 will likely rise somewhere between 0.29 m and 0.59 m with respect to 1985-2005 (Pörtner et al., In press). With the highest emission scenario (RCP8.5) this projection increases to between 0.61 m and 1.10 m. The uncertainties of these predictions (up to 70 % of the mean value) originate mostly from our incomplete understanding of the processes involved in the retreat of ice sheets, especially in Antarctica.

Hydrographic measurements also highlight the global reach of climate variability around Antarctica. Interactions between ocean, ice and atmosphere close to the Antarctic con-

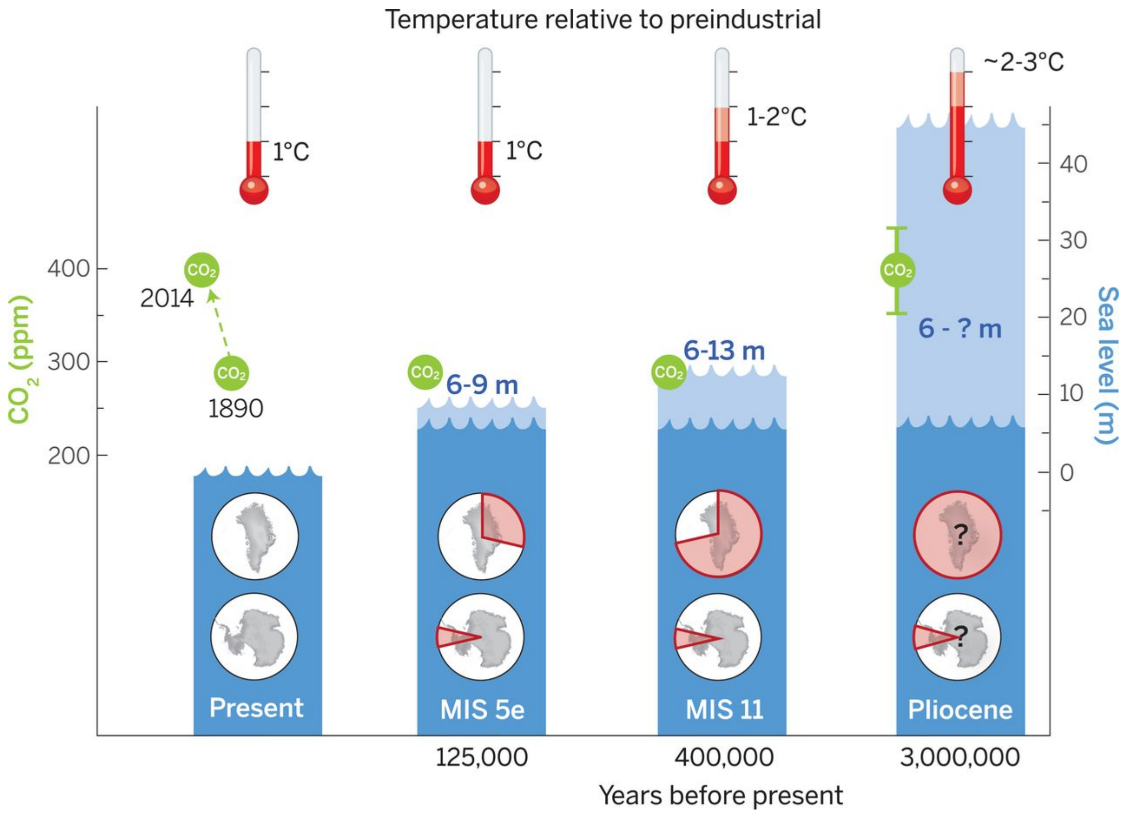

Figure 1.1: Relation between past atmospheric CO2 and Global Mean Sea Level (GMSL). Also shown are peak global mean temperatures and sources of melt water. Red pie charts over Greenland and Antarctica denote the fraction (not location) of ice sheet retreat, and light blue shading indicates the uncertainty of the GMSL maximum. Current sea levels are more than 6 mlower than during past periods with similar atmospheric carbon dioxide concentrations, stressing the transient nature of the current GMSL state. Only by including substantial loss of Antarctic ice can past sea levels be explained. Reproduced by Dutton et al. (2015).

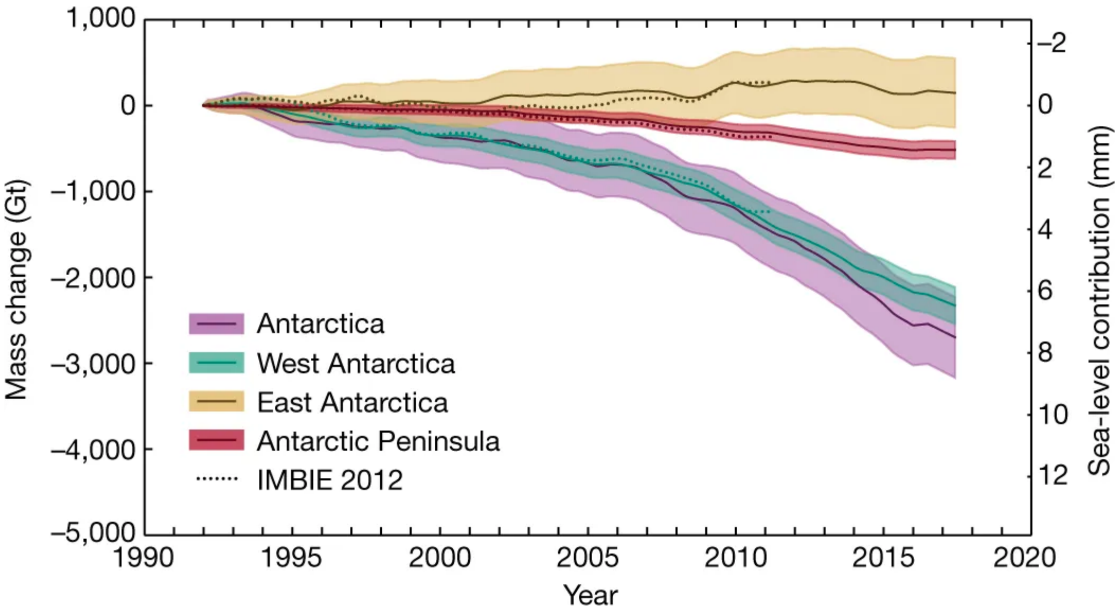

Figure 1.2: Cumulative mass change of the Antarctic Ice Sheets since 1992. Shaded areas indicate the estimated 1σ uncertainty and the dashed lines show the result of a similar but earlier assessment. Antarctic Ice Sheet mass loss is accelerating with west Antarctica as the main contributor. Reproduced from Fig. 2 of Shepherd et al. (2018).

tinent results in the formation of Antarctic Bottom Water (AABW), one of the densest and deepest water masses in global ocean basins (e.g. Gordon, 2001). Repeated hydrographic measurements between the 1980's and the 2000's show that AABW is cooling and freshening (see Fig. 1.3; Purkey and Johnson, 2013) and a reduction of the meridional overturning circulation in the North Atlantic has been linked to decreased AABW volume (Johnson et al., 2008). Further, southern hemisphere westerly winds are strengthening and shifting polewards, driving warm waters at mid depth onto the Antarctic continental shelf (Spence et al., 2014). In agreement, rapid warming of continental shelf bottom waters has already been observed in some regions (Schmidtko et al., 2014) and related glacial melt water increase might explain the strengthening signal in Antarctic sea ice (e.g. Bronselaer et al., 2018).

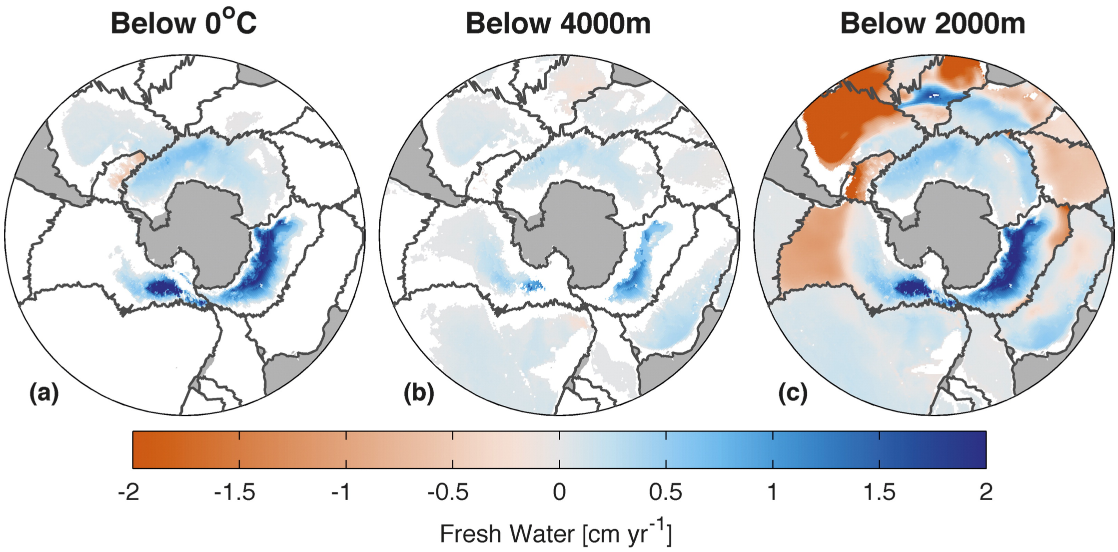

Figure 1.3: Freshening of Antarctic Bottom Water. Local vertical freshwater fluxes into water columns below (a) 0 °C, (b) 4000 m and (c) 2000 m. Ocean freshening below 0 °C close to Antarctica and at the greatest depths of global ocean basins suggest that changes on the Antarctic continental shelf cause a freshening of Antarctic Bottom Water. Freshwater fluxes are calculated from observed water mass salinity changes between the 1980s and 2000s. Gray lines indicate basin boundaries. Reproduced from Fig. 5 of Purkey and Johnson (2013).

1.2 The Role of Ice Shelf Basal Melting

Ocean-driven melting at the base of Antarctic ice shelves has been shown to be responsible for the current observed ice sheet retreat (Shepherd et al., 2004; Pritchard et al., 2012). Where the Antarctic Ice Sheet drains into the southern ocean, floating ice shelves form with areas of up to $500\,000\,\mathrm{km}^2$ (equivalent to the size of Spain). Ice shelf mass loss from 2003-2012 has accelerated with respect to 1994-2012 (Paolo et al., 2015) and, while floating ice has inconsequential contribution to sea level change, inland glacier retreat has been attributed to ice shelf thinning. Figure 1.4 shows the relation between ocean temperature, ice shelf thinning and ice sheet retreat around Antarctica. Direct evidence that ice shelves reduce ice sheet discharge rates has been observed in the Antarctic Peninsula, where the collapse of the Larsen B ice shelf in 2002 caused an up to a sixfold acceleration of tributary glacier flow (Scambos et al., 2004). This so-called buttressing effect of ice shelves originates from friction between floating ice streams and stationary, grounded ice or bedrock. While ice shelf buttressing comprises a complex interplay of far reaching stresses inside the ice sheet (e.g. Gagliardini et al., 2010), ice shelf thinning is generally most critical along lateral boundaries or where seamounts create pinning points (e.g. Favier et al., 2012; Reese et al., 2018).

Of particular concern are rapid retread mechanisms such as the Marine Ice Sheet Instability (MISI). A positive feedback between ice shelf melting and grounding line retreat along retrograde bed slopes has been hypothesised (Mercer, 1978; Schoof, 2007), and supported by idealized (e.g. Schoof, 2012; Asay-Davis et al., 2016) and realistic (e.g. Cornford et al., 2015; Royston and Gudmundsson, 2016) ice sheet simulation experiments. Such an instability implies tipping points for glacier retreat and some studies argue that these points have already been crossed for rapidly retreating outlet glaciers of the Amundsen Sea Embayment (Joughin et al., 2014; Mouginot et al., 2014). In total, 40 % of the Antarctic ice sheet is grounded below sea level (Fretwell et al., 2013) and, hence, susceptible to rapid retreat. Including mechanisms such as MISI in models of Antarctic ice sheet flow substantially increases sea level rise projections (DeConto and Pollard, 2016).

Ice shelf melting also impacts the ocean with consequences for global climate and ecosystems. Glacial fresh water that leaves the sub-ice shelf cavities can partially offset the effects of brine rejection in sea ice polynyas and increased melt water production has been linked to the suppression of AABW formation (Williams et al., 2016; Silvano et al., 2018). Further, including ice shelves in ocean models leads to sea ice thickening (Hellmer,

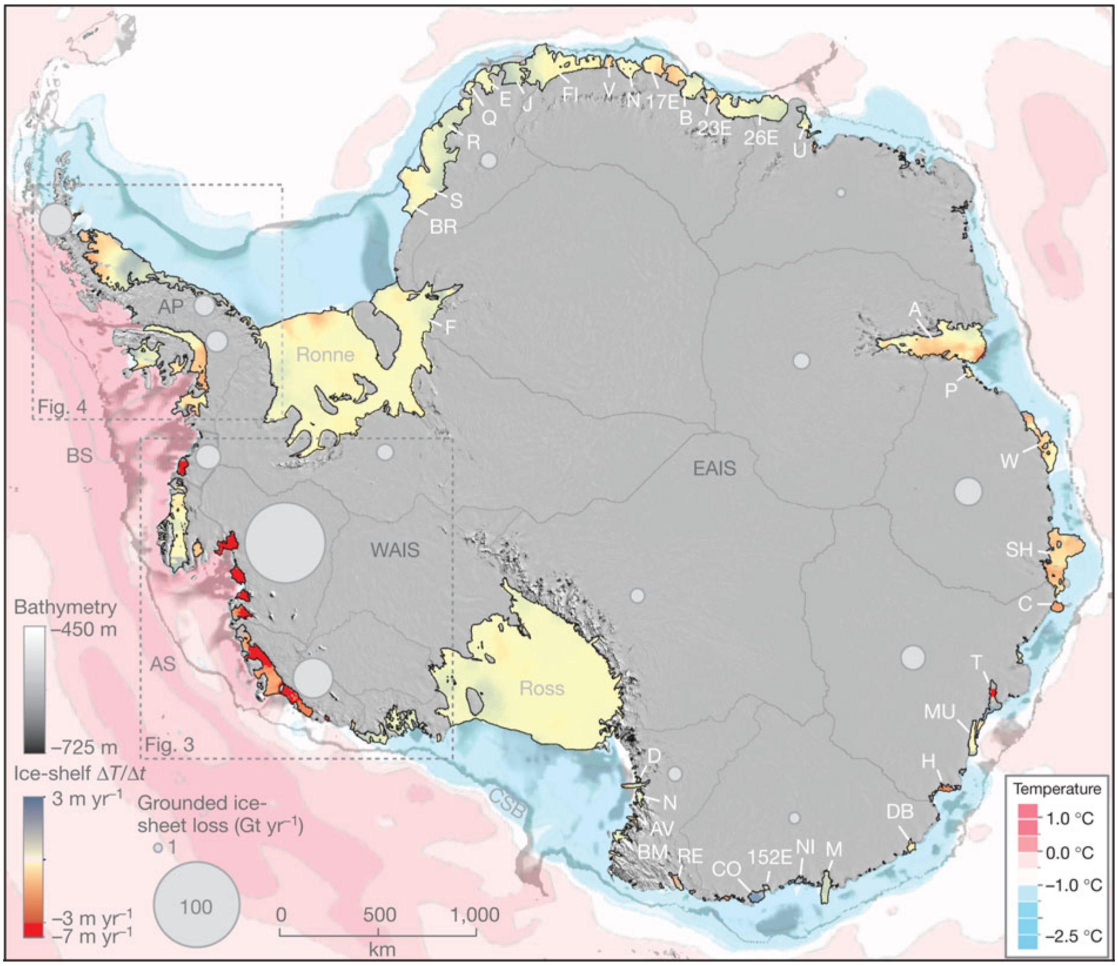

Figure 1.4: Relation between ocean temperature, ice shelf thinning and ice sheet retreat around Antarctica. Seaward of ice shelves, continental shelf bathymetry (gray) and average seafloor potential temperature (colors) estimated from the World Ocean Circulation Experiment Southern Ocean Atlas. Ice shelves show average thickness change between 2003 and 2008 and circles are average ice sheet loss between 1992 and 2006 from adjacent drainage basins (gray contour lines on land). Where warm deep waters reach the coast, ice shelves are thinning rapidly and glaciers retreat. Reproduced from Fig. 2 of Pritchard et al. (2012).

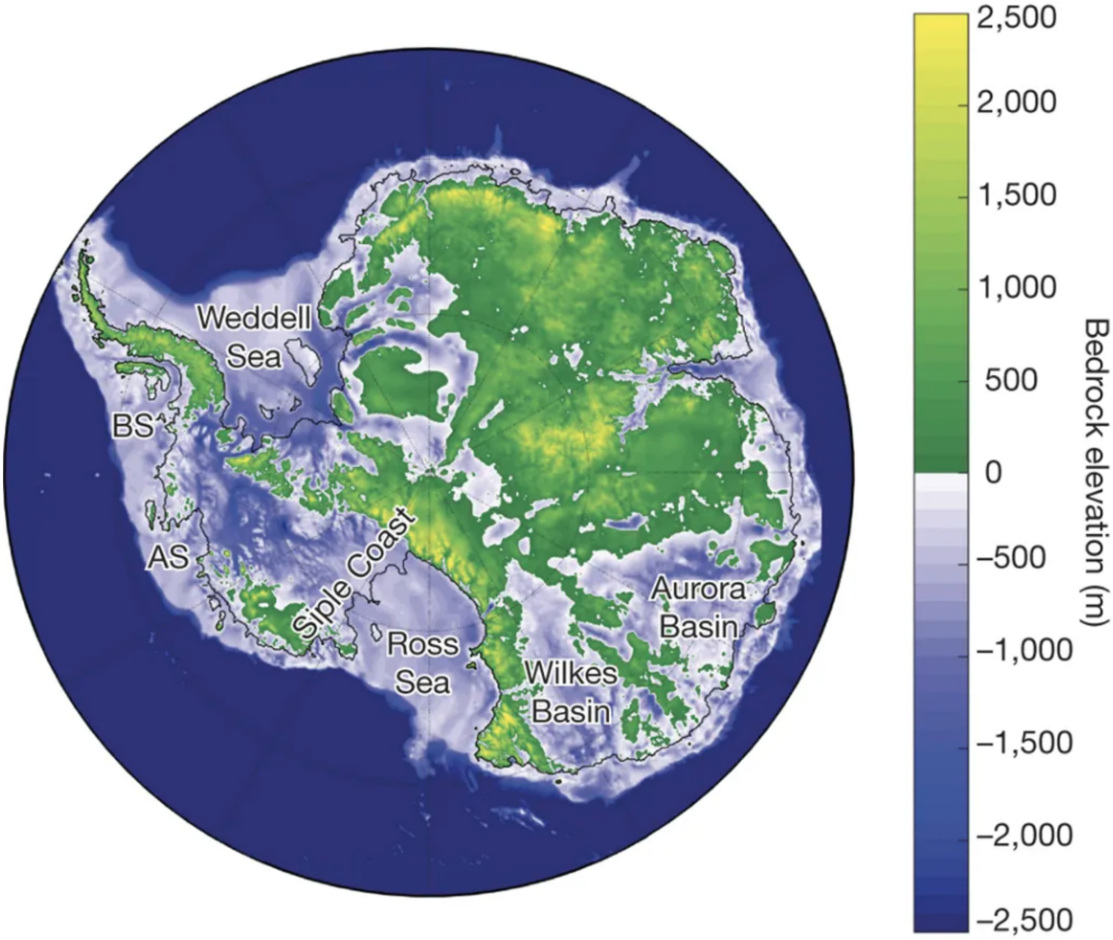

Figure 1.5: Antarctic sea bed elevation. Blue colors denote bedrock that lays below sea level and the gray line indicates the edge of the grounded ice (grounding line). About 40 % of the Antarctic Ice Sheet is grounded below sea level (Fretwell et al., 2013) and, hence, susceptible to rapid glacier retreat. Reproduced from Fig. 1a of DeConto and Pollard (2016).

2004; Liu, 2018) and subsurface warming (Bronselaer et al., 2018), offering largely unexplored feedback mechanisms with the global climate system. There is evidence that changes in ice shelf melting also influences biology, since glacial meltwater is a source of iron, critical for primary production in Antarctic sea ice polynyas (Arrigo et al., 2015).

1.3 Known Drivers of Change

Ice shelf melting is often characterised in three modes (Jacobs et al., 1992, see Fig. 1.6;). The first mode is initiated by High Salinity Shelf Water (HSSW), which is formed by brine rejection in coastal sea ice polynyas. As this dense water sinks to the seafloor and then follows the bed slope, it brings surface freezing point temperatures (about $-1.9\,^{\circ}\mathrm{C}$) to the deepest parts of the ice shelves. Here, the hydrostatic pressure from the water above is so high that it depresses the in situ freezing point (about $0.1\,^{\circ}\mathrm{C}$ per $1000\,\mathrm{m}$), meaning that an inflowing water body has more potential to drive melting. The resulting melt water is fresh and buoyant and rises along the ice draft to shallower regions where it can refreeze back onto the ice (marine ice accretion) or separate from the ice shelf base to form a layer of fresh and cold Ice Shelf Water (ISW). This mode drives an overturning circulation inside the cavity and, if refreezing conditions are met, it literally pumps ice from the grounding lines to shallower parts of the ice shelves (referred to as "The Ice Pump Mechanism"; Lewis and Perkin, 1986).

Mode 2 melting is associated with intrusions of Circumpolar Deep Water (CDW) that drive strong melting at all depths. CDW resides north of the continental shelf break and is mostly prevented from flowing further south by the Antarctic Slope Front (ASF; e.g. Jacobs, 1991). At some places however, CDW intrudes onto the continental shelf and, where it reaches the ice shelf cavities as Modified Circumpolar Deep Water (MCDW), temperatures often still exceed $3\,^{\circ}\mathrm{C}$ above freezing. The strength of MCDW intrusions is regulated by several processes, including bathymetric troughs (Thoma et al., 2008; Assmann et al., 2013), eddies (Stewart and Thompson, 2015; Stewart et al., 2018), thermocline dynamics (Padman et al., 2012; Davis et al., 2018) and wind driven upwelling (Dinniman et al., 2015; Greene et al., 2017).

Mode 3 melting is characterised by advection of warm surface waters under the ice and melting at shallow depths. In the absence of sea ice, solar radiation can heat Antarctic Surface Water (AASW) to temperatures well above freezing. Consequently, warm AASW can drive melting along the vertical cliff face of the ice front and, if advected

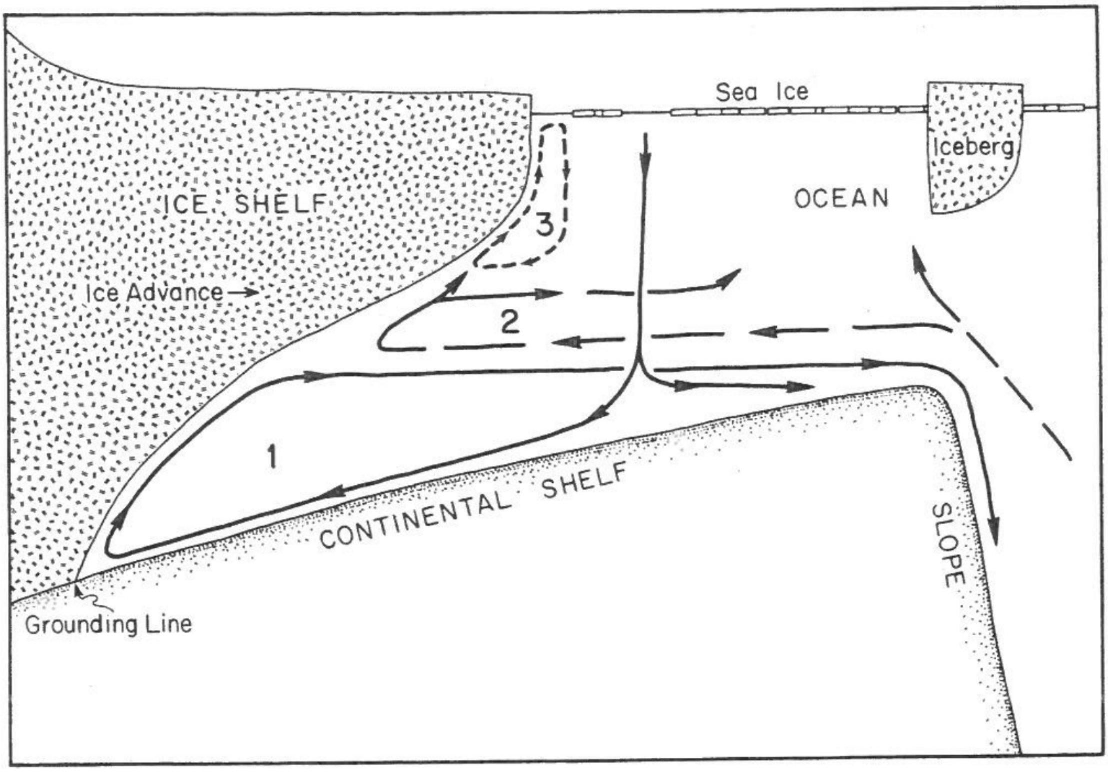

Figure 1.6: Modes of ocean driven ice shelf melting. Mode 1 is driven by brine rejection in sea ice polynyas and the depression of the freezing point with depth, while Mode 2 and 3 are characterised, respectively, by intrusions of warmer off-shelf water or warm surface water under the ice. Reproduced from Fig. 1 of Jacobs et al. (1992).

under the ice, also at the outer regions of the ice shelf cavity. Surface water advection has often been associated with tides and coastal winds (e.g. Arzeno et al., 2014; Zhou et al., 2014; Stewart et al., 2019; Malyarenko et al., 2019).

While all three modes have been observed in different regions of Antarctica, their relative importance for future changes in a continent-wide context is not clear. In the Amundsen-Bellingshausen Seas, CDW intrusions drive some of the strongest melt rates observed around Antarctica (Pritchard et al., 2012; Rignot et al., 2013). Consequently, it is expected that if CDW enters onto the shelf in other regions of Antarctica, the melt regime will shift from the now dominant and more balanced Mode 1 (HSSW driven) to the rapid melting of Mode 2 (CDW driven; e.g. Gwyther et al., 2016). In situ observations at high latitudes are sparse, however, and Antarctic-wide estimates of ice shelf basal melting and the continental shelf ocean imply large uncertainties (e.g. Rignot et al., 2013; Schmidtko et al., 2014). For example, current estimates of Antarctic ice shelf basal melting rely almost exclusively on methods using satellite data and models of surface processes (Rignot et al., 2013; Depoorter et al., 2013; Liu et al., 2015). Surface models include several sources of uncertainty (e.g. Wessem et al., 2018) and satellite observations do not resolve regions close to the ice shelf front (discussed in, e.g. Liu et al., 2015), meaning that a major mode of melting cannot be observed (Mode 3).

Ocean tides are heavily involved in all three melting modes and offer many feedback mechanisms with ice shelf geometry. Tidal currents are known to impact ice shelf-ocean interaction by many means, including vertical mixing, mean flow interaction and turbulence at the ice base (Padman et al., 2018). Activating tides in models of cold water regimes results in a redistribution of melting and refreezing, illustrating how tides are important for controlling spatial distribution of melting, with consequences for ice shelf buttressing (e.g. Makinson et al., 2011; Mueller et al., 2012; Gwyther et al., 2016). Further, tidal current strength is sensitive to the local and far field ice draft geometry (Mueller et al., 2018; Griffiths and Peltier, 2009), offering unexplored feedback mechanisms, from short to glaciological timescales (Arbic et al., 2004; Griffiths and Peltier, 2008). However, present day tidal melting has not yet been studied in an Antarctic-wide context, hindering further conclusions about its role for future changes.

1.4 Towards Predicting the Future

Processes that act across the Antarctic ice-ocean interface have many scales, but computational costs limit the representations of these processes in numerical models. The spatio-temporal scales of known ice shelf-ocean interactions are vast, reaching from millimetres and seconds in the ice-ocean boundary layer (e.g. Holland and Jenkins, 1999) to global and millennial when considering the coupling between ocean melting and ice sheet dynamics (see Fig. 1.7; e.g. Colleoni et al., 2018). All of these processes are studied by means of numerical models, but limited grid resolution defines the range of scales that each single simulation can resolve at once. For example, regional models of Antarctic ice shelf-ocean interaction (e.g. Galton-Fenzi et al., 2012; Nakayama et al., 2017) include only a crude parameterisation of the the complex interplay of turbulence and convection within the ice-ocean boundary layer, processes that are accurately resolved in direct numerical simulations (e.g. Gayen et al., 2016; Mondal et al., 2019). At the other end of the spectrum, current International Panel on Climate Change (IPCC) climate projections use Ocean General Circulation Models (OGCMs) that do not include the effects of glacial melt water at all, potentially missing important feedback mechanisms (discussed in Bronselaer et al., 2018). Solutions to some of these challenges might lay within the use of unstructured or nested grids that offer variable resolutions within one model (Dinniman et al., 2016).

Circum-Antarctic applications play a particular role in the chain of modelling. Many three dimensional models of Antarctic ice shelf-ocean interaction are now available (see Dinniman et al., 2016, for review; later developed Mathiot et al., 2017; Naughten et al., 2018b). These models differ, for example, in the choice of the vertical coordinate system (depth, terrain-following or hybrid), which has been shown to have large consequences for the predicted melting (Gwyther et al., 2020). Developing these models is important, as they will provide the ocean component in coupled ice sheet-ocean models, ultimately needed to improve sea level rise projections (Asay-Davis et al., 2017). Also, compared to regional applications, continent-wide models are less constrained by boundary conditions and they allow studying processes in a comprehensive and consistent manner (e.g. Dinniman et al., 2015).

However, some processes, known to be important for ice shelf-ocean interaction, have yet to be included in large scale models. While the critical effects of tides and eddies are now resolved in most regional modelling studies, continent-wide applications do not include tides yet and are often run at horizontal resolutions that are too coarse to

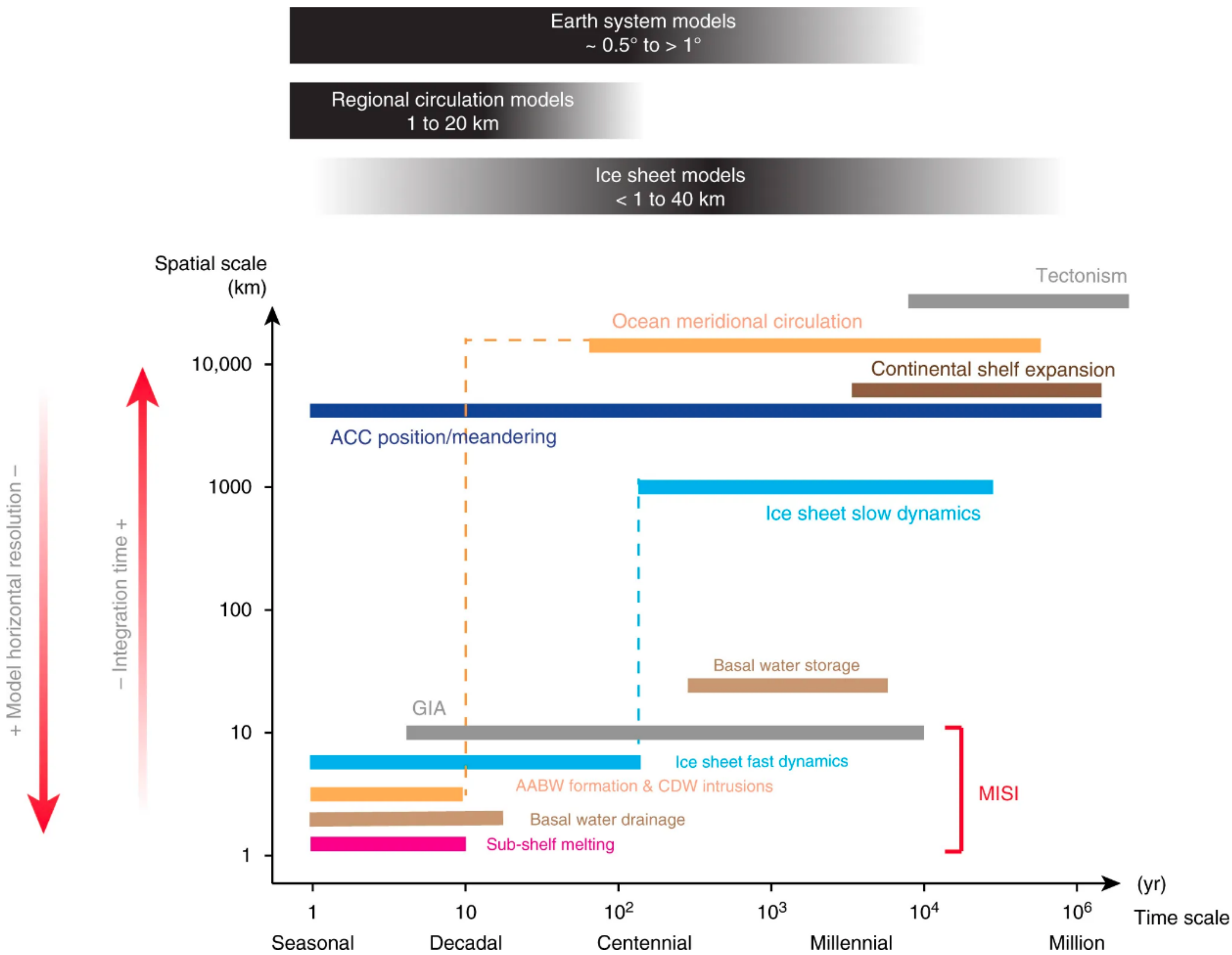

Figure 1.7: Spatio-temporal scales of processes across the Antarctic ice-ocean-bed interfaces. Also shown are approximate horizontal resolutions of numerical models used to resolve these processes (gray bars at the top) and the inverse relation between model resolution and integration time is indicated by the red arrows at the left. Ice shelf basal melting acts on small scales, but connects large scale ice sheet and ocean dynamics via processes such as the Marine Ice Sheet Instability (MISI). Accurately resolving these smaller scale processes in climate simulations is expensive. Other abbreviations are Glacial Isostatic Adjustment (GIA), Antarctic Circumpolar Current (ACC), Antarctic Bottom Water (ABBW) and Circumpolar Deep Water (CDW). Reproduced from Fig. 7 of Colleoni et al. (2018).

resolve eddies on the continental shelf (Nakayama et al., 2014b; Dinniman et al., 2016). Fig. 1.8 demonstrates the effect of resolving eddies on bottom layer temperatures in the Amundsen-Bellingshausen Seas. Other potentially important processes include, for example, diffusive convection in the boundary layer (e.g. Kimura et al., 2014; Begeman et al., 2018) or discharge of subglacial lakes (for inventory of subglacial lakes see Smith et al., 2009; see Jenkins, 2011, for impact on ice shelf melting), but these processes have not yet even been studied in regional models.

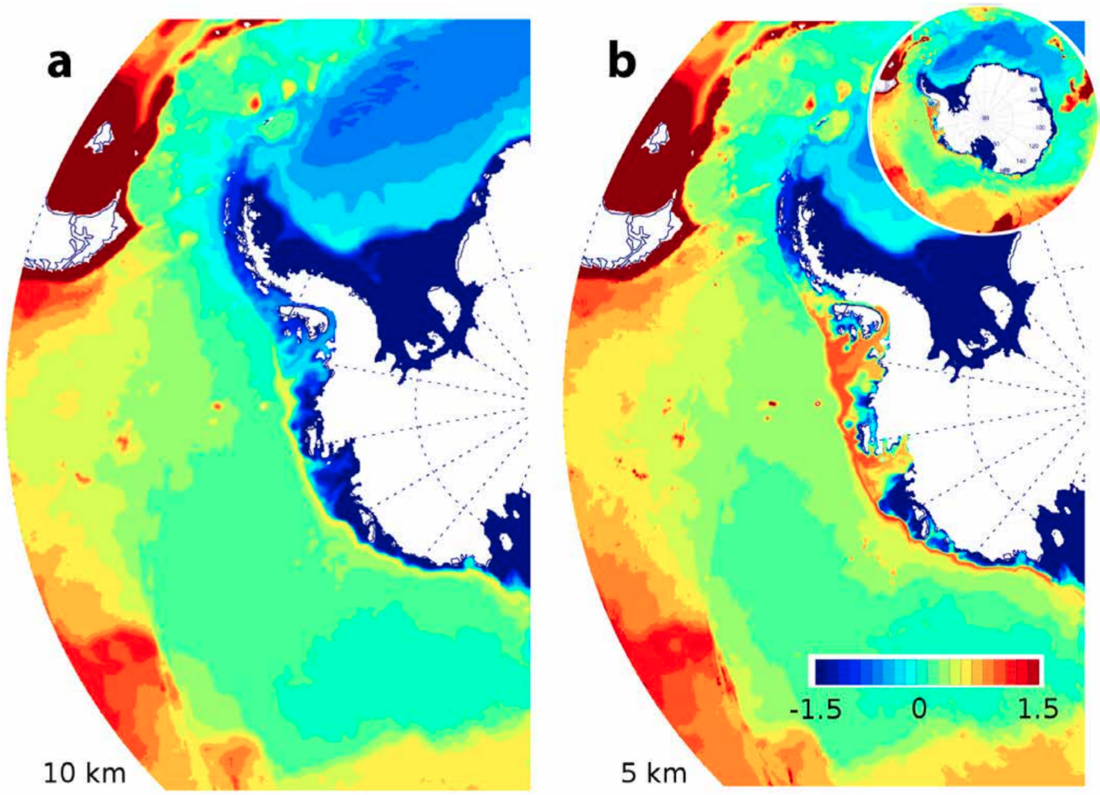

Figure 1.8: The importance of horizontal model resolution for deep warm water intrusions. Bottom layer temperature in the Amundsen-Bellingshausen Seas and other parts of West Antarctica from a model experiment with (a) 10 km and (b) 5 km horizontal resolution (model from Dinniman et al., 2015; similar to Nakayama et al., 2014b). Increasing the resolution dramatically improves the model representation of Circumpolar Deep Water on the Amundsen-Bellingshausen Seas continental shelf. Reproduced from Fig. 4 of Dinniman et al. (2016).

1.5 Research Gap

A large component of the uncertainty in sea level rise projections originates from our incomplete understanding about how the Antarctic ice sheet will respond to climate change. Changes in ice shelf basal melting plays a major role for inland ice sheet dynamics. However, we have yet to unravel all the relevant ocean processes involved in ice shelf melting, motivating continued development of methods to better study ocean-ice sheet interaction and ice sheet evolution. In more detail, the following research gaps have been identified:

- Ocean modelling comprises an essential tool for research in Antarctic ice shelf-ocean interaction. Available Antarctic-wide applications, however, lack important physics, such as eddies and tides, and regional models do not resolve important teleconnections. The role of other potentially important processes, such as subglacial discharge and diffusive convection, have yet to be explored in any kind of realistic setting.

- There is strong evidence that feedback mechanisms between ice sheet evolution and ocean driven melting can cause rapid glacier retreat. Coupled ice sheet-ocean models resolve these feedbacks, but Antarctic-wide application has yet to be developed. Such models are ultimately needed to improve future predictions of the Antarctic contribution to sea level rise.

- Satellite observations have revealed the critical role of CDW intrusions for Antarctic ice shelf melting. The underlying methodology, however, has limitations that inhibits similar conclusions being made for other modes of melting. For example, Mode 3 melting (surface-heated water) is difficult to detect with currently used satellite methods.

- While the importance of tides for ice shelf-melting has been shown in many regional studies, the role of tides in Antarctic-wide ice-ocean interaction is unknown.

1.6 Thesis Objectives

To address these gaps in our understanding this thesis is concerned primarily with three objectives:

1. **To develop and evaluate the Whole Antarctic Ocean Model (WAOM), a new circum-Antarctic configuration of the Regional Ocean Modelling System (ROMS) that includes tides and an eddy resolving resolution.** ROMS has been used for simulating ice shelf-ocean interaction at regional scales (e.g. Galton-Fenzi et al., 2012; Cougnon et al., 2013; Gwyther et al., 2014). In this thesis, we simulate the full circum-Antarctic domain without compromising on the resolved processes, that is including tides and running the model at an eddy resolving resolution. This approach includes teleconnections and state-of-the-art model dynamics. Parallel efforts have been undertaken with the development of MetROMS (Naughten et al., 2018b), a circum-Antarctic application of ROMS that has been augmented by the sea ice model CICE (Community Ice CodE; Hunke et al., 2015)). The parallel effort is warranted, as MetROMS has been designed to study sea ice-ocean-ice shelf interaction over long timescales, while the development of WAOM is focused on accurate predictions of current continental shelf processes at high resolution.

2. **To assess whether deep, warm water intrusions are the main source for Antarctic basal melting.** Simulations with WAOM will provide estimates of Antarctic ice shelf melting at high resolution independent from satellite observations and surface models. These estimates have great potential to reveal new insights into the governing mechanisms that drive melting.

3. **To determine the importance of tides for controlling Antarctic-wide ice shelf melting and conditions in the continental shelf seas.** WAOM is the first continent-wide ocean-ice shelf model that includes tides and, thus, is well suited to derive an important first quantification of Antarctic-wide tidal melting. Further, we aim to explore the exact mechanisms by which tides impact Antarctic ice shelf-ocean interaction.

The remainder of this thesis is organised as follows:

Chapter 2 presents the development and evaluation of WAOM. Here the model design choices as well as applied boundary conditions and forcing products are described. The year 2007 is chosen as a representative year for present day conditions, and the spin up procedure, which accounts for the different scales of resolved processes, is described. A grid convergence study is performed and the model output is evaluated against observations and smaller scale modelling studies where available. Strengths and limitations of

WAOM are compared to similar models, and recommendations for future applications and development are given.

Chapter 3 uses the methodology of Chapter 2 to derive a new high resolution estimate of ice shelf basal melting around Antarctica. Modelled melt rates are integrated over different depth ranges and the resulting distribution is compared against an estimate based on previously published melt rates derived from satellite data. Further, the water masses present at shallow depths in the sub-ice shelf cavity are determined and the seasonal variation in shallow ice melting is compared against temperature variations of the adjacent continental shelf ocean at different depths. We discuss how changes in the surface ocean might impact future Antarctic mass loss.

Chapter 4 applies a downscaled version of WAOM to determine the impact of tides. The sensitivity of mean model results to the presence of tides is quantified, with analysed quantities including ice shelf melting as well as coastal hydrography. Further, by means of spectral analysis techniques, the roles of individual tidal processes for changes close to the ice base are disentangled. The last section of this chapter discusses the potential of prescribing, rather than explicitly resolving, the effects of tides in large scale climate and ice sheet models.

Chapter 5 synthesises the outcomes of this thesis and proposes future research.

Note that Chapters 2, 3 and 4 are standalone manuscripts suitable for publication. They appear here in close to the final form for submission and, thus, some repetition is inherent in the motivation and model description sections. However, to provide a coherent development of the ideas, we added preambles to these chapters that outline the connections between them. References and supplemental material of all chapters have been compiled at the end of the thesis.

All salinities stated in our results are on the Practical Salinity Scale, and therefore are unitless, unless otherwise stated.

Chapter 2

The Whole Antarctic Ocean Model (WAOM v1.0): Development and Evaluation

Preamble

In Chapter 1 the current state of research into Antarctic ice shelf-ocean interaction has been discussed and this discussion has led to the formulation of three main objectives for this thesis (see Section 1.6). The first of these objectives is concerned with the improvement of current generation models of Antarctic ice shelf-ocean interaction. This chapter (Chapter 2) addresses this aim by describing the development and evaluation of WAOM v1.0.

Much time and resources have been dedicated to this part of the thesis, as it comprises most of the methodology for Chapter 3 and 4. Further, the wider community can benefit from the model development work, as the code is open access. Efforts are already underway to use WAOM in coupled ice sheet-ocean simulations, which expands the value of this chapter beyond the thesis objectives.

Abstract

The Regional Ocean Modeling System (ROMS), including an ice shelf component, has been applied on a circum-Antarctic domain to derive estimates of ice shelf basal melting. Significant improvements made compared to previous models of this scale are the inclusion of tides and a horizontal spatial resolution of 2 km, which is sufficient to resolve onshelf heat transport by bathymetric troughs and eddy scale circulation. We choose to run the model with ocean-atmosphere-sea ice conditions from the year 2007, to represent nominal present day climate. We force the ocean surface with buoyancy fluxes derived from sea ice concentration observations and wind stress from ERA-Interim atmospheric reanalysis. Boundary conditions are derived from the ECCO2 ocean reanalysis, while tides are incorporated as sea surface height and barotropic currents. The accuracy of tidal height signals close to the coast is comparable to those simulated from widely-used barotropic tide models, while off-shelf hydrography agrees well with the Southern Ocean State Estimate (SOSE) model. On the shelf, most details of ice shelf-ocean interaction are consistent with results from regional modelling and observational studies, although a paucity of observational data (particularly taken during 2007) prohibits a full verification. We conclude that our improved model is well suited to derive a new estimate of present day Antarctic ice shelf melting at high resolution and is able to quantify its sensitivity to tides.

2.1 Introduction

Modelling of Antarctic ice shelf-ocean interaction is critical to predicting future changes in sea level and climate. Antarctic glaciers drain into floating ice shelves and melting or marine ice accretion at the base of these ice shelves changes their ability to buttress inland ice sheet discharge (e.g. Dupont and Alley, 2005; Gudmundsson, 2013; Pritchard et al., 2012). In turn, glacial melt water impacts the surrounding oceans with consequences for global ocean circulation and climate (e.g. Jacobs, 2004; Purkey and Johnson, 2013). Ocean models that include an ice shelf component are playing a key role in estimating the current state of ocean-ice shelf interaction (e.g. Galton-Fenzi et al., 2012; Gwyther et al., 2014; Hattermann et al., 2014), understanding the underlying mechanisms of ice shelf melting (e.g Makinson et al., 2011; Hattermann, 2018; Gwyther et al., 2018) and predicting future changes (Kusahara and Hasumi, 2013; Mueller et al., 2018; Naughten et al., 2018a). Within these models, Antarctic-wide applications are of particular interest, as they resolve ice shelf teleconnections (Gwyther et al., 2014; Silvano et al., 2018) and smaller ice shelves with less research focus, all around the continent (Timmermann et al., 2012). Further, consistent model design and parameter choices in large scale models make it easier to compare different regions, and coupled ice sheet-ocean models for climate predictions will ultimately need Antarctic-wide domains (Asay-Davis et al., 2017).

The accuracy of circum-Antarctic ocean-ice shelf models, however, suffers from incomplete model dynamics and poorly represented subgrid scale processes. Many ocean models with pan-Antarctic coverage have now been augmented by an ice shelf component (e.g. Hellmer, 2004; Timmermann et al., 2012; Kusahara and Hasumi, 2013; Dinniman et al., 2015; Schodlok et al., 2016; Mathiot et al., 2017; Naughten et al., 2018b; for review see Dinniman et al., 2016; Asay-Davis et al., 2017). Their results for present day conditions, however, often disagree with available observations and vary widely between models (e.g., see Fig. 2.15 for estimates of basal mass loss from major ice shelves). Part of these discrepancies originate from boundary conditions and model design (e.g. Dinniman et al., 2015; Naughten et al., 2018b). The integrity of model dynamics, however, is also questionable, since certain physical processes that have been identified as critical in regional studies, have not yet been included in large scale applications (Dinniman et al., 2016). One of these critical processes is ocean tides, which interact with ice shelves in several ways, most importantly through ice shelf basal melting (Padman et al., 2018). Regional studies have shown that tidal currents can heavily modulate local melt rates (e.g Makinson et al., 2011; Mueller et al., 2012, 2018), but, to our best knowledge, tides have not yet been included in Antarctic-wide ocean-ice shelf models. Further, Antarctic ice shelf-ocean models are typically run at horizontal resolutions of 10-20 km. While this is high in the context of global ocean and climate simulations, bathymetric troughs and eddies on the Antarctic continental shelf are not resolved (Dinniman et al., 2016). Both of these features, however, have been identified to transport heat from the deep ocean shoreward and not resolving them leads to underestimates of ice shelf melting in some regions (for the importance of troughs see Thoma et al., 2008; Assmann et al., 2013; for eddies see Stewart and Thompson, 2015; Stewart et al., 2018). Resolving tides and eddies is expensive, as they require a fine temporal and spatial discretisation, but including them in large scale models is seen as a major step towards more accurate representations of the polar regions.

Model evaluation and efficient tuning is hindered by sparse in situ observations, both beneath ice shelves and on the continental shelf. Model parameters in regional studies are usually calibrated (e.g. Nakayama et al., 2017), but to approach similar efforts with large scale models, suitable Antarctic-wide observations need to be compiled first. Nevertheless, evaluation of selected quantities helps to identify large biases and evaluate model performance. For this purpose, previous studies have often utilised ice shelf melt rates derived from satellite observations and models of firn processes (e.g. Schodlok et al., 2016), and selected Southern Ocean quantities from observations and reanalysis products (e.g. Naughten et al., 2018b). These measures, however, have limitations. For example, while satellite studies provide uncertainty bounds for melt rates averaged over ice shelves or ice flow lines (as in Rignot et al., 2013; Depoorter et al., 2013; Liu et al., 2015), the uncertainty of high resolution data is unknown. Further, ocean reanalysis products, such as the Southern Ocean State Estimate (SOSE; Mazloff et al., 2010), assimilate most of the available data from elephant-seals, ships and Argo Floats, but observations on the Antarctic continental shelf are sparse and the underlying ocean models do not account for ice shelf melting and, hence, the resulting freshwater release.

Here we describe the development and evaluation of a new circum-Antarctic ocean-ice shelf model that aims to overcome some of the shortcomings of previous studies. The Whole Antarctic Ocean Model (WAOM v1.0) includes tides and an eddy resolving horizontal resolution of 2 km and, thus, includes all the model physics of state-of-the-art regional applications. Establishing an evaluation matrix and rigorous model tuning is out of the scope of this study, but we aim to convince the reader that WAOM is capable of simulating an equilibrated and realistic version of present day conditions by comparing model results against a selection of established estimates of Southern Ocean quantities and ice shelf melting for the chosen period of 2007.

The following section (Sect. 2) describes the model and experiments performed in this study. In Section 3, we evaluate tidal accuracy, investigate resolution effects and compare model results against selected off-shelf hydrography from SOSE and climatologies from the World Ocean Atlas (WOA18) as well as estimates of ice shelf-ocean interaction from regional studies and large scale satellite observations. This is followed by a discussion of WAOM's key strengths and limitations, as well as future development and research questions suitable for exploration with our model (Sect. 4). The last section (Sect. 5) summarises and concludes this study.

2.2 Model Description

2.2.1 General Approach

The code that is underlying WAOM has been developed over a decade by our research group in Tasmania and established its integrity in the wider community in many regional and idealized applications (Galton-Fenzi et al., 2012; Cougnon et al., 2013; Gwyther et al., 2014, 2016). In this study we use our experience to upscale the code to a circum-Antarctic domain. WAOM v1.0 (Richter, 2020a) and the scripts used for pre- and post-processing (Richter, 2020b) are open source and can be downloaded and developed on github.

2.2.2 ROMS and Ice-Ocean Thermodynamics

WAOM's backbone is the Regional Ocean Modeling System (ROMS v3.6). ROMS is a free-surface, terrain-following, primitive equations ocean model framework (Shchepetkin 2005) that allows treatment of advection and diffusion in the ocean in a multitude of ways and on different grid configurations. For WAOM we use a spherical coordinate grid (south polar projection) and solve, for example, horizontal and vertical tracer advection using the 4th-order Akima advection scheme, while closing turbulent vertical mixing with the scheme from Large et al. (1994) (see Tab. D.1 and D.2 for all activated options and key parameter choices, respectively).

For ice ocean-thermodynamics, we use the 3-equation melt parameterisation developed by Hellmer and Olbers (1989), refined by Holland and Jenkins (1999) and implemented into ROMS by Galton-Fenzi et al. (2012). The parameterisation accounts for thermal and haline driving across the ice-ocean boundary layer, velocity dependent exchange coefficients following McPhee (1987) and the case of molecular diffusion alone Gwyther et al. (2016). The exact equations used for ice-ocean interaction in WAOM are described in Gwyther et al. (2016).

2.2.3 Domain, Topography and Spatial Discretisation

The rectangular domain is shown in Figure 2.1 and covers all of the Antarctic ice shelf cavities and adjacent continental shelf regions. Spatial discretisation in the vertical uses 31 terrain-following layers with enhanced resolution at top and bottom and results in top layer thicknesses under the ice varying from 0.5 m to 8.3 m (stretching function and parameters used in transformation equations shown at Tab. D.2). In the horizontal we apply uniform grid spacing with resolutions of 10 km, 4 km and 2 km, which results in 52, 130 and 260 million computational cells, respectively. We note that the design of WAOM requires masking of about 36 % of the cells due to land area.

The ice draft and bottom topography south of 60 °S have been derived from Bedmap2 (Fretwell et al., 2013) and north of 60 °S (outside the Bedmap2 boundaries) have been taken from RTopo-2 (Schaffer et al., 2016). Calculating the horizontal pressure gradient at steep sloping topography in terrain-following coordinates is known to generate spurious currents and mixing (Mellor et al., 1994, 1998). Pressure Gradient Force (PGF) error is a well known caveat of sigma-coordinate ocean models and the very reason why they are not used when an accurate representation of the deep ocean is important (Griffies et al., 2000, e.g. in ocean climate simulations; see). On the shelf, however, sigma-coordinates have strong advantages compared to other options (such as z or density defined coordinates), in particular when simulating ice-shelf ocean interaction (see Discussion in, e.g. Naughten et al., 2018b). ROMS is designed to minimise this issue by applying the splines density Jacobian method for the calculation of the pressure gradient force. Nevertheless smoothing of bathymetry and ice draft is recommended (e.g. Sikirić et al., 2009), in particular considering the almost vertical cliff face at the ice shelf front (also discussed in Naughten et al., 2018b). Using the Mellor-Ezer-Oey algorithm (Mellor et al., 1994) we smooth the bathymetry and ice draft iteratively until a maximum slope factor $r = (h_i - h_{i+1})/(h_i + h_{i+1}) \leq 0.3$ is satisfied (h describes either water column thickness or sea floor depth). Further, for numerical stability, we artificially deepen the bathymetry in shallow ice shelf grounding zones to obey a minimum water column thickness of 20 m. While this step might impact local ice shelf ocean-interaction, it has been shown not to affect ice shelf average melt rates and 20 m is considered one of the smallest modifications possible (Schnaase and Timmermann, 2019).

Table 2.1 summarises the computational costs associated with running the model on the Australian National Computing Infrastructure (NCI) supercomputer Raijin. On the resulting grids with 10 km, 4 km and 2 km resolution the 3-D equations integrate stably with timesteps of, respectively, 900 s, 360 s and 180 s. This leads, for example, to a cost of 6,800 CPU hours for 1 year of simulated period at 4 km resolution. We note that upscaling of the computational architecture for the highest resolution was obscured by the fact that the parallel input-output did not work. Serial input-output puts the computational burden onto one random CPU, requiring us to choose a suboptimal architecture with few CPUs and large RAM per CPU. This issue should be addressed in future studies.

2.2.4 Forcing and Boundary Conditions

At the surface, we apply daily buoyancy fluxes derived from sea ice concentration observations (Tamura et al., 2011) and daily wind stress calculated from ERA-Interim 10-m winds and bulk flux formula (Dee et al., 2011). Prescribing surface buoyancy fluxes, rather than including a sea ice model, is likely to more accurately capture polynyas that form in the lee of fast ice and icebergs, and are critical to resolve accurate ice shelf melting in cold regimes (see Mode 2 melting described by Jacobs et al., 1992). We tune the surface forcing by reducing positive heat flux into the ocean to half its original value, omit brine injection when the ocean is warmer than the freezing point and relax surface temperatures towards freezing when they are being forced below freezing. Further, to avoid model drift, the surface ocean is relaxed over long timescales to the solution from SOSE (Mazloff et al., 2010), using a heat flux into the ocean of $40\,\mathrm{W\,m^{-2}\,{}^{\circ}C^{-1}}$ and a salinity relaxation timescale of one month. We do not account for the effect of sea ice on wind stress or frazil ice formation (as in, e.g. Galton-Fenzi et al., 2012). We do not force the surface layer to freezing conditions in the presence of sea ice.

Open boundary conditions are taken from the ECCO2 reanalysis (Menemenlis et al., 2008) and consists of monthly values for sea surface height, barotropic and baroclinic velocities, and temperature and salinity. The model solution, however, mostly dictates the conditions at the boundary, as we nudge inflow and outflow with timescales of 1 day and 1 year, respectively. This way we reduce boundary effects related to ACC frontal jets to a degree that the mean circulation close to the continental shelf is not impacted (see Fig. F.9). We do, however, find spuriously large summer mixed layer depths in the Ross Sea (see Fig. H.5), likely related to remaining boundary effects. Initial ocean temperatures and salinities are also derived from ECCO2 and values under the ice shelves are extrapolated from the ice front. Thirteen major tidal constituents (M2, S2, N2, K2, K1, O1, P1, Q1, MF, MM, M4, MS4, MN4) are derived from the global tidal solution TPXO7.2 (Egbert and Erofeeva, 2002) and also introduced along the northern boundaries of WAOM using sea surface height and barotropic currents.

2.2.5 Spin Up and Experiments

For this study we simulate the year 2007. Forcing with single year conditions captures daily to seasonal variability, while allowing us to run the model to quasi-equilibrium with our given supercomputing resources. At the time of development, all data products used to force the model covered the period from 2005 to 2011 and we found that sea ice buoyancy fluxes and wind stress from the year 2007 are a non-anomalous representation of the period from 1992 to 2011.

To further save computational costs we perform most of the spin up at lower horizontal resolutions. This idea takes advantage of the fact that the temporal and spatial scales of ocean processes are correlated, that is the largest spatial features, such as the Weddell Sea gyre, also take the longest time to develop. Figure 2.2 visualizes our spin-up procedure. The 10 km version of the model is integrated for 5 years, before the on shelf ocean reaches a quasi equilibrium and its solution is used to initialise the 4 km run. Analogously, the 4 km run is stepped forward in time for 2 years before the final 2 km simulation is initiated and integrated for another year and three month. Interpolation of lower resolution solutions to the higher resolution grids is performed using a nearest neighbour method. This can result in artificially large pressure gradients between neighbouring cells, causing model instability. We address this issue by running the first day of each high resolution simulation with a reduced timestep. The ocean state after one day is then used to initiate the actual high resolution run. The main results are taken from the final year of the 2 km run.

2.2.6 Analysis

To calculate basal mass loss from individual ice shelves we use ice shelf boundaries from the MEaSURES Antarctic boundaries dataset (Mouginot et al., 2016). This dataset reflects the 2007 state, while Bedmap2 ice thickness data is mostly based on laser altimetry data from 1994 to 1995. Restricting the ice shelf area to the intersect of Bedmap2 and MEaSURES excludes parts of the ice shelf front in some regions and a narrow frame of thin ice along the open coastlines (see Fig. B.1).

For the evaluation of the ocean hydrography, we use data from WOA18 and SOSE. WOA18 climatologies do not account for interannual variability and are most accurate in summer, when sea ice has its minimum extend and the vast majority of observations are taken. As mentioned earlier, SOSE assimilates many observations from elephant-seals, ships and Argo floats in the Southern Ocean, making it very accurate where such observations exist (Mazloff et al., 2010). On the shelf, however, observations are sparse and the ocean dynamics used to integrate SOSE do not include ice shelf interaction. Hence, we expect SOSE to have large biases close to the ice and we only use its solution for the off-shelf ocean to evaluate WAOM.

We define the off-shelf ocean as south of 65°N and north of the 1500 m isobath. Here we compare the summer mean (December, January and February) of the WOA18 climatology from 2005 to 2017 against the summer mean of 2007 as predicted by WAOM. We also include the prediction of the 2007 summer mean from ECCO2, which provides the initial and boundary conditions for WAOM. Differences in bottom layer hydrography between WOA18, ECCO2 and WAOM are assessed using annual means, as we expect little seasonality at such great depths. Finally, off-shelf stratification is evaluated using example transects from the 2007 mean state of SOSE.

On the shelf (south of the 1500 m isobath), we compare the summer mean of the 2005-2017 climatology from WOA18 against the 2007 summer prediction of WAOM. Longitudinal transects have been chosen, where CTD data from voyages underlies the WOA18 product (see Figure F.2). For the comparisons (on-shelf and off-shelf), estimates from WAOM and ECCO2 have been interpolated onto the WOA18 grid (1/4° and up to 102 depth levels) using nearest neighbours.

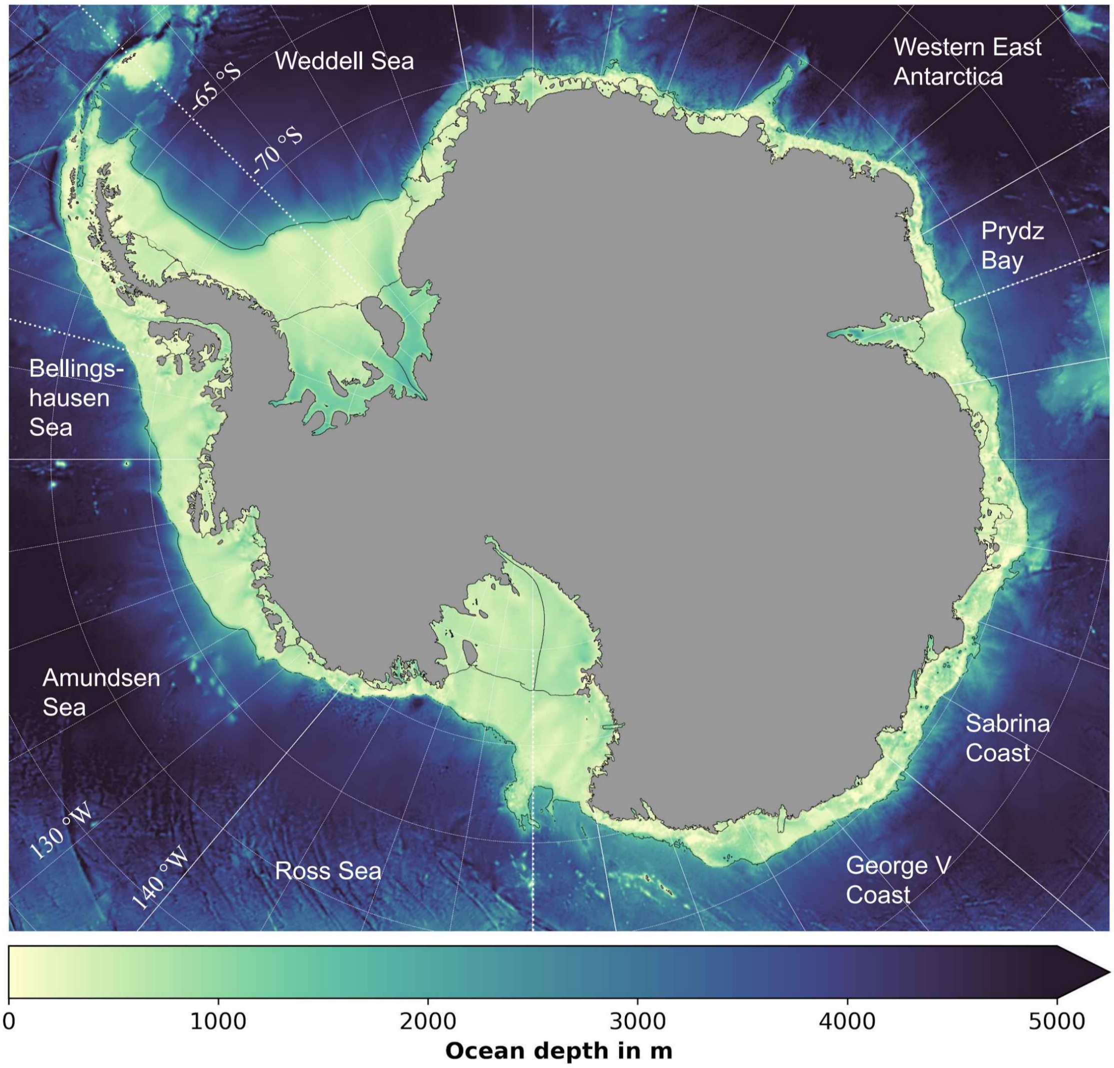

Figure 2.1: Model domain and bathymetry. Figure boundaries denote the model domain and colors show sea floor depth (also inside the sub-ice shelf cavities). Thin black lines are boundaries for the ice shelves and the continental shelf used in this study. Thin white lines are longitudes and latitudes. Labels denote ocean sectors, while bold white lines indicate their boundaries. Dotted white lines are longitude transects used in Figs. 2.8a to 2.8d.

Model Resolution	10 km	4 km	2 km
Period simulated	1 year	1 year	1 year
CPU hours	280 h	6,840 h	40,030 h
Architecture	Sandy Bridge	Sandy Bridge	Broadwell
Number of CPUs	256	2304	224
Memory	51 GB	2.9 TB	876 GB
Walltime	1 h	3 h	142 h
Storage for 1 3D field	40 MB	250 MB	1 GB

Table 2.1: Computational requirements at different resolutions. WAOM has been run on the supercomputer Raijin from the National Computing Infrastructure (NCI) in Australia. Sandy Bridge architecture stands for 2x8 core Intel Xeon E5-2670 2.6GHz with 32 GB RAM per node and Broadwell is 2x14 core Intel Xeon E5-2690v4 2.6GHz with 128 GB RAM per node. We needed to ensure a high RAM per CPU for the 2 km application as input-output was handled in serial.

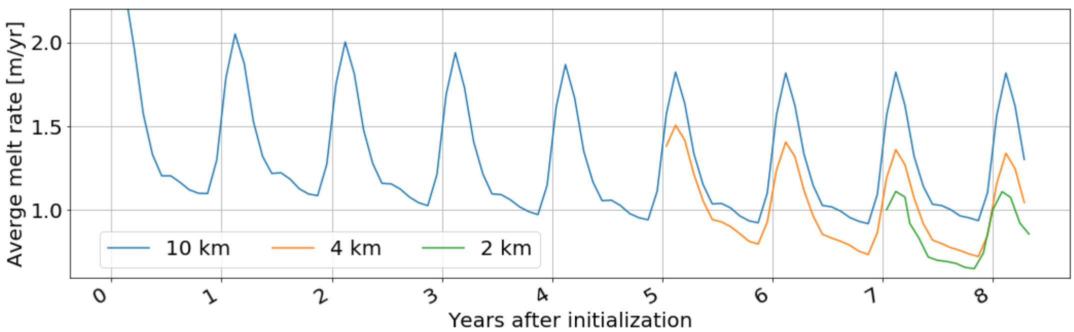

Figure 2.2: Spin up procedure. We spin up large scale processes at lower resolution and find that ice shelf average melting is a good diagnostic for the state of the continental shelf ocean. This way, the total spin up time for the final year of the 2 km-resolution solution is 7 years and 3 months. Model output is plotted as average of every month.

2.3 Results

2.3.1 Tides Evaluation

Following King and Padman (2005), we assess the accuracy of tides in the model by comparing tidal height signals against 69 Antarctic Tide Gauge (ATG) station data, including observations from tide gauges, gravimetric data and GPS records of ice shelf surface elevation. For this we use 365 days of hourly sea surface elevation model output from the 10 km-horizontal resolution simulation. Evaluating tides at higher resolution would have taken considerably more resources and we expect the improvement of accuracy with finer grid spacing to be incremental. We interpolate the model data to the coordinates of each of the 69 tide gauge stations using nearest neighbour interpolation. For the four major tidal constituents M2, S2, K1 and O1, we recover amplitudes H and phases G from the sea surface height time series using classical tidal harmonic analysis (Pawlowicz et al., 2002), and then calculate the complex amplitude $Z = H\cos G + i \sin G$ as a representation of the tidal energy. We disregard stations for a certain constituent if no ATG data is available, the nearest ocean cell is further than 50 km (5 grid cells) away or the tidal harmonic analysis fails to converge. We also disregard 3 stations, which are noted as partially grounded and show non-sinusoidal and complex behaviour (70 Amery IS, 43 Rutford ISTR, 106 Evans ISTR). The Antarctic-wide accuracy of complex amplitudes for each constituent is assessed using root-mean-square (RMS) errors (defined as σ_x) as follows:

$$\sigma_x = \sqrt{\frac{1}{2N}\sum_{j=1}^{N}\left[Z_j^m - Z_j^o\right]^2}\,, \tag{2.1}$$

whereby m and o superscripts denote modelled and observed, respectively, and N is the number of stations. To get a single measure for model bias in tidal energy, the combined RMS error is calculated as

$$\sigma_{comb} = \sqrt{\frac{1}{2N}\sum_{k=1}^{4}\sum_{j=1}^{N}\left[Z_j^m - Z_j^o\right]^2}\,, \tag{2.2}$$

where the differences are also summed over all four constituents k = [M2,S2,O1,K1].

The model has a combined RMS error of 20 cm, which is within the accuracy of state-of-the-art 2D Antarctic tide models (assessed by King and Padman, 2005). Table 2 summarizes the outcomes of the tidal height accuracy analysis, while Figure 3 shows complex amplitude differences for each of the four constituents at each tide gauge station. Most of the bias comes from the semidiurnal constituents M2 and S2 and from sites at the grounding line deep under the large ice shelves. In these shallow regions, semidiurnal tides reach maximum amplitudes of 3 metres (e.g. Griffiths and Peltier, 2008), while bathymetry and ice draft are very uncertain. Tidal strength is sensitive to water column thickness and, thus, we attribute most of the tidal bias in WAOM to uncertainties in the sub-ice shelf cavity geometry of Bedmap2.

	M2	S2	O1	K1
Number of ATG stations	98	91	87	79
mean ATG amp in m	0.42	0.30	0.30	0.32
RMSD amp in m	0.14	0.12	0.07	0.10
relative RMSD amp in %	33	39	25	30
RMSD phase in deg	27.17	22.69	17.82	12.64
RMSD complex amp in m	0.14	0.11	0.06	0.08
Combined complex RMSD in m		0.20		

Table 2.2: Summary of tidal height comparison against Antarctic Tide Gauge Records using Root-Mean-Square-Differences (RMSD). RMSD amplitude relative to ATG is also included.

Further, the relative differences in tidal height amplitude reveal systematically overestimated tidal strength in the Ross Sea. While the relative RMSDs for each constituent (RMSD amp ÷ mean ATG amp) are less than 40 % (Tab. 2.2), the relative difference for individual stations can exceed 300 % (for M2 and S2 at the same station under the Ross Ice Shelf; see G.1 and Fig. G.1). Indeed, the spatial distribution of the relative errors reveals that WAOM systematically overestimates tidal strength of the semi-diurnal constituents in the Ross Sea with differences often exceeding 80 % (see Fig. G.2 and G.3). In contrast, diurnal tides are generally underestimated and deviations are more balanced around the coast. Most stations feature differences below 35 % and maximum differences do not exceed 100 % (Station Lokroy at the Antarctic Peninsula for O1 and K1).

2.3.2 Resolution Effects

The model solution of the continental shelf ocean converges with increasing resolution. We assess the impact of horizontal resolution on the continental shelf ocean by analysing

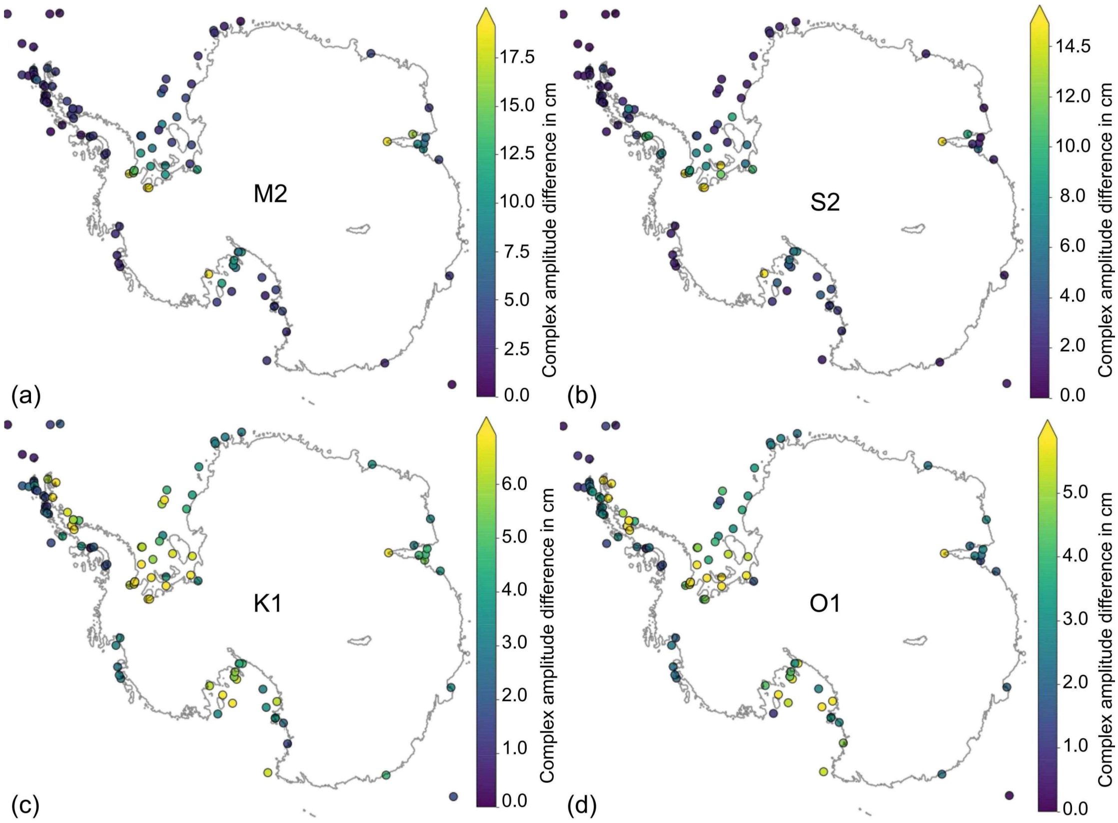

Figure 2.3: Spatial distributions of tidal height accuracy. Complex amplitude differences between the model solution and Antarctic Tide Gauge records are shown for the major tidal constituents (a) M2, (b) S2, (c) K1 and (d) O1. The largest biases occur at the deep grounding lines of the large ice shelves, where the water column thickness is uncertain.

changes in annual mean ocean temperature and average ice shelf melting. To ensure consistency, we compare the 2 km result against lower resolution solutions with equivalent overall simulation time, that is 365 days after 7 years and three months (the overlap in Fig. 2.2). The results of the grid convergence study are shown in Figure 2.4. We find that ocean temperatures as well as melt rates converge when increasing the grid resolution first from 10 km to 4 km (equivalent 250 %) and then to 2 km (equivalent 500 %). We note that several aspects related to model resolution have been changed simultaneously (bathymetry, ice draft topography, horizontal viscosity, horizontal diffusion, the the model's ability to resolve physical processes such as internal tides and eddies). Thus, we use the term "model" in its widest possible sense here, referring to all these aspects together. Demonstrating convergence of WAOM as a whole is an important first step, proving consistency between our understanding and the models behaviour. Attribution of change to the individual resolution dependent aspects is also important, but out of the scope of this study, as it would require several additional series of experiments (discussed later).

When increasing the grid resolution from 10 km to 4 km, the shelf ocean cools at many places, most possibly related to better resolved tidal processes. We find that resolution-induced changes in continental shelf temperature are governed by the ocean at depth (not shown). Figure 2.5 shows how bottom sigma layer temperatures change with increasing resolution. The ocean cools at many places when refining the horizontal grid spacing from 10 km to 4 km (Fig. 2.5a). Differences exceed 1 °C in the eastern Bellingshausen Sea and in the eastern Ross Sea, and are on the order of 0.25 °C in the Amundsen Sea and around the East Antarctic coastline. Activating tides in the model at 4 km leads to similar changes in continental shelf temperature (see Fig. 4.4 of Chapter 4), hinting at the important role of fine resolution tidal effects.

In contrast, increasing the resolution further (from 4 km to 2 km, see Fig. 2.5b) leads to a warming of the Amundsen-Bellingshausen Seas continental shelf. Even though the shelf temperature of the total domain still decreases slightly at the second resolution step, the Amundsen-Bellingshausen Seas is warming. As mentioned earlier, this phenomenon is often associated with shoreward heat transport by eddies that need a grid spacing on the order of 1 km to be resolved by ocean models (Dinniman et al., 2016; Mack et al., 2019). The cooling north of Nickerson, Sulzberg and Swinburne Ice Shelves might be a consequence of this warming, as the continental shelf current drives melt water from the Amundsen-Bellingshausen Seas mostly westward (Nakayama et al., 2017).

Convergence of the model solution does not necessitate convergence towards reality.

Indeed, comparing the bottom layer temperature of WAOM at its three resolutions against WOA18 climatologies reveals that the model solution diverges slightly from observations as resolution increases (see Appendix F Fig. F.8). This behaviour likely has a multitude of reasons, possibly related to artificial diffusion, the impact of resolution on surface forcing and boundary conditions, smoothing of ice draft and bottom topography at different resolutions, the representation of internal tides and its interplay with vertical mixing schemes, etc. We rate a further investigation into the reasons for this behaviour as out of the scope of this study, but note that we expect a convergence towards reality if each version of the model would have been tuned perfectly.

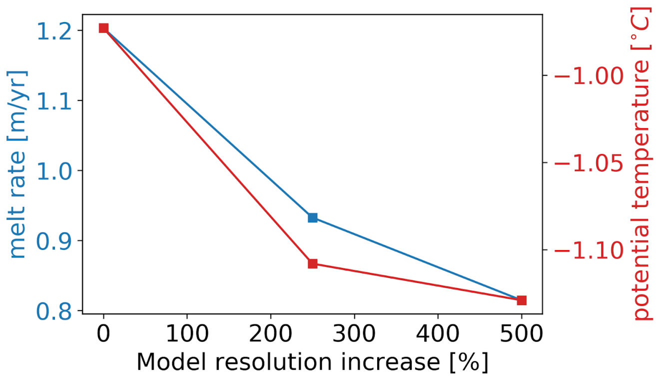

Figure 2.4: Grid convergence. Annual means of average melt rate and continental shelf potential temperature resolved at the different horizontal resolutions: 10 km (0 % increase), 4 km (250 % increase) and 2 km (500 % increase). Continental shelf temperatures have been calculated for depths shallower than 1500 m and including the ice shelf cavities (see Fig. 2.1). Continental shelf processes converge when grid spacing is refined.

2.3.3 Off Shelf Hydrography

To assess the broad-scale hydrography simulated in WAOM, we compare results against WOA18 summer climatologies and SOSE, a high quality ocean reanalysis product (See Section 2.2.6). Figure 2.6 compares the temperature-salinity distribution (TS-distribution) of the summer mean climatology from WOA18 (2005-2017; December, January, February) against the 2007 summer mean from ECCO2 and WAOM. Overall WAOM's off shelf ocean has a warm and fresh bias. While Circumpolar Deep Water (CDW) at intermediate depths is well represented, Antarctic Surface Water (AASW) is to fresh and salty compared to WOA18. WOA18's AASW is mostly limited to tem-

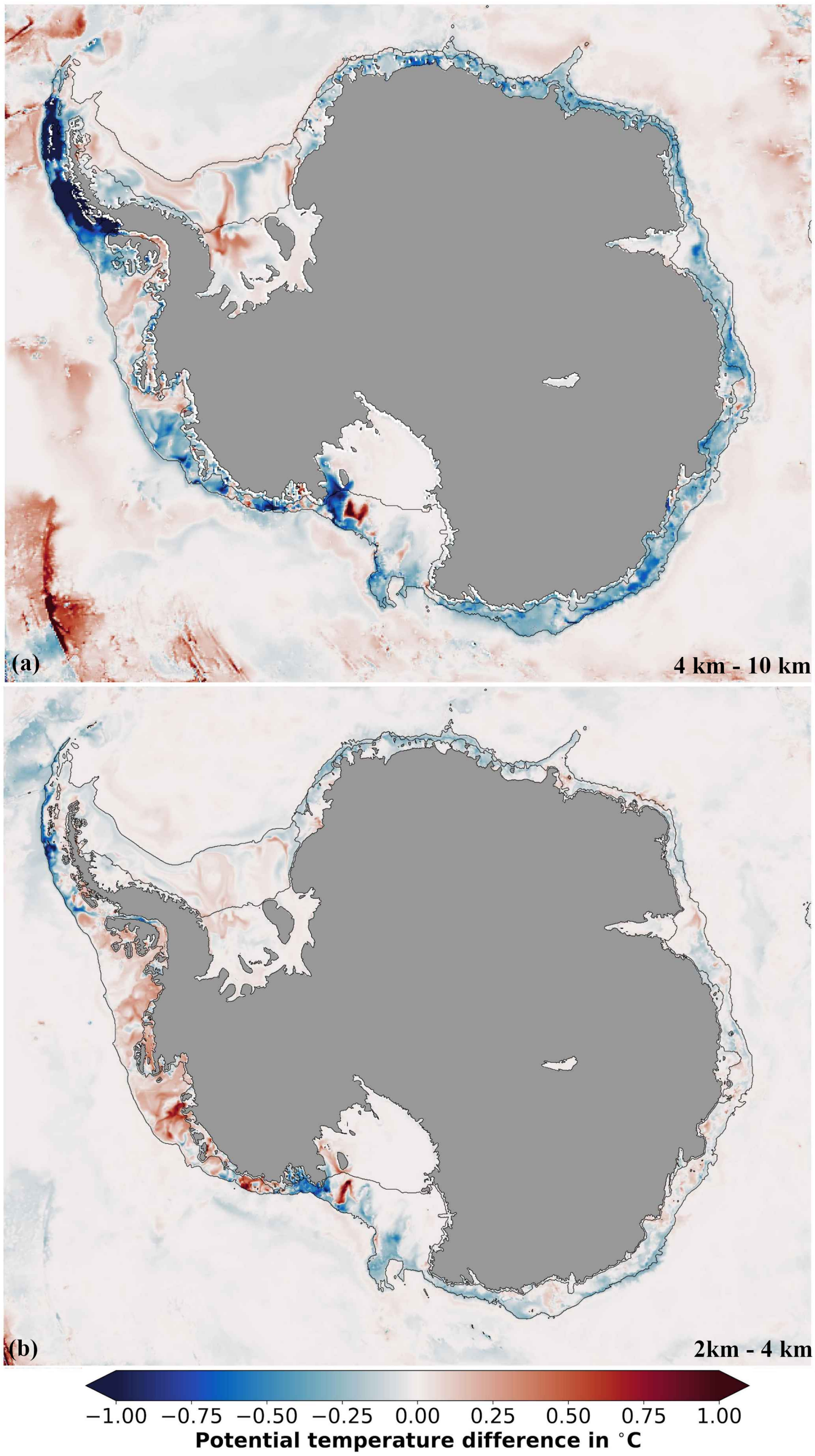

Figure 2.5: The effect of model resolution on deep ocean temperature. Change in annual average bottom sigma-layer potential temperature when increasing the horizontal model resolution from (a) 10 km to 4 km and (b) 4 km to 2 km. Black contour lines indicate the 1500 m isobath and ice shelf fronts.

peratures less than 0 °C and salinities more than 33.75, but WAOM's surface waters are in part warmer than 4 °C and fresher than a salinity of 33.0. These spuriously warm and fresh surface waters affect the properties of adjacent water masses at intermediate depths, effectively warping the overall picture of the TS-distribution away from the freezing point. ECCO2 shows a warm and fresh bias towards the surface too, but the overall extend and impact is less than in WAOM. Water masses close to the freezing point are still apparent in ECCO2 and AASW with temperatures above 2 °C do not show much mixing with deeper waters. Bottom Waters in WAOM are slightly warmer than WOA18 suggest (Ross Sea Bottom Water, RSBW, and Weddell Sea Bottom Water, WSBW, by about 0.5 °C) or to fresh to be distinguished from CDW in this analysis (Antarctic Bottom Water, AABW). ECCO2 shows little sign of RSBW and WSBW.

Figure 2.7 compares the annual mean bottom layer hydrography of the WOA18 climatology from 2005 to 2017 against the 2007 mean from ECCO2 and WAOM. As in Figure 2.6, WAOM shows a warm bias by about 0.5 °C, which can now clearly be attributed to the initial and boundary conditions from ECCO2. This finding agrees with our understanding about the ventilation time of the deep ocean, which exceeds our 7 year spin-up by far. Bottom layer salinities in both models agree very well with WOA18, as differences are mostly constrained to less than 0.05 (often to fresh in both models). In comparison to the GCM, WAOM shows a cooling signal in the Weddell Sea and salinification in the Weddell and Ross Seas, which supports the existence of deep water formation processes in WAOM.

Figure 2.8 compares longitudinal transects of the 2007 annual mean temperature and salinity as resolved by WAOM and SOSE. The stratification of WAOM agrees well with SOSE for the off-shelf ocean and, as expected, diverges towards the ice shelves In the open ocean away from the continental shelf break, the solutions agree and this supports realistic boundary constraints and mixing processes in WAOM. Towards the shelf break and on the continental shelf WAOM resolves substantially colder and fresher waters compared to SOSE, which we interpret as the result of melt water from the ice shelf cavities.

WAOM also often shows stronger vertical mixing close towards the continental shelf, possibly caused by surface forcing or pressure gradient errors. The ocean close to the continental shelf is often well mixed in WAOM, but remains relatively stratified in SOSE (as, e.g., can be seen in Prydz Bay transect, Fig. 2.8d) and this could have various reasons. First, brine rejection in sea ice polynyas is known to cause deep mixing of the entire water column (e.g. Silvano et al., 2018). While WAOM and SOSE use the

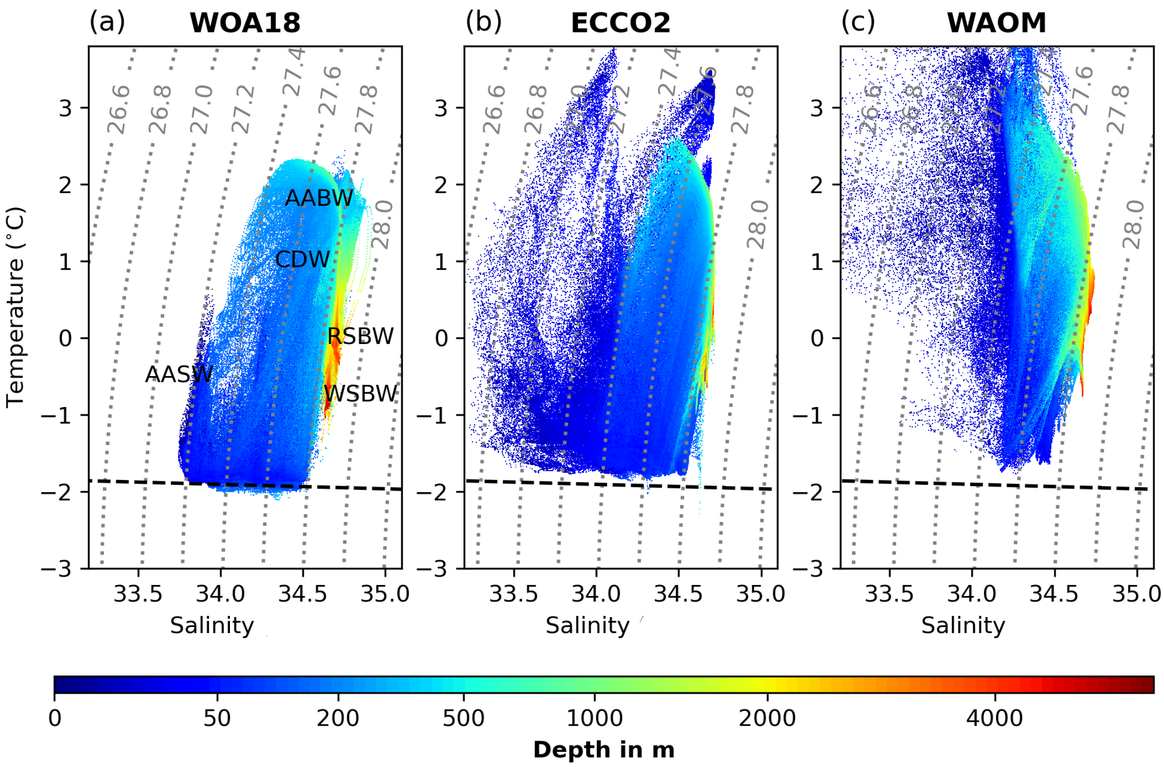

Figure 2.6: Off-shelf summer water masses compared against observations. Potential temperature-salinity-depth distribution of the water masses north of the continental shelf and south of 65°S in summer (average of December, January and February) in (a) WOA18, (b) ECCO2 and (c) WAOM. WOA18 data is the seasonal climatology from 2005 to 2017, while ECCO2 and WAOM is 2007 only. ECCO2 is shown as it provides the boundary and initial conditions for WAOM. Prior to the analysis data from WAOM and ECCO2 has been interpolated on the WOA18 grid (1/4 degree, up to 102 depth levels, using nearest neighbours). For the analysis, each grid cell has been sorted into 1000x1000 temperature and salinity bins and the depth shown for each bin is the volume-weighted average of all the grid cells in this bin. The dashed black lines show the freezing point at the surface and the dotted grey lines are potential density anomaly contours (in km $m^{-3}-1000$; referenced to the surface). Labels show different water masses referred to in the text: AABW indicates Antarctic Bottom Water, WSBW indicates Weddell Sea bottom water, RSBW indicates Ross Sea bottom water, CDW indicates Circumpolar Deep Water, AASW indicates Antarctic Surface Water, and ISW indicates Ice-Shelf Water.

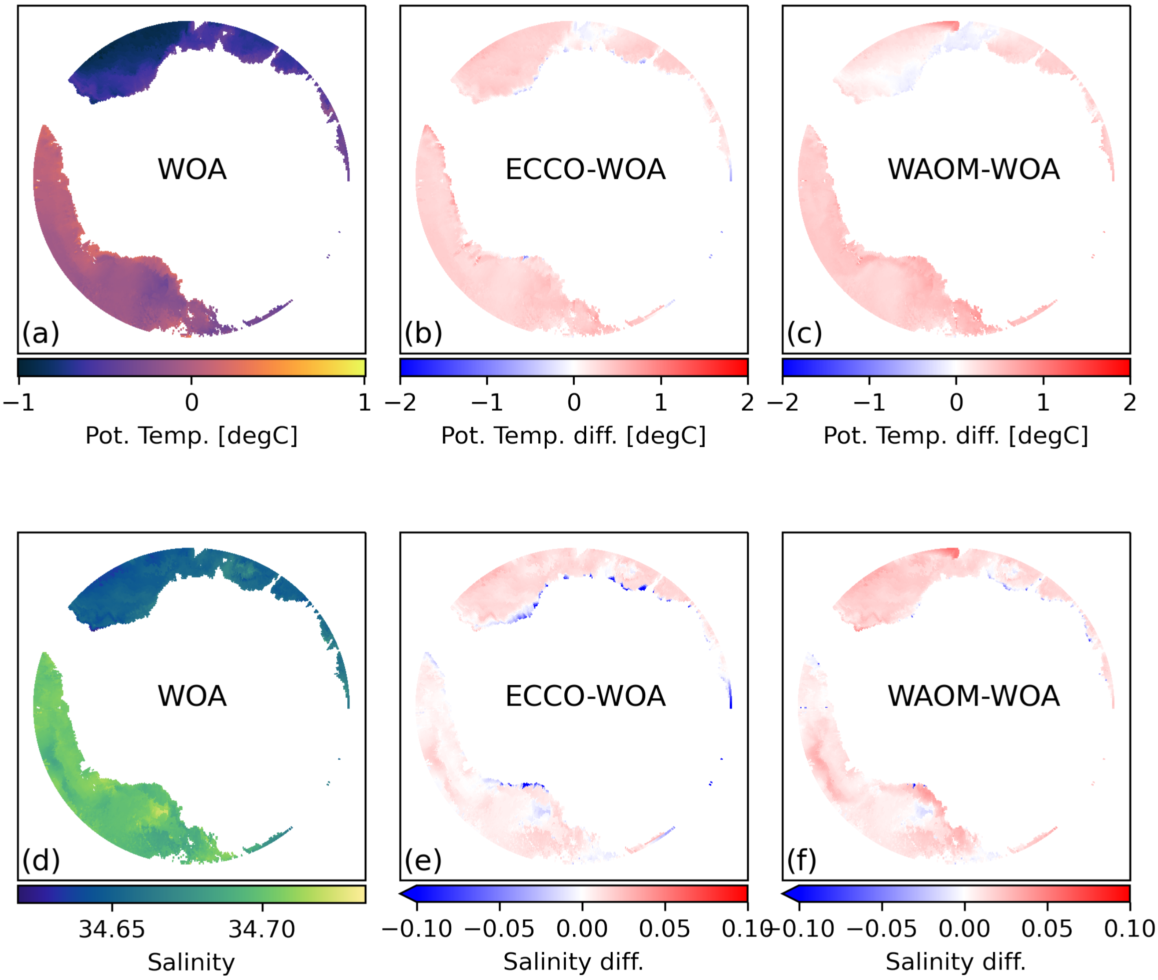

Figure 2.7: Mean bottom water hydrography compared against observations. (a) WOA18 bottom layer potential temperature mean from 2005 to 2017 and difference to (b) 2007 mean from ECCO2 and (c) 2007 mean from WAOM. (d) to (f) is the same for salinity. ECCO2 is shown as it provides the boundary and initial conditions for WAOM. WAOM and ECCO has been interpolated on WOA18 grid prior to comparison (1/4 degree, up to 102 depth levels, using nearest neighbours).

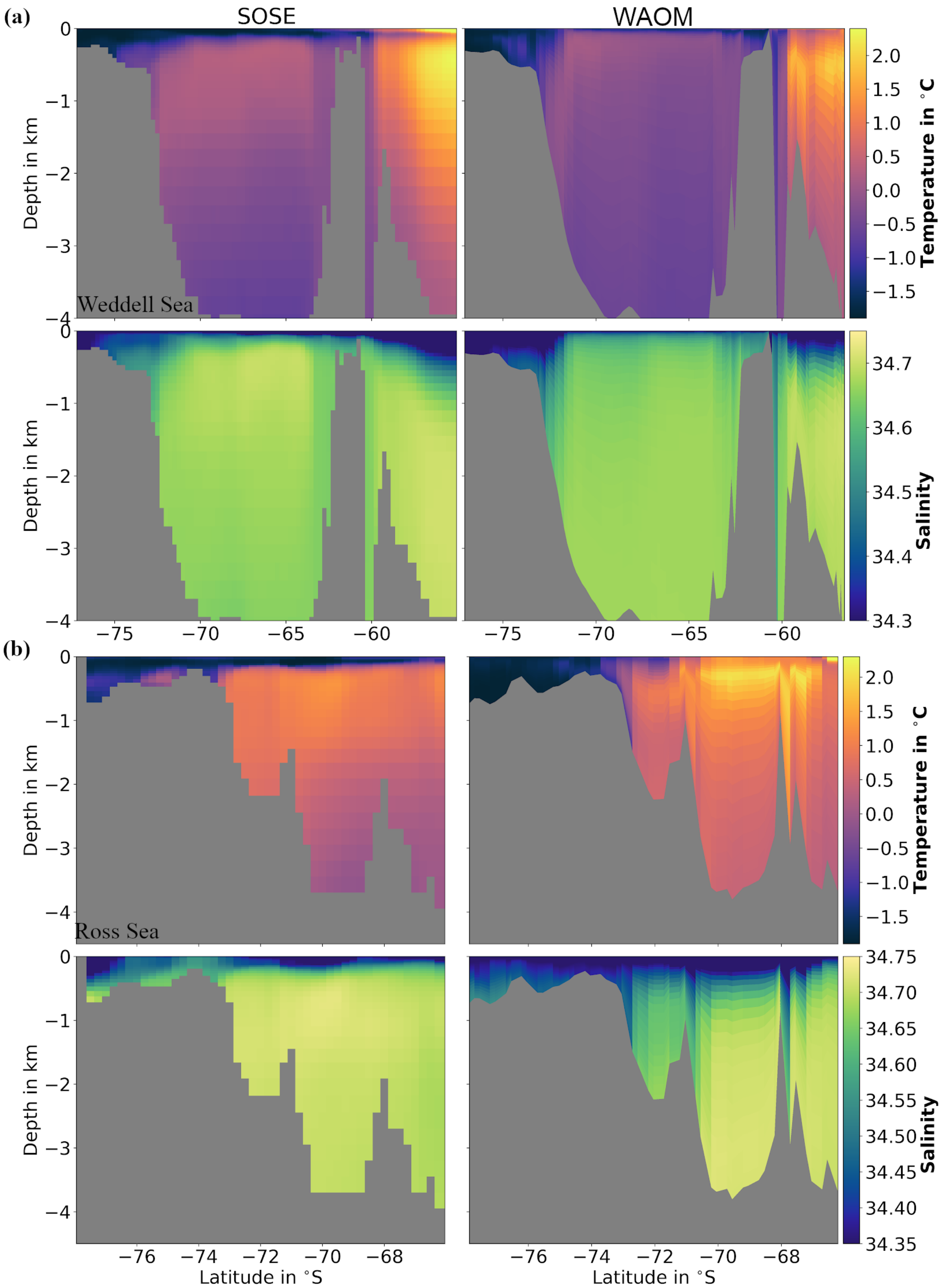

Figure 2.8: 2007 mean Temperature-Salinity distribution of SOSE and WAOM in (a) the Weddell Sea along 45 °W, (b) Ross Sea along 180 °W, (c) Bellingshausen Sea along 75 °W and (d) Prydz Bay along 70 °E. Transect locations are shown in Figure 2.1.

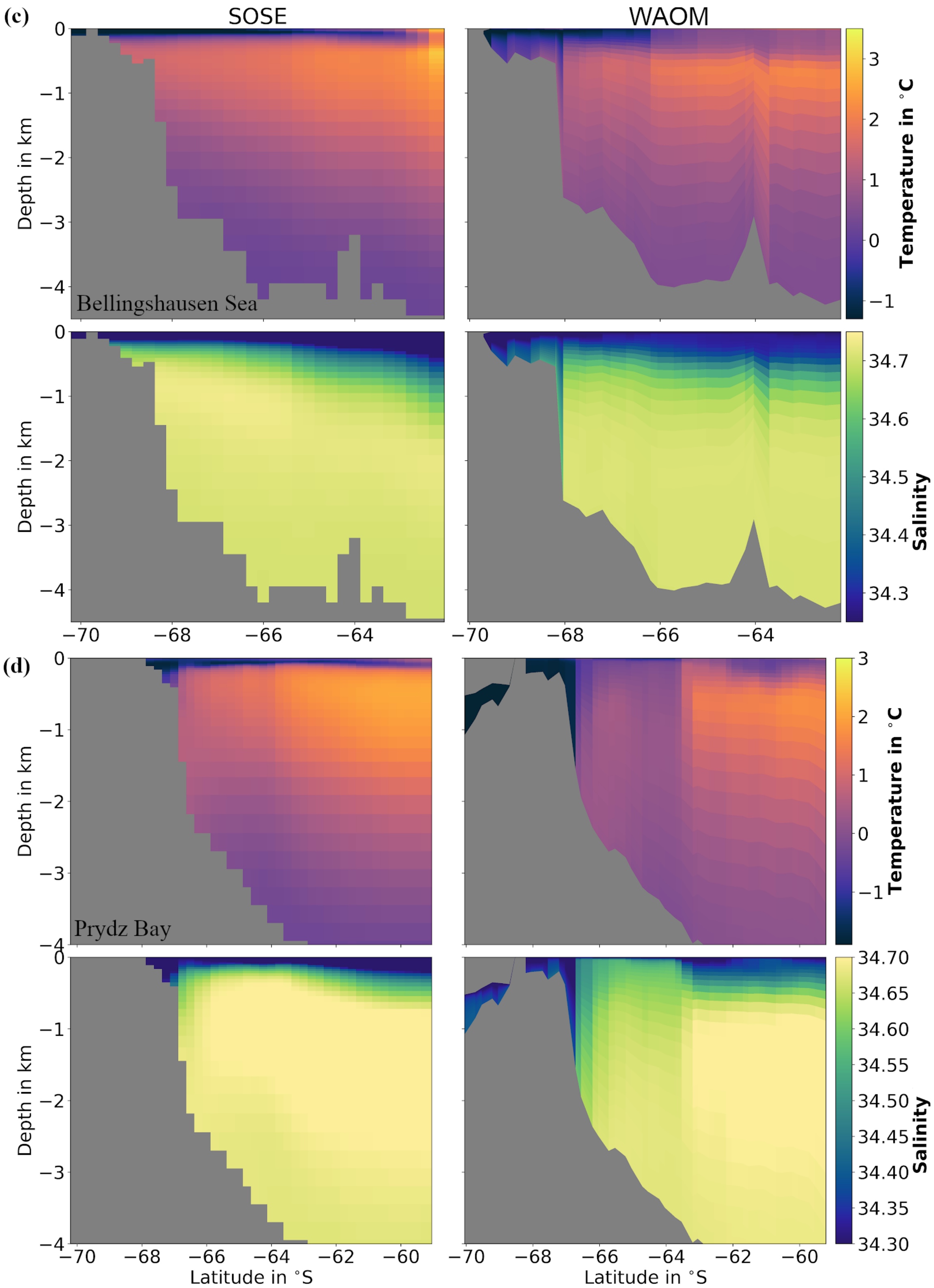

Figure 2.8: 2007 mean Temperature-Salinity distribution of SOSE and WAOM in (a) the Weddell Sea along 45 °W, (b) Ross Sea along 180 °W, (c) Bellingshausen Sea along 75 °W and (d) Prydz Bay along 70 °E. Transect locations are shown in Figure 2.1. (cont.)

same mixed layer parameterisation (KPP), different surface forcing and melt water in WAOM might change the sensitivity to deep convection. Second, spurious currents from pressure gradient errors at steep sloping topography in sigma-coordinate ocean models might also contribute to more mixing in WAOM (Mellor et al., 1994, 1998). This argument is supported by the fact that WAOM produces enhanced mixing also in the vicinity of deep ocean ridges, e.g., in the Ross Sea (Fig. 2.8b). Tidal currents are known to contribute to ocean mixing (e.g. Padman et al., 2009) and SOSE does not include tides. Deactivating tides in the WAOM, however, does not significantly reduce the deep mixing (e.g. in the Ross Seas, see Fig. F.11). Hence, we exclude tides as a possible source for the here discussed differences in mixing to SOSE.

WAOM has been designed to resolve accurate ice-shelf ocean interaction on the continental shelf. Off-shelf regions should be seen as extended boundary condition, rather than part of the model's solution. The models performance in these parts of the domain should be interpreted in this context.

2.3.4 On Shelf Hydrography

Observations on the continental shelf are sparse and cover only short periods of time, which often do not coincide with our simulation. In the following section, first, we showcase that the model qualitatively captures many of the known, critical features of the on-shelf hydrography around Antarctica and, second, compare model results against WOA18 climatologies.

WAOM resolves the important water masses in the Weddell Sea, including Warm Deep Water (WDW) and large amounts of ISW (as shown in Fig. 2.9; see Nicholls et al., 2009, their Fig. 3). Figure 2.10a shows a temperature-salinity transect in front of the Filchner Ice Shelf at 35 °W. This transect reveals that ISW resides at the bottom of the Filchner trough while warmer waters at mid depth resemble characteristics of Modified Weddell Deep Water or Eastern Shelf Water (also shown by Nicholls et al., 2009, their Fig. 7).

In contrast, deep waters in the Amundsen Sea sector feature some of the highest temperatures of the entire Antarctic continental shelf (see Fig. 2.9). Figure 2.10b shows the temperature and salinity distributions along 106 °W, indicating that these CDW intrusions are overlaid by colder Winter Water and only held stable by a large gradient in salinity (in agreement with, e.g. Jacobs et al., 2011).

Figure 2.10c shows a temperature-salinity transect on the continental shelf of Prydz Bay

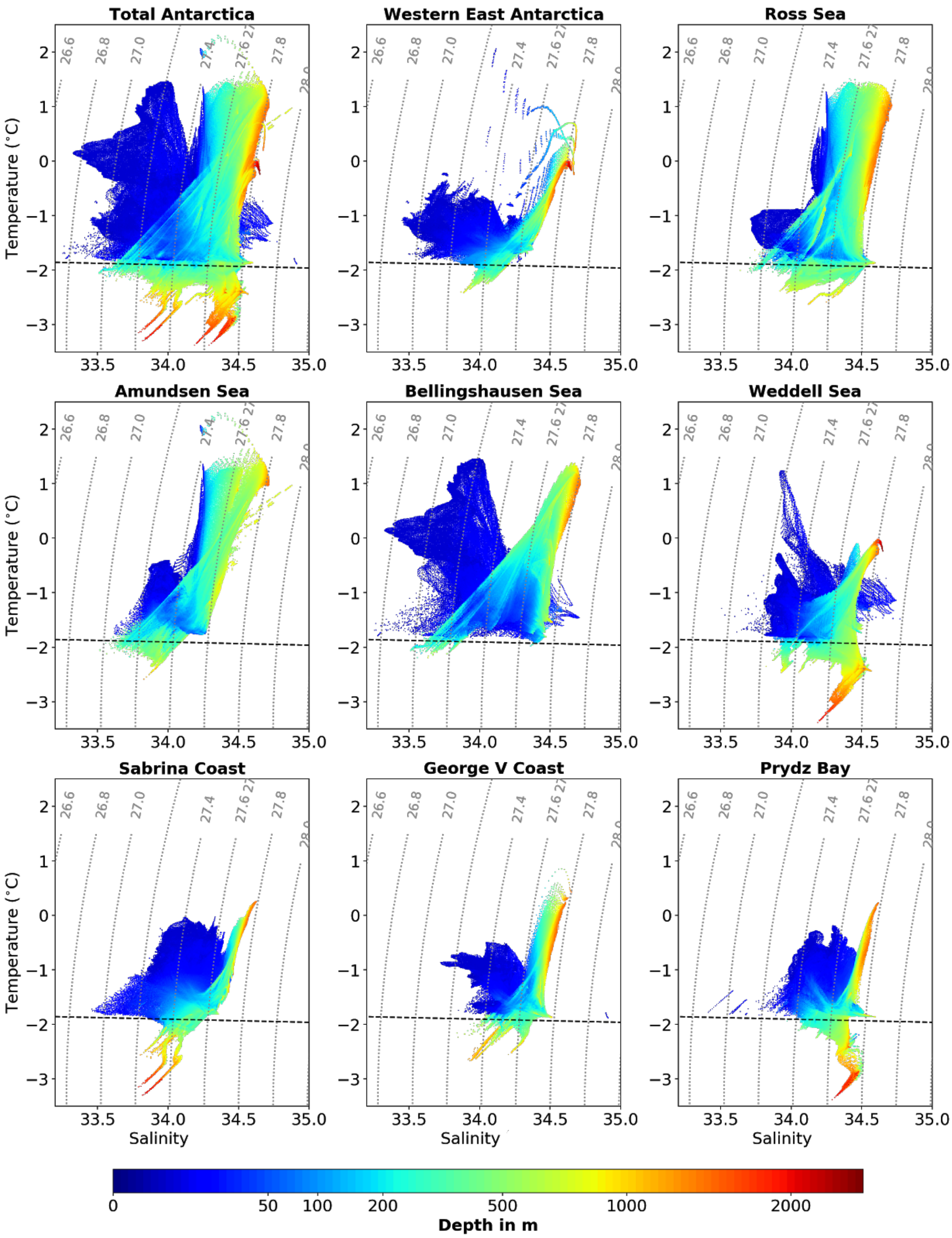

Figure 2.9: WAOM's water masses on the continental shelf for individual sectors. Same as Fig. 2.6c, but for the continental shelf ocean and separated into individual sectors. The analysis has been performed on the model grid. The sub-ice shelf ocean is included and the continental shelf is defined using the 1500 m isobath (shown together with the sector boundaries in Fig. 2.1).

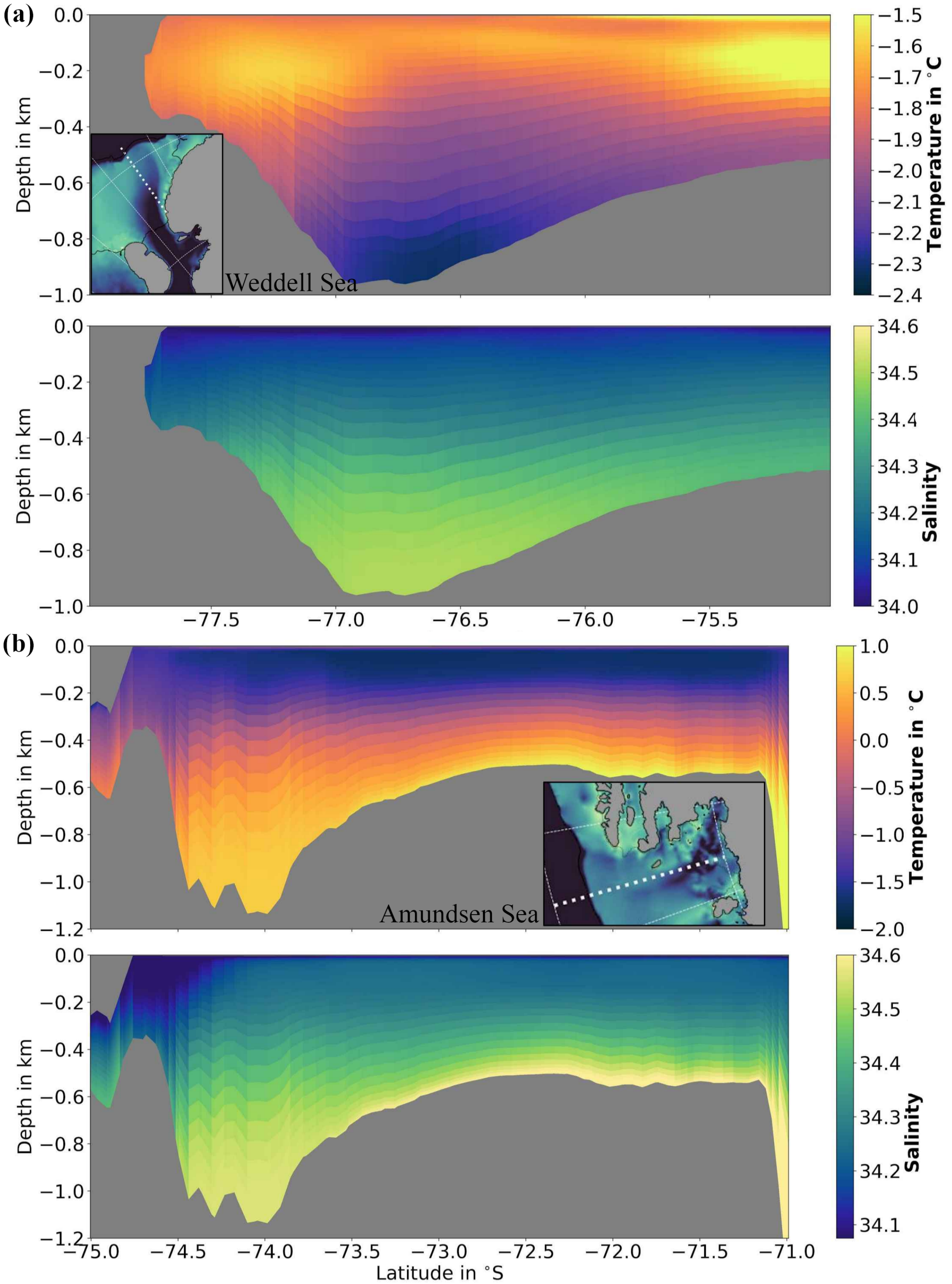

Figure 2.10: Temperature-Salinity distribution on (a) the Weddell Sea continental shelf at 35 °W, (b) the Amundsen Sea at 106 °W, (c) the Prydz Bay at 72 °E and (d) the Sabrina Coast at 120 °E. Inlets show the transect locations.

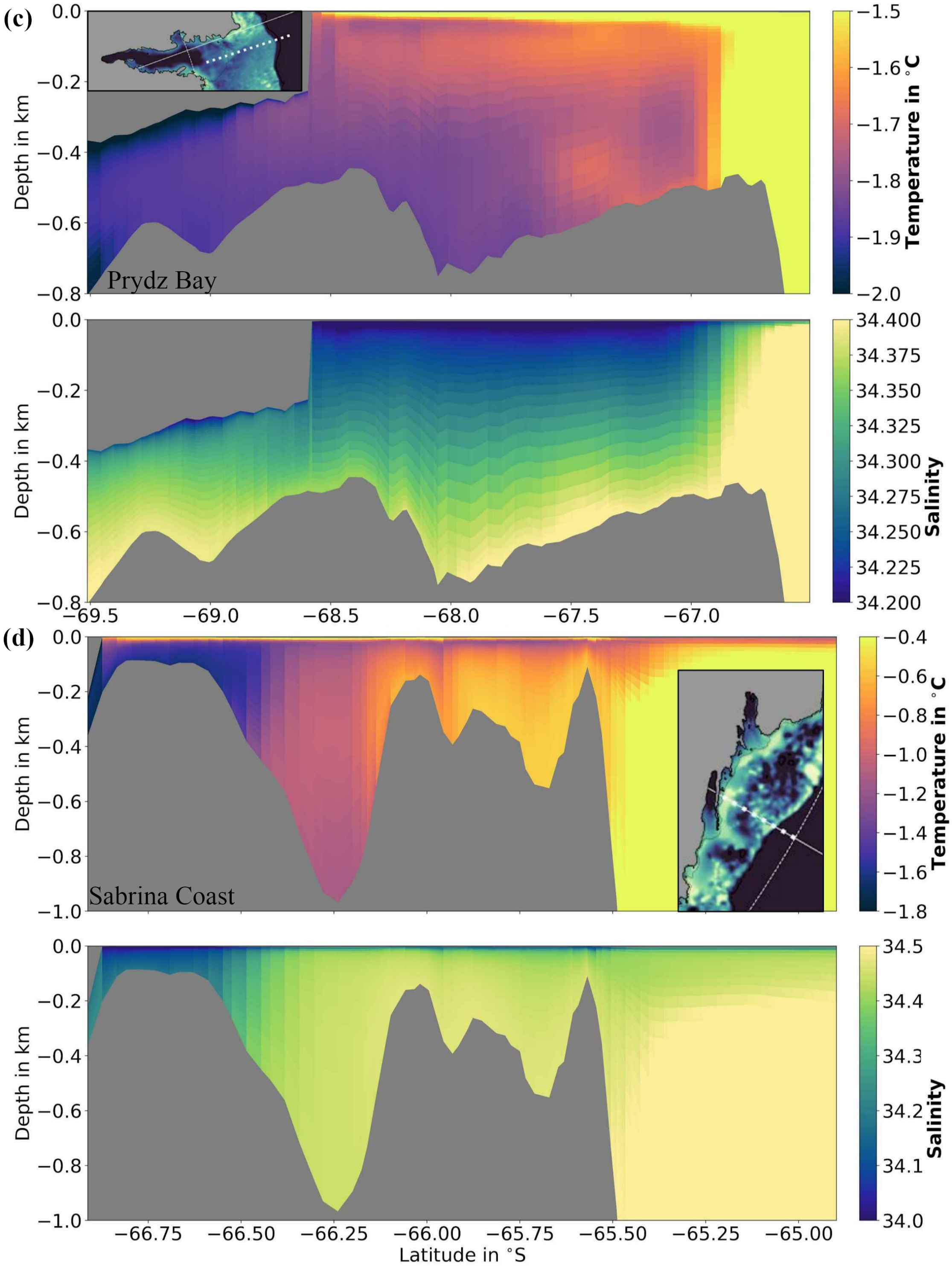

Figure 2.10: Temperature-Salinity distribution on (a) the Weddell Sea continental shelf at 35 °W, (b) the Amundsen Sea at 106 °W, (c) the Prydz Bay at 72 °E and (d) the Sabrina Coast at 120 °E. Inlets show the transect locations. (cont.)

along 72 °E. Inside the Amery Ice Shelf cavity HSSW and ISW can be seen at the bottom and top of the water column, respectively. Further, we detect Dense Shelf Water with salinities of more than 34.5 at depth greater than 500 m (Fig. 2.9, described by, e.g. Williams et al., 2016). CDW is held back from entering the continental shelf in this region by the Antarctic Slope Front (in agreement with, e.g. Guo et al., 2019, their Fig. 2).

Along the Sabrina and George V coasts, however, some MCDW crosses the continental shelf break, e.g. in front of the Totten Ice Shelf. This is demonstrated by the temperature-salinity distribution along 120°E in Figure 2.10d. Once on the shelf MCDW competes with the lighter WW which occupies most parts of the shelf ocean close to the coast (in agreement with, e.g. Silvano et al., 2017, their Fig. 2 and 3).

AASW with temperatures well above freezing can be seen in all transects (Fig. 2.10a to 2.10d). We identify advection of these surface waters into the outer cavities of the Amery ice shelf (see Fig. 2.10c) and the Totten ice shelf (see Fig. 2.10d; in agreement with Silvano et al., 2017, their Fig. 2).

WAOM shows signs of Winter Water (WW) in most regions. WW is a water mass close to the surface that is formed in winter due to heat loss to the atmosphere and salinification as sea ice forms. During summer, WW is eroded as the surface warms and the upper ocean restratifies. WW typically has temperatures close to freezing and salinities between 34.0 to 34.4 (e.g. see Nicholls et al., 2009; Jacobs et al., 2011; Williams et al., 2011). A clear identification of WW in WAOM is made difficult by our evaluation strategy, which only compares summer or annual averages. Nevertheless, we detect signs of WW below a warm surface layer (AASW) in most regions. For example, as mentioned before, Figure 2.10b shows a cold layer from just below the surface up to 200 m depth that overlays warmer CDW in the Amundsen Sea (also visible in TS-space, see Fig. 2.9). That WW occupies most of the upper 300 m in this region is also stated in observational studies (see, e.g. Davis et al., 2018; Jacobs et al., 2011). A similar scenario (CDW overlaid by WW) has also been observed at the Sabrina coast in front of the Totten and Moscow University Ice Shelves (Silvano et al., 2017) and WAOM reproduces this feature at the outer continental shelf (see Fig. 2.10d). In cold water regions, WW is also apparent. The TS-distribution of the Weddell Sea continental shelf (Fig. 2.9) indicates surface water close to freezing with salinities above 34.0, similar to the TS-distribution derived by Nicholls et al. (2009). Finally, in Prydz Bay, observations close to the continental shelf break (see Figure 2 from Guo et al. (2019)) hint towards a fresh and cold subsurface layer on the shelf in this region in good agreement with model results (Fig. 2.10c).

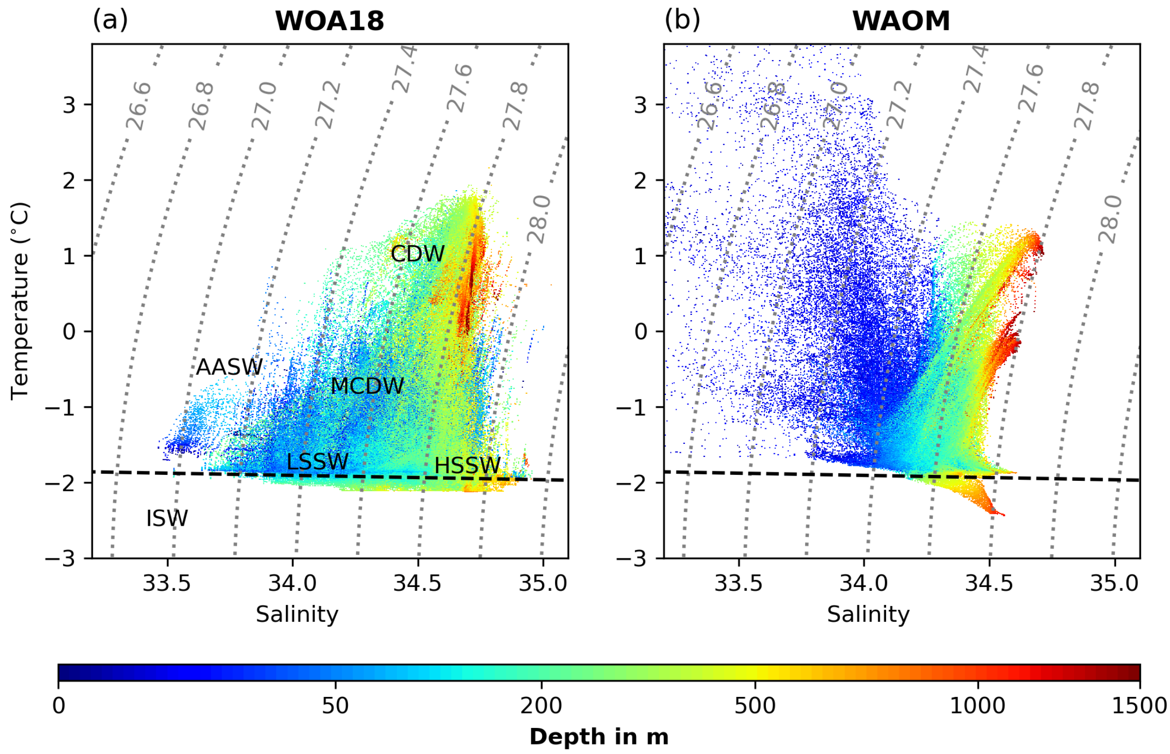

Figure 2.11: Potential temperature-salinity-depth distribution of the water masses on the continental shelf (excluding the ice shelf cavities) in summer (average of December, January and February) in (a) WOA18, (b) WAOM. WOA18 data is the seasonal climatology from 2005 to 2017, while WAOM is 2007 summer only. For analysis details see caption of Figure 2.6. Labels show different water masses: CDW indicates Circumpolar Deep Water, MCDW indicates Modified Circumpolar Deep Water, LSSW indicates low-salinity shelf water, HSSW indicates high-salinity shelf water, AASW indicates Antarctic Surface Water, and ISW indicates Ice-Shelf Water.

Figure 2.11 compares the Temperature-Salinity-Depth distribution of WAOM's on-shelf water masses in summer with the summer climatologies of WOA18. Most subsurface waters (CDW, MCDW and Low Salinity Shelf Water) are well represented in the pan-Antarctic picture. AASW is too warm and fresh, but differences to WOA18 are smaller in magnitude than for the off-shelf ocean and shows less impact on deep waters. In WOA18 surface waters are generally colder than 0 °C and saltier than 33.5, while WAOM's AASW can be as warm as 3 °C and as fresh as 33.0. In contrast to the off-shelf, the impact on deeper waters is mostly restricted to LSSW, as only little mixing occurs at temperatures

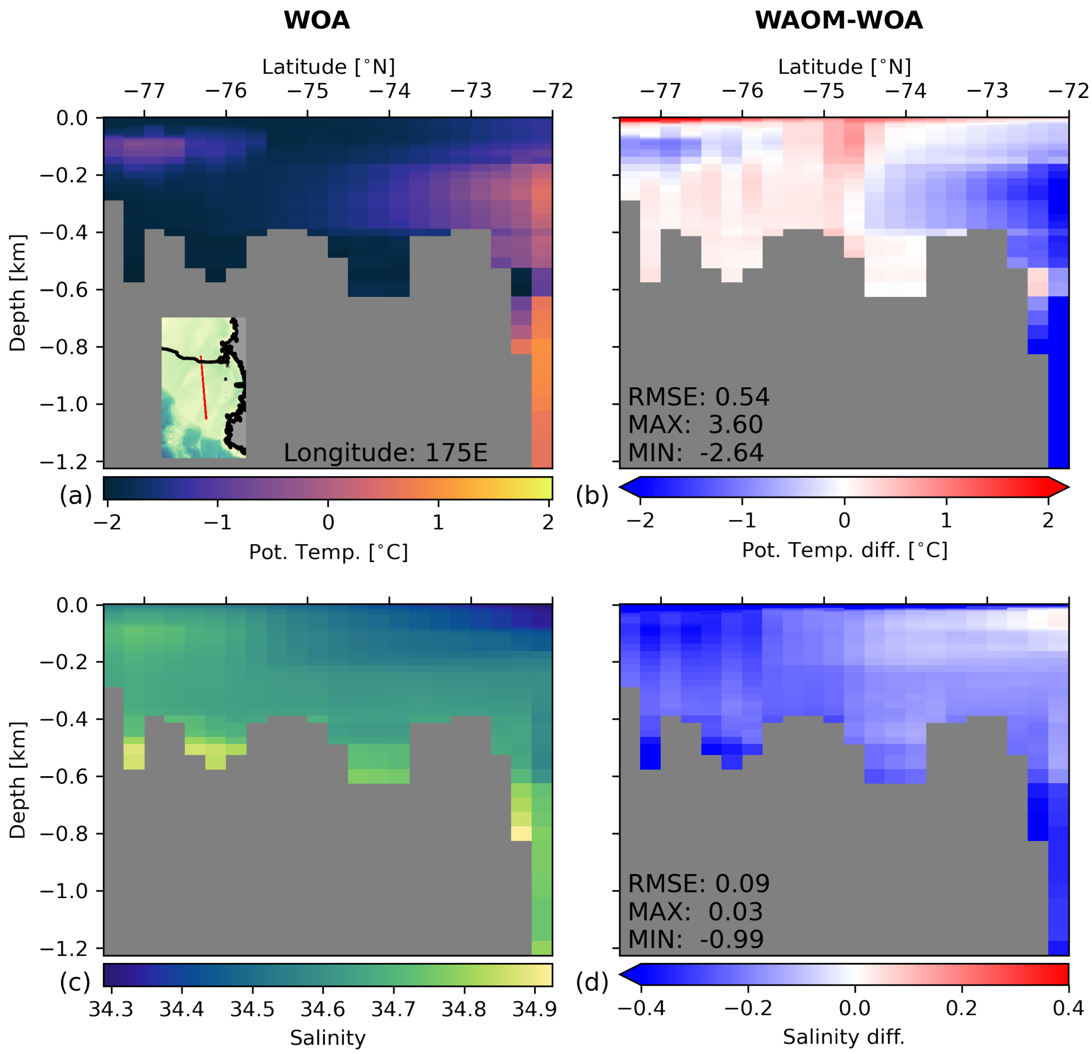

Figure 2.12: Temperature and Salinity transect on the Ross Sea continental shelf (175E) compared against observations. (a) and (c) are WOA18 2005-2017 summer (DJF) climatology mean and (b) and (d) are different from WAOM 2007 summer mean (WAOM-WOA18). WAOM data has been interpolated to WOA18 grid using nearest neighbours.

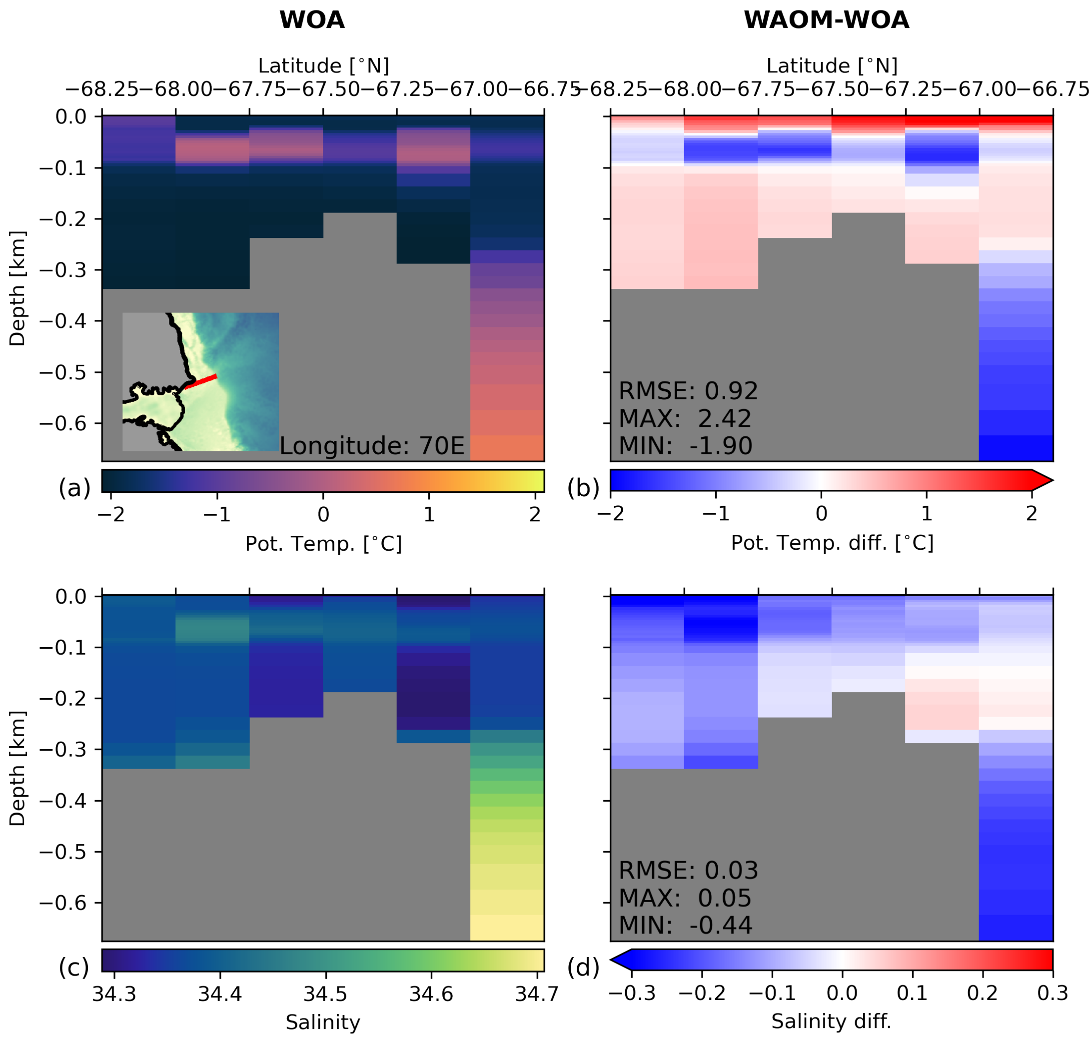

Figure 2.13: Temperature and Salinity transect on the Prydz Bay continental shelf (70E) compared against observations. (a) and (c) are WOA18 2005-2017 summer (DJF) climatology mean and (b) and (d) are different from WAOM 2007 summer mean (WAOM-WOA18). WAOM data has been interpolated to WOA18 grid using nearest neighbour interpolation.

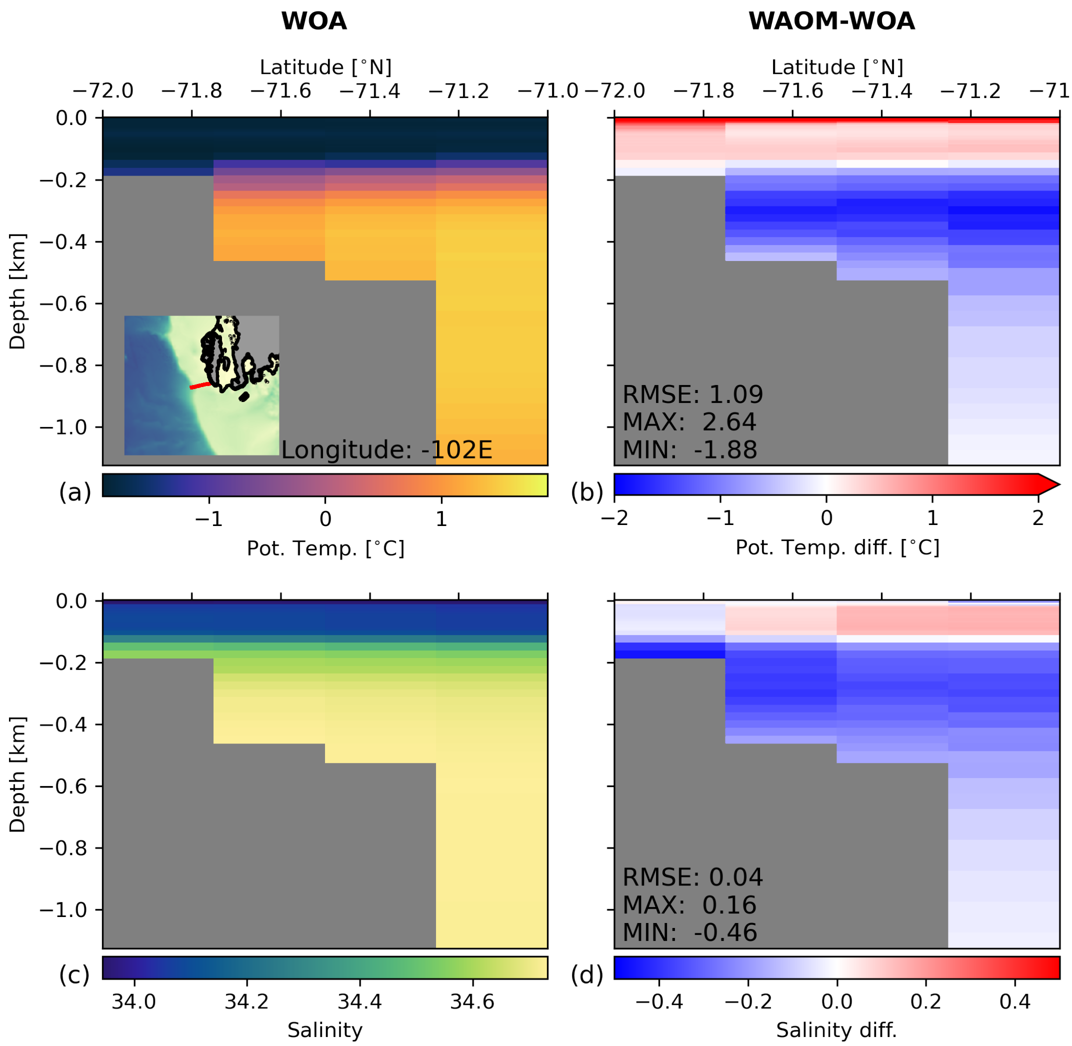

Figure 2.14: Temperature and Salinity transect on the Bellingshausen Sea continental shelf (102W) compared against observations. (a) and (c) are WOA18 2005-2017 summer (DJF) climatology mean and (b) and (d) are different from WAOM 2007 summer mean (WAOM-WOA18). WAOM data has been interpolated to WOA18 grid using nearest neighbours.

higher than $-1.0\,°C$.

Shelf waters with densities higher than $1027.8\,kg\,m^{-3}$ are not well represented in WAOM (Fig. 2.11). Only very little HSSW (freezing point temperatures and salinities higher than 34.5) is apparent in the model. Likewise, other dense shelf waters with higher temperatures (such as Warm Deep Water in the Weddell Sea) are well restricted by $1027.8\,kg\,m^{-3}$. In contrary to WOA18, ISW with temperatures well below freezing is apparent in WAOM.

Figure 2.12 to 2.14 and F.3 to F.5 compare longitudinal transects of temperature and salinity in summer (see 2.2.6). They confirm the biases identified earlier in TS-space. A warm surface bias is apparent in all transects (except in the Ross Sea transects along 150°W). Close to the ice, temperatures can be up to $3.6\,°C$ higher than WOA18 suggest (Ross Sea transect 175°W). We expect Dense Shelf Waters to occupy the bathymetric troughs on the Ross Sea and Prydz Bay continental shelf and, in agreement with earlier findings, water masses here have a tendency to be fresher than WOA18 suggest. In these regions, we detect up to 0.4 fresher waters in WOAM (Ross Sea 175°E). We do not identify systematic biases at intermediate depths. Differences are diverse with Root-Mean-Square-Errors (for entire transects) with temperatures ranging from $2.3\,°C$ to $0.54\,°C$ and salinities from 0.09 to 0.01. We do note, however, that discrepancies often decrease towards the coast (e.g. see transects along 150°W, 70°E and 60°E).

Evaluation of the mean circulation on or close to the Antarctic continental shelf in a comprehensive manner is difficult (see Discussion by Charlotte Huneke et al., 2019; Naughten et al., 2018b; see Gwyther et al., 2018 for a discussion of interannual vs. intrinsic variability). Too few long term current meter records exist to build up a pan-Antarctic map and methods based on sea surface height (e.g. used to constrain the ACC, see Sokolov and Rintoul, 2009) do not work in the presence of sea ice. Other studies have demonstrated ROMS ability of producing realistic slope and coastal currents using selected observations (Charlotte Huneke et al., 2019; Naughten et al., 2018b). Pursuing this efforts for WAOM is out of the scope of this study. Figure F.9 shows the model prediction of 2007 mean barotropic currents close to and on the continental shelf. WAOM reproduces many of the known features, such as the southern limb of the ACC around the Kerguelen Plateau, the southern limbs of the Ross and Weddell Sea Gyres, the Antarctic Slope Current (e.g. around East Antarctica) and the Antarctic Coastal Current (apparent in, e.g. Prydz Bay and in front of the Totten Ice Shelf). The strength of the currents is realistic.

2.3.5 Ice Shelf Melting

Estimates of ice shelf basal mass loss generally agree with satellite observations in many regions. Figure 2.15 compares mass loss estimates for major ice shelves and Antarctica in total from this study against estimates from satellite observations and other ocean models (see Tab. A.1 for underlying data). Using all ice in the model (according to Bedmap2, see Section 2.2.6), we calculate a total mass loss of 1209 Gt/yr (equivalent to an average melt rate of 0.82 m/yr). This is only 4 % below the range of estimates based on remote sensing data and models of surface processes (1263 Gt/yr to 1737 Gt/yr; Rignot et al., 2013; Depoorter et al., 2013; Liu et al., 2015). Regionally, the model and data show larger differences for some ice shelves (Pine Island, Getz, combined Brunt and Riiser-Larsen, Shackleton, combined Totten and Moscow University), but are in agreement or close to others (George VI, Abbot, combined Fimbulisen and Jelbart, Filchner-Ronne, Larsen C, Ross, Amery). In most regions of disagreement (Pine Island, Getz, Shackleton, combined Totten and Moscow University), satellite estimates suggest higher melting consistent with results from regional studies (e.g. Gwyther et al., 2014, for Totten and Moscow University Ice Shelves; Dutrieux et al., 2013, and Shean et al., 2018, for Pine Island Ice Shelf; Jacobs et al., 2013, for Getz Ice Shelf). The estimates from the other models have a large spread, often spanning orders of magnitudes for individual ice shelves. While this can partly be attributed to the different model designs, it also demonstrates the degree of uncertainty associated with modelling of pan-Antarctic ice shelf melting.

Melting and refreezing at high resolution shows that WAOM resolves many of the key features known from observations. Figure 2.16 presents ice shelf basal melt rates and bottom layer temperature around Antarctica from this study. In cold regimes, for example, HSSW often drives strong melting along deep grounding lines followed by refreezing along western outflows (defined as Mode 1 melting by Jacobs et al., 1992). WAOM's melt rates resemble this pattern at many places under the large cold water ice shelves in agreement with regional studies (e.g. under the Filchner-Ronne Ice Shelf in agreement with Holland et al., 2007; under the Larsen C Ice Shelf in agreement with Holland et al., 2009; under the Amery Ice Shelf in agreement with Galton-Fenzi et al., 2012).

It is further known that ice-ocean interaction in the Amundsen-Bellingshausen Seas is governed by intrusions of warm CDW that drive strong melting at all depths (Mode 2 melting; see, e.g. Pritchard et al., 2012; Rignot et al., 2013). WAOM resolves this mode of melting for most ice shelves in this region and features bottom layer temperatures comparable to that observed (often warmer than 1 °C; see, e.g. Schmidtko et al., 2014, their Fig. 1A; Pritchard et al., 2012, their Fig. 2). Why is it then, that some of the ice shelves in this region feature melt rates lower than observed despite sufficiently warm water on the shelf? To address this question, we chose Pine Island Glacier (PIG) ice shelf as an example and compare ocean conditions at the ice front and along the trough that leads up to the front against observations by Jacobs et al. (2011). At the shelf break, bottom layer temperatures are comparable to observed ones (about 3.5 °C above freezing; compare Fig. F.7 transect 1 and 2 against Jacobs et al., 2011 their Fig. 2a transects 5 and 6) indicating that enough CDW is transported onto the shelf. At the ice front, however, bottom layer temperatures are about 1.0 °C lower then observed (compare Fig. F.6c with Jacobs et al., 2011 their Fig. 2b), suggesting that too little of this CDW actually reaches the cavity entrance. Velocities across the cavity opening are realistic (compare Fig. F.6d with Jacobs et al., 2011 their Fig. 4c) and temperatures inside the cavity resemble the conditions at the front (Fig. F.6b), suggesting realistic heat transport across the cavity entrance. In summary, this example investigation supports that the cold bias of some of the warm water ice shelves is caused by spuriously low cross shelf heat transport.

WAOM also resolves other features in cold water regions that agree with observations. For example, the model indicates enhanced melting in the northwestern part of Ronne Ice Shelf, while predicting refreezing north of Henry Ice Rise and east of Berkner Island. All of these features are also reported by Joughin and Padman (2003) and Rignot et al. (2013), even though the magnitude and extent of marine ice accretion is generally lower in the model. Further, the model predicts elevated melt rates along the deep keel of the Fimbul Ice Shelf and this has also been reported by a well constrained regional simulation by Hattermann et al. (2014).

The final melting mode (Mode 3) describes elevated melt rates close to the ice front and WAOM suggests that this melting is apparent everywhere. Jacobs et al. (1992) hypothesise that intrusions of warm surface waters cause strong melting at the frontal zone of ice shelves (often defined as outermost 50 km) at most places around Antarctica. In situ observations have confirmed Mode 3 melting for parts of the Ross, McMurdow and Fimbul Ice Shelf (e.g. Hattermann et al., 2012; Stern et al., 2013; Stewart et al., 2019) and WAOM suggests elevated melt rates in all these regions, with melt rate magnitudes comparable to the observations: about 3 m/yr at the Ross ice shelf front (see Horgan et al., 2011; Stewart et al., 2019) and about 1 m/yr at Windless Bight (see Stern et al., 2013). The simulation results further suggest ice shelf front melting is not limited to these regions, but rather is a widespread feature (further discussed in Chapter 3).

2.4 Discussion

Compared to other models, WAOM includes an eddy resolving resolution, tides and surface buoyancy fluxes from sea ice observations, a first for a circum-Antarctic ice-ocean simulation. These features are critical for resolving ocean-ice shelf interactions accurately and, thus, we consider ice shelf melting and the causal oceanic mechanisms at improved resolution as WAOM's most valuable contribution to ice shelf-ocean research. These melt rates are fully independent from satellite based approaches and will provide new, quantitative insights into the driving mechanisms of ice shelf melting in a pan-Antarctic context. Further, idealized studies have started to explore the average behaviour of the ice shelf cavity system, including its response to a warming ocean (e.g. Holland et al., 2008; Little et al., 2009; Gwyther et al., 2016; Holland, 2017). WAOM provides 176 realistic ice shelf cavities with a single simulation spanning the entire range of present day geometries and ocean conditions. Exploring relations in the average quantities between these systems might help to extrapolate the overall future response of ice shelf melting around Antarctica. Finally, ocean-models are well suited for perturbation experiments and, in the case of WAOM, these can be used to study ocean-ice processes in more detail, for example, the impact of tides or ice shelf teleconnections.

Against expectations, decreasing the model resolution results in an overall warming of the continental shelf ocean possibly related to less accurate resolved tidal processes. Previous studies without tides generally suggest a warming trend of the continental shelf when increasing the resolution from tens of kilometres to kilometres (e.g. Dinniman et al., 2015; Naughten et al., 2018b). This behaviour has been attributed to better resolved bathymetric features, such as troughs, and eddies that act to increase heat transport onto the shelf (Nakayama et al., 2014b; Stewart and Thompson, 2015). The results presented here support the importance of shoreward heat flux by eddies and bathymetry in some regions, e.g., the Amundsen-Bellingshausen Seas. The overall picture, however, is dominated by different processes. Compared to our best guess at reality (2 km resolution and with tides), decreasing the horizontal resolution or deactivating tides (see Chapter 4) leads to a warmer continental shelf with similar regional changes. It appears that a poor representation of tides could cause overestimated heat transport onto the shelf or underestimated heat loss out of the shelf ocean. The latter could be caused by decreased heat loss to the surface or a spuriously low conversion rate of heat into ice

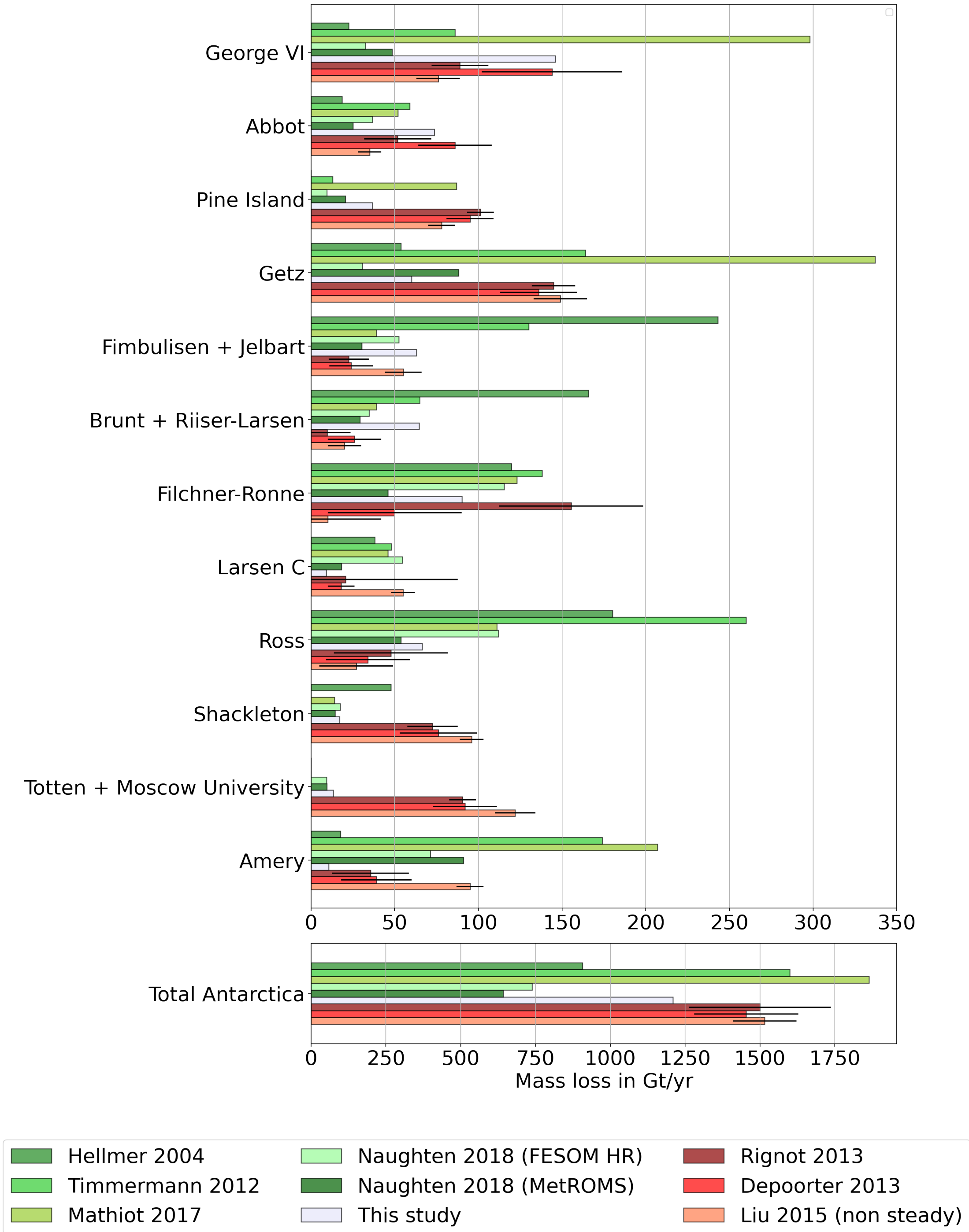

Figure 2.15: Ice shelf basal mass loss from models and satellite observations (equiv. Tab. A.1). Estimates of ice shelf basal mass loss for total Antarctica and major ice shelves individually derived from previous ocean-models (Hellmer, 2004; Timmermann et al., 2012; Mathiot et al., 2017; Naughten et al., 2018b), this study and methods combining satellite data with models of surface processes (Rignot et al., 2013; Depoorter et al., 2013; Liu et al., 2015).

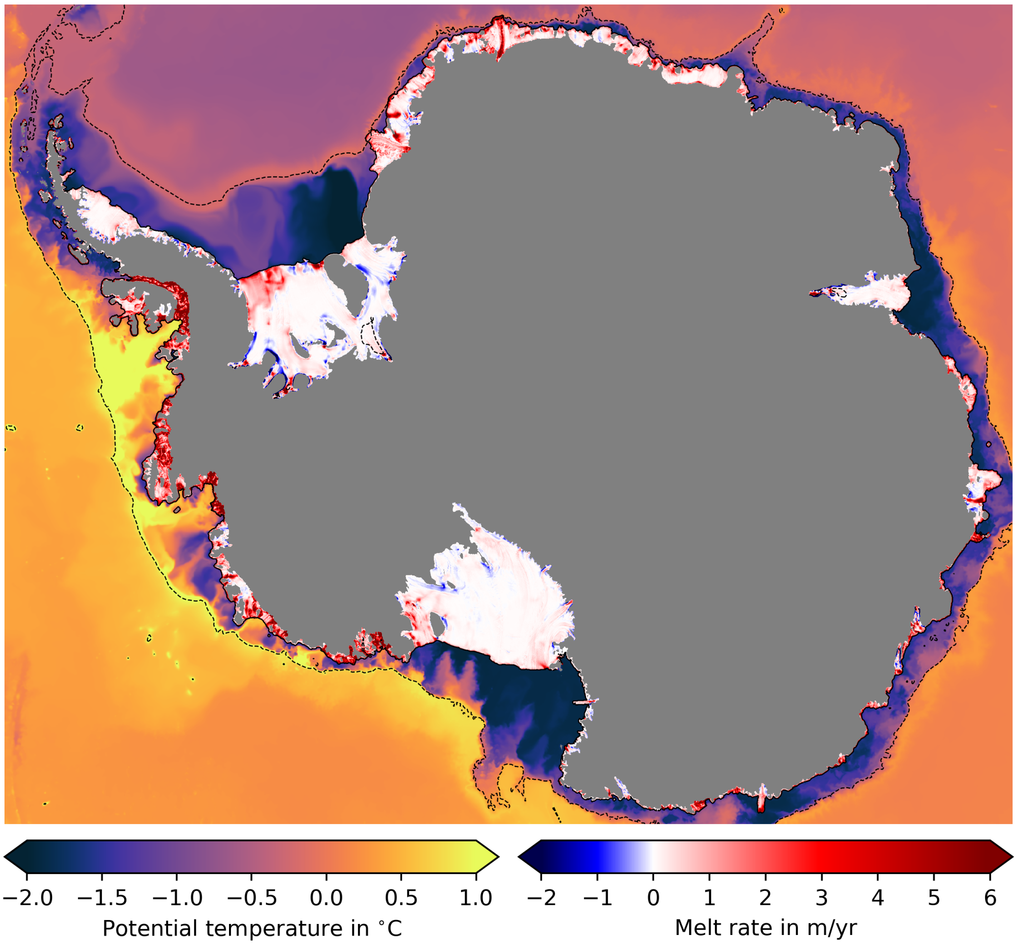

Figure 2.16: Ice shelf melting and bottom layer temperatures. Annual ice shelf basal melt rate is shown where ice shelves are present (negative is refreezing, note the shifted colorbar). Colors seaward of ice shelves show the annual average bottom sigma layer potential temperature. Thin black lines represent the 1500 m isobath.

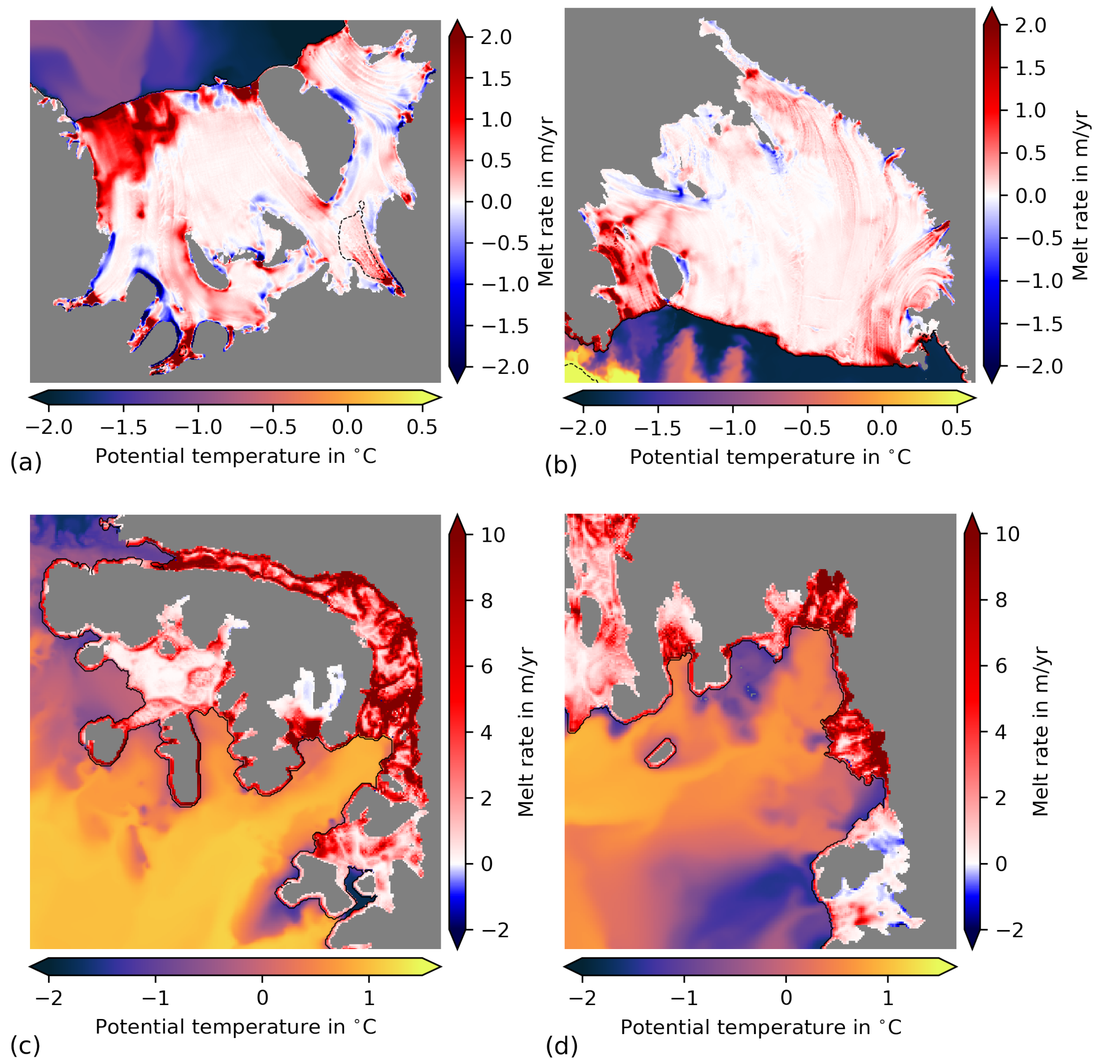

Figure 2.16: Ice shelf melting and bottom layer temperatures (cont.). Zoom-ins show (a) Filchner-Ronne Ice Shelf, (b) Ross Ice Shelf, (c) East Bellingshausen Sea and (d) Pine Island Bay.

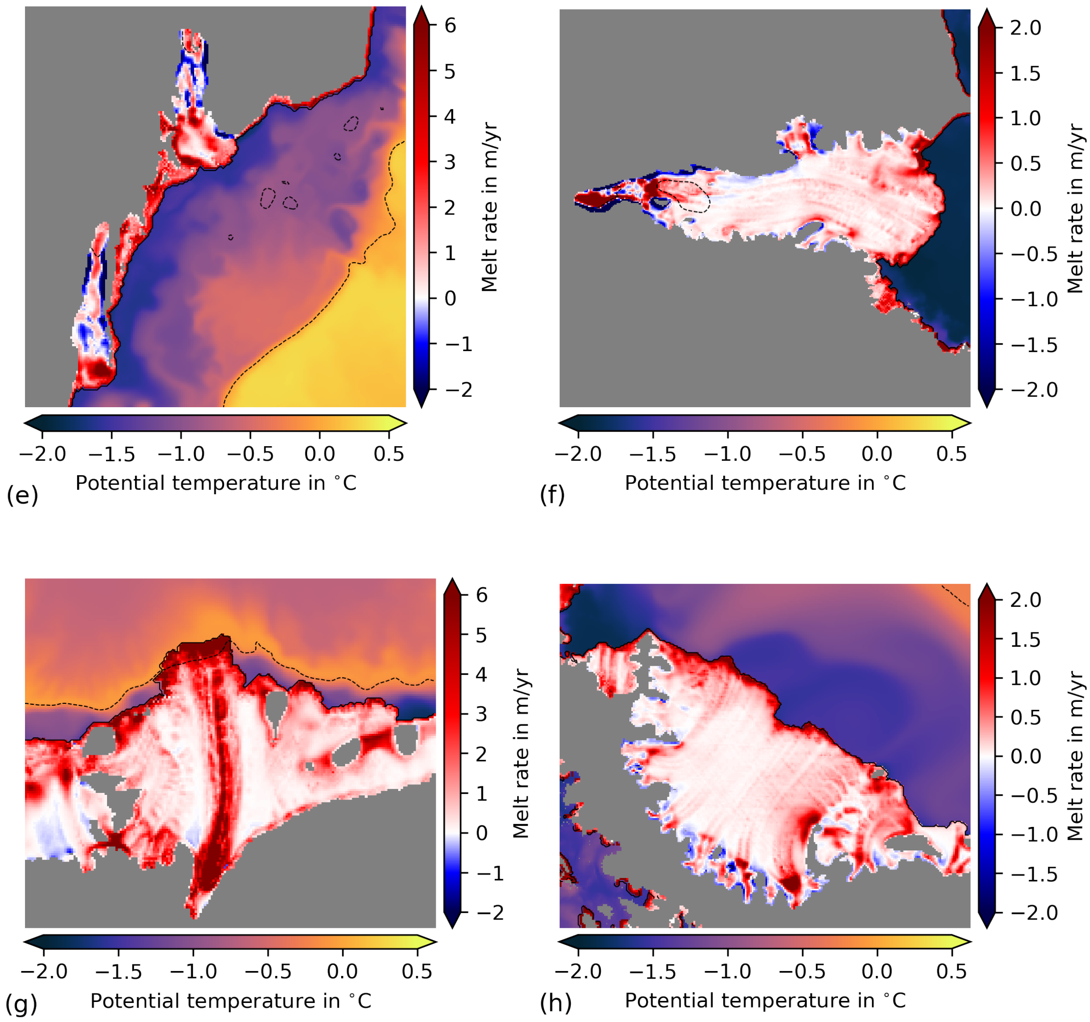

Figure 2.16: Ice shelf melting and bottom layer temperatures (cont.). Zoom-ins show (e) Totten and Moscow University ice shelves, (f) Amery Ice Shelf, (g) Fimbul Ice Shelf, and (h) Larsen B, C and D ice shelves.

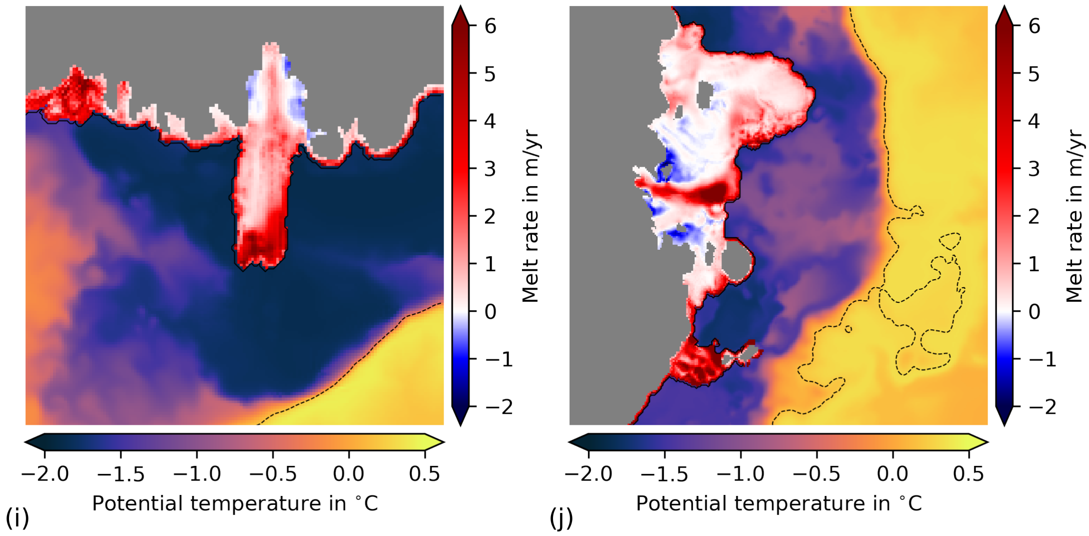

Figure 2.16: Ice shelf melting and bottom layer temperatures (cont.). Zoom-ins show (i) Mertz Glacier Ice Shelf and (j) Shackleton Ice Shelf.

shelf melting. Further experiments are needed to clearly isolate the effects of tides at different resolutions (further outlined below). The finding presented here hints towards the importance of resolving tides at at least 4 km horizontal resolution in large-scale models.

Quantifying changes in the heat budget of the continental shelf ocean and determining the exact tidal mechanism responsible for the model behaviour will require future studies. We hypothesise, however, that vertical mixing on the continental shelf due to internal tide breaking could play an important role. This is based on the following. First, by means of a high resolution circum-Antarctic simulation, Stewart et al. (2018) conclude that tide driven exchanges across the continental shelf break are mostly balanced by mean flow, and, second, the generation of internal tides is sensitive to horizontal model resolution with 4 km being sufficient to resolve the most critical aspects (Robertson, 2006; Padman et al., 2006).

WAOM underestimates melting for some ice shelves and we speculate boundary conditions to be the cause. A cold bias in the Amundsen-Bellingshausen Seas is a common issue in large scale models (e.g. Naughten et al., 2018b) and has been attributed to, either, insufficient transport of deep ocean heat onto the continental shelf (as mentioned earlier), insufficient transport of onshelf heat into the sub-ice shelf cavities or underestimated conversion efficiency of heat into melting inside the cavity (Nakayama et al., 2014b; Dinniman et al., 2015). In our simulation, onshelf ocean temperatures in the Amundsen-Bellingshausen Seas are comparable to observations and where deep warm water intrusions reach the ice shelf cavities melt rates also agree (e.g. for George V and Abbot). For some cases (e.g. Pine Island Glacier and Getz), however, WAOM underestimates melting. For Pine Island Glacier, we have identified insufficient heat flux across the shelf as the main source of the cold bias. Bathymetric troughs are known to be a primary mechanism for cross shelf heat transport (Thoma et al., 2008, e.g.) and a new bathymetric product by Millan et al. (2017) reveals additional troughs in this region. This information has yet to be included in WAOM. Likewise, a regional model by Gwyther et al. (2014) resolves continental shelf temperatures similar to WOAM, but uses a cavity thickness which is 5 times larger along the centreline compared to Bedmap2, and this model resolves melt rates comparable to satellite estimates. Therefore, we rate inaccuracies in the bathymetry as a likely source for the cold bias seen for some of warm water ice shelves in WAOM. Conversely, shore-ward transport of CDW has also been related to thermocline depth modulated by local wind forcing (Davis et al., 2018). We do not account for the effect of sea ice on surface wind stress in the model and, thus, this might effect the ability of CDW to cross bathymetric ridges on the shelf. Seasonal heat flux calculations could be used in future studies to reveal if the inaccuracies are largest in winter when sea ice would have its biggest influence.

The representation of surface fluxes in WAOM should be adjusted in future studies. We have identified that AASW in summer are considerably warmer and fresher than WOA18 climatologies suggest. We can not explain these differences with inter-annual variability, as 2007 is not an anomalously warm year (according to the sea ice extend record of the last 40 years; see Parkinson, 2019). The GCM that provides our boundary and initial conditions shows a similar bias, but the surface layer is too well mixed and ventilated to attribute WAOM surface biases to ECCO2 conditions. Instead, we suspect the applied surface flux schemes to be responsible. In this first version of WAOM, we adjust surface fluxes with tuning parameters established in regional applications and surface relaxation schemes, which has not been tested before. Hence, we attribute the warm surface water bias to overzealous heat flux into the ocean in summer or not enough heat flux out of the ocean in winter. SOSE ensures freezing conditions in the presence of sea ice and resolves large amounts of AASW close to freezing (see Fig. F.1). Including such a condition in WAOM might prove beneficial, but would require information about sea ice extent. Further, WAOM shows only little sign of HSSW and this propagates into a fresh bias of dense waters on the continental shelf. WAOM's salt flux from sea ice polynyas in winter (see F.10) compares well against observational estimates by Tamura et al. (2011) and regional studies that use the same model design (mixing schemes, tides) do not report a lack of HSSW (Galton-Fenzi et al., 2012; Cougnon et al., 2013; Gwyther et al., 2014). Hence, the suppression of HSSW formation is likely also related to the spuriously warm AASW in WAOM. Both of these biases (warm ASSW and too little HSSW) are likely to affect ice shelf melting, as AASW has been shown to advect under the ice in some places (e.g. Stewart et al., 2019) and HSSW is known to drive deep grounding line melting in cold regimes (Jacobs et al., 1992). However, we rate the overall magnitude of the biases as not substantial enough to prohibit a first application of the model to scientific questions. Interpretation of model results, however, should carefully consider these findings.

We consider unresolved sea ice-ocean interactions as the major limitation of WAOM. The ocean connects ice shelf melting and sea ice in a complex manner (Hellmer, 2004; Padman et al., 2018), having motivated many previous studies to include sea ice models (e.g. Hellmer, 2004; Timmermann et al., 2012; Naughten et al., 2018b). This study, however, prioritises accurate polynyas by prescribing surface fluxes from sea ice observations. While this is likely to result in more accurate melt rates at the base of the ice shelves, WAOM can not be used to study processes for which sea ice interaction is critical. Future efforts aiming to use WAOM for simulating periods beyond the observational record will need to incorporate a dynamic sea ice model or carefully prescribe surface flux anomalies. Further, the forcing schemes of this first version of WAOM have been designed for studying phenomena with hourly to seasonal timescales (e.g. tides and summer surface water advection). To address scientific questions related to inter-annual change, these schemes will need to be extended first.

The many wasted land cells in WAOM's domain could also be considered a limitation, but the model design simplifies future coupling with models of ice sheet flow. WAOM's spherical grid using a south polar projection necessitates masking of more than one third of all computational cells, wasting valuable resources with the model integration timestep. This design, however, has been chosen to simplify future efforts that aim to couple WAOM with models of Antarctic ice sheet flow (e.g. Jong et al., 2017), as these coupled models are ultimately needed to improve sea level rise predictions (e.g. Colleoni et al., 2018). Also in regards to coupling, ROMS includes routines to resolve sediment transport and passive tracers (see, e.g. Dinniman et al., 2003; Sherwood et al., 2018, for applications) and activating these options in WAOM will likely be of interest for geological and biological studies.

To further improve the accuracy of WAOM, future development should focus on the following aspects.

- Establishing an evaluation matrix for circum-Antarctic ice shelf-ocean models would open the path for efficient parameter tuning (similar to Nakayama et al., 2017) and allow the community to compare the performance between different models (see Naughten et al., 2018b). Many kinds of observations are useful for this, including ice shelf basal melting from phase-sensitive radar (ApRES), as well as ocean measurements from Conductivity(Salinity)-Temperature-Depth (CTD) sensors, Acoustic Doppler Current Profilers (ADCP) and turbulence measurement packages. These ocean instruments can be mounted on Autonomous Underwater Vehicles (AUVs) with under ice capability, underwater gliders, drifting floats, moorings and Seals. When rating the model performance against such observations, uncertainties of the underlying methods and the spatial and temporal variability of the observed quantities must be carefully considered.

  ApRES seems particularly suitable for large scale model evaluation as it comprises a robust and cheap method to observe basal melt rates over longer time periods. As more ApRES measurements are becoming available, their compilation could provide the backbone for such an evaluation matrix, similar to tide gauge measurements for tidal accuracy (King and Padman, 2005). Comparison of a wide array of ApRES data is already underway with the NECKLACE programme[1].

- Future field campaigns should be guided by model results. ApRES measurements are particularly valuable where high resolution satellite estimates have their greatest uncertainties, that is in calving regions and close to grounding lines. Although, crevasses are often present in these regions and can impede the successful interpretation of ApRES results.

- Accurate bathymetry on the open continental shelf and inside the sub-ice shelf cavities is essential to resolve warm water intrusions, critical for ice shelf melting and consequent melt water export. Thus, the model bathymetry should be updated according to regional surveys (e.g. Millan et al., 2017; Nash, 2019).

- Studying individual aspects of the model will help gain trust in quantitative results. Schnaase and Timmermann (2019), for example, show that artificially deepening

[1]NECKLACE programme: http://www.soos.aq/news/current-news/330-necklace-workshop-update.

the water column thickness near grounding zones (necessary for numerical stability), does not affect ice shelf average melt rates, and Malyarenko et al. (2019) suggest that the unrealistic ice front representation in sigma-coordinates, could actually account for unresolved small scale processes. Wind stress has been shown to impact ice shelf melting (Davis et al., 2018; Greene et al., 2017), but how sea ice modulates momentum flux from the atmosphere into the ocean is still an open question (Lüpkes and Birnbaum, 2005; Nøst et al., 2011).

- The number of wasted land cells in WAOM could be reduced by applying nested grids with coarser resolution in ice sheet areas.
- Finally, including parallel input-output in WAOM would allow for efficient parallelisation at 2 km resolution. The gain in computational cost might make longer simulation periods feasible or allow for a further increase in horizontal resolution until continental shelf quantities converge.

We propose the following experiments to harness the strengths of WAOM.

- Deactivating tides in the model would lead to a first estimate of the impact of tides on Antarctic-wide ice shelf melting and can likely be used to gain further insights into the mechanisms governing tidal melt.
- Experiments that trace individual water masses, such as ISW or AASW, could be used to study the role of ice shelf teleconnections in a pan-Antarctic context or attribute ice shelf mass loss to the individual melting modes.
- To reduce model bias related to HSSW and AASW, sensitivity studies should quantify the impact of surface buoyancy flux tuning. These studies should focus on the relaxation timescales used for sea surface salinity and temperature restoring to estimates from SOSE, as well as the tuning aspects applied to the daily buoyancy fluxes and developed for regional applications. Implementing a scheme that ensures freezing conditions in the presence of sea ice might prove beneficial.
- Extending the resolution study introduced here would help to attribute the convergence behavior to individual aspects of the model. Future experiments should be designed to isolate effects due to changes in bathymetry, ice draft, tides and sub-gridscale turbulence parameterisation. This way, changes in shore-ward heat flux with increasing model resolution could be more be more clearly related to troughs, eddies and internal tides.

- Finally, applying anomalies from future climate projections to the boundary forcing (e.g. from CMIP5; Taylor et al., 2011) could be used to study the response of Antarctic ice shelf melting to warming oceans. This experiment would not just add another estimate that complements other model results by Naughten et al. (2018b), but offers valuable sample points of the average behaviour of the ice shelf cavity system.

2.5 Summary and Conclusion

Here, we present the Whole Antarctic Ocean Model (WAOM v.1.0). WAOM overcomes two major shortcomings of previous circum-Antarctic ocean-ice shelf models by the inclusion of tides and a horizontal resolution which is high enough to resolve critical shoreward heat transport by eddies (e.g. Dinniman et al., 2016). We have simulated present day conditions by spinning up the model to a quasi equilibrium with repeated 2007-forcing.

Overall, model results compare well against available observations. Continental shelf ocean temperatures and ice shelf melting converge with increasing model resolution, but a further refinement to 1 km grid spacing is likely needed to reach asymptotic behaviour. The accuracy of tidal height signals at the coast is comparable to state-of-the-art barotropic tide models. In the Ross Sea, however, the major semidiurnal constituents M2 and S2 are systematically overestimated with differences exceeding 300 % at individual locations. Differences in other Antarctic regions are less noteworthy. The off-shelf hydrography resembles many aspects of WOA18 summer climatologies, but features a warm and fresh bias at the surface. On the continental shelf, where observations are sparse, WAOM resolves realistic hydrography, e.g., featuring bottom layer temperatures of 1 °C in the Amundsen-Bellingshausen Seas and WDW production in the Weddell Sea. The warm bias of AASW is also apparent on the shelf, but to a lesser degree. Spuriously small amounts of HSSW are produced, causing a fresh bias of dense shelf waters. Ice shelf melting and marine ice accretion at high resolution show that WAOM captures the known modes of melting, often in agreement with regional studies. Ice shelf average melt rates agree with satellite observations at many places, but indicate a cold bias for some of the warm water ice shelves in the Amundsen-Bellingshausen Seas as well as the Totten and Moscow-University Ice Shelf System. We attribute these discrepancies to insufficient heat flux across the continental shelf, likely due to regional uncertainties in bathymetry or wind stress.

To further improve WAOM, future studies should mostly focus on compiling available observations of ice-ocean interaction around Antarctica. Efforts are underway to collect all available ApRES measurements of ice shelf basal melting around Antarctica (the NECKLACE programme) and this could form the base for a consistent evaluation matrix of large scale ice shelf-ocean models. Such a framework would not just help to tune model parameters in an efficient manner, but also compare the performance between different models and, thus, focus community model development. Further, the bathymetry in WAOM should be updated where regional products are available and future studies should target individual, uncertain aspects in the model, such as how sea ice modulates wind stress and the representation of surface water advection under the ice front. To reduce known biases related to AASW and HSSW, surface buoyancy flux tuning should be optimised.

Resolving ice shelf-ocean interaction at high resolution is the main purpose of WAOM. The only available estimate of Antarctic-wide ice shelf basal melting at high resolution has been derived from satellite observations and models of surface processes with unknown uncertainty (Rignot et al., 2013). Thus, new estimates derived from a fully independent method, that also offers an ocean consistent to the melt rates, is likely to result in new insights into the governing processes that drive Antarctic ice shelf melting. Further, WAOM is well suited for giving a first estimate of circum-Antarctic tidal melting and to explore the average behaviour of all ice shelf cavity systems found around the continent. WAOM is not coupled to a dynamic sea ice model and, thus, future simulations will need estimates of sea ice-ocean fluxes from climate models. Alternatively, WAOM could be coupled to a sea ice model, in a manner similar to Naughten et al. (2018b).

To reduce uncertainties in predictions of future sea level rise and climate, models will ultimately need to resolve interaction between the Antarctic ice sheet and the Southern Ocean over glaciological timescales (e.g. Colleoni et al., 2018). Code that communicates the shared properties between ice sheet and ocean models is now available (Jong et al., 2017), and idealized and regional applications with ROMS show promising results (Asay-Davis et al., 2017). WAOM has been designed to provide the ocean component of a coupled Antarctic-wide application and this study presented development and evaluation of a present day simulation and is a major step towards this goal.

Chapter 3

Antarctic Ice Shelf basal melting at shallow depths

Preamble

In the preceding chapter (Chapter 2) the development and evaluation of a new Antarctic ice shelf-ocean model with improved accuracy has been described. This chapter (Chapter 3) builds upon these results to determine if ice shelf melting around Antarctica is exclusively driven by deep warm water intrusions. Hence, this chapter addresses the second main objective derived in Section 1.6. Note that this chapter has been written in a concise and focused format that presents the main findings together with their discussion and conclusion.

Abstract

Understanding the processes involved in basal melting of Antarctic ice shelves is important to quantify the rate at which Antarctica will lose mass. Current research of ice shelf-ocean interaction is almost exclusively guided by satellite derived estimates of Antarctic-wide ice shelf melting, which highlight deep warm water intrusions and melting along ice shelf grounding lines. Ocean modelling comprises an independent method to study ice shelf-ocean interactions, but current continent-scale applications lack resolution and important physics. Here we present Antarctic-wide estimates of ice shelf basal melting from a state-of-the-art ocean model, which addresses many of the shortcomings of previous models. We estimate a total basal mass loss of 1207 Gt/yr from which 79 % comes from ice shallower than 400 m deep. Previously published satellite estimates also highlight the mass loss contribution from shallow depths, but simulated melt rates shallower than 200 m deep are three times higher than satellite estimates suggest, leading to a total mass loss contribution of 33 %. Ice shallower than 200 m deep is often confined to the ice front and while recent in situ observations confirm enhanced front melting, methods using satellite data do not resolve these areas. In the model, melting of ice shallower than 200 m deep triples in summer, when solar heated surface waters advect under the ice. Thus, to improve Antarctic mass loss predictions, research should not just focus on deep warm water intrusions, but also the processes that control surface water advection and melting at shallow depths.

3.1 Introduction

Ice shelf basal melting and refreezing can change the thickness and stability of ice shelves, impacting their buttressing ability against inland ice sheet discharge and therefore influencing sea level rise (Reese et al., 2018). Basal melting further impacts the surrounding oceans with consequences for global ocean circulation and climate (Bronselaer et al., 2018; Golledge et al., 2019).

Studying ocean-ice shelf interaction at a continent scale is difficult, as only few direct observations exist. For Antarctic-wide estimates of ice shelf basal melting we currently rely almost exclusively on methods that use satellite data to infer basal melting as the missing component in a mass budget analysis (Rignot et al., 2013; Depoorter et al., 2013; Liu et al., 2015). The accuracy of these methods suffers from uncertainties in the satellite data itself, poor estimates of calving and the use of atmospheric models for near-surface firn processes. While ice shelf averages derived from budgets across ice shelf or ice flow line boundaries often agree within their uncertainties, high resolution results do not integrate to the same values and their uncertainty has not been quantified (Fig. 3.1, Table A.1).

Ocean models which include an ice shelf component have also been used to study Antarctic-wide ice shelf melting at high resolution (Hellmer, 2004; Losch, 2008; Timmermann et al., 2012; Naughten et al., 2018b). However, these models often neglect important ocean dynamics, such as eddies and tides (Dinniman et al., 2016), and do not resolve many of the smaller ice shelves (Hellmer, 2004; Timmermann et al., 2012; Naughten et al., 2018b), leading to large biases in their quantitative results. Developing these models is important, because their estimates are fully independent from the uncertainties related to methods using satellite data (Schodlok et al., 2016), they resolve an ocean that is consistent with the melt rates, and they are ultimately used to predict past and future changes (Hellmer et al., 2012; Obase et al., 2017; Naughten et al., 2018a).

The lack of independent estimates of Antarctic ice shelf melting hinders our understanding of the oceanic processes involved. Observations and models suggest that intrusions of warm deep water masses that cross the continental shelf break and reach the ice shelf cavities can explain the large scale differences in melting around Antarctica (Rignot et al., 2013; Pritchard et al., 2012), and hence many studies have focused on processes controlling the strength and depth of these intrusions (Thoma et al., 2008; Kimura et al., 2017; Greene et al., 2017; Stewart et al., 2018; Davis et al., 2018; Hattermann, 2018). However, there is some evidence from regional studies that seasonal advection of solar heated surface waters can drive strong melting near the ice front (Horgan et al., 2011; Stern et al., 2013; Arzeno et al., 2014; Hattermann et al., 2012) or control the basal mass balance of entire ice shelves (Zhou et al., 2014; Hattermann et al., 2014; Joughin and Padman, 2003). Notably, recent in situ observations from the Ross Ice Shelf suggest that surface waters from a nearby polynya drive melting at shallow depths at an order of magnitude higher rate than the shelf-wide average (Stewart et al., 2019).

Here we present a new estimate of Antarctic-wide ice shelf melting at high resolution derived from a state-of-the-art ocean model. The aims of this study are to quantify the mass loss contribution from different depth ranges and provide Antarctic-wide context for the role of surface water driven melting. In the following, shallow refers to depths from 0 m to 200 m, intermediate to 200 m to 400 m, and deep to below 400 m.

3.2 Methods

3.2.1 Model Description

The fundamental design and parameter choices of the Whole Antarctic Ocean Model (WAOM) have been developed over a decade by our research group in Tasmania and evaluated in many regional studies (Galton-Fenzi et al., 2012; Cougnon et al., 2013; Gwyther et al., 2014). The code consists of the Regional Ocean Modeling System (ROMS) version 3.6 (Shchepetkin and McWilliams, 2005) augmented by an ice shelf component (Galton-Fenzi et al., 2012). We use a three equation melt parameterisation (Hellmer and Olbers, 1989; Holland and Jenkins, 1999) that includes velocity dependent exchange coefficients (McPhee, 1987) and a modification that accounts for molecular diffusion alone (Gwyther et al., 2016).

The rectangular domain covers all Antarctic ice shelf cavities and adjacent continental shelf seas (Fig. 3.2) and is discretized with uniform 2 km horizontal grid spacing and 31 terrain following vertical levels. The three dimensional grid including the land mask comprises 260 million cells. Ice draft and bottom topography south of 60 °S have been derived from the Bedmap2 dataset (Fretwell et al., 2013) and bathymetry values north of 60 °S (outside the Bedmap2 boundaries) have been taken from RTopo-2 (Schaffer et al., 2016). We smooth the ice draft and bathymetry using the Mellor-Ezer-Oey algorithm (Mellor et al., 1994) and artificially deepen the bathymetry under the ice to 20 m minimum water column thickness to ensure numerical stability.

Boundaries for 176 individual ice shelves are taken from the MEaSURES Antarctic Boundaries dataset (Mouginot et al., 2016). We note that while the MEaSURES boundaries are close the 2007 state, Bedmap2 ice shelf thickness is mostly based on laser altimetry data from 1994 to 1995 (Griggs and Bamber, 2011).

The nature of sigma coordinates and necessary smoothing of the ice draft, results in an unrealistic representation of the ice front with a cavity inward sloping topography rather than a vertical cliff face. This is likely to increase water mass exchanges across the ice front. Recent observations, however, suggest that a smooth ice front mimics an underappreciated wedge mechanism: that is, melting along the submarine part of the vertical ice face tends to slope isopycnals under the ice front and provides a pathway for summer surfaces water inflow (Malyarenko et al., 2019). The model results support this idea, as simulated melt rates of the outermost cells compare well against in situ observations from the front of the north-western Ross Ice Shelf (Stewart et al., 2019). The question of whether sigma-coordinates provide a realistic representation of surface water intrusions under the ice in all Antarctic regions, will have to be explored in future studies and as more observations become available.

3.2.2 Experiments

For this study we simulate the year 2007 and force the model with daily buoyancy fluxes derived from heat flux calculations and satellite derived sea ice data (Tamura et al., 2011), and daily wind stress calculated from Era-Interim 10-m winds and bulk flux formula (Dee et al., 2011). We perform surface relaxation to sea surface temperature and salinity to estimates from the Southern Ocean State Estimate reanalysis (Mazloff et al., 2010) using a 365 day time scale. Furthermore, we ensure that positive salt flux (to parameterise sea ice formation) occurs only when sea surface temperatures are at or below the in situ freezing point. We do not account for the effect of sea ice on wind stress or include an explicit model of frazil ice (Galton-Fenzi et al., 2012). Prescribing surface fluxes in (ROMS), rather than including a fully interactive dynamic sea-ice model, has been proven successful in several regional studies around Antarctica (Galton-Fenzi et al., 2012; Cougnon et al., 2013; Gwyther et al., 2014; Hattermann et al., 2014).

We force tides as sea surface height and barotropic currents along the lateral boundaries, accounting for the 13 major constituents derived from the global tidal solution TPXO7.2 (Egbert and Erofeeva, 2002). Tidal height signals along the coast compare well against Antarctic tide gauge records with a combined root mean square error of the four major constituents of 27 cm (King and Padman, 2005). Open boundary conditions are derived from the ECCO2 reanalysis for 2007 (Menemenlis et al., 2008) and consist of monthly values for sea surface height, barotropic and baroclinic velocities, temperature and salinity. Initial temperatures and salinities for the 1st of January 2007 are also derived from ECCO2, whereby values under the ice shelves are extrapolated from the ice front. To save computational costs we perform most of the spin up at lower horizontal resolutions using repeated 2007 forcing. A 10 km version of the model is integrated for 5 years, by which time conditions on the continental shelf have reached a quasi equilibrium. The final state is used to initialise the 4 km run. Analogously the 4 km run is integrated for 2 years before the final 2 km simulation is initiated and integrated for another year and three months. Diffusion and viscosity parameters have been scaled linearly with grid size. The analysis is based on 5 day averages of the final 12 months of the 2 km run.

3.2.3 Satellite Estimates

To confirm the importance of mass loss from shallow to intermediate ice, we compare our results against the depth distribution of previously published satellite estimates of ice shelf melting around Antarctica. At the time of writing only one high resolution product of ice shelf melting around Antarctica is available at the moment (Rignot et al., 2013). A new high resolution estimate, however, is currently under review and confirms a dominant mass loss from shallow to intermediate ice (private communication, Adusumilli, 2018). To derive the total mass loss and depth distribution of the published data, we interpolated the melt rates as well as ice shelf masks on the model grid and used ice draft data from Bedmap2. The MEaSURES ice shelf boundaries have been used to calculate mass loss of individual ice shelves.

3.3 Results, Discussion and Conclusion

3.3.1 Antarctic Ice Shelf Basal Melting From a State-of-the-Art Ocean Model

We simulate circum-Antarctic ice shelf melting during 2007 by upscaling an ocean-ice shelf code, which has been well established in regional studies (see Sect. 3.2; Galton-Fenzi et al., 2012; Cougnon et al., 2013; Gwyther et al., 2014). Major improvements compared to previous large-scale models are the inclusion of tides and an eddy resolving resolution.

Tidal currents have been shown to modulate ice shelf basal melting by enhancing the turbulence at the ice shelf base, as well as by increasing vertical mixing and interacting with mean circulation upstream (Padman et al., 2018). A high horizontal resolution is necessary to resolve critical shoreward heat transport by bathymetric troughs and eddies (Stewart et al., 2018; Nakayama et al., 2014b) as well as the ocean circulation under small ice shelves around the continent (Hellmer, 2004; Timmermann et al., 2012). With 2 km resolution we resolve more than 1.6 million km^2 of ice (Fig. 3.2) and calculate mass loss quantities for 176 individual ice shelves (results for all ice shelves are accessible online[1]; see Table C.1 for total and sector-wise quantities and Fig. B.2 for ice shelf boundaries).

We calculate a total basal mass loss of 1207 Gt/yr, which is close to, but 4 % below the range of estimates based on remote sensing data and models of surface processes (1263 Gt/yr to 1737 Gt/yr; Rignot et al., 2013; Depoorter et al., 2013; Liu et al., 2015). Regionally, the model and data show larger differences for some ice shelves (Pine Island, Getz, combined Brunt and Riiser-Larsen, Shackleton, combined Totten and Moscow University), but are in agreement or close to others (George VI, Abbot, combined Fimbulisen and Jelbart, Filchner-Ronne, Larsen C, Ross, Amery; Fig. 3.1; Table A.1). In most regions of disagreement (Pine Island, Getz, Shackleton, combined Totten and Moscow University), satellite estimates and estimates from regional studies suggest higher melting (Gwyther et al., 2014; Dutrieux et al., 2013; Shean et al., 2018; Jacobs et al., 2013), indicating a systematic bias for warm water ice shelves in our model. We note that these model deficiencies do not impact the conclusions of this study, as artificially increasing melt rates in high-melt areas, the Amundsen-Bellingshausen Seas, by a factor of two only changes the mass loss fraction of ice shallower than 400 m by 0.01 %.

Other biases have been reported for WAOM (see Chapter 2 Section 2.5). The model features a warm bias of the surface ocean in summer and a spuriously deep summer mix layer in the Ross Sea. The spuriously warm surface waters, however, cool down to a realistic level on the continental shelf in most regions (compare Fig. H.6 against Pellichero et al., 2017 their Fig. 3). Also, the bias in mixed layer depth is confined to the Eastern Ross Sea and translates onto the continental shelf only in front of Land, Nickerson and Sulzberger Ice Shelves (see Fig. H.5). We do acknowledge, however, that a spuriously deep mixed layer at the shelf break can affect the water masses that are transported onto the shelf. Hence, melting under the eastern part of Ross Ice Shelf might also be impacted. Overall, we rate these biases as not substantial enough to challenge

[1] https://data.utas.edu.au/metadata/5d9ee4e6-99e8-46f0-b6c2-cc869a5e3d06

the main conclusions of this study.

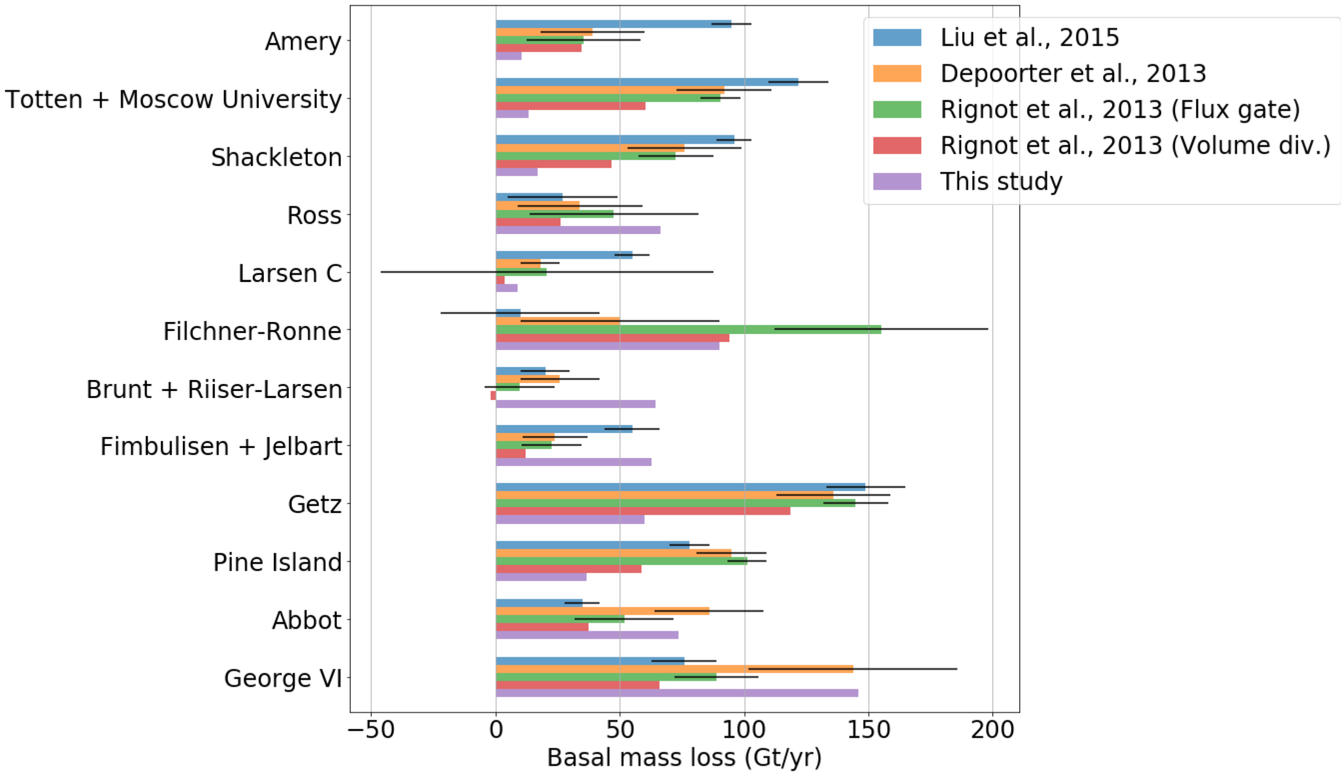

Figure 3.1: Basal mass loss estimates for 12 of the larger ice shelves around Antarctica from this study and satellite derived estimates (Rignot et al., 2013; Depoorter et al., 2013; Liu et al., 2015). Volume div. denotes estimates derived from integrating high resolution results (see Sect. 3.2.3; see Table A.1 for data).

Our model is capable of resolving smaller-scale melt features known from observations and regional modelling studies (Fig. 3.2). For example, in the Amundsen-Bellingshausen Seas, where deep warm water intrusion cause strong melting of most ice shelves, the Wilkes Ice Shelf, which features an unusually shallow ice draft, melts at a considerably lower rate (80 % lower than its neighbour George VI Ice Shelf, Padman et al., 2012). Further examples can be found in the Weddell Sea under the Filchner-Ronne and Larsen C Ice Shelf, where strong melting in the deep grounding line regions of inflowing ice streams is followed by refreezing along western outflows (Joughin and Padman, 2003; Holland et al., 2007, 2009), and in East Antarctica under the Fimbul Ice Shelf, where the model predicts isolated high melt rates along the deep keel of the Jutulstraumen Glacier (Hattermann et al., 2014). Finally, under the Ross Ice Shelf strong melting is resolved at the ice front just east of Ross Island with melt rates of up to 10 m/yr (Arzeno et al., 2014; Stewart et al., 2019). Resolving these smaller scale processes is important as their Antarctic-wide impact might be large.

3.3.2 The Contribution From Different Depths

Our simulation suggests that 79 % (954 Gt/yr) of Antarctic ice shelf basal mass loss comes from ice that is shallower than 400 m (Fig 3.2, Fig 3.3). Even though the model predicts the highest melt rates at the greatest depths (on average 5.2 m/yr from 2200 m to 2300 m), such deep ice only exists in a few regions (such as near the grounding lines of the Filchner-Ronne, Ross, and Amery Ice Shelves; see Fig. H.8) and hence its area-integrated contribution to the total mass loss is relatively small. Between 200 and 400 m depth, melt rates are moderate (0.8 m/yr), but since almost half of the ice shelf drafts occur between these depths (48 %; see Fig. H.9), mass loss integrates to its largest contribution (46 %). Towards the ice front (200 m and shallower) melting increases (up to 1.9 m/yr for the shallowest 100 m) and a relatively small area (17 %) integrates to a large mass loss contribution (33 %). Melting from ice shallower than 400 m is the dominant source of ice shelf basal mass loss in all individual Antarctic regions with ice shallower than 200 m alone making up substantial amounts (Table C.1).

The depth distribution of Antarctic ice shelf melting derived from satellite methods (Rignot et al., 2013) confirms the importance of shallow to intermediate ice (see Sect. 3.2.3, Fig. C.1). 48 % (428 Gt/yr) of the total mass loss (897 Gt/yr) comes from ice that is shallower than 400 m, despite up to ten times higher melting at greater depths (up to 11.3 m/yr for the 2000 m to 2100 m depth bin). Most of the difference in shallow mass loss fraction between the model and the data originates from depths shallower than 200 m (only 10 %, 93 Gt/yr, of the total mass loss). Sampling dynamic ice shelf fronts is difficult using low spatial and temporal resolution satellite data, meaning they may not fully represent change in these regions. For instance, calving events during the sampling periods require boundaries several km away from the actual termini of the ice shelves, leaving ice shelf melting close to the front unresolved (Liu et al., 2015). Recent in situ observations, however, highlight enhanced melting below this part of the world's largest ice shelf, the Ross Ice Shelf, with melt rates up to an order of magnitude higher than the shelf average (Stewart et al., 2019).

Small, fringing, parts of the ice shelf produce a large fraction of the ice shelf melt. In the model, much of this shallow ice (0 m to 200 m) is confined along the ice front

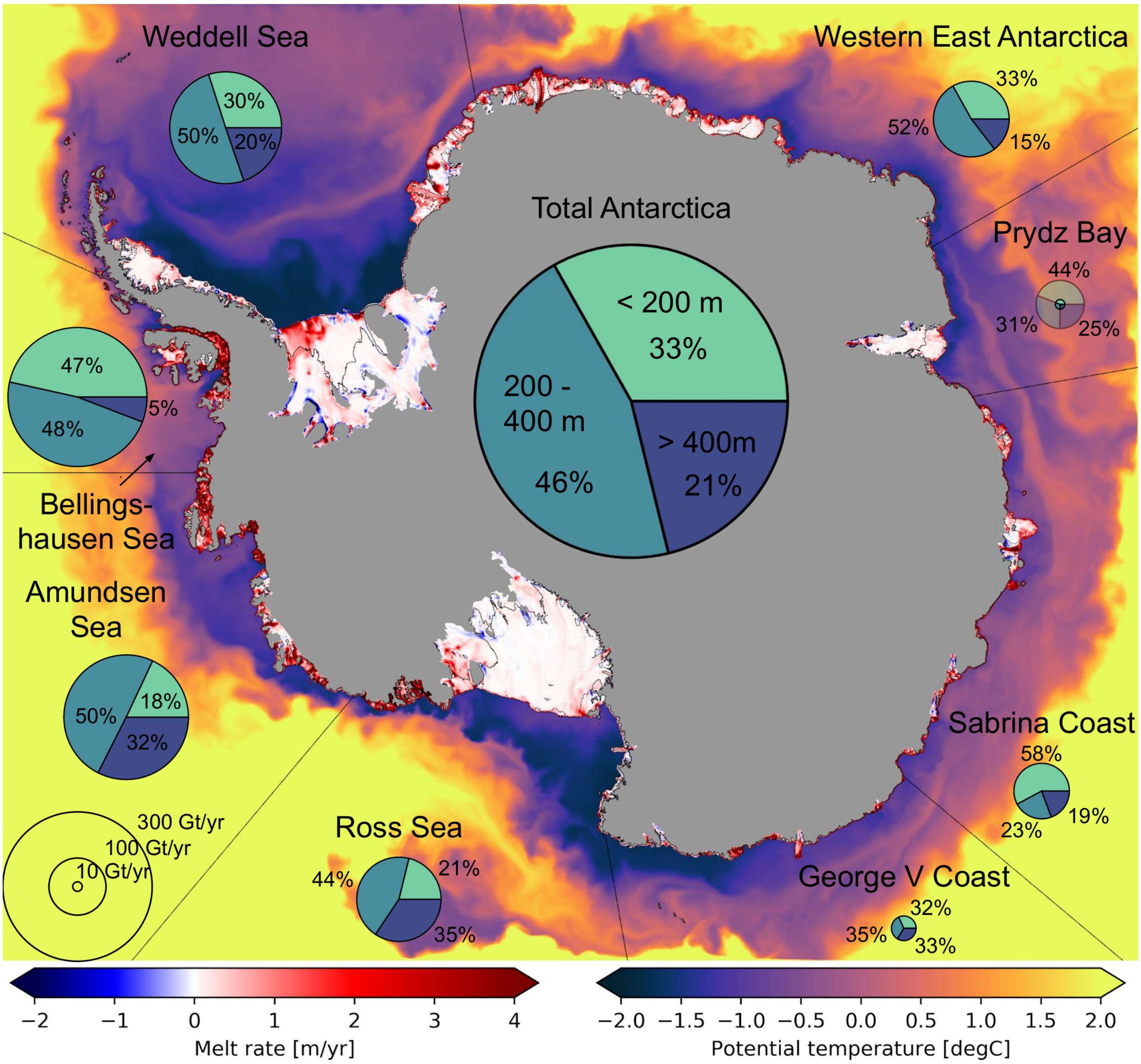

Figure 3.2: Ice shelf basal melting and surface ocean temperature around Antarctica. Seaward of ice shelves, 2007 average potential temperature of the surface ocean (uppermost sigma layer). Within ice shelves, 2007 average basal melt rate. Solid and dashed lines indicate 400 m and 200 m ice draft, respectively. Pie chart areas are proportional to the mass loss from each sector, in Gt/yr. Pie chart partitions indicate mass loss integrated over depth ranges (shallower than 200 m, between 200 m and 400 m, deeper than 400 m). Total Antarctica and Prydz Bay pie charts have been scaled for ease of readability. Basal melting shallower than 200 m contributes substantial amounts to the mass loss in all regions and the surface ocean often features temperatures above freezing close to the ice. See Appendix H Figure H.7 for regional details.

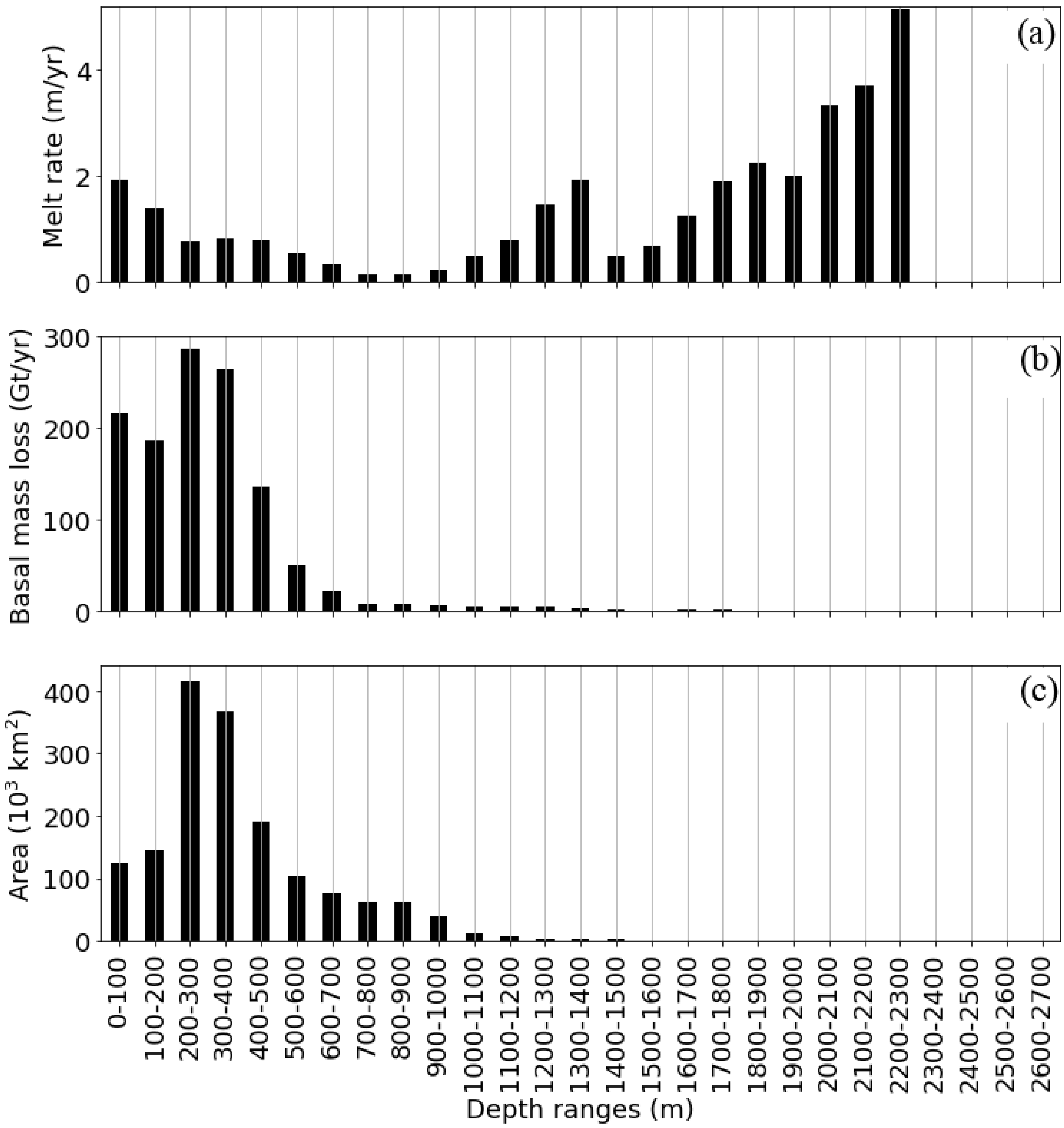

Figure 3.3: Ice shelf basal melt rates, mass loss and area at different depths. (a) 2007 ice shelf melting averaged over 100 m depth ranges. (b) Integrated mass loss. (c) Integrated area of ice shelf draft. Moderate melt rates at shallow to intermediate depths integrate to highest mass loss contributions, due to large available area.

and in small ice shelves all around the continent (Fig. 3.2, Fig. B.2). The outermost 6 km of all ice shelves coincide with 41 % of the ice shelf draft that is shallower than 200 m and, hence, is not well captured by satellite methods but has a large mass loss contribution (379 Gt/yr, 31 %, Tab. I.1). Similarly, categorizing the ice shelves by areal extent reveals that ice shelves that are smaller than $5000\,\mathrm{km}^2$ contain 39 % of all the ice shallower than 200 m and integrate to a total mass loss contribution of 378 Gt/yr (31 %). By showing that excessive amounts of ice are lost from the ice front and small ice shelves, our results suggest that reduced accuracy of basal melting in these regions, due to sampling limitations or coarse model resolution, implies substantial uncertainty in the overall mass budget of Antarctica's ice shelves. For example, the unresolved areas of high resolution satellite data account for 336 Gt/yr of mass loss in the model, which would bring the total mass loss close to estimates derived from flux gate analysis.

3.3.3 The Surface Ocean as Driver of Change

The model results suggest that advection of solar heated surface waters is an important driver of shallow ice melting. The surface ocean adjacent to the ice is often significantly warmer than the freezing point (Fig. 3.2). Solar radiation heats the surface of the Southern Ocean to more than 10 °C above freezing in summer, but on the Antarctic continental shelf, Antarctic Surface Water (AASW) is cooled by a thick sea ice cover in winter and glacial melt water all through the year. Warm streams from offshore are brought towards and around the coast by barotropic large-scale circulation, such as the Weddell Gyre or the Antarctic coastal current. Eddies can mix warm water shoreward or upwell heat from greater depth, as apparent in the Bellingshausen Seas, while sea ice polynyas open a pathway for solar heating close to coast even in winter, e.g. near the Ross Ice Shelf front (Stewart et al., 2019). In our simulation, all these effects combined result in an upper continental shelf ocean (first 100 m) with a mean temperature of $-1.1\,°\mathrm{C}$ ($0.75\,°\mathrm{C}$ above the surface freezing point).

In some cold water regions, warm deep waters upwell to depths shallower than 400 m, often mixing with warm surface waters in summer. In many regions the annual mean sub-surface temperature maximum is located below 400 m depth, excluding CDW and WDW as sources for shallow ice melting (Amundsen-Bellingshausen Seas, Western Weddell Sea, most of narrow continental shelf regions in East Antarctica; see Fig. H.1, H.2 and H.3). In some cold water regions, however, the sub-surface temperature maximum is shallower than 400 m (or even 200 m) indicating the potential of warm deep waters to contribute to melting at intermediate to shallow depths (e.g. in the Ross Sea, in Prydz Bay, Eastern Weddell Sea and George V Land Coast). In most of these regions, the sub-surface temperature maximum close to the ice front, however, shoals up into the upper ocean in summer, indicating AASW downwelling and a mixed regime. Downwelling of the surface water layer to depths below 200 m has been observed at some places (Stern et al., 2013; Zhou et al., 2014; Stewart et al., 2019) and is also apparent in the model, e.g. at the Ross ice shelf front (see Fig. H.4).

That warm AASW is indeed advecting under the ice front and reaches the shallow parts of many ice shelves is indicated by the temperature-salinity distribution of water inside the ice shelf cavities (Fig. 3.4). AASW typically has temperatures above freezing point and potential densities below 27.6 $\mathrm{kg\,m^{-3}}$. Similar characteristics, however, can arise when warmer and denser Modified Circumpolar Deep Water (MCDW) mix with fresh and cold melt water. The mixing process is visible in the temperature-salinity space as lines with characteristic slope (Gade lines; Gade, 1979) and, thus, the absence of these lines indicates surface water origin for an ambiguous sample point. Following this argument, we identify AASW up to 200 m deep in western East Antarctica, Prydz Bay, the Weddell Sea, and the Sabrina and George V Coasts. From 200 m to 400 m depth the above mentioned mixed regime is apparent (AASW and warmer deep waters, such as CDW or WDW). This regime likely contains substantial amounts of heat sourced from solar radiation at the surface, but we can not clearly trace the water mass origins using standard water mass characteristics analysis.

The extent to which surface water advection controls melt rates of shallow ice becomes evident by comparing the seasonal cycle in melt rates from different depths (Fig. 3.5). During southern hemisphere winter and spring (June to December) melt rates at all depths are relatively constant. In summer, however, melting of ice shallower than 200 m increases on average by 2.5 m/yr (200 %), with regional differences ranging from 1.5 m/yr (75 %) in the Bellingshausen Sea up to 7 m/yr (over 1000 %) in Prydz Bay, Sabrina Coast and George V Coast, while melt rates of deeper ice do not increase much above winter values. This distinct seasonal cycle is closely correlated to the surface ocean temperature of the adjacent continental shelf, suggesting that a fast heat transfer mechanism, such as advection, is at play. Figure H.4 shows monthly mean transects of potential temperature and salinity across the Ross Ice Shelf front, demonstrating AASW downwelling in summer and consequent advection under the ice in our model. In western East Antarctica, the Amundsen Sea, and along the Sabrina and George V Coasts, deep ocean temperatures and melt rates show signs of this seasonal variation, indicating the

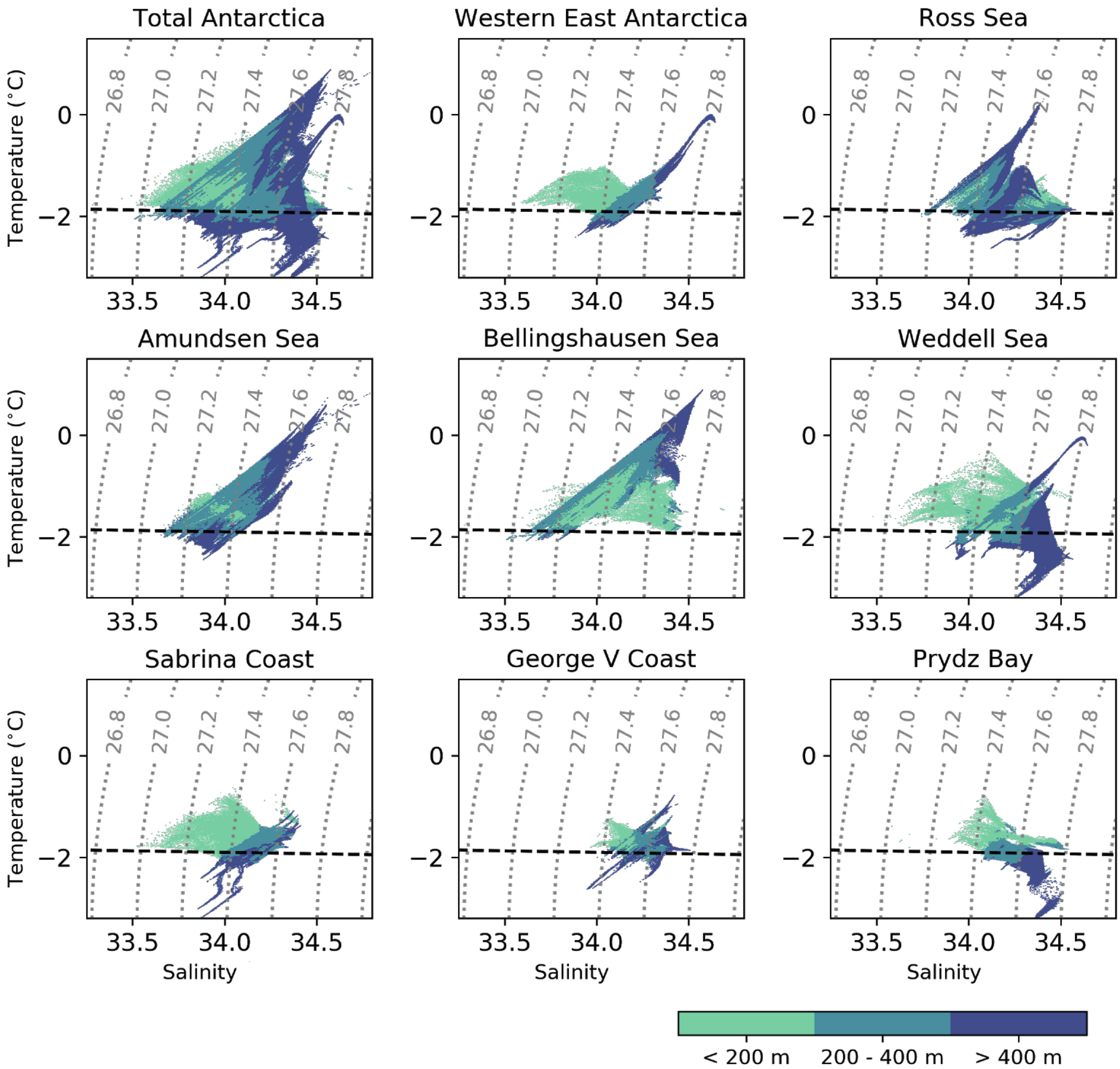

Figure 3.4: Water masses present below the ice shelves. Potential Temperature-Salinity distribution of the ocean inside the ice shelf cavities for total Antarctica and each individual sector. Each grid box is sorted into 1000x1000 temperature and salinity bins and coloured based on depth. The surface freezing point is indicated by a dashed black line, and potential density contours ($\mathrm{kg\,m^{-3}}$) by dashed gray lines.

influence of surface processes even below 200 m depth.

In situ observations confirm the importance of surface water driven melting at some locations around Antarctica. The idea of melt driven by warm surface water intrusions under the ice shelf frontal zone, also known as “Mode 3” melting, has been known for quite some time (Jacobs et al., 1992) and confirmed by in situ observations (Stern et al., 2013; Arzeno et al., 2014; Hattermann et al., 2012; Stewart et al., 2019; Malyarenko et al., 2019) and high resolution satellite data (Horgan et al., 2011). Our results suggest that surface water-driven melting is a wide-spread feature around Antarctica, causing a substantial contribution to the total mass loss.

Surface water driven melting is likely affected by small scale coastal processes, subject to respond to perturbations on rapid timescales and offering different feedback mechanisms than processes at depth. Global atmospheric warming is likely to directly increase upper ocean temperatures (Durack et al., 2018), but seasonal sea ice cover controls the exposure to solar radiation and can change dramatically over yearly timescales (Parkinson, 2019). Further, easterly winds close to Antarctica are predicted to gain strength (Kushner et al., 2001) and the associated shoreward Ekman transport might cause enhanced AASW downwelling at the ice front (Zhou et al., 2014; Sverdrup, 1954). How changes in seasonal ice cover will impact the mean wind stress imported into the ocean is not well understood (Lüpkes and Birnbaum, 2005). Finally, ice shelf thinning or large break up events do not just expose further inland ice to the surface ocean, but the consequent change in water column thickness also affects local tides (Mueller et al., 2018), which have often been suggested as one of the main drivers of water mass exchange across the ice front (Jacobs et al., 1992; Makinson and Nicholls, 1999; MacAyeal, 1985). Seasonal sea ice, coastal winds and ice shelf geometry can change on short time-scales and its effects on surface water driven melting provide the means for a very dynamic response of shallow ice mass loss to climate change.

Recent research of Antarctic mass loss has focused on warm water intrusions in the deep ocean and melting along ice shelf grounding lines, but the modelling results and analysis presented here suggest that shallower processes also play a fundamental role. Not resolving these processes in models used to predict future climate might have far reaching consequences. The amount and depth at which glacial melt water is injected into the ocean impacts local water mass transformation with consequences for global ocean circulation and climate (Bronselaer et al., 2018; Golledge et al., 2019). The role of shallow ice melting for ice sheet dynamics are less clear. Integrating the instantaneous buttressing flux response for all ice shelf parts shallower than 400 m results in 34 % of the

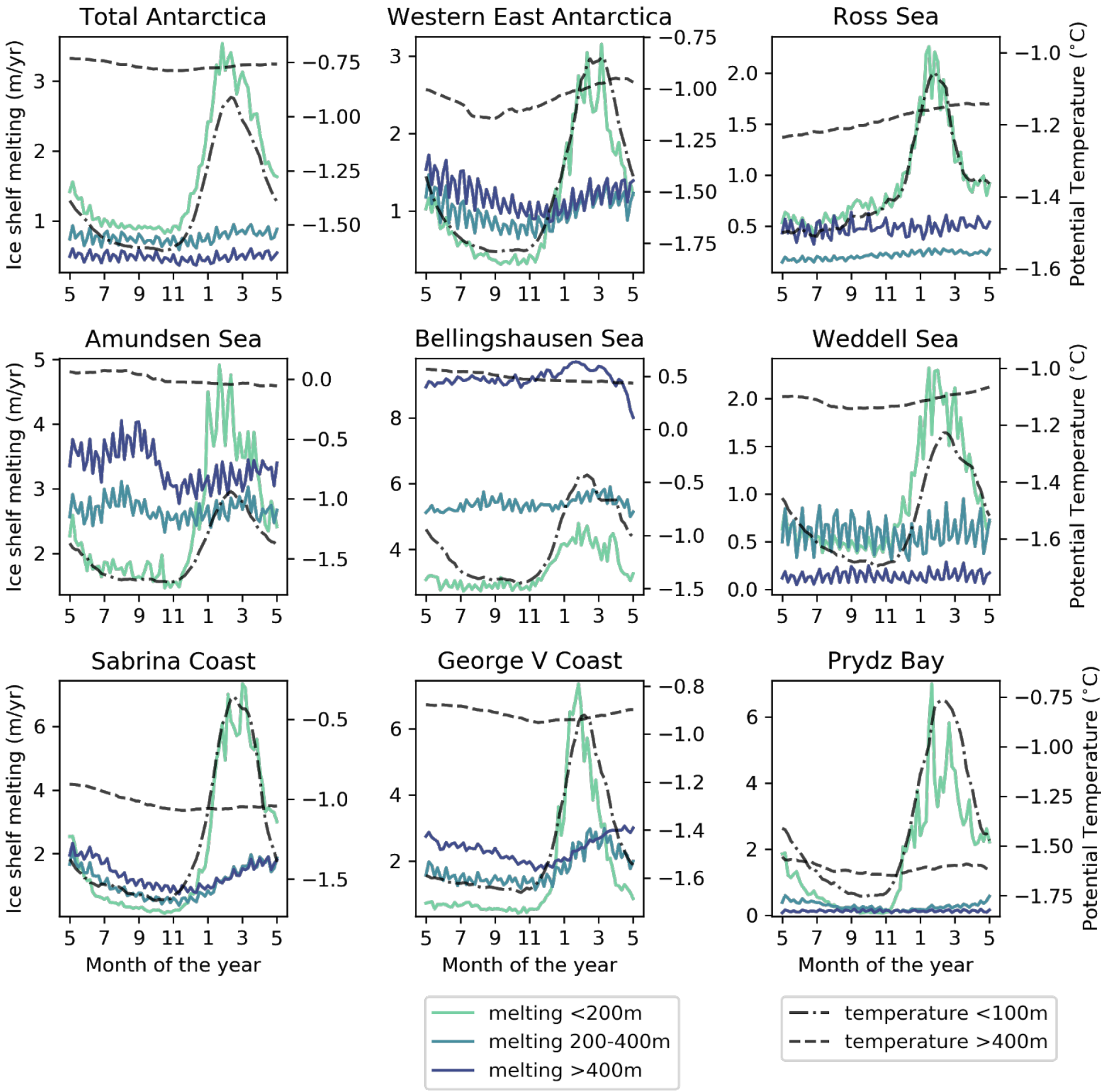

Figure 3.5: Relationship between ice shelf melting at different depths and adjacent surface and deep ocean temperature. Potential temperature is volume averaged over the continental shelf, above 100 m as well as below 400 m. The continental shelf is defined using the 1000 m isobath and excluding ice shelf cavities. Ice shelf melting is area averaged for ice shallower than 200 m, between 200 m and 400 m, and deeper than 400 m. Both are 5 day means and shown for total Antarctica and each individual sector.

response of deeper ice (Reese et al., 2018). Over decadal time scales, however, melting at shallow depths might precondition calving (Padman et al., 2012) and, at many places close to lateral boundaries or pinning points, ice shelves will undergo structural changes with even little ice front retreat (Fürst et al., 2016). To quantify these longer term effects, fully coupled ocean-ice sheet models will ultimately be needed.

Chapter 4

Tidal Modulation of Antarctic Ice Shelf Melting

Preamble

By means of the model developed in Chapter 2, the preceding chapter (Chapter 3) has shown that surface water intrusions play a substantial role for ice shelf melting around Antarctica. This chapter (Chapter 4) further harnesses the potential of the model to quantify the impact of tides and, thus, address the third objective established in Section 1.6. The experiences gained during model evaluation (Chapter 2) and result interpretation (Chapter 3) helped to guide the experimental design and discussion of this chapter.

Abstract

Tides influence basal melting of individual Antarctic ice shelves, but their net impact on Antarctic-wide ice-ocean interaction has yet to be constrained. Here we quantify the impact of tides on ice shelf melting and the continental shelf seas by means of a 4 km resolution circum-Antarctic ocean model. Activating tides in the model increases the total basal mass loss by 57 Gt/yr (4 %), while decreasing continental shelf temperatures by 0.04 °C, indicating a slightly more efficient conversion of ocean heat into ice shelf melting. Regional variations can be larger, with melt rate modulations exceeding 500 % and temperatures changing by more than 0.5 °C, highlighting the importance of capturing tides for robust modelling of glacier systems and coastal oceans. Tide-induced changes around the Antarctic Peninsula have a dipolar distribution with decreased ocean temperatures and reduced melting towards the Bellingshausen Sea and warming along the continental shelf break on the Weddell Sea side. This warming extends under the Ronne Ice Shelf, which also features one of the highest increases in area-averaged basal melting (128 %) when tides are included. Further, by means of a singular spectrum analysis, we explore the processes that cause variations in melting and its drivers in the boundary layer over periods of up to one month. At most places friction velocity varies at tidal timescales (one day or faster), while thermal driving changes at slower rates (longer than one day). In some key regions under the large cold-water ice shelves, however, thermal driving varies faster than friction velocity and this can not be explained by tidal modulations in boundary layer exchange rates alone. Our results suggest that large scale ocean models aiming to predict accurate ice shelf melt rates will need to explicitly resolve tides.

4.1 Introduction

Changes in the ocean have been identified to drive melting at the base of Antarctic ice shelves with consequences for sea-level rise and global climate (e.g. Pritchard et al., 2012; Liu et al., 2015; Bronselaer et al., 2018). The oceanic mechanisms that govern the heat transport across the continental shelf and within sub-ice shelf cavities, however, remain poorly understood and quantified, causing large uncertainties in the prediction of future changes (e.g. Asay-Davis et al., 2017; Turner et al., 2017).

One relevant mechanism is ocean tides, as they interact with ice shelves in many ways including ice shelf basal melting (Padman et al., 2018). At the ice base, tidal currents enhance the turbulent exchange of heat and salt through the ice-ocean boundary layer and, hence, modulate local melt rates as well as melt water driven buoyant plumes that affect ice-ocean interaction downstream (MacAyeal, 1984; Makinson and Nicholls, 1999). Away from the ice shelf base, friction at the sea bed and underneath static sea ice contributes to ocean mixing (e.g. Padman et al., 2009; Llanillo et al., 2019), as does breaking of internal waves excited by tidal oscillating flow over steep sloping topography (e.g. Padman et al., 2006; Foldvik et al., 1990). Further, tidal currents can be rectified into a mean flow component (Loder, 1980) with velocity magnitudes comparable to the ambient circulation (Padman et al., 2009; MacAyeal, 1985). By means of these mechanisms, tides are thought to play a fundamental role in the heat transport across the continental shelf break (Padman et al., 2009; Stewart et al., 2018), vertical mixing and advection at the ice front (Gammelsrod and Slotsvik, 1981; Foldvik et al., 1985; Makinson and Nicholls, 1999) and upwelling of warm deep water inside sub-ice shelf cavities (MacAyeal, 1984). The roles of these processes for ice shelf-ocean interaction in an Antarctic-wide context, however, are not well understood, restraining reliable parameterisations in large scale climate simulations (Asay-Davis et al., 2017; Jourdain et al., 2019).

Regional ocean-ice shelf models that explicitly resolve tides have now been successfully applied to all large ice shelves around Antarctica (e.g. Makinson et al., 2011; Mueller et al., 2012, 2018; Galton-Fenzi et al., 2012; Robertson, 2013; Arzeno et al., 2014; Mack et al., 2017; Jourdain et al., 2019). The combined domains, however, do not cover all of the Antarctic coastline, neglecting the potentially important contribution of small ice shelves (discussed in, e.g. Timmermann et al., 2012) and ice shelf teleconnections (Gwyther et al., 2014; Silvano et al., 2018). Also, inconsistent design and parameter choices make it difficult to identify the governing processes on a continent-wide scale.

In contrast, Ocean General Circulation Models (OGCMs) that have global coverage and include tidal currents have not been augmented by an ice shelf component (Savage et al., 2017; Stewart et al., 2018). To our best knowledge, no Antarctic-wide ocean model that resolves ice shelf interactions and tides simultaneously has so-far been developed (Asay-Davis et al., 2017).

Here, using an Antarctic-wide ocean-ice shelf model that explicitly resolves tides, we quantify the impact of tidal currents on ice shelf basal melting and the continental shelf ocean. Further, we analyse the temporal variability of the melt drivers at the ice base over periods of up to one month to explore the mechanisms that govern tidal melting.

The following section (Sect. 2) describes the model, experiments and analysis techniques used in this study. Section 3 presents the results. First, we show tide-induced annual mean changes in ice shelf melting and the continental shelf ocean. Second, we present spectral characteristics of the melt drivers at the ice base in the presence of tides. The frequency spectrum ranges from hourly to fortnightly. The result section is followed by a discussion of the implications for larger scale modelling efforts including ice sheets and global oceans (Sect. 4). The last section (Sect. 5) summarises and concludes this study.

4.2 Methods

4.2.1 Model Description

We derive estimates of ice shelf-ocean interaction using the Whole Antarctic Ocean Model (WAOM) at 4 km horizontal resolution. The model is based on the Regional Ocean Modeling System (ROMS) version 3.6 (Shchepetkin and McWilliams, 2005), which uses terrain-following vertical coordinates, and has been augmented by an ice shelf component (Galton-Fenzi et al., 2012). Thermodynamic ice-ocean interaction is described using the three equation melt parameterisation (Hellmer and Olbers, 1989; Holland and Jenkins, 1999) including velocity dependent exchange coefficients (McPhee, 1987) and a modification that accounts for molecular diffusion alone (Gwyther et al., 2016).

The domain covers the entire Antarctic continental shelf including all ice shelf cavities (as shown in Fig. 4.1). The bathymetry and ice draft topography has been taken from the Bedmap2 dataset (Fretwell et al., 2013), while boundaries for 139 individual ice shelves are based on the MEaSURES Antarctic boundaries dataset (Mouginot et al., 2016). A well known caveat of terrain following coordinates are pressure gradient errors in regions of steep sloping topography, ultimately driving spurious circulation patterns (Mellor et al., 1994, 1998). To minimise pressure gradient errors in WAOM, we smooth the ice draft and bottom topography using the Mellor-Ezer-Oey algorithm until a maximum Haney factor of 0.3 is reached. Further, we artificially deepen the seafloor to a minimum water column thickness of 20 m to ensure numerical stability (see Schnaase and Timmermann, 2019, for implications). The ocean is discretised using a uniform horizontal grid spacing of 4 km and 31 vertical levels with enhanced resolution towards the surface and seafloor. Running the model for one year with 2304 CPUs on 2x8 core Intel Xeon E5-2670 (Sandy Bridge) Nodes costs about 7000 CPU-hours.

4.2.2 Simulations

For this study we perform two model simulations with ocean-atmosphere-sea ice conditions from the year 2007, one with tidal forcing and one without tides. In the tidal run, we force the 13 major constituents (M2, S2, N2, K2, K1, O1, P1, Q1, MF, MM, M4, MS4, MN4) derived from the global tidal solution TPXO7.2 (Egbert and Erofeeva, 2002) as sea surface height and barotropic currents along the northern boundary of the domain (north of 60°S). In this way we achieve an accuracy in the tidal height signal around the coast of Antarctica that is comparable to available barotropic tide models (assessed in King and Padman, 2005). Our combined root-mean-square error in tidal height complex amplitude assessed against Antarctic Tide Gauge records is 27 cm (see Chapter 2 for tide evaluation).

Open boundary conditions and surface fluxes are identical in both simulations. The ocean outside the model domain is described using the ECCO2 reanalysis (Menemenlis et al., 2008) and includes sea surface height, barotropic and baroclinic velocities, temperature and salinity. At the surface, we prescribe daily heat and salt fluxes, which have been derived using satellite sea ice data and heat flux calculations (Tamura et al., 2011), and daily wind stress is calculated from ERA-Interim 10-m winds and bulk flux formula (Dee et al., 2011). To constrain model drift, sea surface temperature and salinity are relaxed, on an annual timescale, to estimates from the Southern Ocean State Estimate reanalysis (Mazloff et al., 2010). Furthermore, we ensure that positive salt flux from sea ice formation occurs only when sea surface temperatures are at or below freezing. We do not account for the effect of sea ice on wind stress or include an explicit model of frazil ice (as in, e.g. Galton-Fenzi et al., 2012).

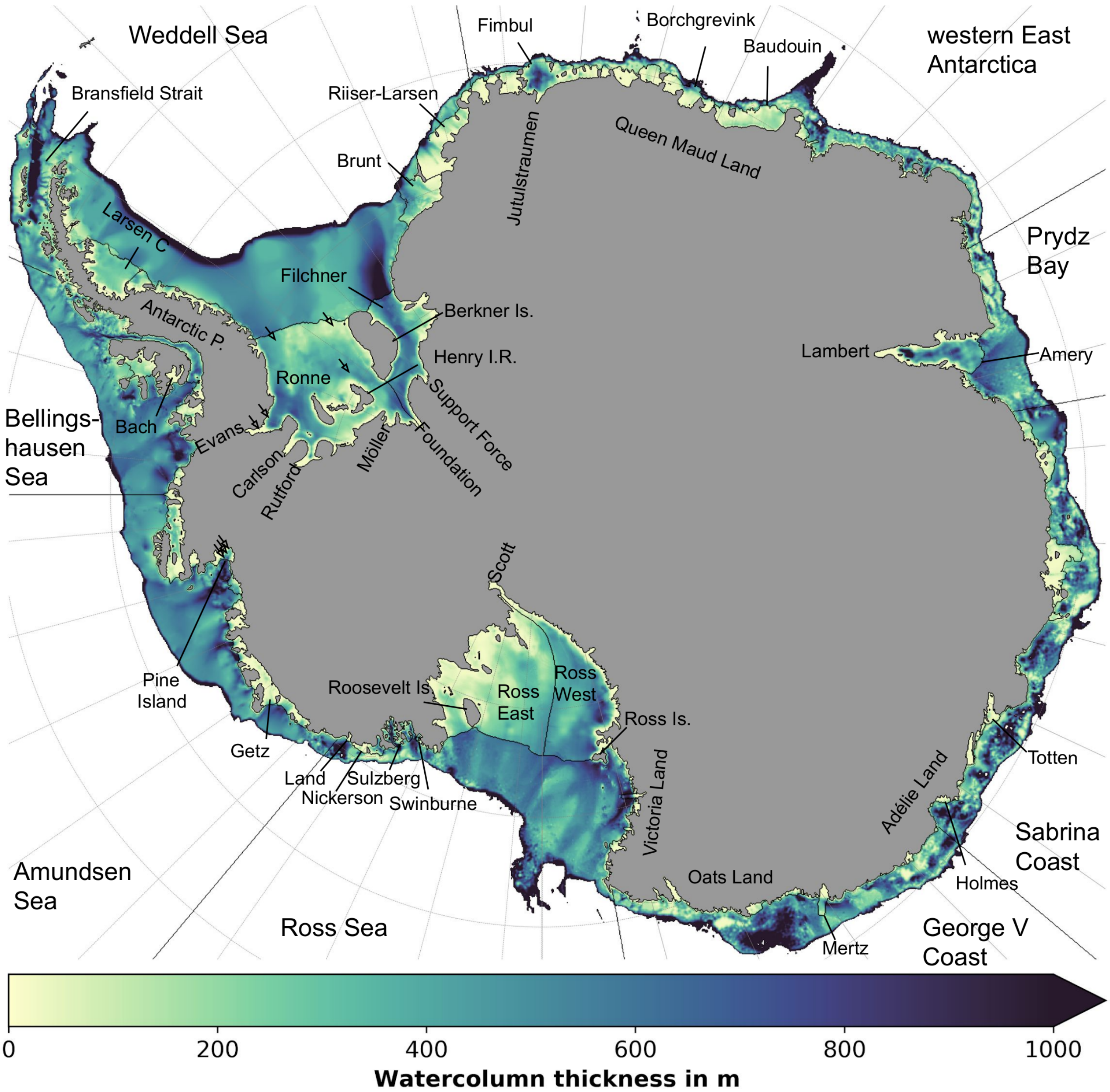

Figure 4.1: Study area and water column thickness on the continental shelf. Colours show the seafloor depth on the open continental shelf and water column thickness where ice shelves are present. The labels indicate locations referred to in the text with ice sheet regions and tributary glaciers on land, and ice shelves and ocean sectors on water. Arrows under Ronne and Pine Island Ice Shelf indicate the locations of the time series shown in Fig. 4.8. Abbreviations are Island (Is.), Ice Rise (I.R.) and Peninsula (P.).

Initial temperatures and salinities are also derived from ECCO2, whereby we extrapolate values under the ice shelves from ice front conditions. The tidal and non-tidal case have been run separately for 5 years using a 10 km version of the model followed by 2 years at 4 km resolution. By performing parts of the spin up at lower resolution, we save computational costs, while still ensuring a quasi-equilibrium of the continental shelf ocean. Annual average results have been derived from the final year of the 4 km simulations, while mean tidal current speed and time series analysis is based on additional subsequent integration for 30 days (January) of the tidal case.

4.2.3 Analysis

The spatial characteristics of the mean tidal current speed are calculated as:

$$|u|_{tide} = \left\langle \sqrt{u_b^2 + v_b^2} \right\rangle_t \qquad [\mathrm{m\ s^{-1}}] \ , \tag{4.1}$$

whereby u_b and v_b are the orthogonal components of hourly averaged barotropic currents of the 30 day simulation with tides and $\langle\rangle_t$ denote temporal averaging. With 30 days we cover 2 full spring-neap cycles of the major semidiurnal and diurnal tidal constituents M2, S2, K1 and O1. Tidal currents typically reach a maximum speed of two times $|u|_{tide}$.

By means of Singular Spectrum Analysis (SSA; Elsner and Tsonis, 1996), we decompose variations in the melt drivers at the ice base to infer the role of tidal currents. SSA is a powerful time series analysis technique, that has been used before to derive insights into global climate models (Monselesan et al., 2015) and ice shelf-ocean interaction (Gwyther et al., 2018). The method is based on singular value decomposition of the time lagged covariance matrix and can be used to calculate the variance contribution from individual frequency ranges. In this study we use SSA to determine the in-band contribution of processes faster than 24 hours to the total variance of 30 day signals; we attribute this contribution to tidal currents alone, as they are the primary source of sub-daily variability in the model.

We apply this technique to thermal driving (T^*) and friction velocity (u^*). Thermal driving is defined as the difference in temperature across the ice-ocean boundary layer (see Holland and Jenkins, 1999):

$$T^* = T_M - T_B \ [^\circ\mathrm{C}]. \tag{4.2}$$

T_M denotes the temperature of the mixed layer under the ice base. T_B describes the temperature at the ice-ocean interface and is assumed to be the freezing point temperature, T_f. T_B is calculated as

$$T_B = T_f = 0.0939 - 0.057 S_B + 7.6410 \times 10^{-4} z_{ice} \text{ [°C]}, \tag{4.3}$$

where S_B denotes the salinity at the ice-ocean interface and z_{ice} the ice shelf draft. The friction velocity (u^*) controls the exchange rates of heat and salt through the boundary layer and is calculated using the surface quadratic stress of the upper most sigma layer:

$$u^* = \sqrt{C_d}|u| \text{ [m/s]}. \tag{4.4}$$

$C_d = 5 \times 10^{-3}$ is a quadratic drag coefficient and $|u|$ is the magnitude of the upper most sigma layer current. Change in the covariation of T^* and u^* is a good approximation for melt rate variations when using the three equation melt parameterisation (e.g. Jourdain et al., 2019):

$$w_b \propto u^* T^* \qquad [\text{m yr}^{-1}] \;. \tag{4.5}$$

Applying the SSA to T^* and u^*, rather than melt rates directly, offers a first step towards separating the processes that drive melting (e.g. Mueller et al., 2018).

4.3 Results

4.3.1 Mean Changes in Ice Shelf Melting and Coastal Oceans

The area-integrated impact of tides on modelled annual-average melting and continental shelf ocean temperatures is small as shown in Table 4.1. The total basal mass loss increases by 4 % when including tides in the model, while ocean temperatures slightly drop, indicating more melt water and an overall increase in the efficiency at which heat is converted to melting.

Despite weak overall effects, the impact of tides on ice shelf melting in individual regions can be large (cancelling each other out for the whole Antarctic). These regional differences are important for many research questions, for example, localised sensitivity

	Without tides	**With tides**	**Difference**
Average melt rate	0.90 m/yr	0.93 m/yr	0.04 m/yr
Basal mass loss	1388 Gt/yr	1445 Gt/yr	57 Gt/yr
Continental shelf potential temperature	-1.38 °C	-1.42 °C	-0.04 °C

Table 4.1: Tide induced absolute difference in area averaged melt rate, basal mass loss and continental shelf ocean temperatures for all Antarctic ice shelves (averaging Fig. 4.2c and Fig. 4.4b). Continental shelf temperatures have been calculated using a depth at the shelf break of 1000 m and including the sub-ice shelf cavities.

to reduced ice shelf buttressing. Figure 4.2 presents the spatial distribution of ice shelf melting around Antarctica as well as the sensitivity of these melt rates to tides. Tides modulate melting all around the continent (Fig. 4.2c), but mostly impact ice-ocean interaction underneath the large cold cavity ice shelves (Filchner-Ronne, Ross, Amery and Larsen C; Fig. 4.2b), where ambient melt rates are small (Fig. 4.2a). Modulations in melt rate (at model horizontal resolution of 4 km) have a standard deviation (std) of 352 % and can be larger than 100 times of the original melt rate (calculated as $(w_{b\ \text{tides}} - w_{b\ \text{no-tides}})/w_{b\ \text{no-tides}})$ and shown in Figure 4.2c). Areas of increased melting are often in close vicinity of areas of reduced melting or increased marine ice accretion, leading to smaller effects when considering ice shelf area averages (std = 37 %; see Table E.1).

These small scale modulations can often be linked to local tidal current strength. Figure 4.3 shows the barotropic currents associated with tides. These currents include the annual mean circulation (Fig. 4.3a) and the mean tidal current strength (calculated following Eqn. 4.1 and shown in Fig. 4.3b; see Section 4.2.3). Figure 4.4a shows the sensitivity of the mean circulation to tides. The sub-ice shelf cavities can become very narrow where streams of grounded ice drain into the large cold water ice shelves, for example, near Evans, Carlson and Rutford Ice Stream under the Ronne Ice Shelf, near the Lambert Glacier under the Amery Ice Shelf and near Scott Glacier under the Ross Ice Shelf (as shown in Fig. 4.2). Tides accelerate in these grounding line pockets (Fig. 4.3b) and act to strengthen the ice pump mechanism (Lewis and Perkin, 1986) with enhanced melting at depth followed by reduced melt rates (or increased refreezing) along western outflow regions (Fig. 4.2c). A similar pattern is also apparent under the Fimbul Ice Shelf, where a melt increase near the grounding line of the Jutulstraumen Glacier coincides with reduced melt rates all along its keel (Fig. 4.2c). We note that we artificially deepened the bathymetry in narrow grounding zones and all of the regions

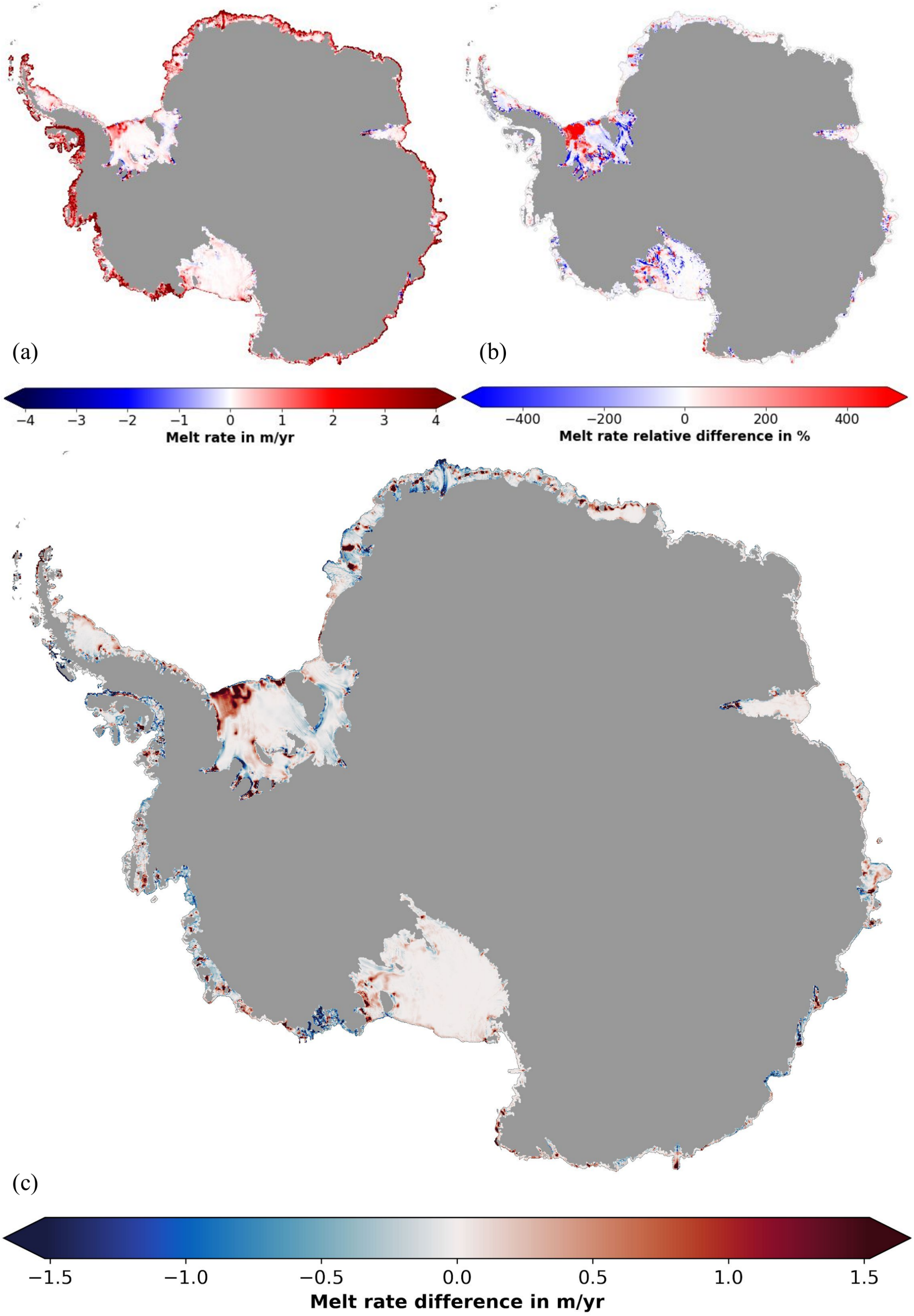

Figure 4.2: Tidal melting of Antarctic ice shelves. a) Annual average ice shelf melting for the case with tides, b) its relative difference to the case without tides $((w_{b\ \text{tides}} - w_{b\ \text{no-tides}})/w_{b\ \text{no-tides}})$ and c) its absolute difference to the case without tides $(w_{b\ \text{tides}} - w_{b\ \text{no-tides}})$.

mentioned above are affected by this approach (see Section 4.2.1). We also note that peaks in tidal velocity away from the grounding zones often coincides with localised melt increases, for example, underneath Riiser-Larsen Ice Shelf and the ice shelves of Queen Maud Land, but also in the Amundsen-Bellingshausen Seas underneath the Getz and Bach ice shelves. Tides also act to increase the Antarctic Slope Current (shown in Fig. 4.4a) at many places (e.g. in the Ross Sea, western Weddell Sea and in East Antarctica; see Fig. 4.5b for East Antarctica) and we hypothesise that this impacts water mass transport onto the shelf (e.g. Charlotte Huneke et al., 2019).

Melting in the frontal parts of ice shelves is often associated with local tidal activity. While our results indicate strong melting at the ice shelf front all around the continent (see Fig. 4.2a), in most regions this melting is independent from tides (as shown in Fig. 4.2b). Only at few places do tides contribute substantial amounts to front melting, for example, west of Berkner Island, east of Ross Island and under the Mertz Glacier tongue. Figure 4.4b shows the sensitivity of depth averaged continental shelf ocean temperature to tides and, in the regions mentioned, adjacent shelf temperatures do not show significant warming in the presence of tides. Hence, we attribute front melting at these locations to tidal advection of solar heated surface waters (proposed by Jacobs et al., 1992; see, e.g. Stewart et al., 2019, for observational evidence).

At some locations, tides act to increase melting across larger areas and these locations always coincide with a nearby warming of the continental shelf ocean (compare Fig. 4.2c with Fig. 4.4b). We attribute strong melting underneath the north-western side of the Ronne Ice Shelf to tide driven circulation on the adjacent continental shelf. The M2 tide resonates with the topography of the Weddell Sea causing a large tidal wave to circulate along the coastline of this region. When activating tides in our model, a strong gyre forms with its centre close to the midpoint of the rotating tidal wave, called the amphidromic point (for location of the M2 amphidromic point in the Weddell Sea see, e.g. Rosier et al., 2014, their Fig. 1a). The gyre transports heat across the continental shelf break and causes the Ronne Ice Shelf to feature one of the largest increases in average melting (128 %, equivalent to 44 Gigatons of ice per year, see Table E.1). Tide induced strengthening of warm water intrusions onto the continental shelf can also be seen in the northwestern Ross Sea, around the tip of the Antarctic Peninsula, seaward of Brunt Ice Shelf (eastern Weddell Sea) and in front of Land Ice Shelf (western Amundsen Sea).

Tide induced shelf melting is often followed by decreased ocean temperature and decreased melt rates downstream and we hypothesise melt water teleconnections to be

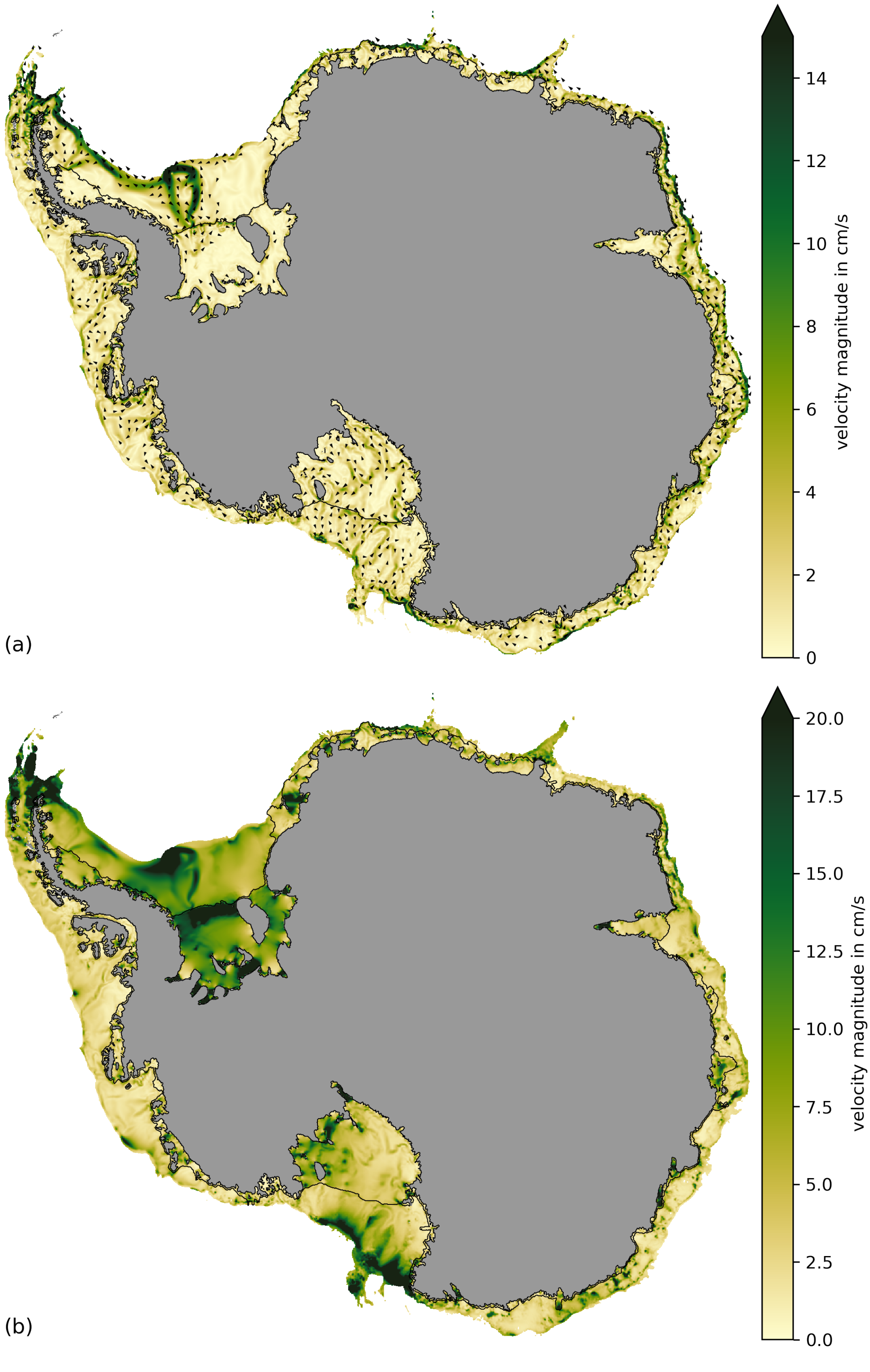

Figure 4.3: Mean and tidal current speed. a) mean barotropic velocities from the simulation with tides, b) mean speed of oscillating tidal currents ($|u|_{tide}$, calculated following Eqn. 4.1; see Section 4.2.3). Arrows in (a) indicate flow direction and are shown only where velocities are stronger than 1 cm/s.

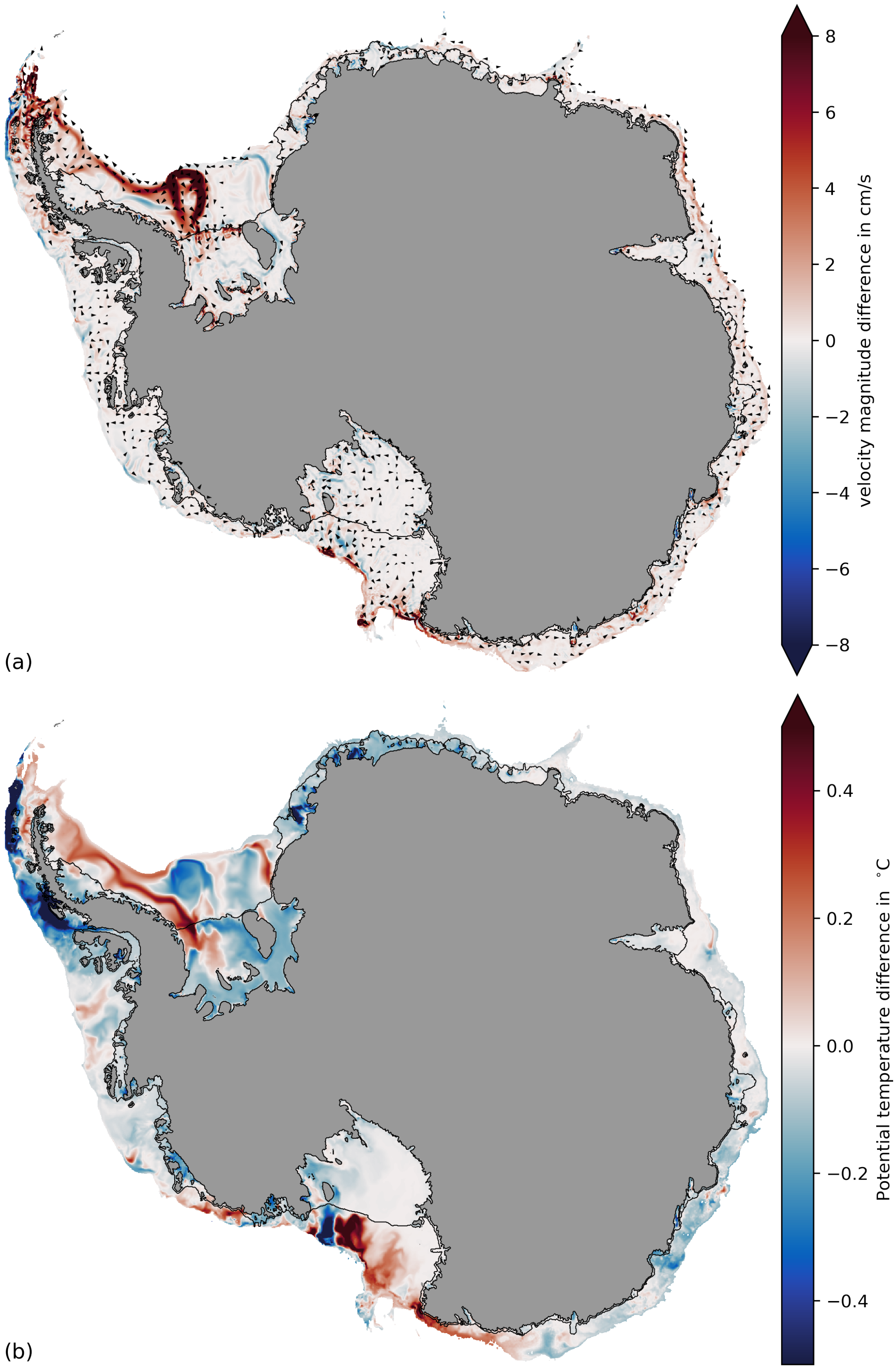

Figure 4.4: Tide induced change in (a) continental shelf barotropic velocity and direction and (b) continental shelf potential temperature. Differences show impact when activating tides in the model (e.g. $\Theta_{\text{tides}} - \Theta_{\text{no-tides}}$). Arrows in (a) are shown only where velocity change is larger than 1 cm/s.

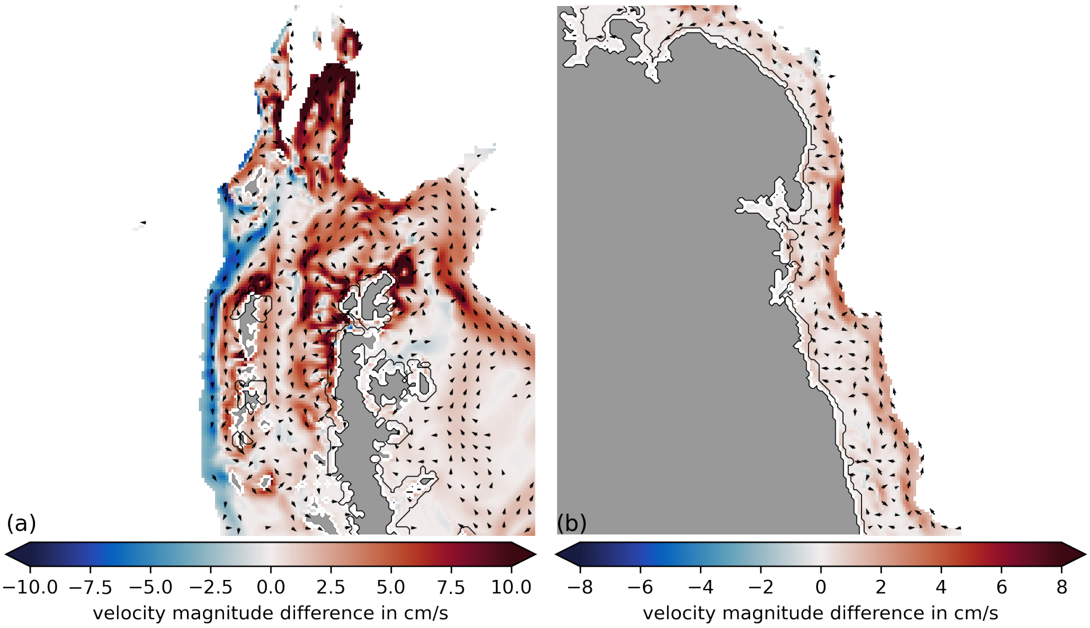

Figure 4.5: Tide induced change in continental shelf barotropic velocity. Same as Figure 4.4a, but showing (a) the tip of the Antarctic Peninsula and (b) the continental shelf near Kemp Land in more detail.

the cause. In the western Amundsen Sea, tide-induced melting underneath the Land Ice Shelf coincides with a reduction in melting of the downstream ice shelves Nickerson, Sulzberg and Swinburne (see Fig. 4.2c) and previous studies have suggested the westward propagation of melt water in this region (Jacobs and Giulivi, 2010; Nakayama et al., 2014a; Biddle et al., 2019). Further, the warming of the western part of the Ronne Ice Shelf Gyre coincides with cooling along its eastern side after passing through the sub-ice shelf cavity (see Fig. 4.4a for tide induced circulation change and Fig. 4.4b for temperature change). Likewise, the predominantly increased melting around Roosevelt Island (eastern Ross Ice Shelf) coincides with an increase in northerly mean flow and strong cooling of the adjacent continental shelf ocean. Cooler waters off the coast of Queen Maud Land only appear after the westward circulation passes through enhanced melting under Baudouin and Borchgrevink Ice Shelves. At a larger scale, the enhanced westward flowing current through Bransfield Strait (Antarctic Peninsula, see Fig. 4.5a) coincides with tide-induced warming and melting in the western Weddell Sea and an overall cooling and reduction in melt rates in the eastern Bellingshausen Sea. Finally, increased melting along Oates Land and the George V Coast coincides with a cooling of the continental shelf seaward of Adélie Land and reduced melting under Holmes Ice Shelf.

4.3.2 Time Series Analysis of Melt Drivers at the Ice Base

After quantifying the impact of tides on annual mean ice shelf melting and coastal oceans, we now explore variations in the melt drivers at the ice base at hourly resolution. The main result of this analysis is that tides control the sub monthly variability of T^* and u^* at most places around Antarctica. The underlying processes are either local with sub daily timescales, or include modulations of buoyant plumes with fortnightly timescales.

The model suggests that tidal currents often directly control T^* where inflowing glaciers form narrow cavities near the grounding line of cold water ice shelves. Figure 4.6 shows maps that indicate how much of the sub-monthly variance of T^* and u^* is driven by processes with sub-daily timescales. Figure 4.7 provides more details of these maps for the Ronne and Amery ice shelves. Based on these maps, we have chosen a few key locations that illustrate differences in T^* and u^* behaviour. Figure 4.8 presents the underlying times series at these locations. T^* and u^* are often directly controlled by tidal currents where, for example, Lambert Glacier (Amery Ice Shelf), Evans, Carlson, Rathford and Moeller Ice Streams (Ronne Ice Shelf) and Scotts Glacier (Ross Ice Shelf) become afloat (as shown in Fig. 4.6c and 4.6d). For example, under Evans Ice Stream, T^* varies at half the frequency as u^* and shows negative values (refreezing) with every second maximum in u^* (Fig 4.8a). We explain this behaviour as being due to tidal advection of High Salinity Shelf Water into the pockets and supercooled water from consequent melting out of it. Interestingly, the transition between inflow and outflow can be so rapid that it reduces the contribution of sub-daily variability to the total variance of u^*. In such a case, the contribution maximum is apparent at the entrance of the narrow channel close to the grounding zone (see, e.g. Amery Ice Shelf grounding zone in Fig. 4.7a).

The meltwater plumes that leave these narrow channels vary less at sub-daily timescales and drive thermal modulations with fortnightly periods. In the adjacent outflow regions of the grounding line melting described above, T^* shows little sub-daily variation, and, in the case of the Evans Ice Stream, changes with the fortnightly cycle of spring and neap tide (Fig. 4.8b). We interpret this signature as meltwater plumes that rectify over daily, but not fortnightly periods.

In other regions with cold-water ice-shelf grounding zones, T^* mostly varies on above daily timescales. Where Support Force and Foundation Ice Streams drain into Ronne Ice Shelf, for example, T^* is dominated by processes acting on timescales longer than one day, while u^* is clearly controlled by the strong tidal currents in these regions (compare Fig. 4.6c against Fig. 4.6d). Here, T^* also exhibits strong fortnightly variations, suggesting the influence from melt water upstream (not shown).

Fortnightly tides also control the strength of the warm water intrusion under Ronne Ice Shelf. The temperatures and velocities at the base of the northwestern Ronne Ice Shelf also exhibit strong modulations following the spring neap tide (shown in Fig. 4.8c). As earlier identified, the source of the warm water intrusions in this area is a tide driven gyre on the adjacent continental shelf and we conclude that the strength of the M2 tide controls the strength of the gyre.

In several regions tidal currents impact the sub-monthly variability of T^* more than that of u^*. At some areas of the trunk of the Filchner-Ronne, Ross and Riiser-Larsen Ice Shelves, sub-daily processes have a larger impact on T^* variability than on u^* variability (as shown by Fig. 4.9). We identify these regions as having strong tidal mixing, which lifts warm water up in the water column and in contact with the ice. Currents in these areas seem to include a strong fortnightly component (e.g. in the North-East of Ronne Ice Shelf and north of Henry Ice Rise, Fig. 4.8d and 4.8e, respectively), indicating the

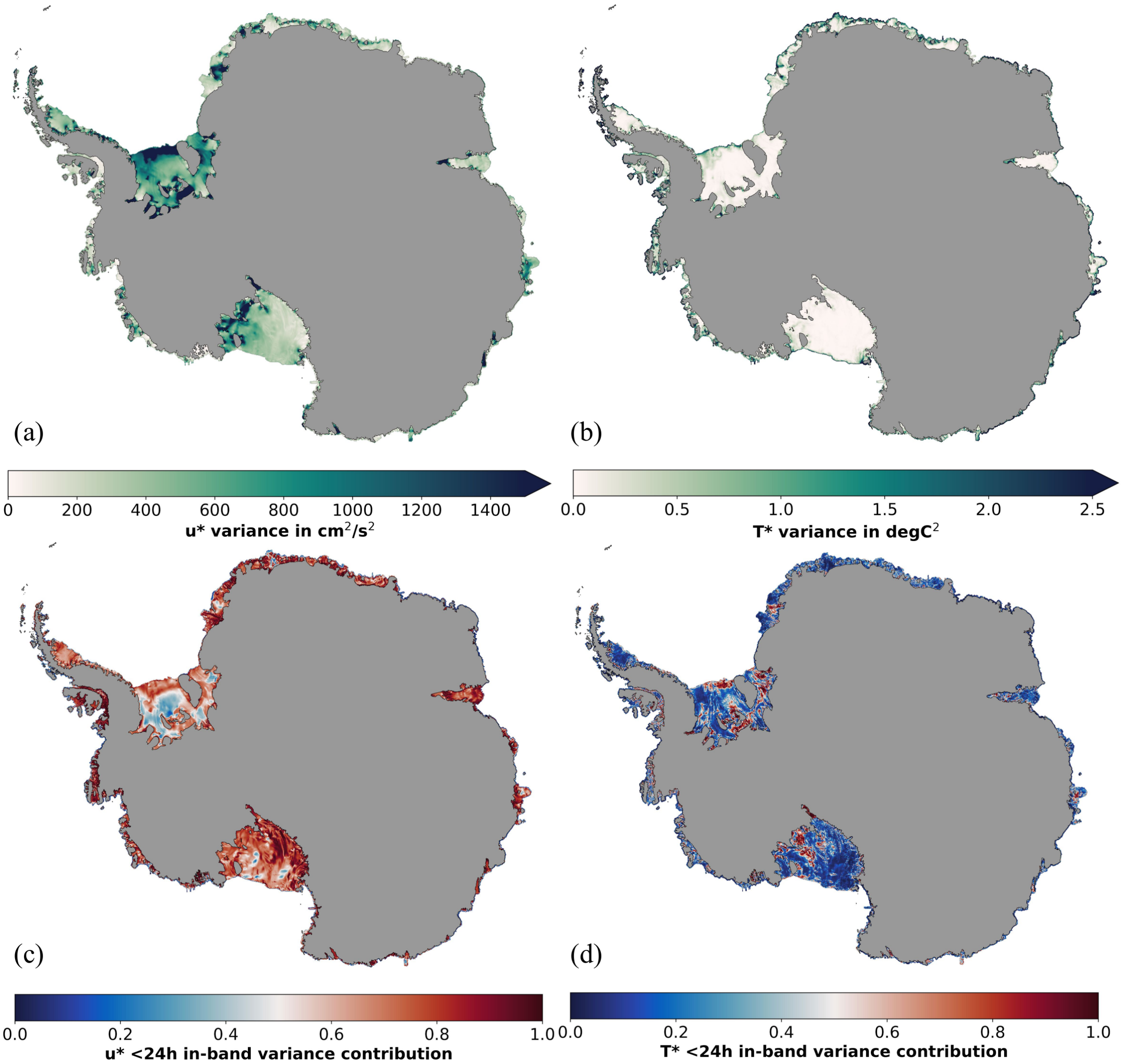

Figure 4.6: Contribution of tidal currents to the sub-monthly variance of the melt drivers at the ice base. (a) Sub-monthly variance of friction velocity (u^*) and (b) thermal driving (T^*) from the run with tides at hourly resolution. Inband contribution from processes acting on timescales faster than one day to the variance of (c) u^* and (d) T^* (0.0 corresponds to 0 % fast-process-contribution, 0.5 to equal contributions from fast and slow processes and 1.0 to 100 % fast-processes-contribution).

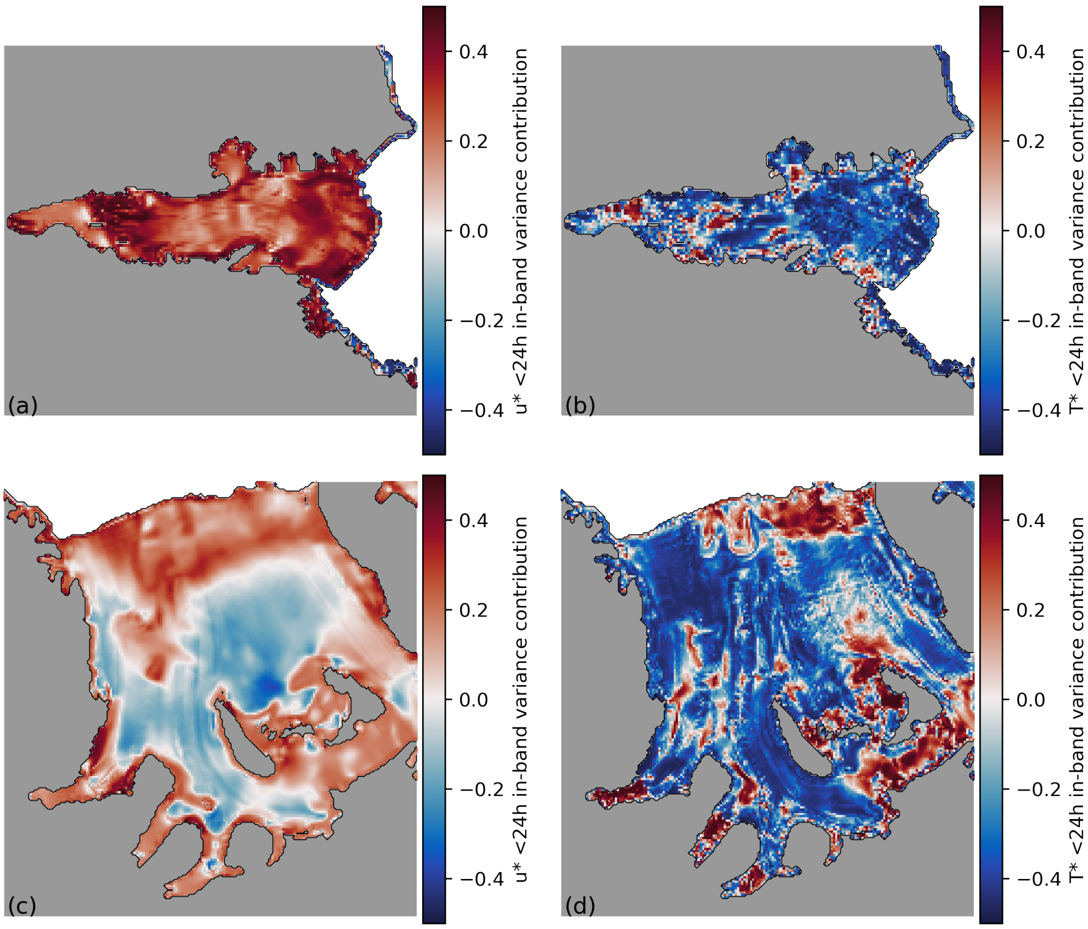

Figure 4.7: Contribution of tidal currents to the sub-monthly variance of the melt drivers at the ice base (details). Same as Fig. 4.6b and c, but zoomed in to show details of Amery ice shelf (a and b), and Ronne Ice Shelf (c and d).

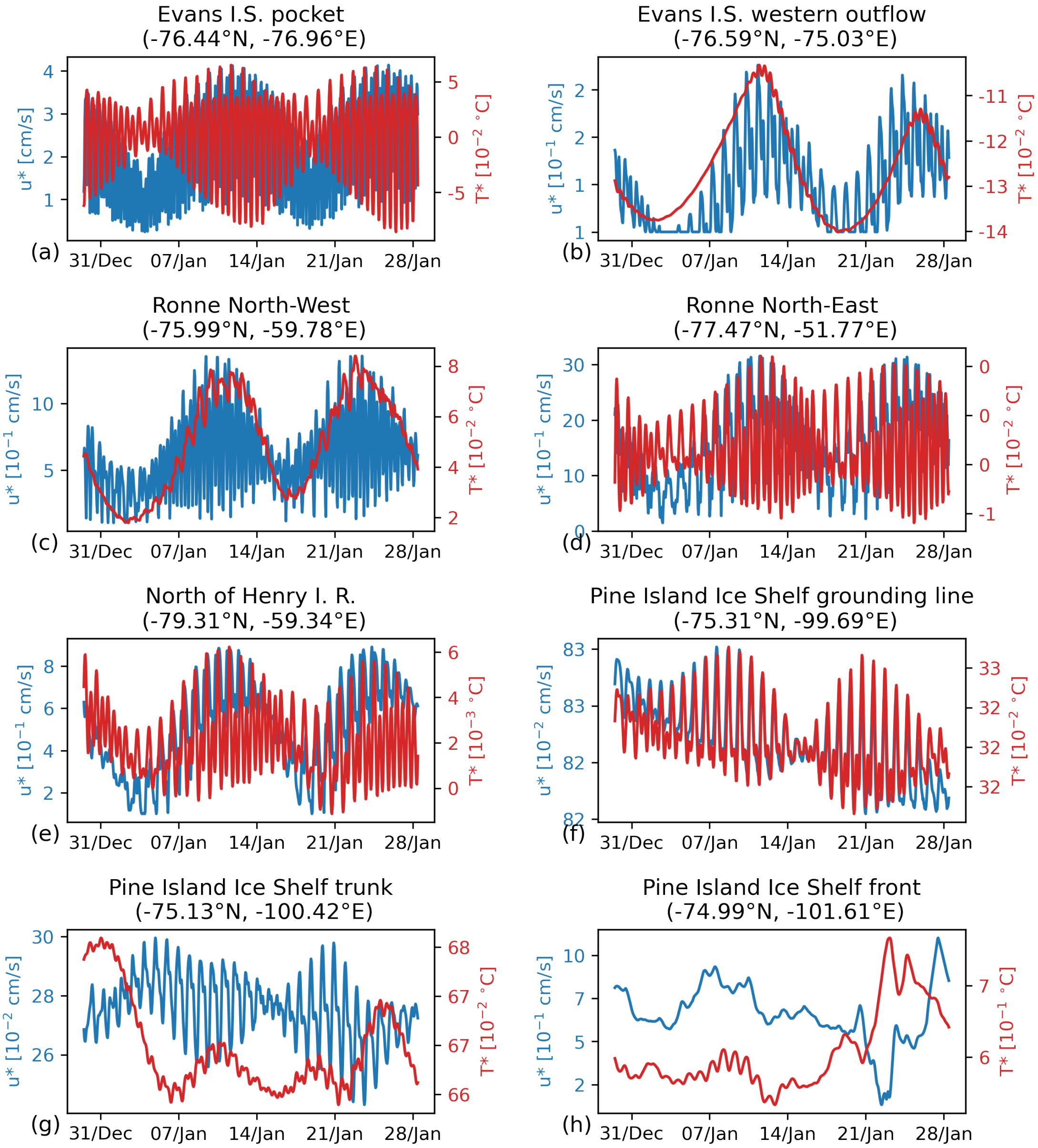

Figure 4.8: Selected time series of melt drivers at the ice base. Hourly average values of the friction velocity (u^*; blue) and thermal driving (T^*; red) during January 2007. Samples are single model grid points and taken from the Evans Ice Stream grounding line pocket (a), its western outflow region (b), the North-West (c) and North-East (d) of Ronne Ice Shelf, north of Henry Ice Rise (e) and, from Pine Island Ice Shelf, the grounding line (f), trunk (g) and front (h). Exact locations are presented in the titles of the sub-figures and indicated by arrows in Fig. 4.1. The magnitude of variability in each place looks to be strongly tidal, but the range of variations (e.g., Pine Island grounding line) can be extremely small.

existence of buoyant plumes, which are possibly induced by the mixing-driven melt. The total sub-monthly variance of T^* in these regions, however, is typically small (Fig. 4.6b), questioning the relevance of this process in a larger context. Sub-daily timescales also contribute more variance to T^* than to u^* in some of the grounding line pockets of Ronne and Ross ice shelves, but this is caused by short transition times of in and outflowing waters that act to reduce the contribution of fast processes to u^* variance (as mentioned earlier).

Tidal currents are also important along the grounding zones of warm water ice shelves. The high melt rates in the Amundsen-Bellingshausen seas (see Fig. 4.2a) are often associated with deep warm water intrusions driven by eddies (e.g. Nakayama et al., 2014b; Dinniman et al., 2016). Even in the presence of strong buoyant plumes, typical for these regimes, the sub-monthly variability of u^* and T^* is often dominated by tidal currents (as shown by Fig. 4.6c and 4.6d). At the Pine Island Ice Shelf grounding line, for example, u^* varies synchronously with T^* (see Fig. 4.8f) and with equal contributions to the longer term variability (as shown in Fig. 4.9). This signature might be associated with tidal advection of warm water into the shallow, well-mixed parts of the cavity.

Other parts of warm water ice shelves, however, show little signs of tidal activity in T^*. In the Amundsen-Bellingshausen Seas, T^* also often varies on above daily-timescales (Fig. 4.6c), but unlike similar regions in colder regimes, we do not find strong fortnightly cycles (as shown in Fig. 4.8g).

Variability in u^* and T^* at the ice front are often not impacted by tidal currents. The overall Antarctic picture of T^* variability up to a month is governed by high values at the front (as shown in Fig. 4.6b) and at most places with dominant contributions from above-daily timescales (e.g. in the Amundsen-Bellingshausen Seas and in East Antarctica; see Fig. 4.6d). In these regions, u^* is also often dominated by long period processes (Fig. 4.6c) and time series of u^* and T^* show only negligible tidal variation (e.g. at the front of the Pine Island Ice Shelf; Fig. 4.8h). We relate this behaviour to a strong buoyant plume, which is restricted to the very front of the ice shelves and likely controlled by the daily variation in surface fluxes or eddies. Only at very few places do tidal currents also impact frontal T^* variability (e.g. around Ross and Roosevelt Island or at the eastern part of the Filchner Ice Shelf). Here, u^* does not exhibit fortnightly cycles and this supports melt driven by tidal advection of warm surface waters (as mentioned earlier).

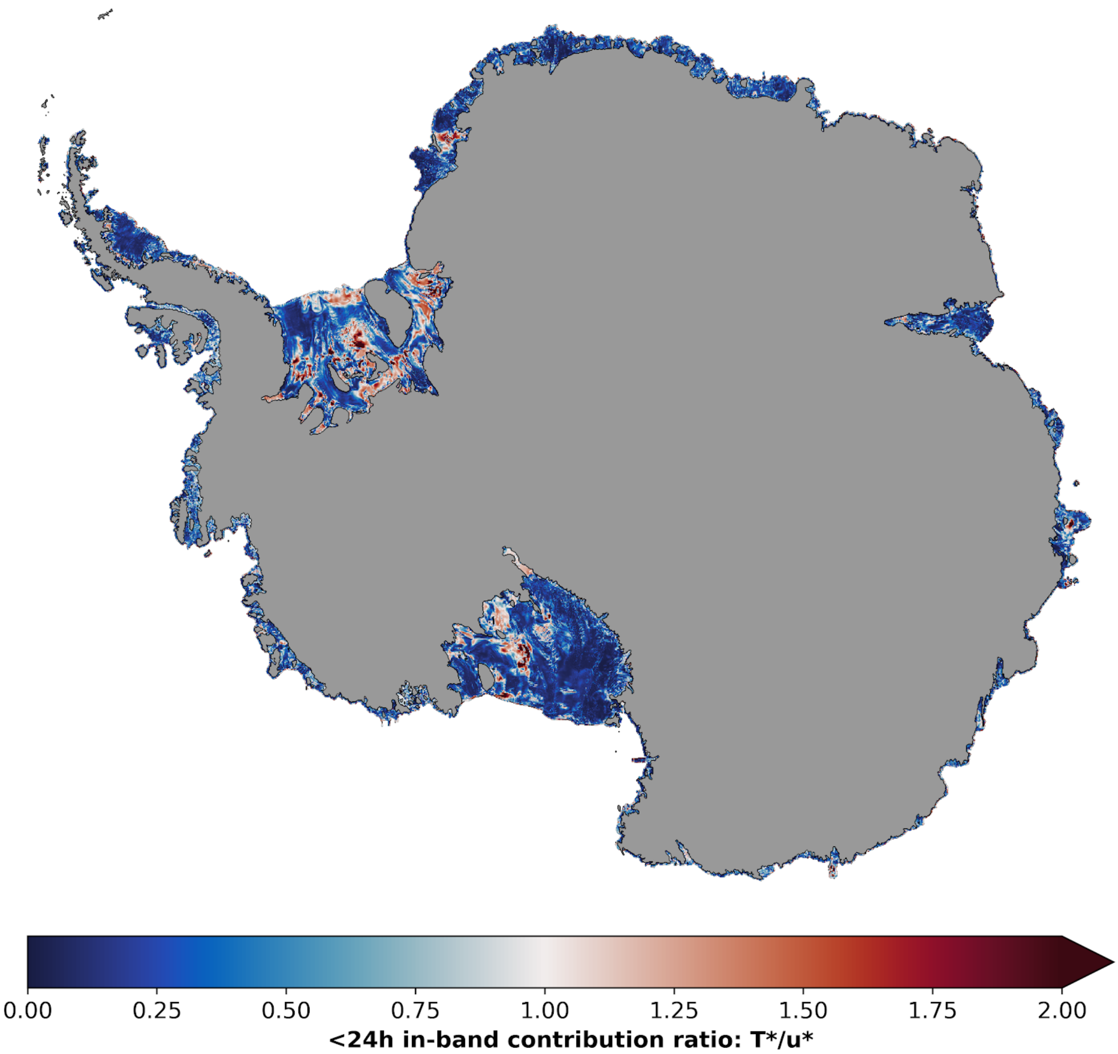

Figure 4.9: Ratio of tidal current variance contribution between the melt drivers at the ice base. The ratio of the T^* fast-process variance contribution (Fig. 4.6d) to the u^* fast-process variance contribution (Fig. 4.6c). In regions with values smaller than 1.0 fast processes impact u^* variance more than T^* variance, while values larger than 1.0 denote the opposite.

4.4 Discussion

We have shown that tidal effects on Antarctic ice shelf-ocean interaction are large and this means that robust modelling of ice shelves or the ice sheet requires inclusion of tides. That is, models including ice shelves, which are critical to the stability of the ice sheet and hence accurate ice sheet projections (Shepherd et al., 2004; Pritchard et al., 2012), need to explicitly resolve tidal currents. Tides are understood to be critically important for ocean-ice shelf interaction (e.g. Padman et al., 2018; Galton-Fenzi et al., 2012), but resolving tides in larger scale models is expensive. Hence, several studies have focused on attempts to include the influence of tides on ice shelf melting without explicitly resolving tidal currents. Jourdain et al. (2019), for example, accounts for tide-driven changes in modelled melting of the Amundsen Sea ice shelves by adding a tidal component to the description of the friction velocity (following, e.g. Jenkins et al., 2010; similar to enhancing bottom drag in non-tide-resolving estuary models). The results of this study, however, suggest that such approaches would cause large biases in circum-Antarctic ice sheet projections.

We identified that under large parts of the cold water ice shelves tidal currents primarily interact with ice shelf melting by changing temperatures at the ice base, rather than velocities. Further, tide-induced warm water intrusions on the Weddell Sea continental shelf cause significant increases in mass loss from nearby ice shelves. Ocean changes are most pronounced near the continental shelf break and, hence, we suspect tidal mixing or rectified currents to be the driving mechanism, rather than cavity overturning from buoyant meltwater plumes.

At the ice shelf front, however, tidal currents seem to play a secondary role. Frontal melting has often been related to tidal advection of surface waters (Jacobs et al., 1992; Stewart et al., 2019) and, while the model resolves elevated melt rates of frontal ice all around the continent, tides are involved only at very few locations (e.g. east of Ross Island). Instead, surface fluxes or eddies seem to govern modulations of velocity and temperature at most places, suggesting a very localised buoyancy driven regime. We note, however, that the model might have biases at the outermost cells, as pressure gradient errors in sigma coordinate ocean models require smoothing of vertical boundaries (Mellor et al., 1994, 1998). To which degree a smoothed ice front is actually a better representation of frontal conditions in ocean models (as suggested by Malyarenko et al., 2019), will have to be explored in future studies.

A major limitation of this study originates from the three-equation melt parameterisation used in the model. Observations suggest that in regions with weak currents or strong stratification, the boundary layer exchange rates of heat and salt are controlled by diffusive-convection, rather than shear-driven turbulence, and the three equation melt parameterisation used in the model does not account for this regime (Kimura et al., 2014; Begeman et al., 2018).We speculate, however, that results of this study could be used to inform where diffusive-convection takes place. Future studies aiming to address this question should look for regions where weak flow (mean and tidal) could produce a circulation regime more favourable to the formation of diffusive convection staircases (e.g. George VI Ice Shelf, Kimura et al., 2014).

Future studies should include extended frequency analysis and experiments without thermodynamic ice-ocean interaction. A tidal harmonic analysis could shed more light on the role of the spring-neap tide for buoyant plumes, allow for the attribution of melt modulations to individual tidal constituents and help to interpret borehole observations. Performing this analysis at different months of the year should clarify how seasons impact the tide driven modulations revealed in this study. Further, additional experiments without salt and heat exchange at the ice base would help to identify the role of tide-induced meltwater plumes for exchanges across the continental shelf break and should be compared against the estimates of tide-driven shoreward heat transport of (Stewart et al., 2018).

Tide induced changes in ocean temperature and ice shelf melting exhibit a dipole pattern in many regions, consistent with the idea of ice shelf teleconnections. Regional studies suggest that meltwater can propagate far downstream (Jacobs and Giulivi, 2010; Nakayama et al., 2014a; Biddle et al., 2019) and substantially impact ice-ocean interaction underneath other ice shelves (Gwyther et al., 2014; Silvano et al., 2018). Activating tides in our model can be seen as one large perturbation experiment and results suggest that ice shelf teleconnections are a widespread phenomenon (see Fig. 4.4). A strong, tide-induced coastal current (shown in Fig. 4.5a) appears to transport glacial melt water even around the tip of the Antarctic Peninsula from the Weddell to the Bellingshausen Sea. A westward flowing coastal current through Bransfield Straight has also been observed (Heywood et al., 2004; Thompson et al., 2009). To confirm that the dipole pattern seen in this study are indeed related to downstream propagation of melt water, future studies should include passive tracer in the model (similar to, e.g., Nakayama et al., 2014a) and extend the simulation time to several years. Such analysis would be crucial to inform boundary locations and conditions of regional models.

Despite the small integrated mass loss change due to tides, the consequences for ice sheet dynamics might be large. The buttressing importance of floating ice can vary by several orders of magnitude within one ice shelf, with regions close to grounding lines, lateral boundaries or pinning points generally being the most important for ice sheet stability (Gudmundsson, 2013; Reese et al., 2018). Our model predicts that the strongest changes in basal mass loss often occur in exactly these parts of the ice shelves. Within these regions, however, increased melting is often in close vicinity to equally strong reduction in melting or enhanced refreezing, making it difficult to assess the overall impact on buttressing. Diagnostic experiments with ice sheet flow models could be used to quantify the instantaneous response of tide-driven ice shelf thinning on the ice flux across the grounding lines (similar to experiments by Reese et al., 2018). Such an approach, however, does not include longer term consequences.

Antarctic tides are sensitive to changes in ice shelf geometry and sea levels, offering potential feedback on ice sheet relevant timescales. Antarctic tides can be interpreted as waves that propagate around the continent and barotropic ocean models show that shifts in sea levels, grounding line location and ice draft depth significantly alters their propagation and dissipation (Griffiths and Peltier, 2009; Rosier et al., 2014; Wilmes and Green, 2014). Ice shelf retreat in simulations by Rosier et al. (2014), for example, produces an overall increase of M2 dissipation by more than 40 % (see their Table 1) and here we have shown that tides act to increase the conversion efficiency of ocean heat into ice shelf melting, which is also supported by idealized simulations by the study of Gwyther et al. (2016). On a more regional scale, tidal current strength is very sensitive to local changes in the water column thickness, which is set by ice shelf geometry and ocean depth (e.g. Galton-Fenzi et al., 2008; Mueller et al., 2012). Mueller et al. (2018) revealed that slight changes in the draft of the Filchner-Ronne Ice Shelf impacts tide driven melting in areas relevant for inland ice sheet dynamics. More drastic ice retreat in this region, however, might reduce the warm water intrusion under the Ronne Ice Shelf, as the M2 amphidromic point on the Weddell Sea migrates northward (Rosier et al., 2014) and our results suggest a connection between this point and the warm water intrusions. Potential positive and negative feedback between ice geometry, basal melting, and local as well as far field tides will need to be explored using coupled ocean-ice shelf-ice sheet models with Antarctic-wide coverage.

Likewise, regional changes in coastal hydrography due to tides might impact water mass transformation with consequences for global oceans and climate. Brine rejection in sea ice polynyas drives the formation of dense water, which has been linked to Antarctic Bottom Water (Purkey and Johnson, 2013) and the meridional overturning circulation (e.g. Jacobs, 2004). Deep water formation seems to be sensitive to local changes in the ocean, as recent studies show that glacial melt water can offset the densification by polynya activity (Williams et al., 2016; Silvano et al., 2018). Activating tides in our model changes depth average temperatures by up to 0.5 °C in some locations and generates rectified currents with velocities of up to tens of centimetres per second. The relevance of these tidal currents and tidal-driven meltwater for water mass formation and transformation on the Antarctic continental shelf, and indeed on the global oceans and climate, is yet to be explored.

4.5 Summary and Conclusion

The modelling results presented here indicate that tides modulate Antarctic-wide ice shelf basal melting by various means:

- Tide induced warm water intrusions drive strong melting under the northwestern part of Ronne Ice Shelf and are likely driven by processes near the continental shelf break rather than ice-ocean interaction.
- Near the grounding zones of warm and cold water ice shelves, tidal currents control warm water advection and boundary layer exchange rates over sub-monthly timescales.
- These interactions act to strengthen buoyant meltwater plumes, which modulate according to the spring-neap tidal cycle on fortnightly timescales.
- Under some parts of the cold water ice shelves, tidal mixing governs ice-ocean interaction.

The integrated impact on ice shelf basal mass loss and the continental shelf ocean temperature is small, but in opposing directions. Modelled basal mass loss increases only by 4 %, while continental shelf ocean temperatures drop by 0.04 °C. This is in agreement with idealized modelling results of (Gwyther et al., 2016) and indicates a gain in the conversion efficiency of heat into melting. This efficiency is likely to change as Antarctic tides vary in strength over glaciation timescales (Griffiths and Peltier, 2009; Rosier et al., 2014; Wilmes and Green, 2014).

Regional variations, however, can be large with potential consequences for ice sheets and global oceans. Melt modulations at 4 km scale can exceed 500 % and are often located near grounding zones, lateral boundaries and pinning points of cold water ice shelves. These regions are most valuable for the buttressing ability of ice shelves against tributary glacier discharge (Reese et al., 2018), but increased melt is often balanced by reduced melt or increased refreezing nearby, making it difficult to assess the overall impact without ice sheet modelling. Likewise, local changes in depth averaged ocean temperature on the continental shelf can exceed 0.5 °C and deep water formation driven by sea ice polynyas has been shown to be sensitive to such changes (Williams et al., 2016; Silvano et al., 2018).

Tides do not modulate melting at the ice front or below warm water ice shelves away from the grounding zone. In the model, tidal currents directly modulate velocities and temperatures close to the ice front only at a few locations, such as east of Ross Island (also observed by Arzeno et al., 2014). Likewise, fortnightly variations in T^* close to the front only occur where tides drive warm water intrusions under the ice, for example in the northwestern part of Ronne Ice Shelf. In most places, however, frontal melting varies mostly on longer timescales and without fortnightly cycles, suggesting a strong buoyant regime that protects the ice from tidal influences (see also Malyarenko et al., 2019). Further, high melt rates in the Amundsen-Bellingshausen Seas are often related to warm water intrusions driven by non-tidal processes and, away from the grounding zone, the strength of these intrusions also controls ice-ocean interaction on sub-monthly timescales in our model.

In many regions, tide induced melting coincides with a reduction in melt downstream, hinting towards the importance of ice shelf teleconnections. Regional studies suggest that ice shelf melt water can propagate downstream on the continental shelf (Jacobs and Giulivi, 2010; Nakayama et al., 2014a) and connect ice-ocean interaction between ice shelves (Gwyther et al., 2014; Silvano et al., 2018). Results presented here suggest that this is true for many regions around the continent, including the Western Amundsen Sea, along the coast of Queen Maud and Adélie Land and through Bransfield Strait (see Fig. 4.4). Multiyear tracer analysis could be used to confirm our speculation and inform boundary locations and conditions in regional studies.

The absolute numbers presented in this study might be susceptible to model bias, but conclusions about the driving mechanisms are robust. No evaluation matrix for circum-Antarctic ice shelf-ocean models has been developed yet and, hence we present absolute estimates which should be taken with caution. Nevertheless, Antarctic-wide basal mass loss driven by tides is a valuable first estimate and our model has been proven successful in many regional and idealized applications (Galton-Fenzi et al., 2012; Cougnon et al., 2013; Gwyther et al., 2014, 2016), giving us confidence in our conclusions about the driving processes.

We conclude that tidal currents modulate Antarctic ice shelf melting not just by impacting boundary layer exchange rates, but also by means of vertical mixing, advection and continental shelf processes. Hence, parameterisations of tidal melting that account for boundary layer processes alone (as suggested by, e.g. Jourdain et al., 2019) will likely result in large biases in Antarctic-wide applications. Further, tidal strength changes with local and far field ice sheet retreat (e.g. Mueller et al., 2018; Rosier et al., 2014) and there is evidence that consequent changes in meltwater impact ice-ocean interaction far downstream. Hence, models that aim to accurately predict future changes in ice shelf melting will need to explicitly resolve tides and have continent-wide coverage.

Chapter 5

Conclusion

5.1 Summary of Findings

Interactions between the Antarctic ice sheet and the surrounding ocean exert large controls over global sea level and climate. Among these interactions, ocean-driven melting and refreezing at the base of floating ice shelves play particularly important roles, as they govern ice sheet discharge rates and freshening of global oceans. While research is beginning to unravel the complex mechanisms that are involved in ice shelf melting, this knowledge is far from complete. A better understanding of the drivers that cause melting today will help to improve projections of future change.

Observing the processes that take place at high latitudes, however, is difficult. Metres-thick sea ice covers the continental shelf ocean in winter and inhibits scientific voyages to Antarctica. Thus, in situ observations derived using moorings, seals, ice penetrating radar and boreholes do not have enough coverage in space and time to draw large scale conclusions. Further, methods using satellite data models and models of surface processes have been used to infer continent-wide estimates of the ice shelf basal mass balance. The underlying methodology, however, implies large uncertainties of high resolution results.

Ocean modelling is fully independent from satellite methods and now constitutes an essential tool for researching Antarctic ice-ocean interaction. Ocean processes involved in ice shelf melting cover a wide range of scales, reaching from millimetres and seconds to global and millennial, and various numerical models have been used to gain great insights into these processes. Within these models, circum-Antarctic applications are of particular interest, as they allow us to study known, important processes in a continent-wide context and fully independent from satellite limitations.

This thesis applies ocean modelling to advance our understanding of current Antarctic ice shelf-ocean interaction. The overall outcomes of this research have been:

- Development of a state-of-the-art ice shelf-ocean model, with high spatial resolution and inclusion of tides.
- Quantification of the significant impact of solar-heated surface water in driving melting of ice shelves shallower than 200 m.
- Assessment of the role of tides in facilitating on-shelf and sub-cavity heat exchange to all ice shelves in Antarctica.

In Section 1.6, three main objectives were proposed. The following paragraphs repeat these objectives and describe how, and in which chapter, they have been addressed. Secondary outcomes related to each objective are also summarised.

1. **To develop and evaluate WAOM, a new circum-Antarctic configuration of the Regional Ocean Modelling System (ROMS) that includes tides and an eddy resolving resolution.** In Chapter 2, I apply ROMS to a circum-Antarctic domain and simulate 2007 conditions. Tidal forcing is realised in a way that tidal height accuracy along the coast is comparable to current generation barotropic tide models. Further, the grid features a uniform horizontal resolution of 2 km, which is high enough to resolve eddy driven heat flux onto the continental shelf and results in realistic bottom layer temperatures in the Amundsen-Bellingshausen Seas. WAOM resolves small scale ice shelf ocean-interaction in agreement with regional studies and the total ice shelf basal mass loss is close to estimates from methods using satellite observations and models of surface processes. The simulations performed in this chapter are likely the most accurate representation of processes inside Antarctic ice shelf cavities today.

   Secondary outcomes of Chapter 2 are:

   - Ice shelf melt rates and continental shelf ocean temperatures converge with increasing resolution, but a further refinement to 1 km is likely necessary to reach asymptotic behaviour.
   - Tide-topography interactions need to be resolved with at least 4 km horizontal resolution.

- A cold bias for some of the warm water ice shelves was attributed to insufficient heat flux from the continental shelf into the sub-ice shelf cavities, likely caused by bathymetry biases or the representation of surface stress.
- At most places the model resolves elevated melt rates towards the ice shelf front. While only few in situ observations of frontal melting are available, they confirm enhanced ablation with rates comparable to the simulation.
- Future efforts should primarily focus on compiling available observations, as this would open the way to efficient model tuning and intercomparison between studies. A second priority is implementing regional bathymetry updates and windstress modulation by sea ice in the model.
- WAOM is well suited to provide the ocean component in coupled models, but projections outside the observational records require buoyancy fluxes from climate model projections or augmentation by a dynamic sea ice model (e.g. following Naughten et al., 2018b).
- The model (Richter, 2020a) as well as its pre- and post-processing scripts (Richter, 2020b) has been made freely available on github.

2. **To assess whether deep, warm water intrusions are the main source for Antarctic basal melting.** In Chapter 3, the modelling results of Chapter 2 has been analysed in regards to this objective. It is shown that advection of solar heated surface waters also plays a substantial role for the Antarctic mass loss, in addition to deep ocean processes. This conclusion has been reached in two steps. First, ice shelf melting has been integrated over different depth ranges and results show that about a third of the total mass loss originates from ice shallower than 200 m. Second, an ocean analysis reveals that AASW is often present at these depths inside the ice shelf cavities and, further, that the annual variation of shallow ice melting strongly correlates with the seasonal cycle of the adjacent surface ocean temperature. Surface water melting is likely affected by small scale processes close to the ice front. These coastal processes respond to climate change on more rapid timescales than the ocean at depth and need to be included in large scale predictions of future change.

   Related to the second objective, the following outcomes have also been derived.

   - Antarctic ice shelves lose most of their mass from depths shallower than 400 m.
   - Satellite estimates of Antarctic ice shelf melting at high resolution miss an important melting mode.

Deep ice is more valuable for the instantaneous buttressing ability of ice shelves against ice flux across the grounding lines. Longer term effects, however, are less clear.

3. **To determine the importance of tides for controlling changes in Antarctic-wide ice shelf melting and conditions in the continental shelf seas.** In Chapter 4, I conduct additional experiments with the model developed in Chapter 2 at 4 km horizontal resolution. Deactivating tides in the model has little effect on the total mass loss and integrated continental shelf ocean temperatures. Regional variations, however, can be substantial, exceeding 500 % for ice shelf melting and 0.5 °C for depth integrated temperatures. These local changes are likely to impact ice shelf buttressing and water mass transformation on the continental shelf. Thus, the evolution of tides over glacial time scales will likely need to be considered when predicting changes in ice sheets and global oceans.

   During work related to the third objective, the following secondary outcomes have been derived.

   - A tide induced gyre on the Weddell Sea continental shelf drives warm off shelf water under the Ronne Ice Shelf, contributing 150 % to its area average melt rate.
   - In most regions, tides are not involved in melting at the ice front. Instead, model results suggest that surface water advection is driven in most places by non-tidal mechanisms, such as winds or eddies.
   - In many regions, tide induced melting coincides with a reduction in melt downstream, hinting towards the importance of ice shelf teleconnections (e.g. around the Antarctic Peninsula carried by the coastal current).
   - Tides modulate ice shelf melting not only by changing boundary layer exchange rates, but also by means of vertical mixing, advection and processes on the continental shelf. These processes will need to be explicitly resolved to predict accurate Antarctic ice shelf melting.

5.2 Limitations

The model presented in this thesis has limitations, which have guided the choices of research topics. These limitations are related to computational constraints and the design choices made for WAOM regarding unresolved or parameterised processes.

While WAOM brings the sophistication of regional models to a circum-Antarctic domain, there are important processes that are not yet included in state-of-the-art ocean-ice shelf models like WAOM.

- A lack of knowledge of bathymetry is often stated as the main source of uncertainty in ice shelf-ocean simulations (Dinniman et al., 2016). WAOM's cavity geometry is based on Bedmap2, which, at the time of development (2016), was a state-of-the-art product. Since then, however, some regions have been updated, including the discovery of troughs that cross the continental shelf and can be critical for ice shelf cavity processes (e.g. Millan et al., 2017). Many regions remain poorly surveyed, especially underneath ice shelves (Fretwell et al., 2013). In this thesis, bathymetry biases are likely responsible for the cold bias of some of the warm water ice shelves (discussed in Chapter 2). Further, reduced tidal accuracy near the deep grounding lines of large cold water ice shelves has been attributed to biases in cavity geometry, as tides are very sensitive to water column thickness (see Chapter 2).

- WAOM does not include sea ice interaction. Prescribed surface fluxes potentially result in a representation of continental shelf conditions that are more accurate than conditions derived from including a sea ice model (e.g. representation of polynyas). Accurate melt rates are fundamental for the research objective addressed in Chapter 3, but the perturbation experiments in Chapter 4 are likely less realistic without sea ice interaction. Ice shelf melt water is known to impact sea ice concentration (Hellmer, 2004; Padman et al., 2018) and the absence of tides substantially changes Antarctic melt water pathways (outcome of Chapter 4). Exclusion of dynamic sea ice also limits the ability to perform future projections (discussed below).

- The 3-Equation melt parameterisation used in WAOM has known limitations. The parameterisation has been tested in only a few locations and tuned to these regions. There is evidence that melt rates deviate from predictions in other regions, e.g. under George V Ice Shelf (Kimura et al., 2014) and Ross Ice Shelf grounding zone (Begeman et al., 2018). A resulting bias in WAOM could impact quantitative results in Chapter 3 and 4. In addition to melt rates, meltwater plumes and associated conditions on the continental shelf might be affected.

- WAOM does not resolve eddies in the entire domain. Even though WAOM's horizontal resolution of 2 km is fine enough to capture critical eddy processes at the shelf break, it is not sufficient to resolve eddies everywhere in the domain.

Årthun et al. (2013) suggest that eddy driven heat flux across the cavity entrance is important for ice shelf melting. Eddy size is related to water column thickness, stratification and latitude (Chelton et al., 1998) and resolving eddies near the ice front would require horizontal resolutions of 500 m. The importance of these smaller eddies in an Antarctic-wide context is supported by the grid convergence study in Chapter 2, which shows that the continental shelf ocean has not reached asymptotic behaviour at 2 km grid spacing. A further limitation related to grid resolution is that perturbation experiments in Chapter 4 have been conducted at 4 km horizontal resolution and, hence, may not resolve potentially important eddy-tide interactions.

WAOM has been designed to simplify coupling to models of ice sheet flow, but its current version has limitations in regards to larger spatial and temporal scale simulations.

- Simulations with WAOM are computationally intensive. The model requires about 40,000 CPU hours to simulate a single year at 2 km horizontal resolution. While some aspects of the code can be optimised, e.g. in regards to parallel Input/Output and inactive land cells, the gain will not be enough to make simulations with WAOM over climate relevant time scales feasible. This limitation is not inherent to WAOM, but rather arises from the attempt to resolve small scale processes in models with large domains.
- WAOM does not include a dynamic sea ice model. Thus, predictions outside the observational record require surface fluxes from climate simulations. Climate model surface fluxes are not more accurate than fluxes derived from coupling a sea ice model. This compromises the main advantage of prescribing surface fluxes.
- Sigma coordinate ocean models are known to erode deep water masses. Terrain following vertical coordinates produce spurious mixing at steep sloping topography due to pressure gradient force errors (Mellor et al., 1994; discussed in Chapter 2). In the deep ocean, circulation is slow and spurious mixing leads to the erosion of water masses (Griffies et al., 2000; also discussed by Naughten et al., 2018b). Studies conducted in this thesis are focused on continental shelf ocean, but simulation efforts aiming to use WAOM for objectives that require accurate deep ocean properties will be affected by this limitation.

What are the implications of these limitations in the context of the broader research theme? This thesis aims to contribute to our understanding of the processes involved in Antarctic ice sheet retreat (see Section 1.6 for research gap). In particular, I have focused on the interaction between ice shelf basal melting and the continental shelf ocean at an Antarctic-wide scale and for present day conditions (represented by a single year). However, processes that act on above annual time scales and involve interaction of ice shelf melting with evolving ice sheets or global oceans are known to also exert large controls over glacier retreat (Colleoni et al., 2018). The methodology applied in this thesis does not allow for any conclusions to be drawn about these larger scale processes and, thus, implications of thesis results in this regard have been discussed only. To quantify the impact of feedback mechanisms such as MISI or subsurface ocean warming for sea level rise and global climate, coupled models that simultaneously resolve dynamics in global oceans and the Antarctic ice sheet are needed (see DeConto and Pollard, 2016, for large scale application of MISI; see Bronselaer et al., 2018, for subsurface ocean warming). The model developed in the framework of this thesis could be used as a module that communicates the shared quantities without compromising on important small scale ocean processes close to the ice.

5.3 Future Work

In Section 1.6, several research gaps were identified - the outcomes of this thesis address them in part. Future studies that aim to further close these gaps by building on the outcomes of this thesis should either harness the remaining potential of the model output derived in this thesis, perform additional experiments with WAOM or engage in further model development.

Further analysis of the model output from simulations performed in this thesis should focus on the following aspects.

- Idealized studies started to explore the average behaviour of Antarctic ice shelf cavity systems, including their response to ocean warming (Holland et al., 2008; Little et al., 2009; Gwyther et al., 2016; Holland, 2017). The simulations conducted in Chapter 2 provide 176 realistic examples of ice shelf cavity systems spanning the entire spectrum of present day conditions. Relations in the average quantities between these systems could be used to extrapolate the future behaviour of the average Antarctic ice shelf cavity. Further, the perturbation experiments conducted in Chapter 4 could reveal which regions are likely to follow the overall response, or would be most likely to deviate from the mean behaviour.

- The potential of machine learning approaches to reveal new insights from existing model output should be explored. Recent studies have applied machine learning approaches to questions in the fields of geophysical fluid dynamics (Phillips et al., 2020; Rasp et al., 2018). Random forests are a very robust and accessible machine learning technique, which can be used to analyse the importance of predefined features for predicting quantities of interest. Conclusions in Chapter 3 are based on ice draft depth as a predictor for ice shelf melting, but a well constructed random forest analysis could easily test if other geometric quantities are actually more powerful. These quantities could be, for example longitude, ice draft slope, water column thickness, depth normalized by total cavity depth, distance to the grounding line and ice front or the opening angle with the cavity entrance. Random forests can not only quantify the importance of these features to predict melt rates, but also reveal dependencies between them. Applying this technique to cavity averages would be straight forward and involve only little computational expenses. Extension to the four dimensional field of ocean quantities would require more thought and testing, but has the potential to open up entirely new methods for exploring and interpreting model output.

The following additional experiments require minimal changes to the code, but are expected to result in further valuable insights into Antarctic ice shelf-ocean interaction modelling.

- Releasing passive tracers from the base of individual ice shelves would sketch a pan-Antarctic map of ice shelf teleconnections, the importance of which has been indicated by the results in Chapter 2 and 4. Further, to build upon the results of Chapter 3, tracing pathways of AASW and MCDW inside the ice shelf cavities could be used to quantify how much mass loss is driven by surface or off-shelf water.

- Changing the reanalysis product used for surface relaxation from SOSE to ECCO2 would extend the possible simulation period from 2005-2011 to 1992-2017. While simulations with multi year forcing would still require a single year spin-up procedure (as outlined in Chapter 2) and, hence, would be very cost intensive, such experiments would allow to study interannual variability in the model.

- Using WAOM for future projections of ice shelf melting based on CMIP5 scenarios would comprise a valuable complement to the study by Naughten et al. (2018b).

In addition, such experiments would add valuable sample points to the behaviour of ice shelf cavity systems (described earlier). The most straightforward way to provide the necessary surface fluxes is to calculate the anomalies of CMIP5 projections compared to their present day state. Then, apply these anomalies to the surface forcing fields from this study. The resulting forcing fields will contain the spatial pattern of present day, but include trends and temporal changes from future scenarios.

Future model development efforts should prioritize improving WAOM and coupling WAOM with models of ice sheet flow.

- To improve WAOM the establishment of an evaluation matrix should be prioritized. A comparison of a wide array of melt rates from ApRES is already underway with the NECKLACE programme[1] and this could be used to tune the model parameters in an efficient manner (similar to Nakayama et al., 2017), and allow the community to compare models across different studies (discussed by Naughten et al., 2018b; discussed in Sect. 2.4). The optimisation could aim to minimise the model-data misfit of monthly mean melting at ApRES locations using root mean square differences (as done for the assessment of tidal accuracy, see Sect. 2.3.1 and King and Padman, 2005). The following parameters should primarily be targeted for optimisation: the ice-ocean boundary layer exchange coefficients for heat and salt, horizontal background diffusion, horizontal background viscosity, relaxation timescales of surface temperature and salinity, the tuning parameter for positive heat flux into the ocean (see 2.2.4 for more details about surface forcing).

- Further, incorporating a dynamic sea-ice model (similar to Naughten et al., 2018b) would simplify future projections and open the way to study questions for which sea ice interaction is critical. For example, what role do tides play in deep water formation on the Antarctic continental shelf.

- As mentioned above, updating the bathymetry and ice draft with new regional data (e.g. Millan et al., 2017) is considered essential to reduce remaining biases in WAOM and further improve tidal accuracy.

- Coupling WAOM to models of ice sheet flow is ultimately needed to quantify the long term consequences of small scale continental shelf ocean processes for

[1]NECKLACE programme: http://www.soos.aq/news/current-news/330-necklace-workshop-update.

Antarctic glacier retreat. The impact of WAOM's melt rates on instantaneous buttressing could be quantified by means of diagnostic ice sheet models (such as used by Reese et al., 2018). Such approaches, however, do not capture feedback mechanisms between ice sheet evolution and ocean driven ice shelf melting. For example, Chapter 3 highlights shallow ice melting driven by small scale processes in the surface ocean and there is evidence that this could precondition calving (Padman et al., 2012). Many ice shelves feature only a narrow safety band of structurally unimportant ice along the front (Fürst et al., 2016) and, thus, loss of frontal ice due to warming surface oceans could result in run-away glacier retreat. Further, Chapter 4 concludes the importance of tides for regional ice shelf melting. Tides circulate Antarctica in large waves and these waves are sensitive to near and far field ice sheet evolution (Mueller et al., 2018; Rosier et al., 2014). Thus tide driven changes in sub-ice shelf cavity geometry will affect tidal melting close by and in other regions. While the results of this thesis support that feedbacks between ice sheet evolution and small scale ocean processes related to tides and surface water advection impact Antarctic glacier retreat over long timescales, only coupled models can quantify these effects.

The future work suggested above, however, does not address a more fundamental technical challenge, highlighted by the outcomes of this thesis: How can we efficiently resolve kilometre-scale processes on the Antarctic continental shelf in larger scale climate simulations that target periods of up to tens of thousands of years? The answer to this question might lie in entirely new modelling approaches involving varying resolutions in space and time, as well as machine learning algorithms.

The computational costs associated with resolving kilometre-scale oceanic processes in global models and over climate relevant timescales is too large for current generation supercomputers (e.g. Asay-Davis et al., 2017). Variable horizontal resolution realised by grid nesting or unstructured grids might help to reduce the computational burden (Dinniman et al., 2016), but this will likely not be enough to make such simulations feasible in the near future.

The potential of variable temporal resolution has yet to be explored. Large scale ocean models contain different subsystems with widely varying characteristics in terms of spatial and temporal scales, dynamic behaviour, and accuracy requirements. For accurate Antarctic ice shelf-ocean interaction, the ACC, for example, does not need to be resolved with the same temporal and spatial resolution as cavity processes. This concept has partly been accommodated in models using varying grid spacing (realised by unstructured meshes, see e.g. Kimura et al., 2013; Timmermann et al., 2012, or grid nesting, see e.g. Debreu et al., 2012) and mode-splitting (resolving baroclinic and barotropic processes with different time step sizes; see, e.g. Shchepetkin and McWilliams, 2005). The time discretisations, however, are always uniform throughout the domain, making it impossible to be effective for all subsystems. To resolve all ocean phenomena important for Antarctic ice shelf melting at their respective scales, variable grid spacing would need to be combined with multirate time stepping. Multirate time stepping schemes allow for a temporal discretisation that varies in space and time. The time step lengths within each subsystem varies dynamically and automatically within the local dynamical stability constraints. An example of such a scheme has already been developed for a discontinous Galerkin model and applied to a realistic geophysical flow problem (Seny et al., 2013). Further, tipping points separate slow changing stages of Antarctic ice-ocean interaction from periods of rapid evolution (explained in, e.g. Pattyn et al., 2018). While the feedback mechanisms related to rapid changes will likely require a high temporal resolution for the entire period, slow changes might be represented well enough by a mean trend, which is updated from time to time by a short term, high resolution simulation.

Lastly, recent advances in machine learning might prove useful for detecting tipping points and guiding the time step size. Machine learning approaches have revolutionized pattern recognition in human faces and speech and first applications in climate modelling offer promising results (Rasp et al., 2018). To increase computational efficiency in ocean models, for example, the artificial intelligence could be trained on existing high resolution simulations to detect conditions that favour eddy formation. Then, in non-eddy resolving simulations, the algorithm would build and collapse high resolution nested grids to capture eddy life cycles. Further, rapid changes around Antarctica only occur when certain conditions are met, e.g. when grounding lines retreat to retrograde bed slopes (Gudmundsson et al., 2012) or CDW is lifted above the shelf break (Spence et al., 2014). Machine learning models could be trained to detect these conditions and decide about appropriate spatial and temporal resolutions. The basal mass balance in ice sheet simulations over glaciation time scales, for example, could be updated by snap-shots of coupled ice-sheet ocean models and the machine learning algorithm would decide about the updating frequency.

5.4 Final Remarks

Overall, the results of this thesis stress the importance of small scale Antarctic ice shelf-ocean interaction for global sea level rise and climate. The preceding chapters show that kilometre-scale processes related to tide-topography interactions or surface water advection under the ice front exert large controls over ice shelf basal melting around Antarctica and related pathways of melt water. In addition, previous studies have come to similar conclusions with regards to ocean eddies and their role in shoreward heat transport (e.g. Stewart et al., 2018) and the results presented here support these conclusions. These small scale processes impact ice shelf buttressing and water mass transformation on the continental shelf and, thus, play an important role for future changes in sea level rise and climate change. Representation of these small scale processes in models used for climate and sea level rise projections, however, will be challenging, due to the associated computational costs. The solution might lie in combining geophysical models with emerging technologies from the field of machine learning.

Appendix A

Antarctic Ice Shelf Melting From Observations and Models

BML (Gt/yr) w_b (m/yr) Area (10^3 km^2)	This study (MEaSURES)	This study (Bedmap2)	Rignot 2013 (IS flux)	error	Rignot 2013 (hr data)	Liu 2015 (non steady)	error	Liu 2015 (steady state)	error	Depoorter 2013	error	Hellmer 2004	Timmermann 2012	Dinniman 2015	Schodlock 2016	Mathiot 2017	Naughten 2018 (MetROMS)	Naughten 2018 (FESOM HR)
Total Antarctica	**973.34**	**1209.10**	**1500.00**	**237.00**	**896.87**	**1516.00**	**106.00**	**1290.00**	**110.00**	**1454.00**	**174.00**	**906.60**	**1600.00**	**664.00**	**1735.00**	**1864.00**	**642.00**	**739.00**
	0.70	0.82	0.85	0.10	0.64	1.10	0.10	0.90	0.10	0.94	0.11	0.80	1.20	-	1.16		0.52	0.56
	1523.33	1617.62	1561.40		1525.03	1542.11		1542.11		1555.00		1233.00	1510.00	-	1625.00		1349.00	1438.00
Amery	**10.56**	**10.03**	**35.50**	**23.00**	**34.50**	**95.00**	**8.00**	**63.00**	**9.00**	**39.00**	**21.00**	**17.65**	**174.00**			**207.00**	**91.00**	**71.40**
	0.19	0.18	0.58	0.40		1.70	0.10	1.10	0.20	0.65	0.35	0.35	2.90	1.10	1.25	3.73	1.64	1.29
	59.13	60.53	60.65			62.23		62.23		60.00		55.00	67.00			60.65	60.65	60.65
Totten & Moscow Uni.	**13.26**	**18.39**	**90.60**	**8.00**	**60.37**	**122.00**	**12.00**	**90.00**	**12.00**	**92.00**	**19.00**						**9.50**	**9.30**
	1.25	1.52	7.66	0.73		10.68	1.02	7.86	1.02	7.41	1.62				2.06		0.88	0.86
	11.60	13.23	11.83			12.55		12.55		12.00							11.83	11.83
Shackleton	**17.12**	**23.63**	**72.60**	**15.00**	**46.68**	**96.00**	**7.00**	**60.00**	**7.00**	**76.00**	**23.00**	**47.68**				**14.00**	**14.30**	**17.40**
	0.74	0.88	2.78	0.60		3.39	0.26	2.14	0.26	2.20	0.67	1.04			0.52	0.59	0.60	0.73
	25.26	29.21	26.08			31.00		31.04		35.00		50.00				26.08	26.08	26.08
Ross	**66.48**	**69.10**	**47.70**	**34.00**	**26.26**	**27.00**	**22.00**	**71.00**	**25.00**	**34.00**	**25.00**	**180.20**	**260.00**			**111.00**	**53.80**	**112.00**
	0.15	0.15	0.10	0.10		0.10	0.00	0.20	0.10	0.07	0.05	0.49	0.60	0.14	0.36	0.24	0.12	0.24
	490.40	493.61	500.81			497.78		497.81		477.00		401.00	475.00			500.81	500.81	500.81
Larsen C**	**9.08**	**13.12**	**20.70**	**67.00**	**3.90**	**55.00**	**7.00**	**6.00**	**8.00**	**18.00**	**8.00**	**38.13**	**48.00**			**46.00**	**18.20**	**54.70**
	0.22	0.26	0.45	1.00		1.00	0.10	0.10	0.20	0.30	0.14	0.63	1.00	0.35	1.47	1.08	0.43	1.29
	45.62	55.66	46.47			57.04		57.04		60.00		66.00	52.00			46.47	46.47	46.47
Filchner-Ronne	**90.25**	**87.09**	**155.40**	**43.00**	**94.35**	**10.00**	**32.00**	**82.00**	**37.00**	**50.00**	**40.00**	**119.70**	**138.00**			**123.00**	**46.00**	**115.40**
	0.23	0.22	0.32	0.10		0.00	0.10	0.20	0.10	0.12	0.09	0.32	0.35	0.19	0.25	0.30	0.11	0.28
	433.32	433.95	443.14			426.35		426.35		423.00		408.00	438.00			443.14	443.14	443.14
Brunt & Riiser-Larsen	**64.53**	**68.45**	**9.70**	**14.00**	**-1.83**	**20.00**	**10.00**	**37.10**	**10.00**	**26.00**	**16.00**	**165.90**	**65.00**			**39.00**	**29.20**	**34.60**
	0.89	0.93	0.12	0.20		0.25	0.12	0.50	0.14	0.33	0.20	2.38	0.94	0.67	0.28	0.53	0.40	0.47
	78.86	80.65	80.34			81.84		81.84		79.00		76.00	77.00			80.34	80.34	80.34
Fimbulisen & Jelbart*	**62.94**	**67.39**	**22.50**	**12.00**	**12.11**	**55.10**	**11.00**	**46.00**	**11.00**	**24.00**	**13.00**	**243.10**	**130.00**			**39.00**	**30.30**	**52.40**
	1.36	1.41	0.43	0.22		0.75	0.12	0.62	0.15	0.52	0.27	4.91	2.80	1.51	1.16	0.82	0.64	1.11
	50.54	52.20	51.69			78.06		78.06		46.00		54.00	53.00			51.69	51.69	51.69
Getz	**60.12**	**67.13**	**144.90**	**13.00**	**118.72**	**149.00**	**16.00**	**96.00**	**16.00**	**136.00**	**23.00**	**53.64**	**164.00**			**337.00**	**88.10**	**30.60**
	1.99	2.04	4.26	0.40		4.80	0.50	3.10	0.50	4.09	0.68	1.95	5.40	0.66	11.05	10.81	2.83	0.98
	33.05	35.86	34.02			33.74		33.74		33.00		30.00	35.00			34.02	34.02	34.02
Pine Island	**36.65**	**41.18**	**101.20**	**8.00**	**58.65**	**78.00**	**8.00**	**51.00**	**8.00**	**95.00**	**14.00**		**13.00**			**87.00**	**20.50**	**9.50**
	7.03	7.28	16.20	0.10		14.00	1.40	9.10	1.40	15.96	2.38		3.10	1.62	14.91	15.20	3.58	1.66
	5.69	6.18	6.25			6.09		6.09		6.00			5.00			6.25	6.25	6.25
Abbot	**73.63**	**80.93**	**51.80**	**20.00**	**37.50**	**35.00**	**7.00**	**46.00**	**7.00**	**86.00**	**22.00**	**18.60**	**59.00**			**52.00**	**25.00**	**36.60**
	2.60	2.65	1.75	0.60		1.20	0.20	1.60	0.20	2.72	0.70	0.55	2.10	0.34	1.23	1.91	0.92	1.35
	30.90	33.37	29.69			32.51		32.51		32.00		36.00	32.50			29.69	29.69	29.69
George VI***	**145.99**	**152.31**	**89.00**	**17.00**	**66.18**	**76.00**	**13.00**	**56.00**	**13.00**	**144.00**	**42.00**	**22.48**	**86.00**			**298.00**	**48.40**	**32.50**
	6.99	7.06	3.80	0.70		4.02	0.73	2.94	0.67	2.88	0.83	0.43	3.60	1.19	7.99	13.88	2.25	1.51
	22.79	23.50	23.43			20.59		20.59		50.00		57.00	27.00			23.43	23.43	23.43

Table A.1: Antarctic ice shelf basal mass loss from models and satellite observations. Modelling studies are Hellmer (2004); Timmermann et al. (2012); Dinniman et al. (2015); Schodlok et al. (2016); Mathiot et al. (2017); Naughten et al. (2018b) and studies using satellite observations and models of surface processes are Rignot et al. (2013); Depoorter et al. (2013); Liu et al. (2015). Rignot 2013 (hr data) estimates have been calculated by integrating the high resolution solution from Rignot et al. (2013) over ice shelf areas defined by MEaSURES boundaries (Mouginot et al., 2016). Naughten et al. (2018b) and Mathiot et al. (2017) area average melt rates for individual ice shelves have been calculated using area definitions from Rignot et al. (2013). Abbreviations are melt rate (w_b) and Basal Mass Loss (BML).

* Liu et al. (2015) also includes Vigrid, Nivil, Lazarev, Borchgrevink.

** Depoorter et al. (2013) also includes Larsen B.

*** Depoorter et al. (2013) and Hellmer (2004) includes Wilkens and Stange.

Appendix B

Computational Ice Shelf Masks

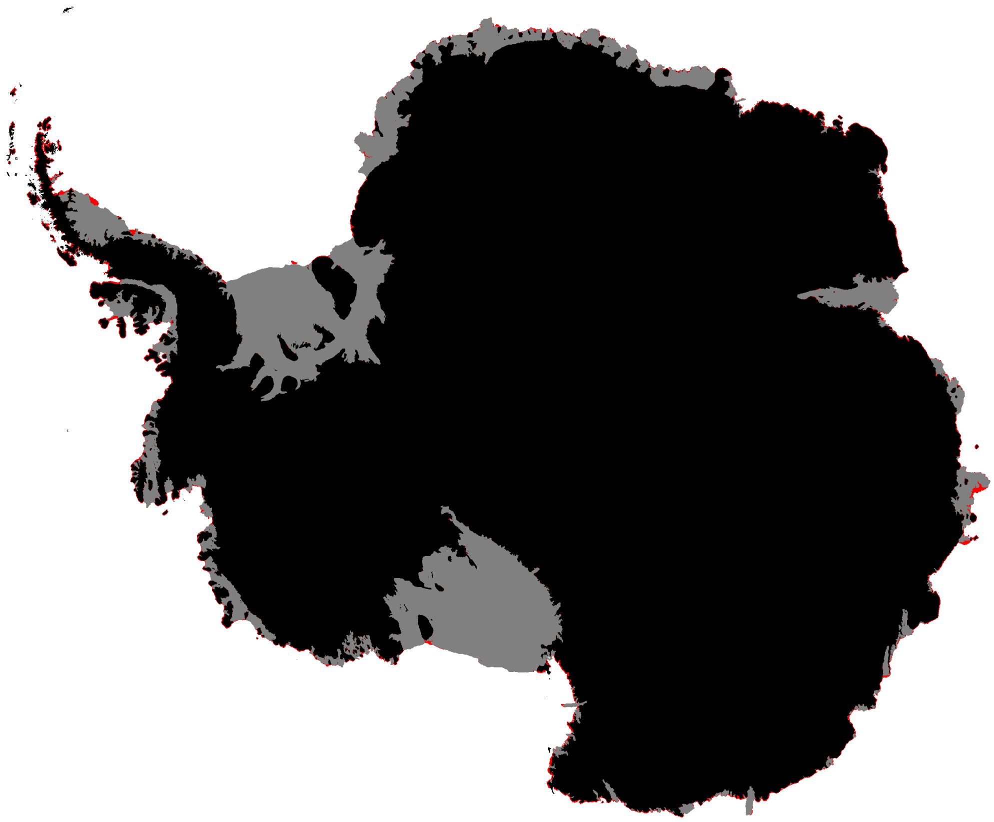

Figure B.1: Difference in ice area definition. Red areas show ice that is excluded when imposing ice shelf boundaries from the MEaSURES Antarctic Boundaries data set (Mouginot et al., 2016) onto the ice draft from Bedmap2 (Fretwell et al., 2013).

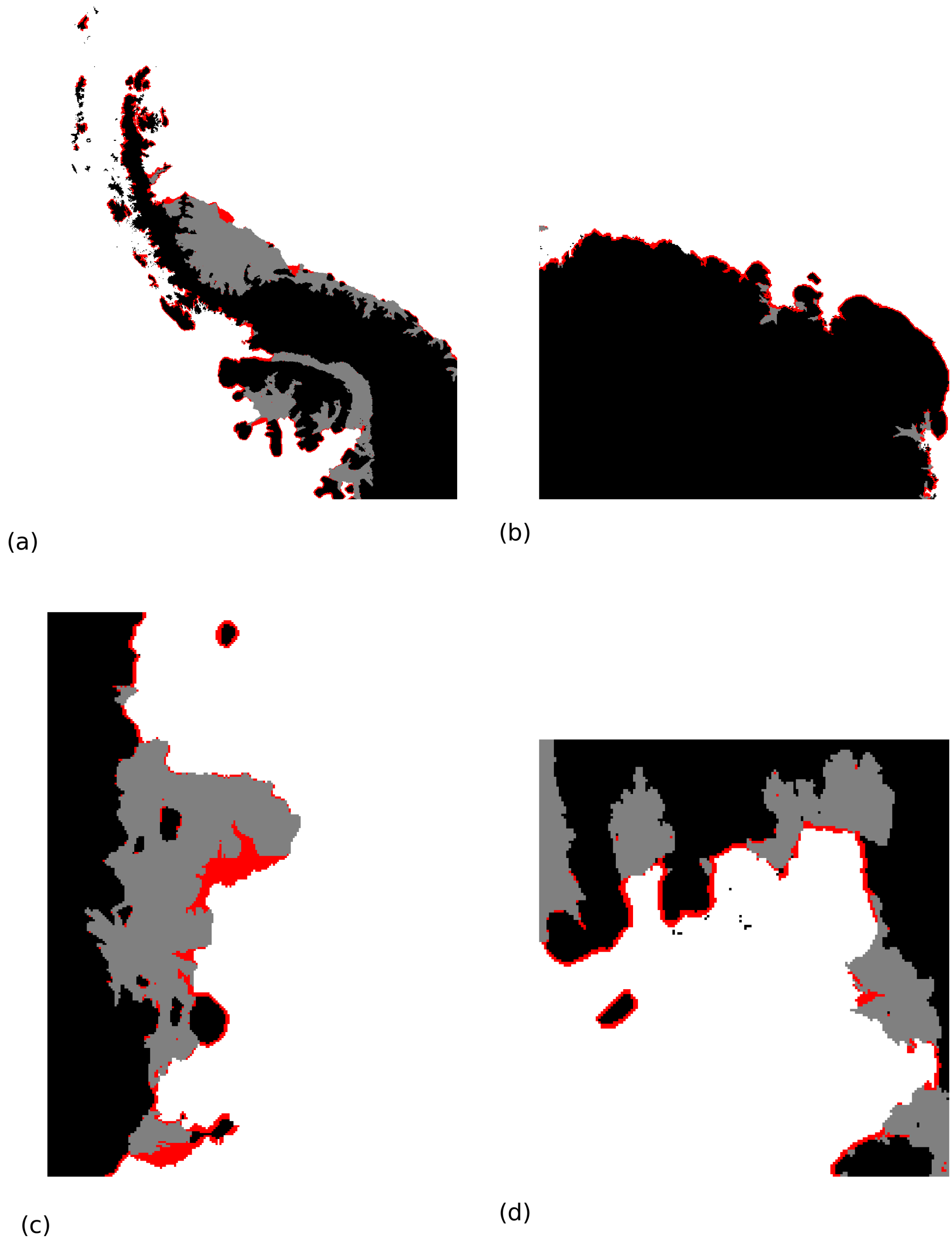

Figure B.1: Difference in ice area definition (cont.). Red areas show ice that is excluded when imposing ice shelf boundaries from the MEaSURES Antarctic Boundaries data set (Mouginot et al., 2016) onto the ice draft from Bedmap2 (Fretwell et al., 2013). Zoom-ins show (a) Antarctic Peninsula, (b) Enderby Land, (c) Shackleton Ice Shelf and (d) Pine Island Bay.

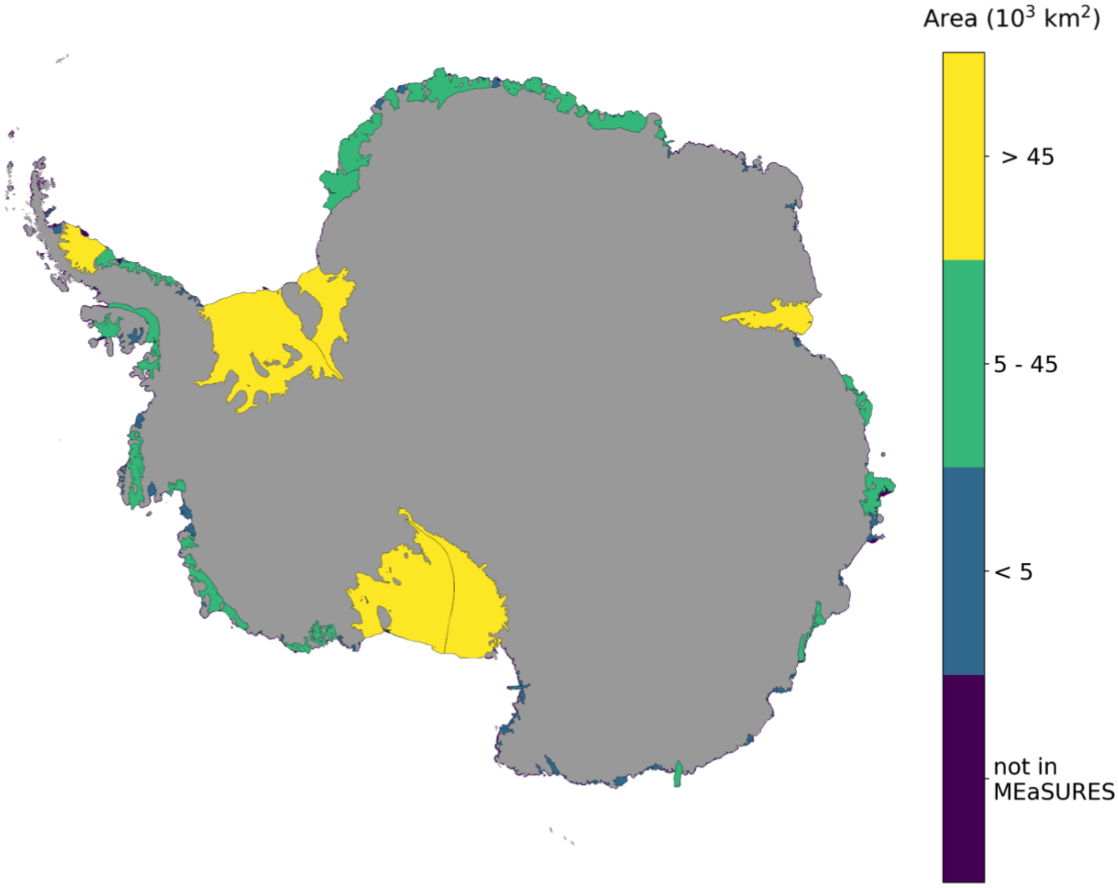

Figure B.2: Ice shelf size classes. Computational masks used to categorize mass loss contributions by ice shelf area. Some ice in the model (based on Bedmap2; Fretwell et al., 2013) is not present in the dataset used for ice shelf boundaries (MEaSURES Antarctic Boundaries dataset; Mouginot et al., 2016). Black lines are ice shelf boundaries.

Appendix C

Depth Distribution of Antarctic Ice Shelf Melting Compared Against Observations

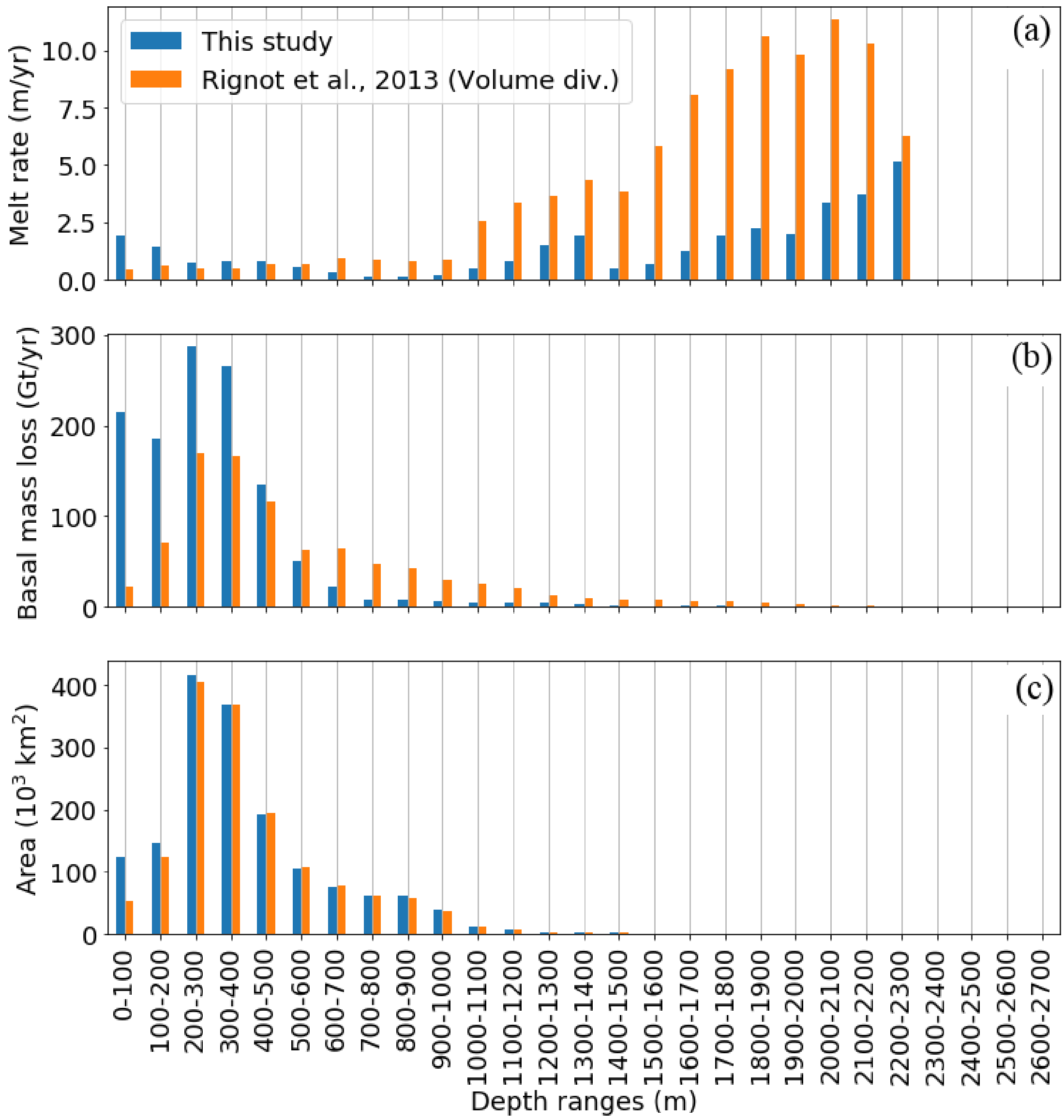

Figure C.1: The depth distribution of ice shelf melting compared against satellite estimates (Rignot et al., 2013). (a) ice shelf melting averaged over 100 m depth ranges. (b) Integrated mass loss using Bedmap2 ice draft (Fretwell et al., 2013). (c) Integrated area of ice shelf drafts. Satellite estimates confirm the importance of the mass loss contribution from ice shallower than 400 m.

Table C.1: Basal mass balance of Antarctic sectors over different depth ranges. 2007 area average melt rate, area and basal mass loss (negative is mass gain) for all depths and ice shelf parts shallower than 200 m deep and shallower than 400 m deep. Quantities are shown for 8 individual sectors (shown in Fig. 2.1) and total Antarctica based on Bedmap2 boundaries (Fretwell et al., 2013). The same qunatities for 176 individual ice shelves can be accessed online[1]. Abbreviations are melt rate (w_b) and Basal Mass Loss (BML)

	w_b (m/yr)	Area (10^3km^2)	BML (Gt/yr)	w_b <200m (m/yr)	Area <200m (%)	BML <200m (%)	w_b <400m (m/yr)	Area <400m (%)	BML <400m (%)
Prydz Bay	0.31	65.53	18.61	1.69	8.09	44.04	0.56	41.78	74.83
George V Coast	1.92	27.03	47.64	1.74	35.27	31.86	1.76	72.72	66.45
Sabrina Coast	1.60	73.26	107.14	2.14	43.21	57.81	1.67	77.08	80.67
Western East Antarctica	1.05	151.28	146.13	1.12	31.25	33.09	1.03	87.19	85.47
Ross Sea	0.33	531.49	162.78	0.94	7.52	21.19	0.29	76.39	65.61
Weddell Sea	0.39	607.57	215.95	0.92	12.62	29.93	0.68	45.72	80.27
Amundsen Sea	2.81	93.28	240.45	2.46	20.62	18.02	2.61	72.71	67.53
Bellingshausen Sea	4.30	68.18	268.34	3.37	59.31	46.53	4.16	97.28	94.17
Total Antarctica	0.81	1617.62	1207.04	1.62	16.70	33.22	0.99	65.11	78.88

[1] https://data.utas.edu.au/metadata/5d9ee4e6-99e8-46f0-b6c2-cc869a5e3d06

Appendix D

Model Configuration

Table D.1: Activated ROMS options in WAOM.

Category	**CPP option**	**Description**
Momentum equations	UV_COR	Coriolis term
	UV_VIS2	harmonic horizontal mixing
	UV_QDRAG	quadratic bottom friction
	UV_ADV	advection terms
	MIX_S_UV	mixing along constant S-surfaces
	SPLINES_VVISC	splines reconstruction of vertical viscosity
pressure gradient	DJ_GRADPS	splines density Jacobian
Tracer equations	TS_A4HADVECTION	4th-order Akima horizontal advection
	TS_A4VADVECTION	4th-order Akima vertical advection
	TS_DIF2	harmonic horizontal mixing
	SALINITY	having salinity
	MIX_ISO_TS	mixing on epineutral (constant RHO) surfaces
	NONLIN_EOS	nonlinear equation of state
	QCORRECTION	net heat flux correction
	SCORRECTION	freshwater flux correction
	SURFACE_OVERFLUX_FIX	corrections for not having a sea ice model
Vertical mixing	LMD_MIXING	Large et al. (1994) interior closure
	LMD_CONVEC	add convective mixing due to shear instability
	RI_SPLINES	splines reconstruction for Richardson Number
	LMD_DDMIX	double-diffusive mixing
	LMD_RIMIX	add diffusivity due to shear instability
	LMD_SKPP	surface boundary layer KPP mixing
	LMD_BKPP	bottom boundary layer KPP mixing
	LMD_NONLOCAL	nonlocal transport
	LMD_SHAPIRO	shapiro filtering boundary layer depth
Bottom stress	LIMIT_BSTRESS	limit the magnitude of bottom stress
Model configuration	SOLVE3D	3D primitive equations
	CURVGRID	curvilinear coordinates grid
	SPHERICAL	spherical grid
	AVERAGES	writing out NLM time-averaged data
	MASKING	land/sea masking
Analytical fields	ANA_BSFLUX	analytical bottom salinity flux
	ANA_BTFLUX	analytical bottom temperature flux
	ANA_SRFLUX	analytical surface shortwave radiation flux
	SPLINES_VDIFF	splines reconstruction of vertical diffusion
Ice shelf	ICESHELF	including ice shelf cavities
	LIMIT_ICESTRESS	limit the magnitude of ice shelf basal stress
	ICESHELF_3EQN_VBC	activate 3-equation ice/ocean thermodynamics
Tides	SSH_TIDES	imposing tidal elevation
	ADD_FSOBC	add tidal elevation to processed OBC data
	UV_TIDES	imposing tidal currents
	ADD_M2OBC	add tidal currents to processed OBC data
	RAMP_TIDES	ramping (over one day) tidal forcing
NetCDF input/output	PERFECT_RESTART	include perfect restart variables

Table D.2: Some key model parameters.

Parameter	**value (10/4/2 km resolution)**
Vertical resolution (# layers)	31
Vertical coordinate transformation equation #	2
Vertical coordinate transformation stretching function #	4
Surface stretching parameter	7
Bottom stretching parameter	8
Critical depth (m)	250
Baroclinic timestep (s)	900/360/180
Barotropic timestep (s)	25/10/5
Horizontal diffusivity ($m^2\,s^{-1}$)	50/20/10
Horizontal viscosity ($m^2\,s^{-1}$)	500/200/100
Tracer relaxation time scale (days)	365
Surface elevation relaxation time scale (days)	3
Barotropic momentum relaxation time scale (days)	3
Baroclinic momentum relaxation time scale (days)	3
Open boundary outflow/inflow nudging factor	365

APPENDIX E

Tide-Driven Ice Shelf Basal Mass Loss

Table E.1: Ice shelf average mass loss due to tides. For 139 individual ice shelves the table shows the area, melt rate (w_b) and Basal Mass Loss (BML) of the run with tides as well as its difference to the run without tides in absolute (e.g. $w_{b\ \text{tides}} - w_{b\ \text{no-tides}}$) and relative ($(w_{b\ \text{tides}} - w_{b\ \text{no-tides}})/w_{b\ \text{no-tides}}$) terms. Ice Shelf boundaries have been taken from the MEaSURES dataset (Mouginot et al., 2016).

	Area (10^3km^2)	**w_b (m/yr)**	**BML (Gt/yr)**	**w_b difference (m/yr)**	**BML difference (Gt/yr)**	**w_b and BML relative difference (%)**
Abbot	29.74	2.57	70.09	0.14	3.95	5.97
Abbot 1	0.24	1.11	0.24	-0.05	-0.01	-4.50
Abbot 2	0.34	0.92	0.28	-0.02	-0.01	-2.23
Abbot 3	0.35	0.39	0.13	-0.01	0.00	-2.31
Abbot 4	0.43	1.34	0.53	-0.02	-0.01	-1.53
Abbot 5	0.54	1.23	0.61	0.03	0.02	2.77
Abbot 6	0.26	0.65	0.15	-0.01	0.00	-1.91
Ainsworth	0.12	0.40	0.05	0.00	0.00	-0.20
Alison	0.08	6.66	0.49	-0.37	-0.03	-5.25
Amery	59.85	0.18	9.68	0.03	1.59	19.73
Astrolabe	0.11	0.72	0.07	-0.07	-0.01	-8.80
Atka	2.14	1.34	2.62	0.12	0.23	9.50
Aviator	0.92	0.26	0.22	0.03	0.02	11.48
Bach	4.61	3.49	14.74	1.11	4.70	46.80
Baudouin	33.40	0.74	22.62	0.18	5.55	32.53
Borchgrevink	21.11	1.51	29.15	0.12	2.27	8.46
Brahms	0.25	2.00	0.47	-0.04	-0.01	-2.15
Brunt Stancomb	36.66	1.03	34.63	0.05	1.65	4.99
Campbell	0.11	0.73	0.08	0.00	0.00	0.09
Cheetham	0.11	0.11	0.01	0.00	0.00	0.76
Chugunov	0.05	0.66	0.03	0.12	0.01	22.72
Conger Glenzer	1.63	3.08	4.58	0.72	1.08	30.78
Cook	3.63	3.72	12.38	-0.18	-0.61	-4.71
Cosgrove	2.94	3.40	9.16	0.13	0.35	4.00
Crosson	3.11	0.69	1.98	-0.05	-0.14	-6.59
Deakin	0.09	2.60	0.22	-0.28	-0.02	-9.64
Dennistoun	0.13	1.40	0.16	0.82	0.10	143.73
Dibble	1.56	2.81	4.01	0.12	0.18	4.59

Table E.1 continued

	Area (10^3km^2)	**w_b (m/yr)**	**BML (Gt/yr)**	**w_b difference (m/yr)**	**BML difference (Gt/yr)**	**w_b and BML relative difference (%)**
Dotson	5.16	0.70	3.33	-0.04	-0.18	-5.21
Drury	0.09	1.56	0.13	0.35	0.03	29.10
Drygalski	2.45	0.73	1.63	0.06	0.13	8.72
Edward VIII	0.43	0.56	0.22	-0.03	-0.01	-4.32
Ekstrom	6.90	1.06	6.69	0.23	1.45	27.69
Erebus	0.05	0.25	0.01	0.03	0.00	14.75
Ferrigno	0.18	6.43	1.04	-0.49	-0.08	-7.02
Filchner	102.07	0.06	5.51	-0.09	-8.31	-60.14
Fimbul	40.69	1.73	64.31	-0.19	-6.96	-9.77
Fisher	0.19	0.83	0.14	0.03	0.00	3.13
Fitzgerald	0.37	0.29	0.10	0.05	0.02	22.97
Flatnes	0.09	0.53	0.05	0.03	0.00	6.22
Fox Glacier	0.08	3.33	0.23	-0.06	0.00	-1.85
Francais	0.09	1.56	0.13	-0.15	-0.01	-8.80
Frost	0.26	2.33	0.56	-0.95	-0.23	-28.88
Garfield	0.06	0.46	0.03	0.02	0.00	4.00
Geikie Inlet	0.33	0.09	0.03	-0.01	0.00	-7.72
George VI	23.15	7.76	164.50	-0.20	-4.28	-2.53
Getz	33.50	1.95	59.97	0.17	5.33	9.76
Getz 1	0.60	1.09	0.59	-0.17	-0.09	-13.22
Gillet	0.17	0.90	0.14	0.33	0.05	56.87
Hamilton	0.21	2.88	0.56	-0.46	-0.09	-13.65
Hannan	0.40	0.30	0.11	-0.01	0.00	-2.17
Harbord Glacier	0.10	0.14	0.01	0.01	0.00	10.54
Helen	0.35	1.98	0.64	-0.05	-0.02	-2.60
Holmes	2.38	1.56	3.40	-0.73	-1.59	-31.87
Holt	0.08	1.11	0.08	0.28	0.02	33.78
Horn Bluff	0.17	1.67	0.26	0.07	0.01	4.17
Hoseason	0.14	1.15	0.15	0.03	0.00	2.32
Hull	0.19	0.97	0.17	0.02	0.00	2.21
Ironside	0.10	0.20	0.02	0.04	0.00	21.93

Table E.1 continued

	Area (10^3km^2)	w_b **(m/yr)**	**BML (Gt/yr)**	w_b **difference (m/yr)**	**BML difference (Gt/yr)**	w_b **and BML relative difference (%)**
Jackson	0.08	0.95	0.07	0.12	0.01	14.47
Jelbart	10.83	1.10	10.96	-0.09	-0.90	-7.58
Land	0.68	3.07	1.92	1.62	1.02	112.06
LarsenA	0.79	0.60	0.44	0.38	0.27	164.36
LarsenB	2.13	0.43	0.83	0.03	0.05	6.82
LarsenC	46.50	0.24	10.17	0.01	0.50	5.20
LarsenD	21.84	0.30	5.96	0.09	1.83	44.41
LarsenD 1	0.06	0.23	0.01	-0.13	-0.01	-35.59
LarsenE	1.25	0.68	0.78	0.29	0.33	74.79
LarsenF	0.87	0.34	0.27	0.12	0.09	51.86
LarsenG	0.47	0.17	0.07	-0.05	-0.02	-21.45
Lauritzen	0.60	2.02	1.10	0.40	0.22	24.98
Lazarev	8.73	0.73	5.80	-0.01	-0.10	-1.74
Lillie	0.86	2.58	2.02	0.26	0.21	11.37
Mariner	2.73	0.69	1.73	0.36	0.90	108.98
Marret	0.05	2.70	0.11	-0.37	-0.02	-12.21
Matusevitch	0.30	4.61	1.26	1.03	0.28	28.72
May Glacier	0.32	2.53	0.75	0.16	0.05	6.77
Mendelssohn	0.48	3.76	1.64	-0.22	-0.09	-5.41
Mertz	5.68	1.40	7.27	0.41	2.13	41.37
Moscow Uni.	6.10	1.38	7.72	-0.24	-1.31	-14.54
Moubray	0.18	0.27	0.04	0.15	0.02	132.46
Mulebreen	0.34	0.52	0.16	-0.03	-0.01	-4.82
Nansen	1.98	0.01	0.02	-0.01	-0.02	-48.74
Nickerson	6.83	3.67	22.93	-0.57	-3.55	-13.42
Ninnis	2.03	2.82	5.25	-0.04	-0.07	-1.23
Nivl	7.53	0.40	2.79	0.09	0.62	28.80
Noll	0.16	4.00	0.58	1.03	0.15	34.55
Nordenskjold	0.29	0.30	0.08	0.02	0.00	6.55
Parker	0.11	0.11	0.01	0.00	0.00	4.78
Philbin Inlet	0.11	0.47	0.05	-0.04	0.00	-8.37

Table E.1 continued

	Area (10^3km^2)	w_b **(m/yr)**	**BML (Gt/yr)**	w_b **difference (m/yr)**	**BML difference (Gt/yr)**	w_b **and BML relative difference (%)**
Pine Island	5.96	7.02	38.32	-0.33	-1.78	-4.44
Porter	0.08	2.04	0.14	-0.04	0.00	-1.71
Pourquoi Pas	0.20	4.91	0.90	-0.44	-0.08	-8.25
Prince Harald	5.66	1.27	6.61	-0.04	-0.23	-3.34
Publications	1.62	0.62	0.93	0.07	0.10	12.24
Quar	2.29	1.71	3.59	-0.08	-0.18	-4.66
Rayner Thyer	0.62	0.28	0.16	0.03	0.02	13.32
Rennick	3.32	0.25	0.77	0.08	0.25	48.91
Richter	0.15	7.91	1.07	-0.80	-0.11	-9.19
Riiser-Larsen	43.53	0.93	37.11	0.04	1.63	4.61
Ronne	333.48	0.26	78.32	0.14	43.93	127.75
Ross East	191.24	0.17	29.30	0.01	2.04	7.47
Ross West	300.76	0.16	43.57	0.04	11.41	35.46
Rund Bay	0.14	1.33	0.17	-0.08	-0.01	-5.60
Shackleton	26.43	0.80	19.37	0.10	2.50	14.84
Shirase	0.74	1.33	0.91	-0.01	-0.01	-1.10
Skallen	0.06	0.30	0.02	0.01	0.00	2.65
Slava	0.38	0.75	0.26	0.03	0.01	3.61
Sorsdal	0.19	1.24	0.21	0.03	0.01	2.79
Stange	8.29	2.50	18.98	0.24	1.83	10.66
Sulzberger	12.47	7.81	89.24	-0.96	-10.97	-10.94
Suter	0.05	0.11	0.00	0.07	0.00	172.75
Suvorov	0.22	1.02	0.21	0.18	0.04	20.85
Swinburne	0.93	12.74	10.88	-0.92	-0.78	-6.71
Thwaites	4.51	7.36	30.36	-0.54	-2.22	-6.82
Tinker	0.15	0.03	0.00	-0.01	0.00	-13.99
Totten	6.14	1.72	9.66	0.27	1.50	18.39
Tracy Tremenchus	2.81	0.86	2.20	0.02	0.05	2.46
Tucker	0.46	0.75	0.32	0.42	0.18	125.72
Underwood	0.20	2.26	0.42	-0.09	-0.02	-3.75

Table E.1 continued

	Area (10^3km^2)	**w_b (m/yr)**	**BML (Gt/yr)**	**w_b difference (m/yr)**	**BML difference (Gt/yr)**	**w_b and BML relative difference (%)**
Utsikkar	0.09	0.73	0.06	0.01	0.00	1.51
Venable	3.31	4.65	14.07	-0.20	-0.62	-4.20
Verdi	0.14	5.41	0.71	-0.13	-0.02	-2.29
Vigrid	2.10	1.07	2.07	0.03	0.06	3.16
Vincennes Bay	1.14	1.99	2.08	-0.06	-0.06	-2.80
Voyeykov	0.69	1.66	1.06	-0.07	-0.05	-4.29
Walgreen Coast 1	0.11	5.95	0.62	-0.55	-0.06	-8.50
Walgreen Coast 2	0.03	2.84	0.08	-0.40	-0.01	-12.40
Watt Bay	0.11	0.68	0.07	-0.11	-0.01	-13.83
West	15.86	1.69	24.58	0.09	1.35	5.79
Whittle	0.11	1.06	0.10	-0.28	-0.03	-20.75
Wilkins	13.04	1.31	15.61	-0.06	-0.76	-4.65
Williamson	0.20	2.67	0.49	-0.24	-0.04	-8.14
Wilma-Robert-Downer	0.91	0.50	0.42	-0.03	-0.03	-5.72
Withrow	0.72	4.09	2.70	-0.83	-0.55	-16.94
Wordie (Harriott)	0.09	0.12	0.01	-0.02	0.00	-12.46
Wordie (Prospect)	0.20	0.19	0.03	0.00	0.00	-1.19
Wylde	0.18	0.22	0.04	0.08	0.01	58.21
Zubchatyy	0.33	0.80	0.24	-0.07	-0.02	-7.50

Appendix F

Additional ocean evaluation

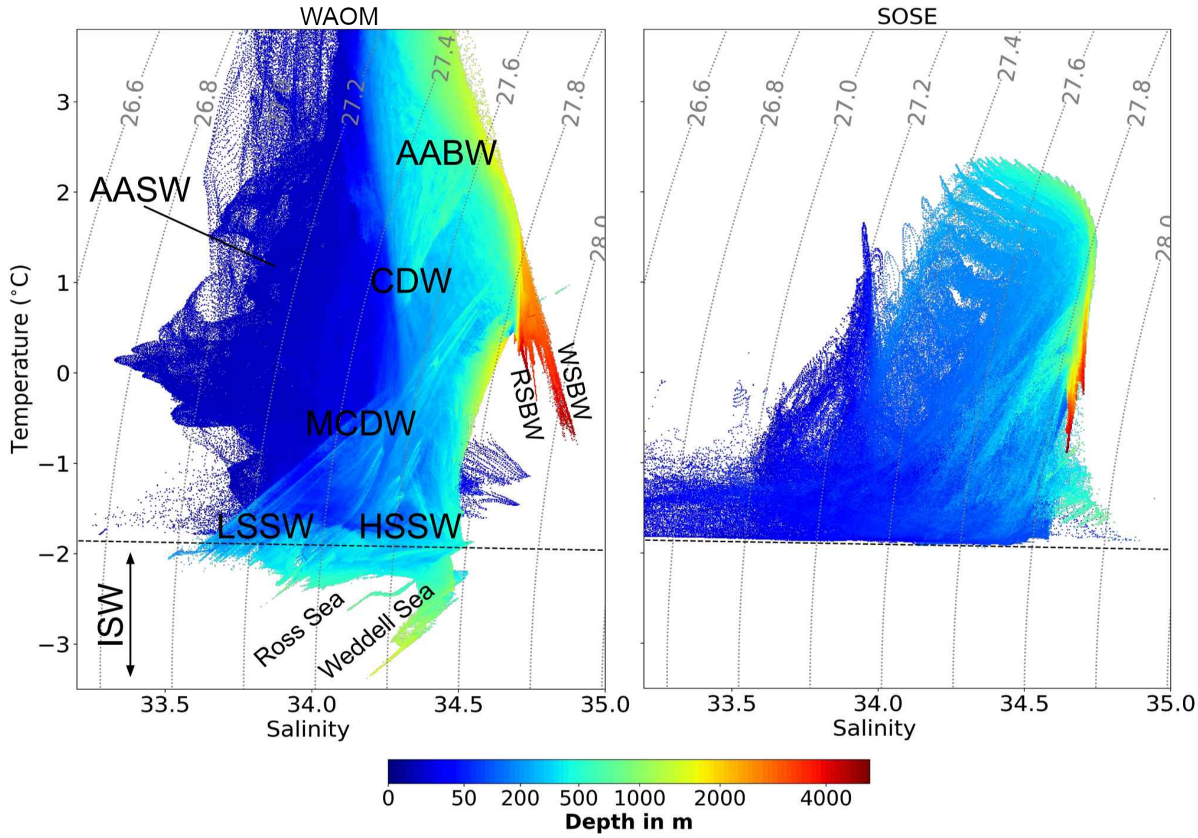

Figure F.1: Water masses resolved by WAOM and SOSE. Potential temperature-salinity-depth distribution of the water masses apparent south of 65°S in (a) WAOM and (b) SOSE. Each grid cell in either model has been sorted into 1000x1000 temperature and salinity bins and the depth shown for each bin is the volume-weighted average of all the grid cells in this bin. The dashed black lines show the freezing point at the surface and the dotted grey lines are potential density anomaly contours (in km $m^{-3}-1000$; referenced to the surface). Labels in (a) indicate the water masses Antarctic Bottom Water (AABW), Weddell Sea Bottom Water (WSBW), Ross Sea Bottom Water (RSBW), Circumpolar Deep Water (CDW), Modified Circumpolar Deep Water (MCDW), Low-Salinity Shelf Water (LSSW), High-Salinity Shelf Water (HSSW), Antarctic Surface Water (AASW) and Ice Shelf Water (ISW). Remaining labels indicate specific regions from where some water masses originate (also see Fig. 2.9).

DATA DISTRIBUTION PLOT:

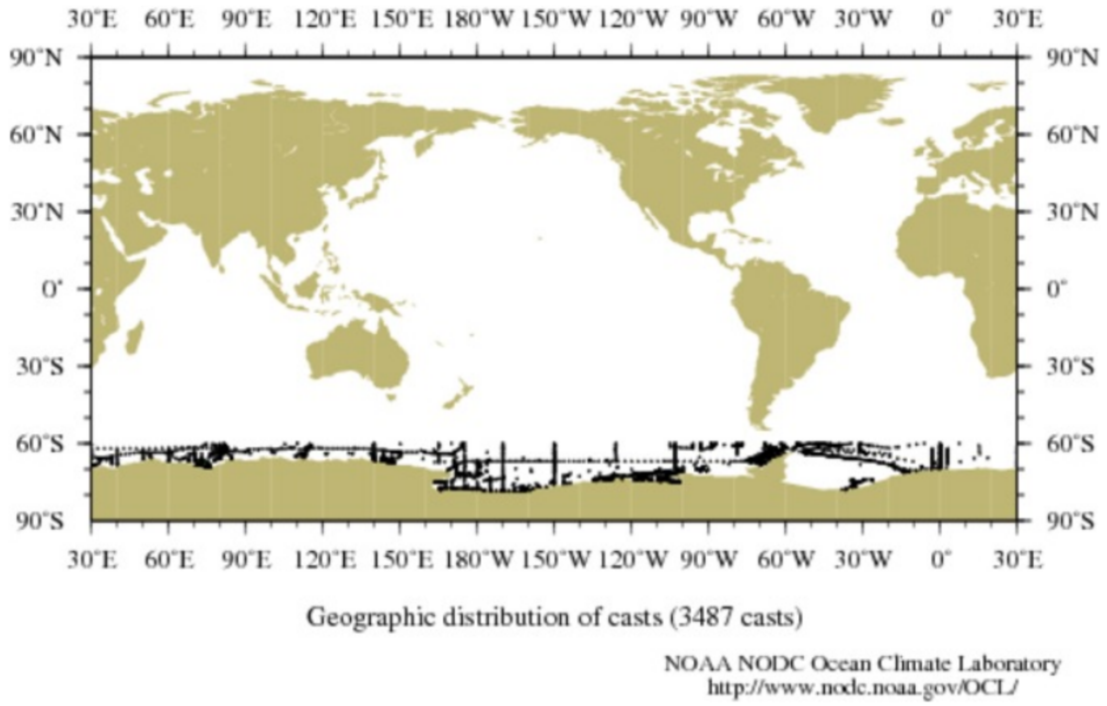

COPY OF YOUR SEARCH CRITERIA:

DEEPEST MEASUREMENTS:>	**400**
OBSERVATION DATES:	**Year** from 2005 to 2017
GEOGRAPHIC COORDINATES:	**Longitude** from -180.0000 to 180.0000; **Latitude** from -60.0000 to -80.0000
DATASET:	CTD,UOR
MEASURED VARIABLES (extract):	Temperature, Salinity

Figure F.2: Sampling distribution underlying WOA18 data. Only CTD casks that reached a depth below 400 m and measured both, Temperature and Salinity, are shown. Distribution clearly shows summer ship tracks (e.g. along longitudes: 170W, 150W, 102W, 40E, 60E, 70E and 175E). The figure has been produced using the World Ocean Database Search Query web application: https://www.nodc.noaa.gov/OC5/SELECT/dbsearch/dbsearch.html.

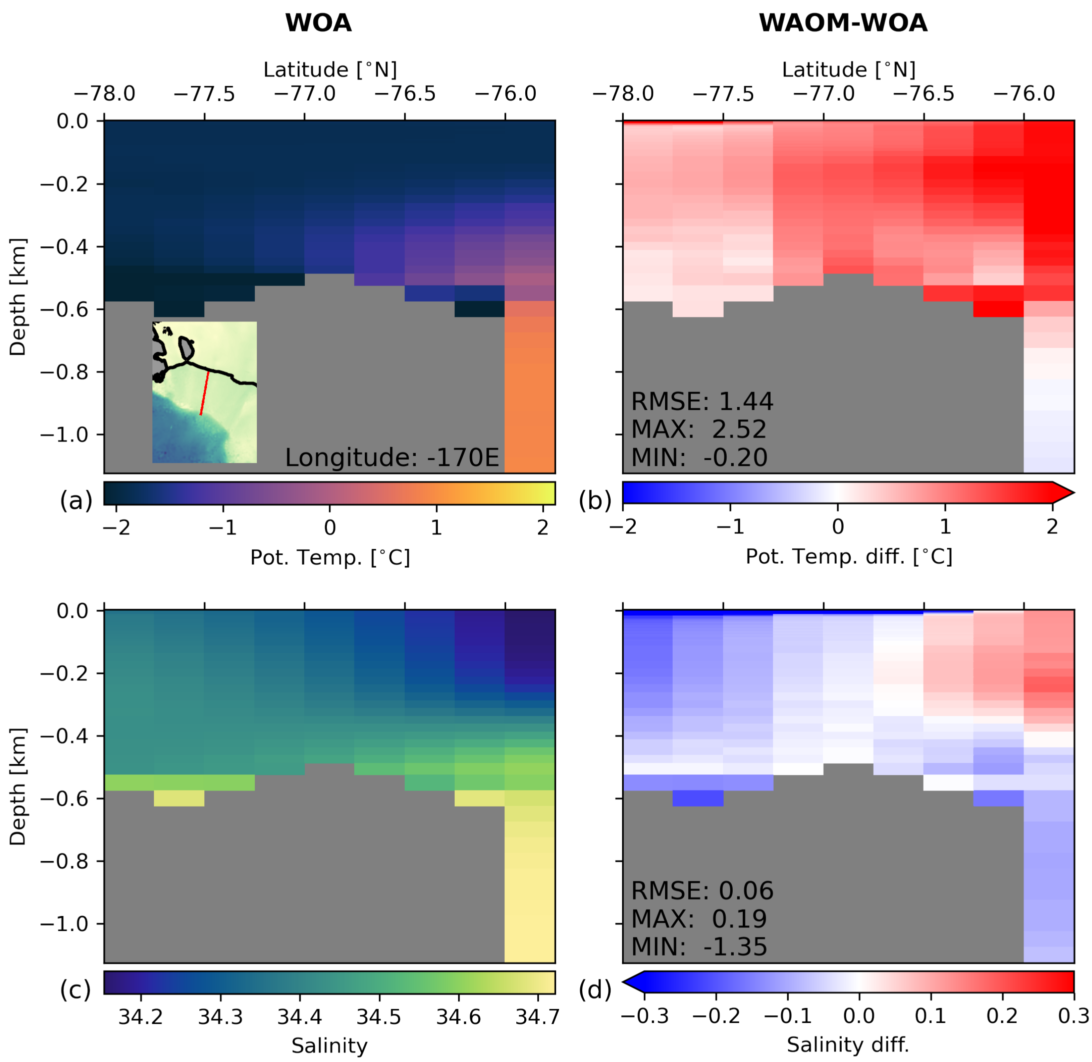

Figure F.3: Temperature and Salinity transect on the Ross Sea continental shelf (170W) compared against observations. (a) and (c) are WOA18 2005-2017 summer (DJF) climatology mean and (b) and (d) are different from WAOM 2007 summer mean (WAOM-WAO18). WAOM data has been interpolated to WOA18 grid using nearest neighbors.

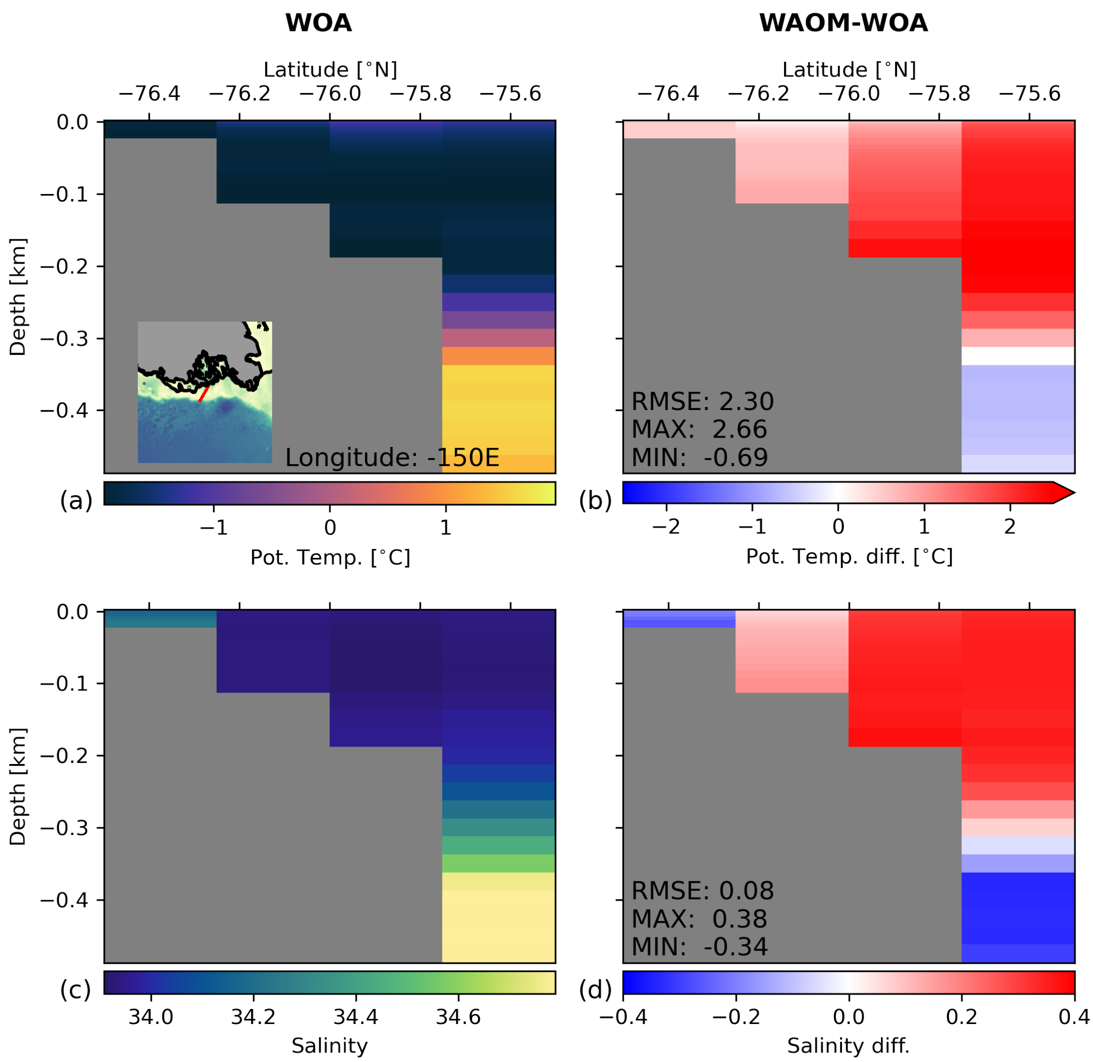

Figure F.4: Temperature and Salinity transect on the Ross Sea continental shelf (150W) compared against observations. (a) and (c) are WOA18 2005-2017 summer (DJF) climatology mean and (b) and (d) are different from WAOM 2007 summer mean (WAOM-WAO18). WAOM data has been interpolated to WOA18 grid using nearest neighbors.

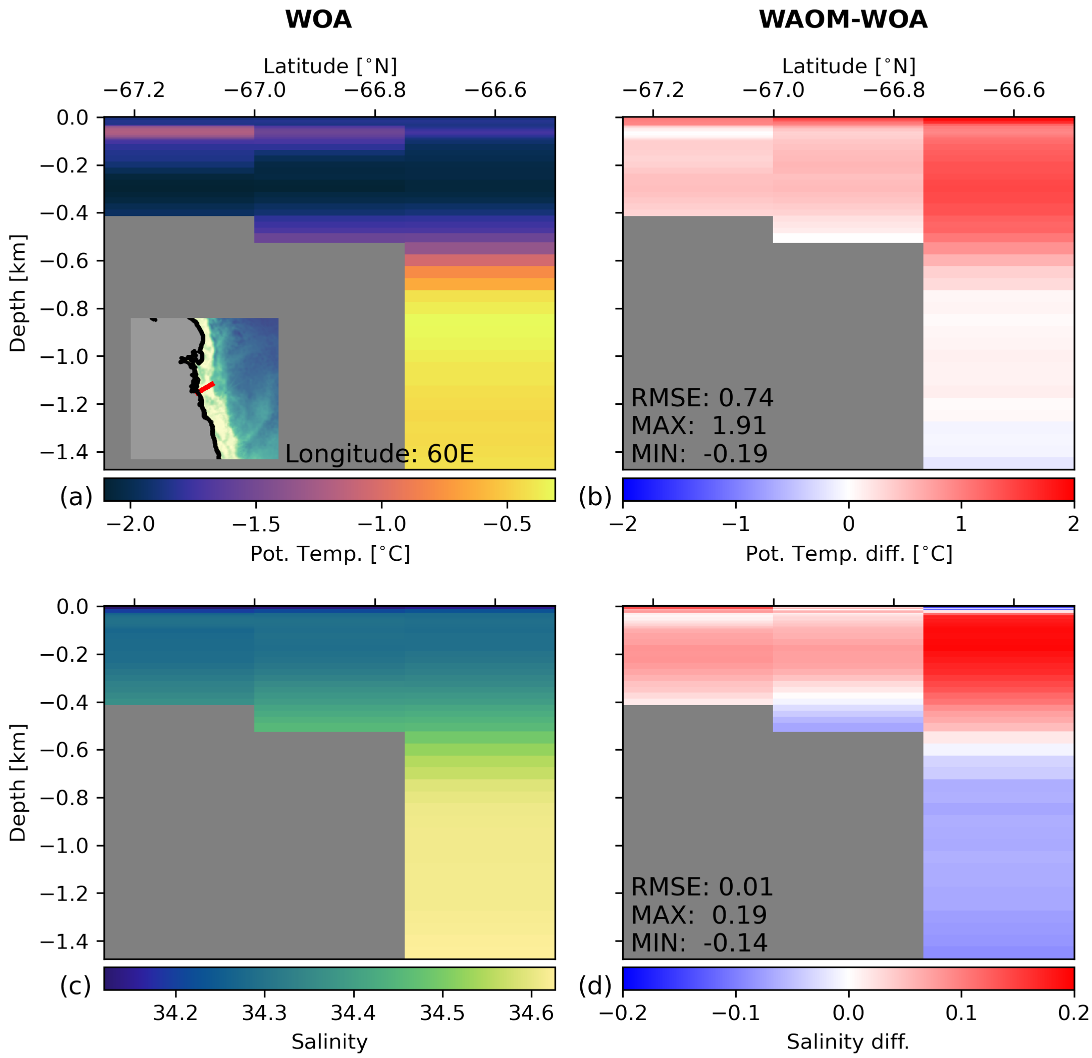

Figure F.5: Temperature and Salinity transect on the East Antarctic continental shelf (60E) compared against observations. (a) and (c) are WOA18 2005-2017 summer (DJF) climatology mean and (b) and (d) are different from WAOM 2007 summer mean (WAOM-WAO18). WAOM data has been interpolated to WOA18 grid using nearest neighbors.

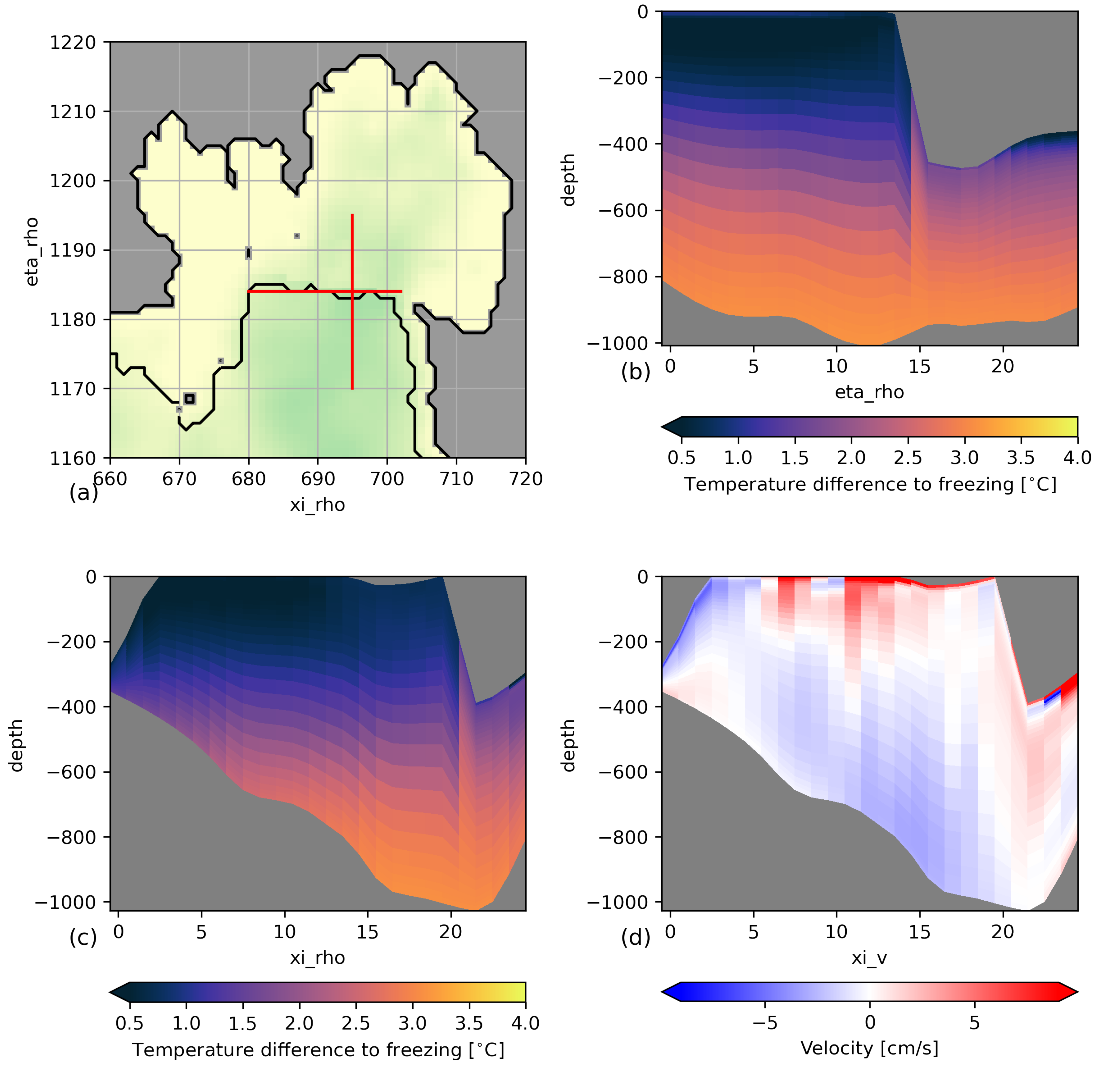

Figure F.6: Ocean conditions at the Pine Island Glacier front. (a) shows the transect locations in model coordinates. (b) and (c) show the in-situ temperature difference to freezing across and along the cavity entrance. (d) presents the velocity magnitude across the cavity entrance (positive is out of the cavity). Colorbars have been scaled to values from Jacobs et al. (2011) (their Fig. 2 and 4). While velocities are comparable to observed ones, deep ocean temperatures are about 1.0 °C to cold.

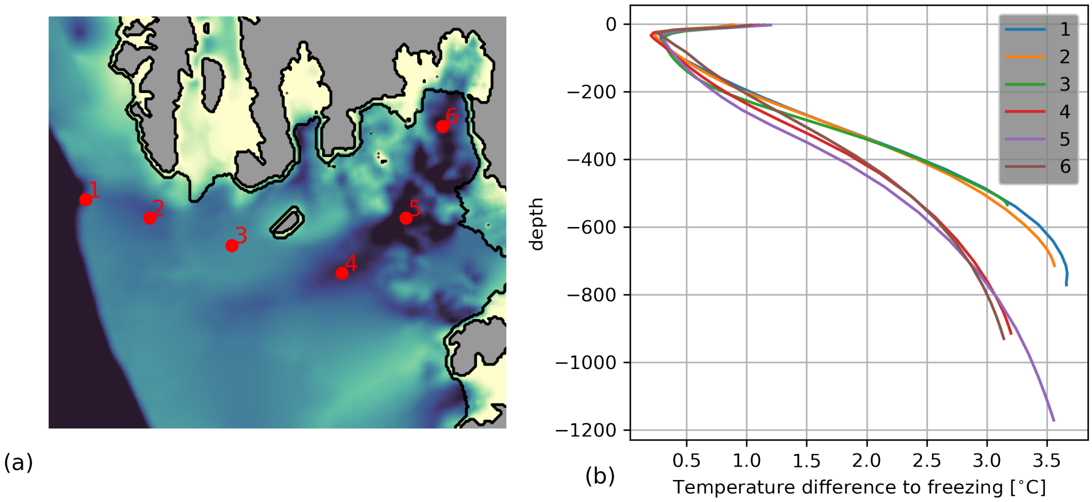

Figure F.7: Temperature change along the Pine Island Bay trough. (a) presents locations of (b) profiles of insitu temperature difference to freezing. Locations have been chosen to reflect the observations presented by Jacobs et al. (2011) (see their Fig. 1 for CTD locations and their Fig. 2 for the respective temperature estimates. While CDW temperatures close to the shelf break agree well with observations (about 3.5 °C above freezing), water within deep bathymetric troughs that lead up to the Pine Island Glacier are to cold (by about 1.0 °C.)

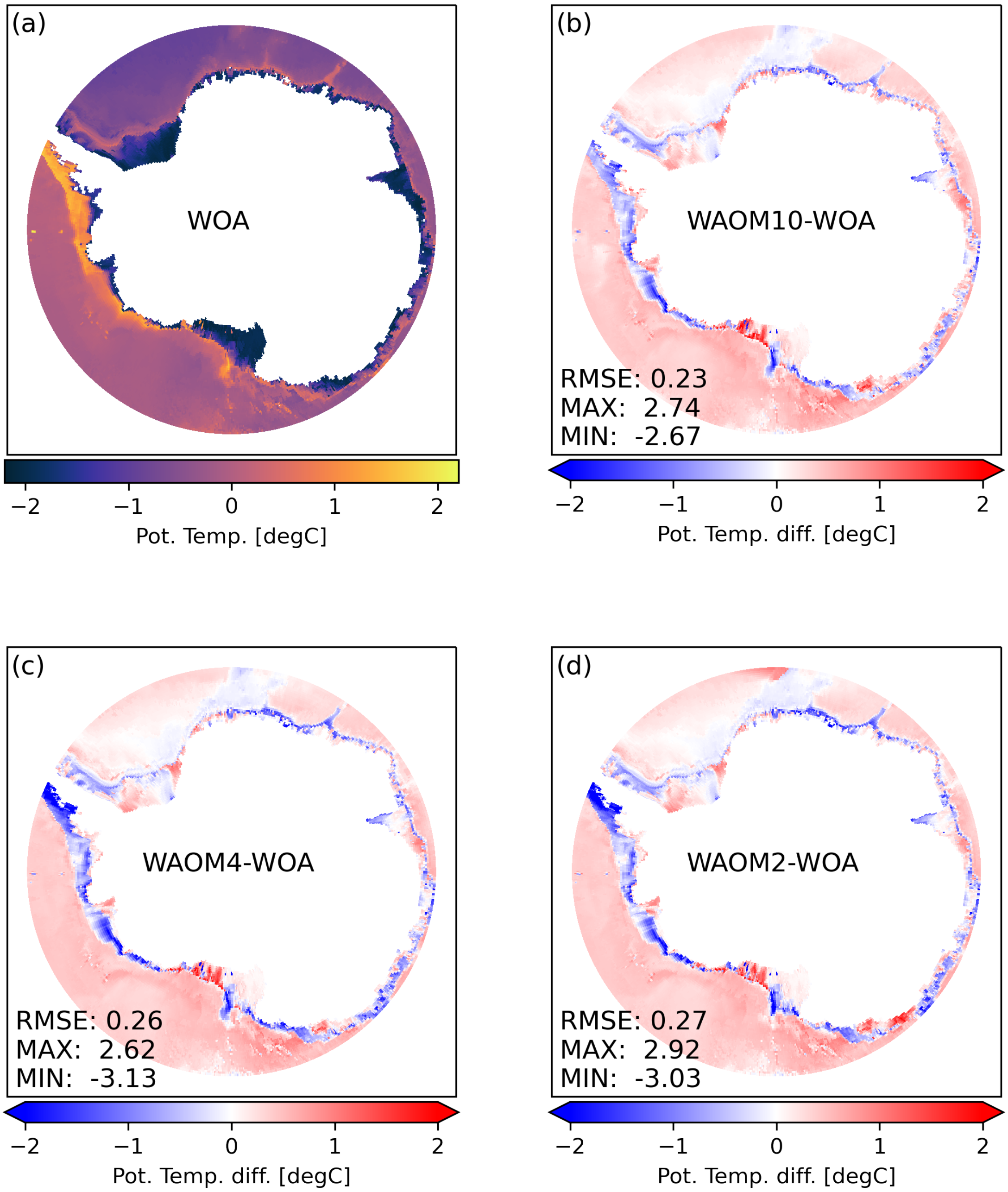

Figure F.8: Mean bottom water potential temperature at different resolutions compared against observations. (a) WOA18 bottom layer potential temperature mean from 2005 to 2017 and difference to 2007 mean from WAOM at (b) 10 km, (c) 4 km and (d) 2km horizontal resolution. WAOM has been interpolated on WOA18 grid prior to comparison ($\frac{1}{4}$ deg; nearest neighbors horizontally and vertically).

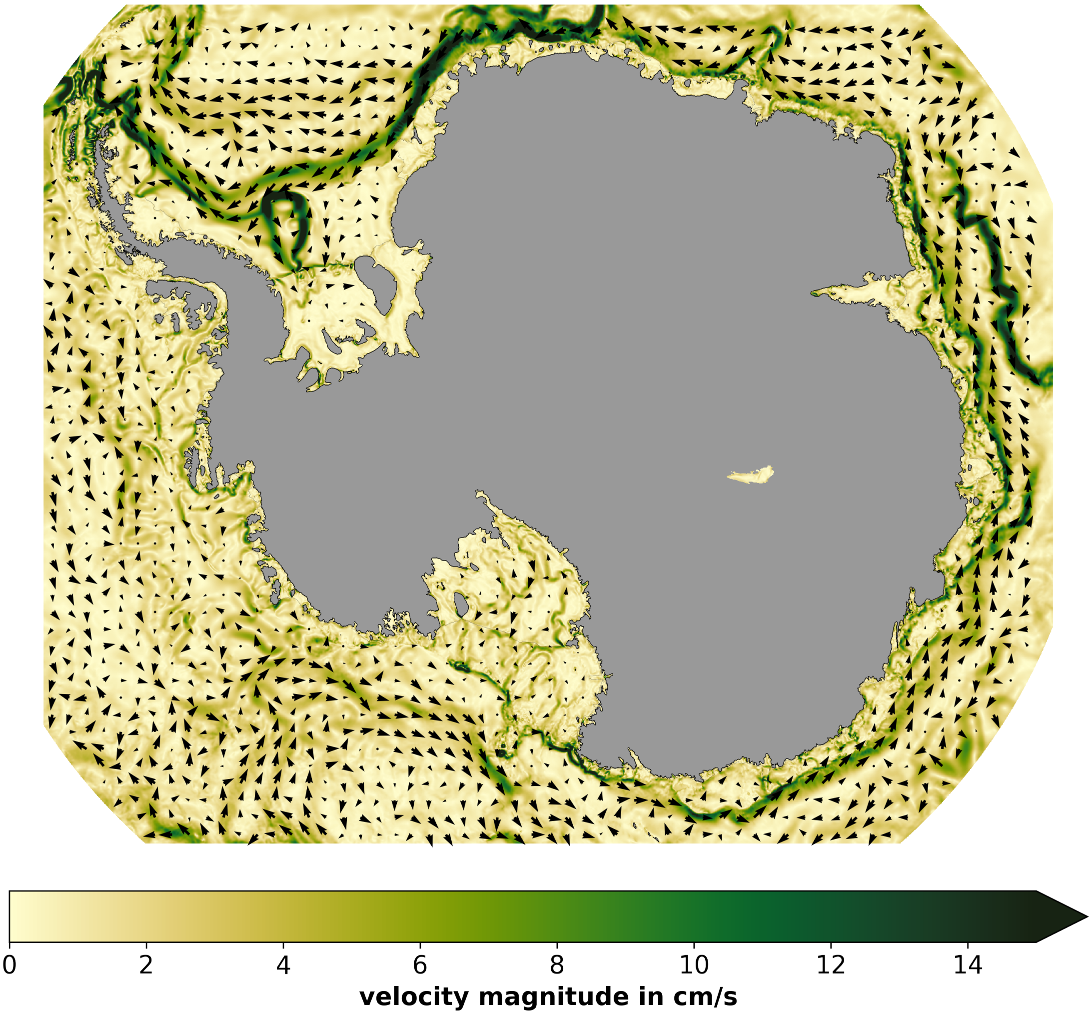

Figure F.9: Mean barotropic currents in WAOM. Colors denote 2007 mean barotropic current velocity magnitude and arrows indicate direction. WAOM reproduces known features, such as the southern limb of the ACC around the Kerguelen Plateau, the southern limbs of the Ross and Weddell Sea Gyres, the slope current (e.g. around East Antarctica) and coastal currents (apparent in, e.g. Prydz Bay and in front of the Totten Ice Shelf).

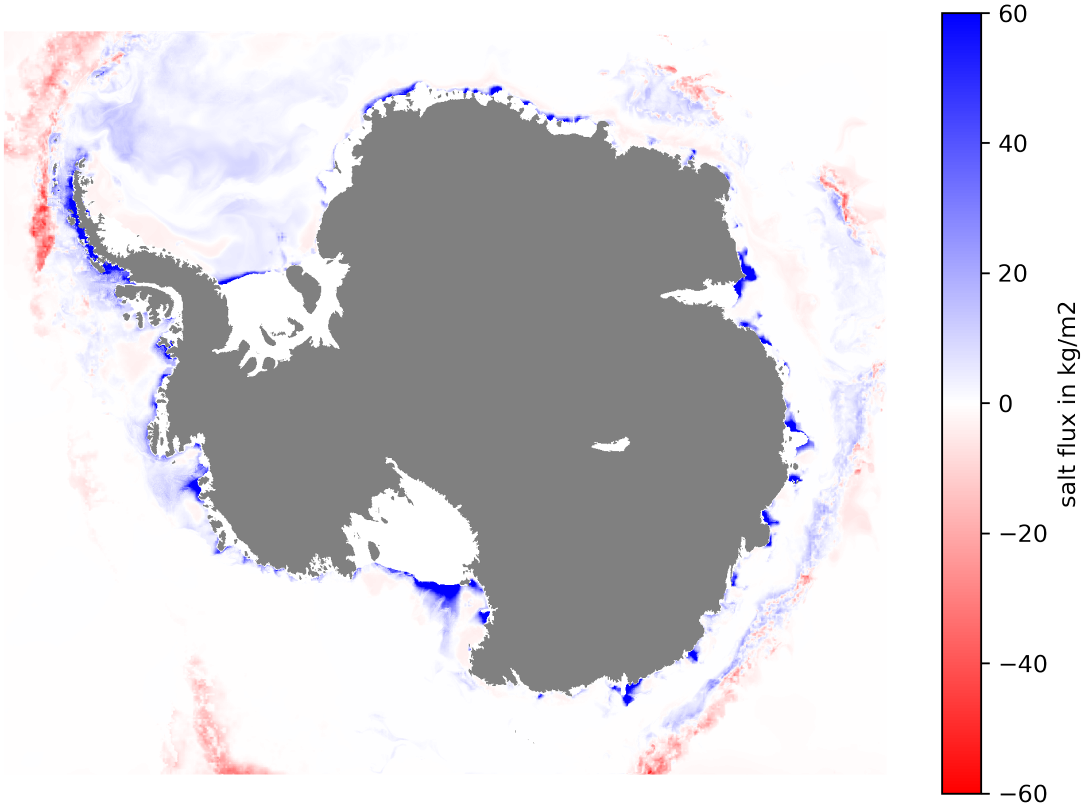

Figure F.10: WAOM's surface salt flux integrated over June, July and August 2007. Positive is into the ocean. The values are derived from model output, that is after relaxation to surface salinity from SOSE and tuning has been applied. The colorbar has been scaled to ease a comparison against observational estimates from Tamura et al. (2011).

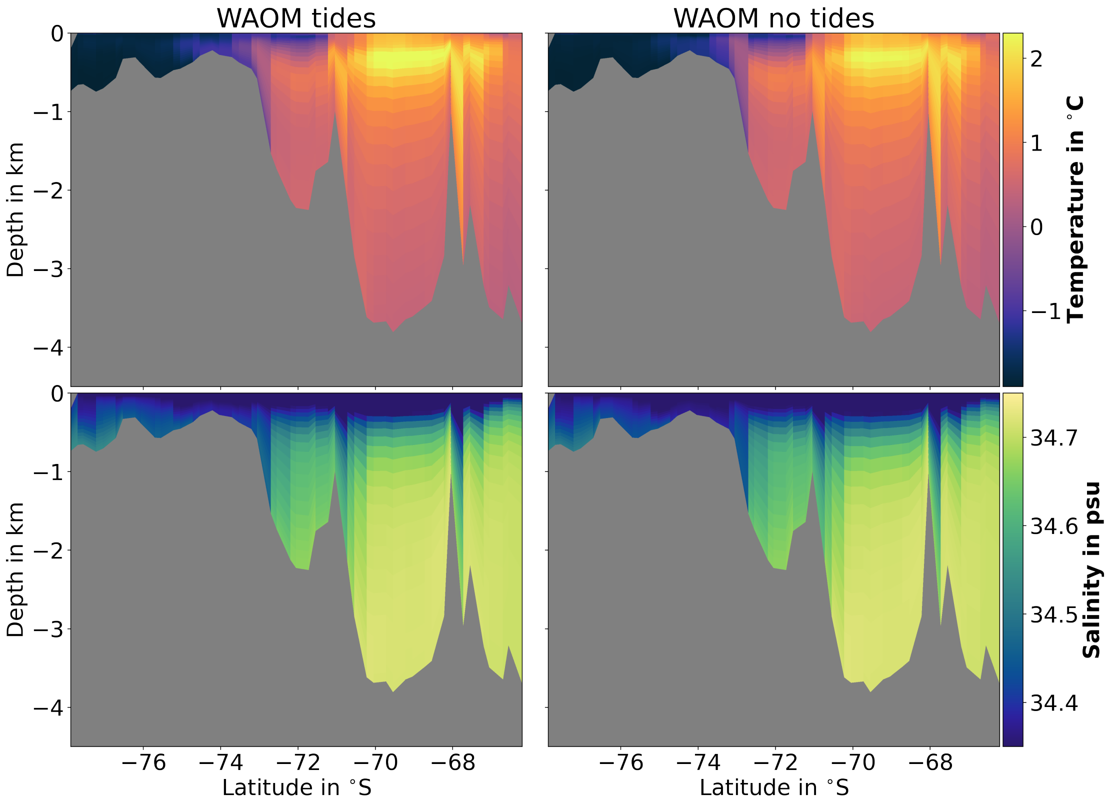

Figure F.11: 2007 mean Temperature-Salinity distribution of WAOM at 4 km horizontal resolution in the Ross Sea along 180 °W, with and without tides. Transect locations are shown in Figure 2.1. Figure 2.8b shows the same transect for SOSE and WAOM at 2 km resolution.

Appendix G

Additional Tide evaluation

Table G.1: Stations with the largest bias in tidal accuracy. For each constituent, the stations with the largest 5 % bias in relative amplitude difference compared to Antarctic Tide Gauge Records are listed. Figure G.1 shows the locations of these stations.

	id	Station name	ampl [m]	rel ampl diff [%]
M2	23	20080- Mawson	0.06	194.83
	28	Base (gravity measurements on the RIS)	0.15	194.05
	34	LAS	0.07	235.21
	37	RI (gravity measurements on the RIS)	0.17	266.65
	73	Ross Ice Shelf DFLT	0.43	337.48
S2	30	c16 (gravity measurements on the RIS)	0.04	195.50
	35	McMurdo	0.07	344.74
	36	O19 (gravity measurements on the RIS)	0.05	249.04
	73	Ross Ice Shelf DFLT	0.43	308.28
	78	Scott Base Tide Gauge	0.06	177.63
O1	29	c13 (gravity measurements on the RIS)	-0.13	39.99
	33	J9 (gravity measurements on the RIS)	-0.15	36.81
	36	O19 (gravity measurements on the RIS)	-0.12	36.19
	55	Lokcroy	-0.29	100.00
	62	Moutonnee Lake (Looks Bad)	0.10	64.60
K1	7	PTC_4_2_03	-0.20	54.40
	55	Lokcroy	-0.29	100.00
	58	Seymour Is. (Marambio Base)	-0.21	51.49
	59	Larsen Nunatak (Matenzio Base)	-0.17	40.26
	62	Moutonnee Lake (Looks Bad)	0.13	72.50

Figure G.1: Locations of Stations listed in Table G.1

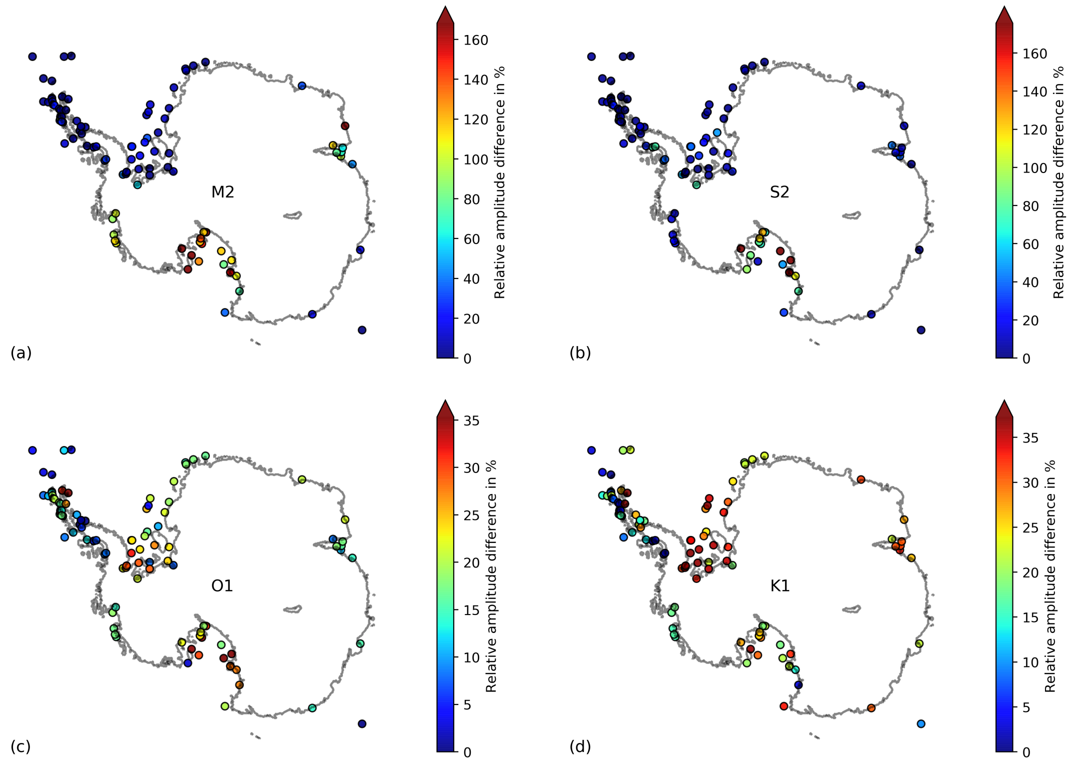

Figure G.2: Spatial distributions of tidal height accuracy. Relative amplitude differences between the model solution and Antarctic Tide Gauge records ($[H_{WAOM} - H_{ATG}]/H_{ATG}$) are shown for the major tidal constituents (a) M2, (b) S2, (c) K1 and (d) O1. The colorbar has been truncated at the 95% quantile. Differences for stations exceeding this limit are presented in Table G.1 and Figure G.1.

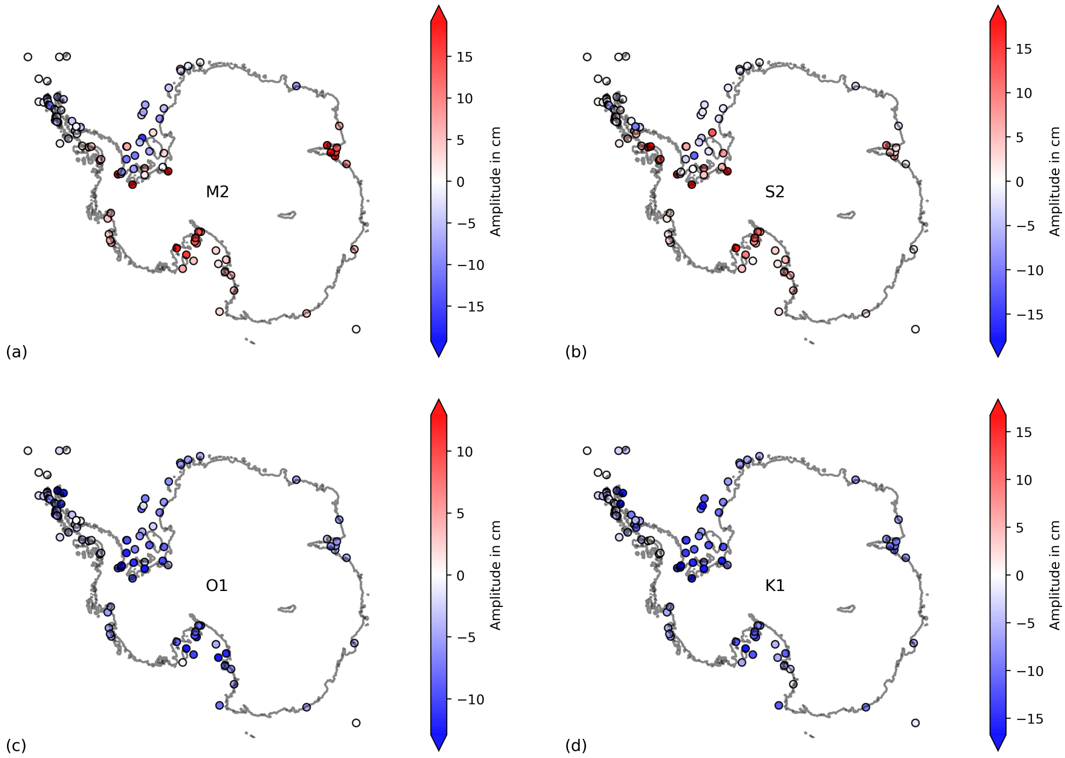

Figure G.3: Spatial distributions of tidal height accuracy in absolute terms. Amplitude differences between the model solution and Antarctic Tide Gauge records ($H_{WAOM} - H_{ATG}$) are shown for the major tidal constituents (a) M2, (b) S2, (c) K1 and (d) O1. The colorbar has been truncated at the 95% quantile.

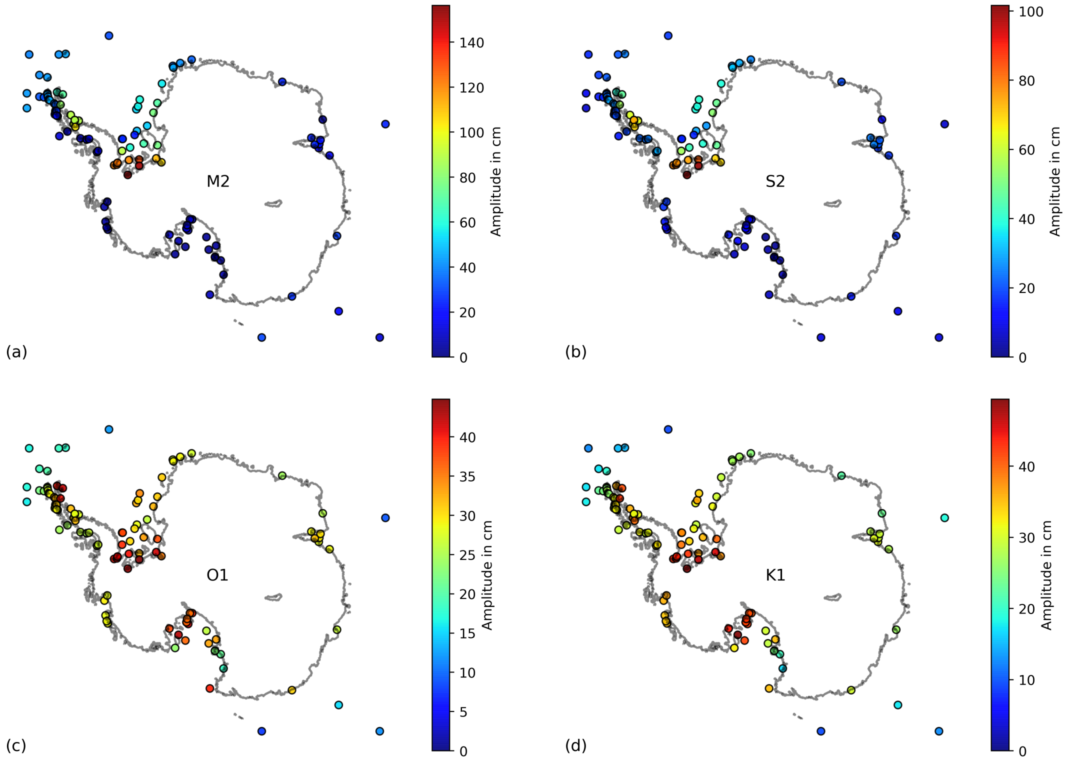

Figure G.4: Spatial distributions of tidal height amplitude. Tidal height amplitude of the Antarctic Tide Gauge records (H_{ATG}) are shown for the major tidal constituents (a) M2, (b) S2, (c) K1 and (d) O1.

Appendix H

Drivers of shallow ice melting

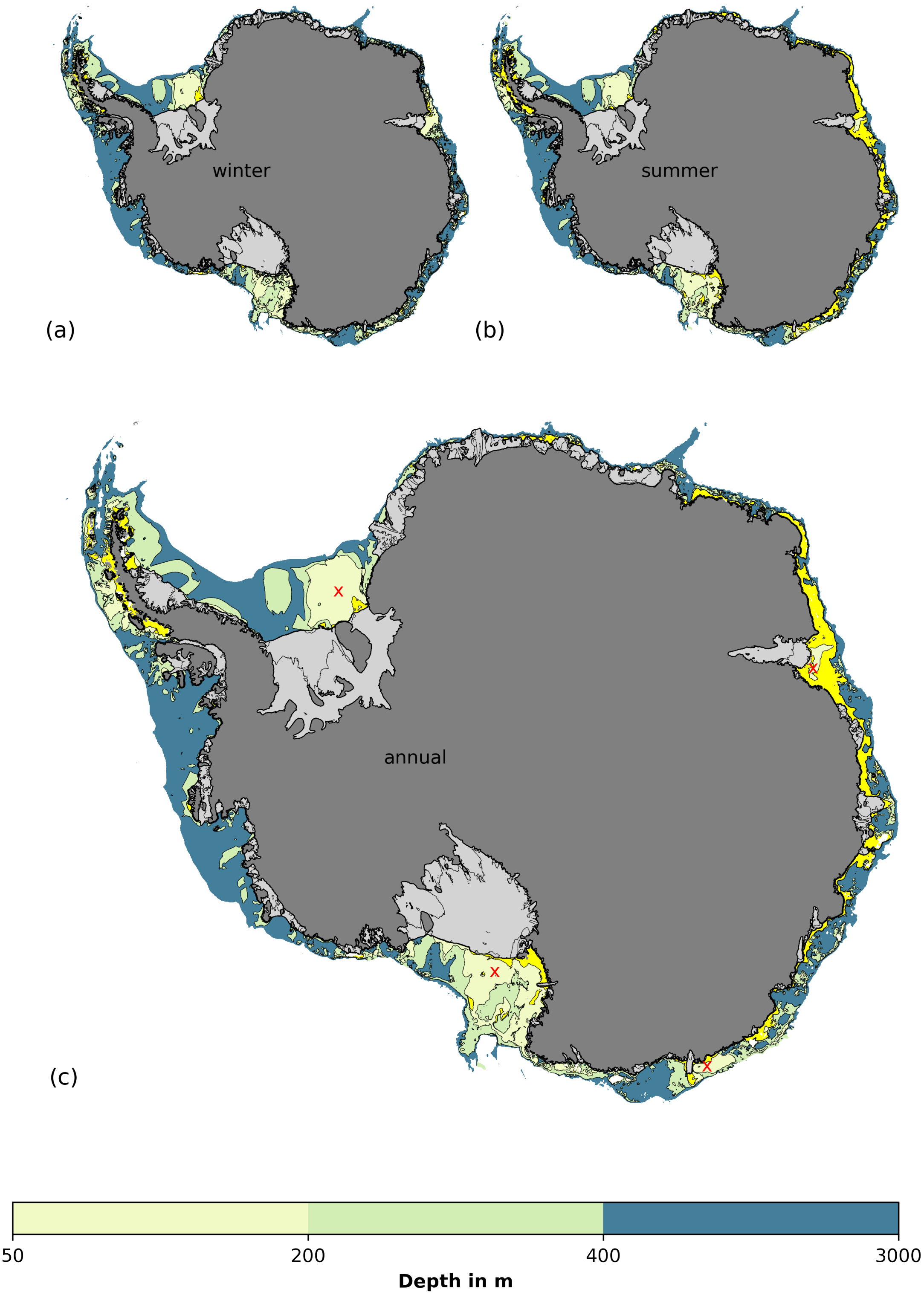

Figure H.1: Modelled Subsurface Temperature Maximum Depth (SSTMD) on the continental shelf in 2007 (a) winter (b) summer and (c) as annual mean. The subsurface is defined as below 50 m depth. Yellow areas are regions where the SSTMD is at 50 m depth. Winter is the mean of June, July and August and summer of December, January and February. Dark gray denotes grounded ice and light gray ice shelves. Contour lines highlight 200 m and 400 m depth for the SSTMD and the ice shelf draft.

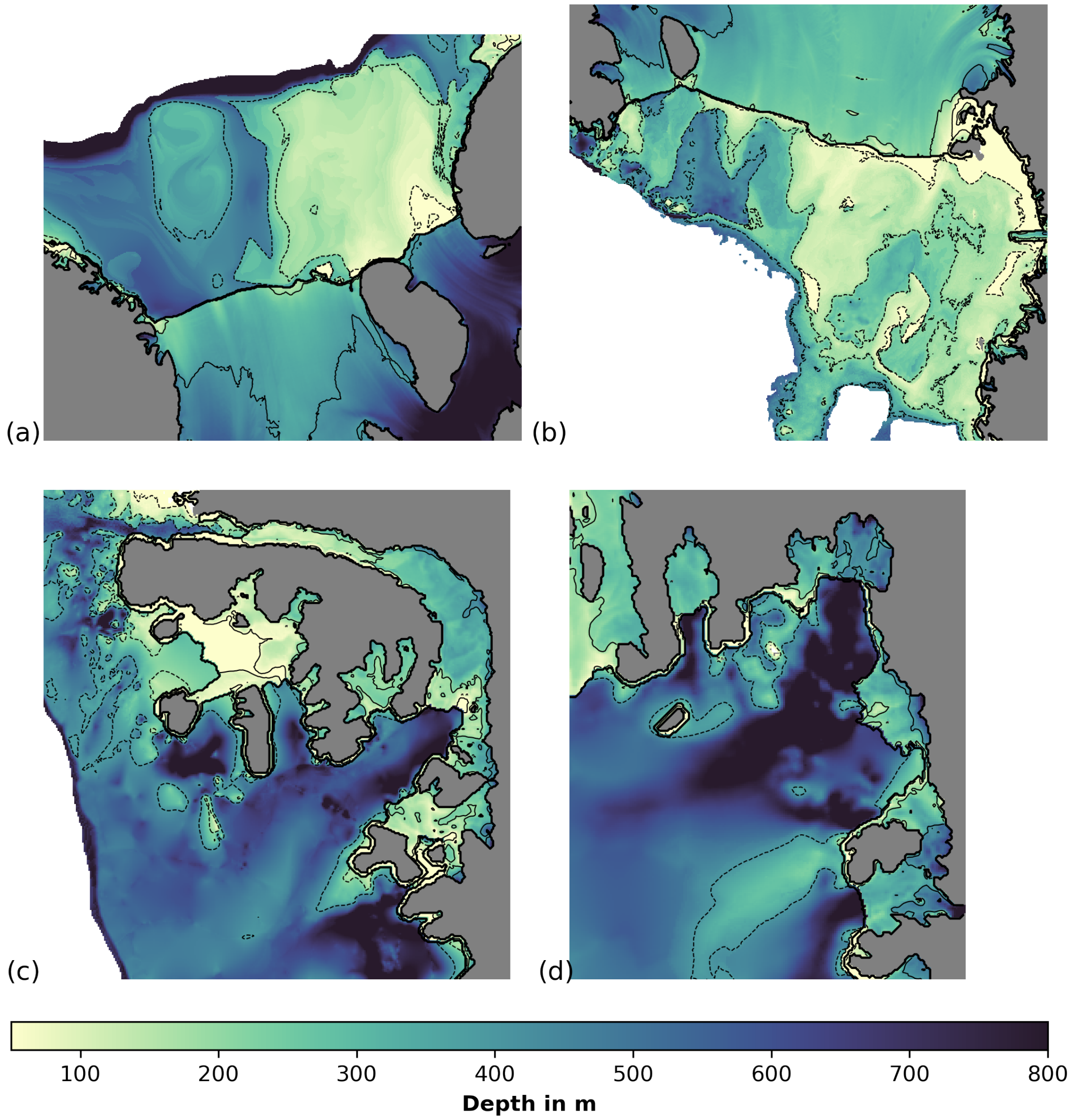

Figure H.2: 2007 mean of modelled Subsurface Temperature Maximum Depth (SSTMD) on the continental shelf. (a) Filchner-Ronne Ice Shelf front, (b) Ross Ice Shelf front, (c) Eastern Bellingshausen Sea and (d) Eastern Amundsen Sea. The Subsurface is defined as below 50 m depth. The color scale has been saturated at 50 m depth. The colors shows the ice shelf draft as well as the SSTM. Contour lines show 400 m and 200 m marks of SSTM (dashed) and ice draft (solid).

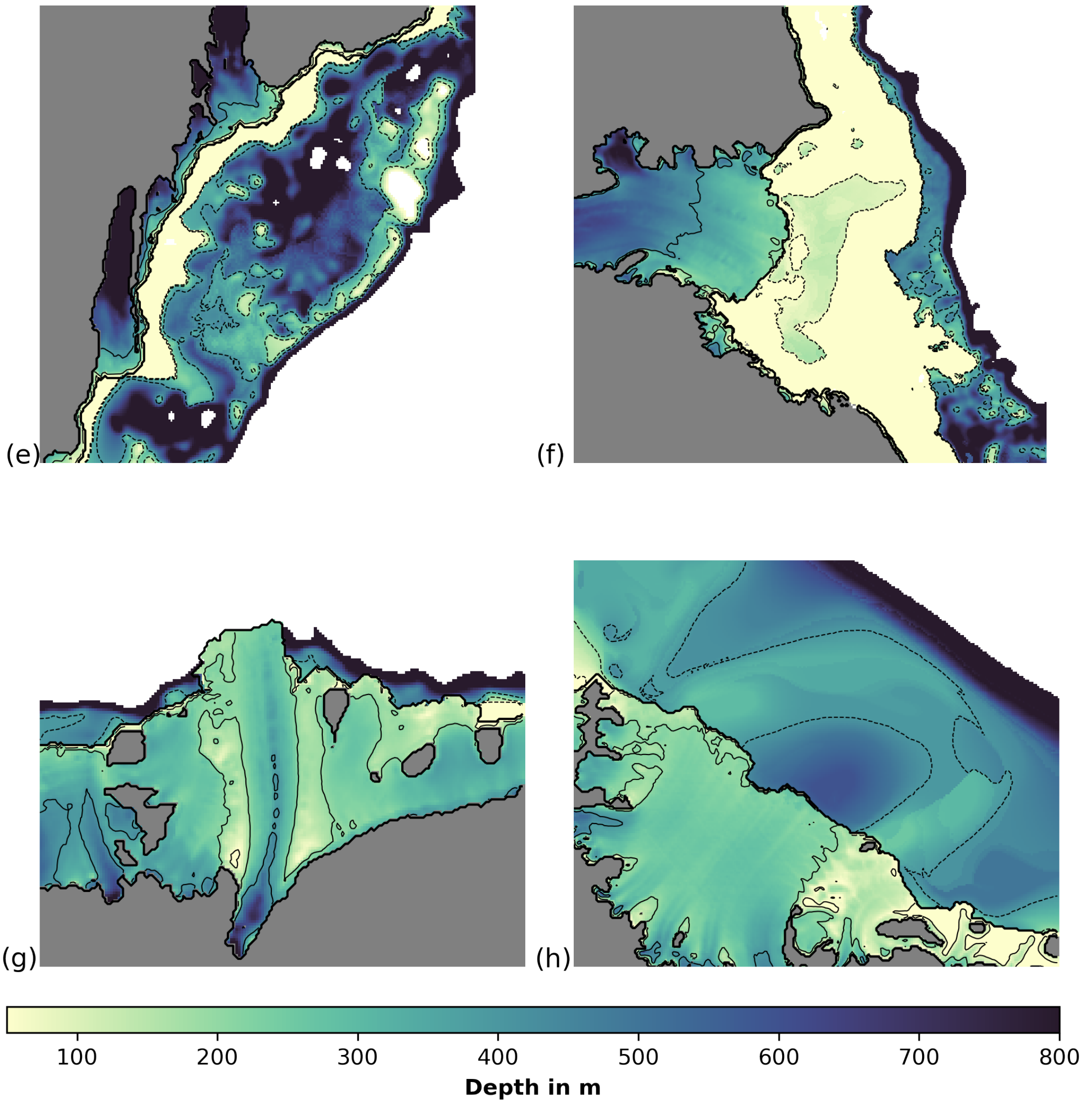

Figure H.2: 2007 mean of modelled Subsurface Temperature Maximum Depth (SSTMD) on the continental shelf (cont.). (e) Coast in front of Totten and Moscow University ice shelves, (f) Prydz Bay, (g) Fimbul Ice Shelf and its narrow shelf region and (h) region around LarsenC Ice Shelf.

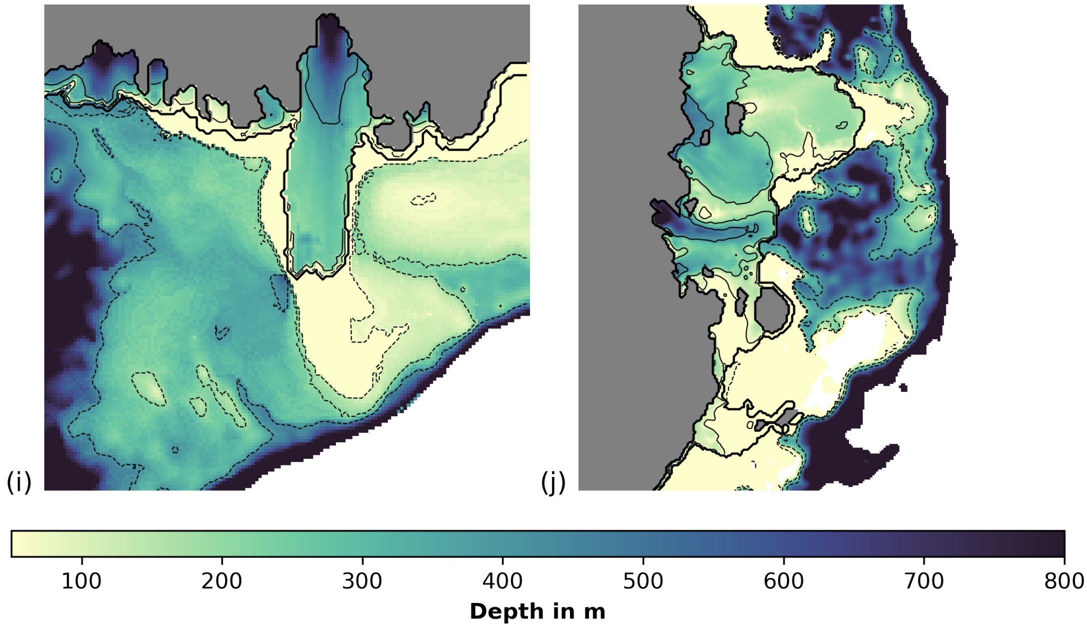

Figure H.2: 2007 mean of modelled Subsurface Temperature Maximum Depth (SSTMD) on the continental shelf (cont.). Region around (i) Mertz Glacier Ice Shelf and (j) Shackleton Ice Shelf.

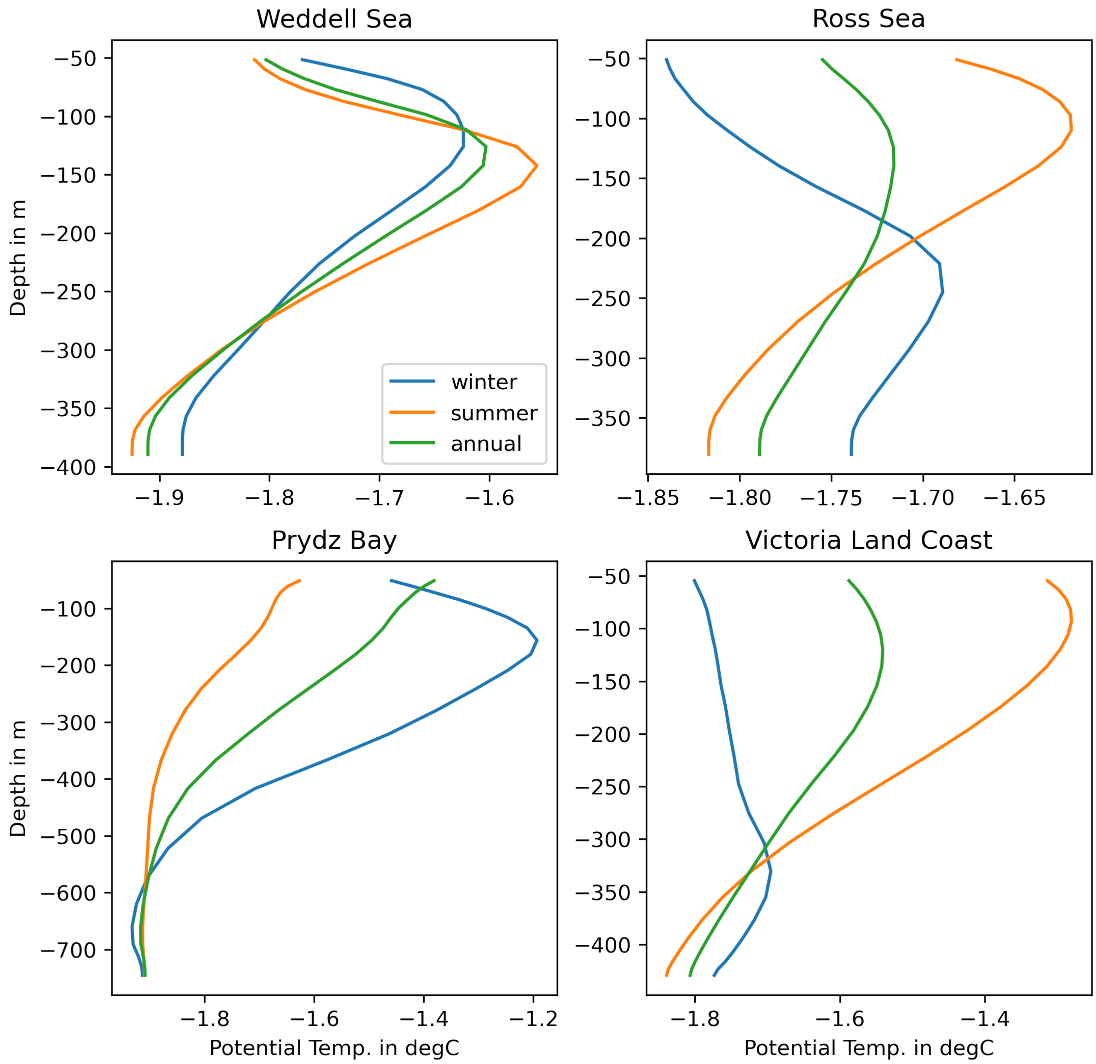

Figure H.3: Example profiles of Potential Temperature over depth for 2007. The locations are marked in Figure H.1c. Winter is the mean of June, July and August and summer of December, January and February.

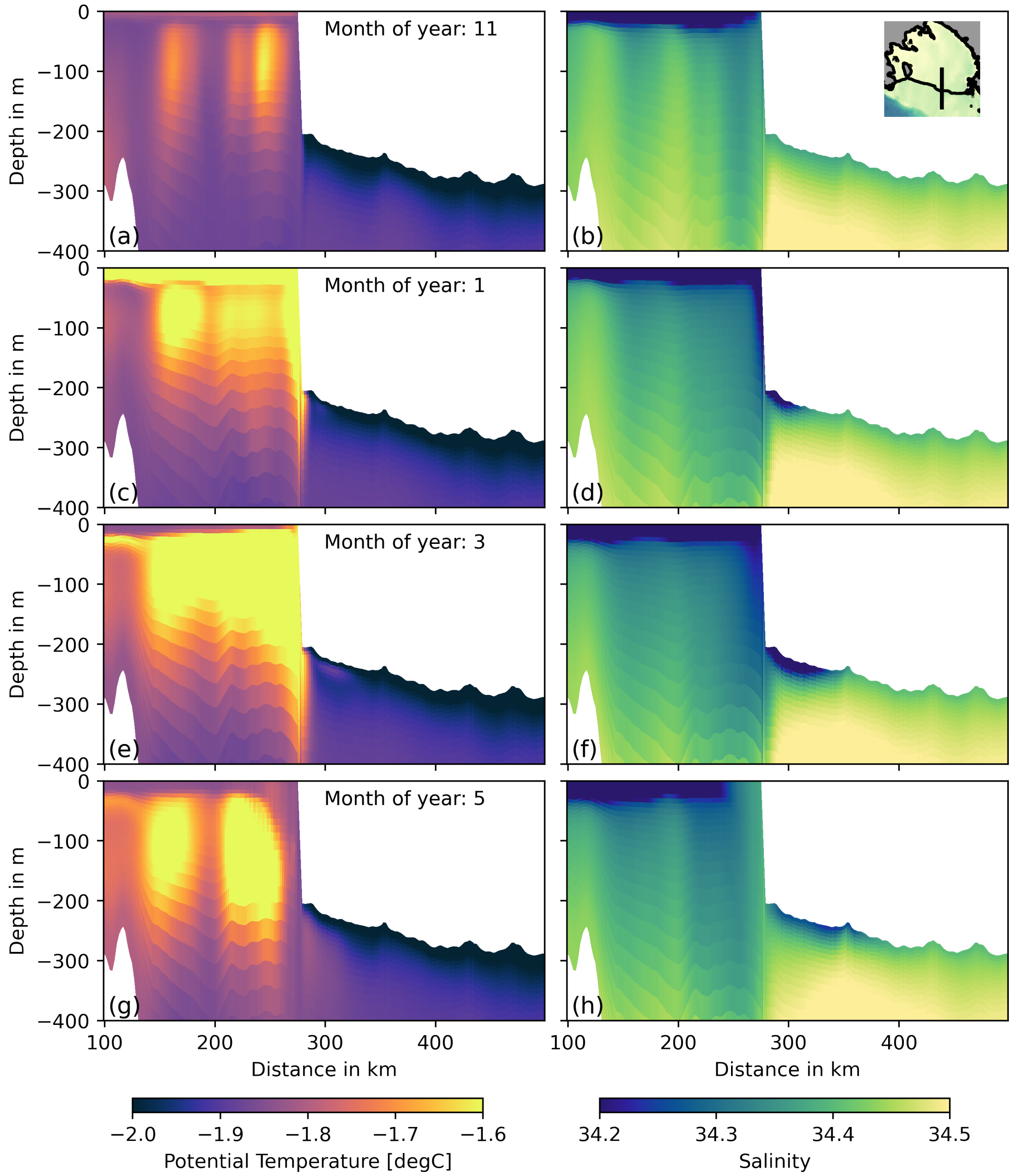

Figure H.4: Example transect across the Ross Ice Shelf front showing monthly means of Potential Temperature (left panels) and Salinity (right panels). (a) and (b) are November, (c) and (d) are January, (e) and (f) are March, and (g) and (h) are May. The location of the transect is shown in the inset of sub-figure (b). The displayed times and color scales are chosen to capture surface water advection under the ice (also see Fig 3.5).

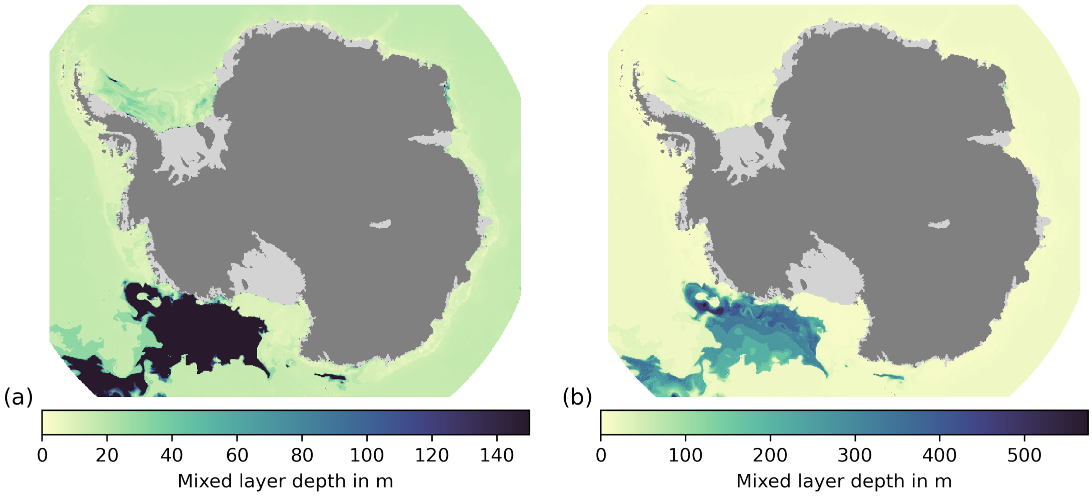

Figure H.5: Mixed layer depth in summer (mean of 2007 December, January and February). The depth is calculated as the shallowest depth where potential density is at least $0.03\,\mathrm{kg\,m^{-3}}$ greater than at the surface. An observational estimate of the summer mix layer depth, which uses the same definition, is presented in Naughten et al. (2018b) (using observations by Pellichero et al., 2017).

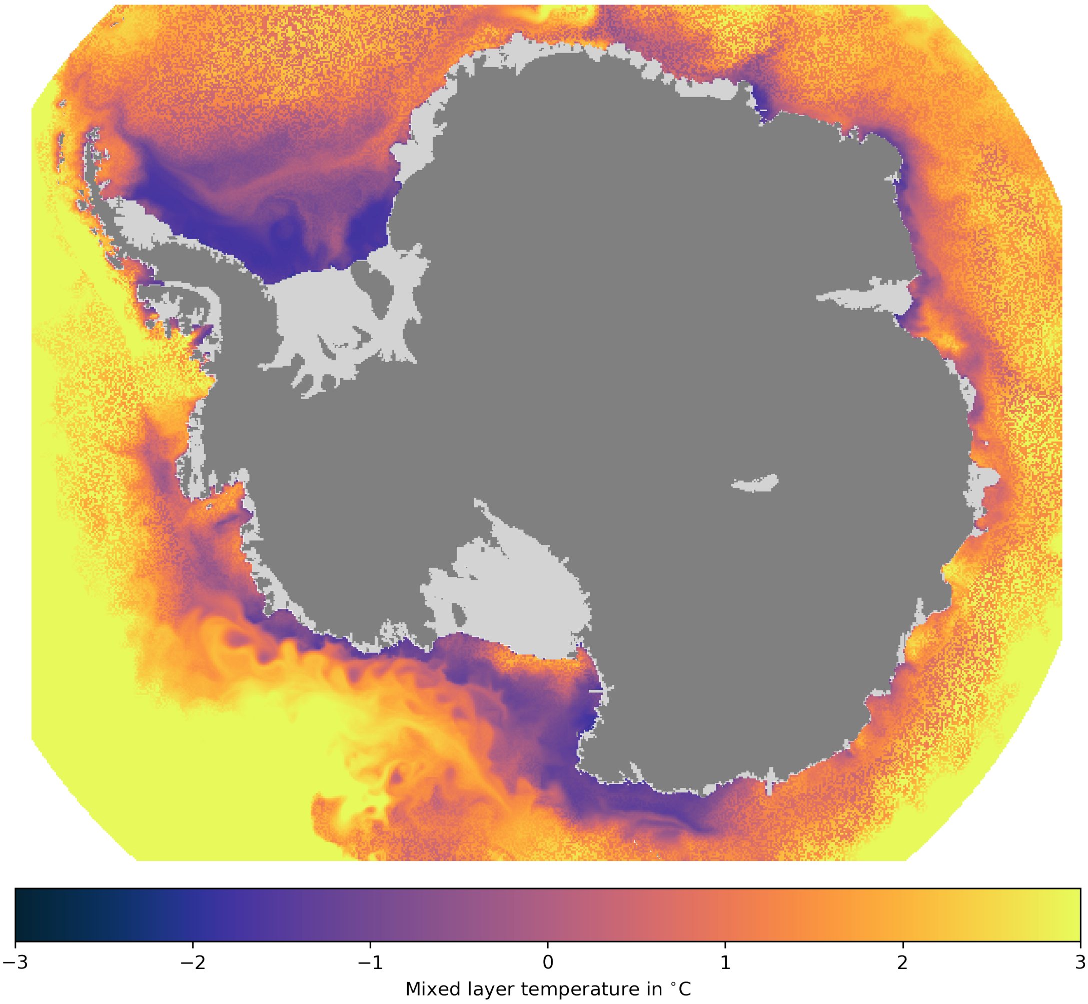

Figure H.6: Mixed layer temperature in summer (mean of 2007 December, January and February). The temperature is the vertical mean over the depth of the mixed layer shown in Figure H.5. An observational estimate of the summer mix layer temperatures are presented by Pellichero et al. (2017)

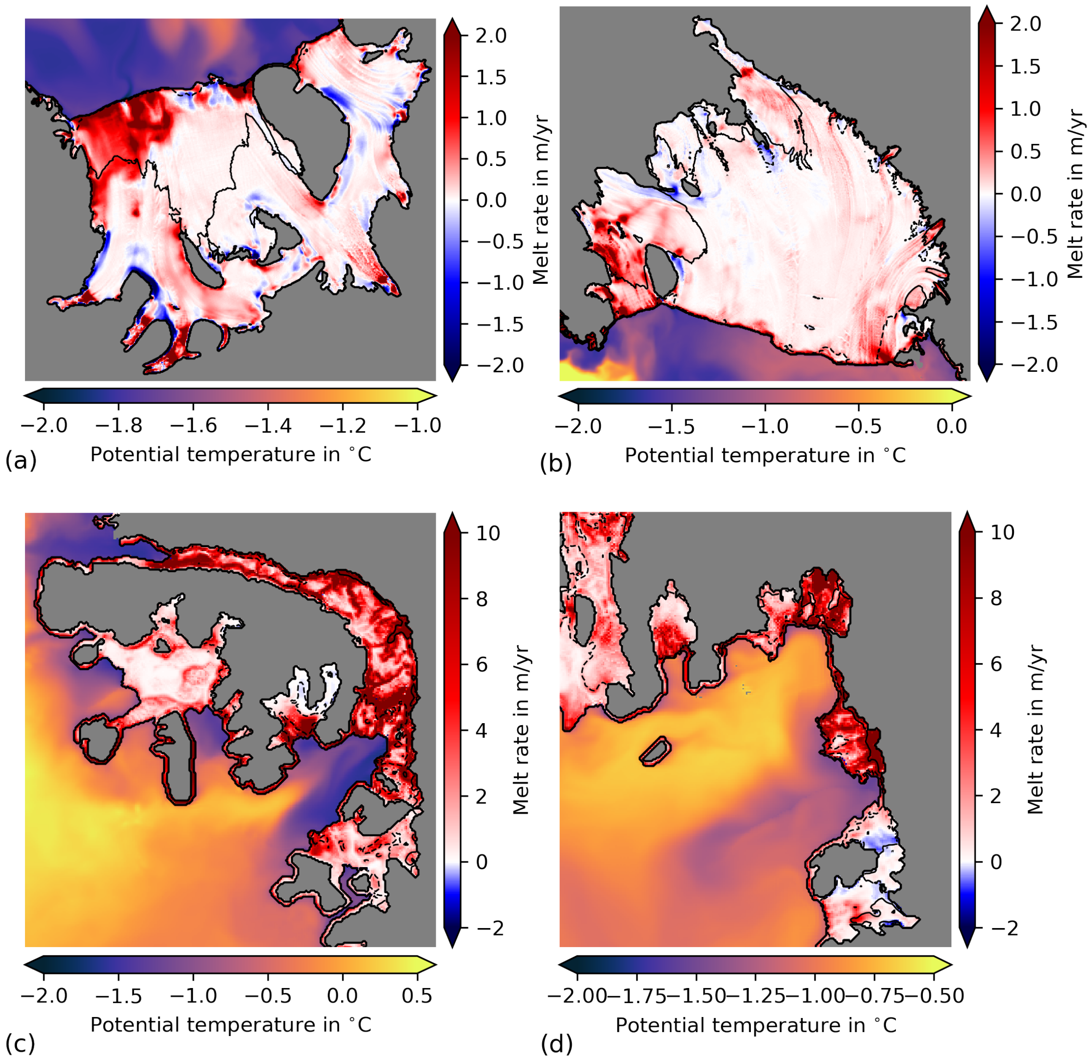

Figure H.7: Ice shelf basal melting and surface ocean temperature around Antarctica (Zoom-ins for Fig. 3.2). Zoom-ins show (a) Filchner-Ronne Ice Shelf, (b) Ross Ice Shelf, (c) Eastern Bellingshausen Sea and (d) Pine Island Bay. Seaward of ice shelves, 2007 average potential temperature of the surface ocean (uppermost sigma layer). Within ice shelves, 2007 average basal melt rate. Solid and dashed lines indicate 400 m and 200 m ice draft, respectively.

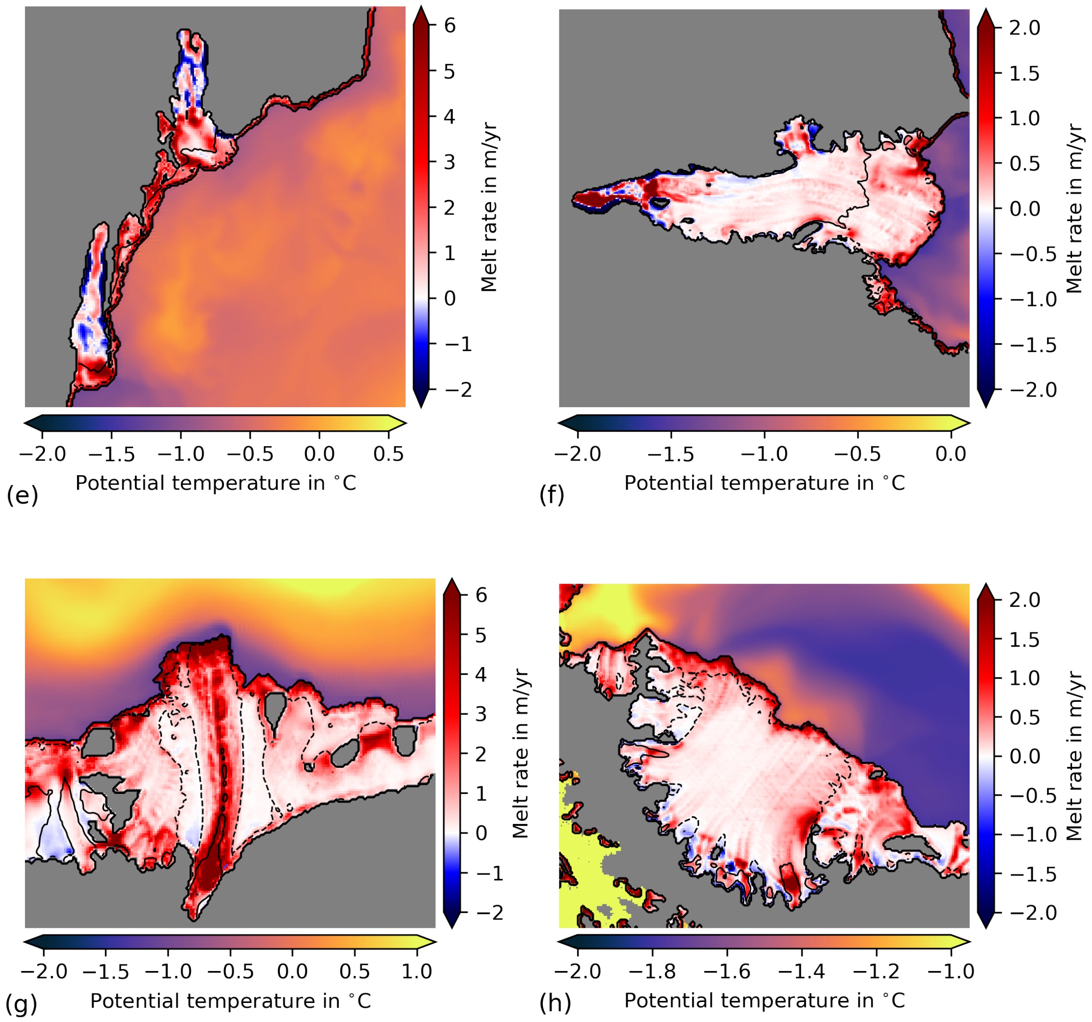

Figure H.7: Ice shelf melting and surface layer temperatures (cont.). Zoom-ins show (e) Totten and Moscow University ice shelves, (f) Amery Ice Shelf, (g) Fimbul Ice Shelf, and (h) Larsen B, C and D ice shelves.

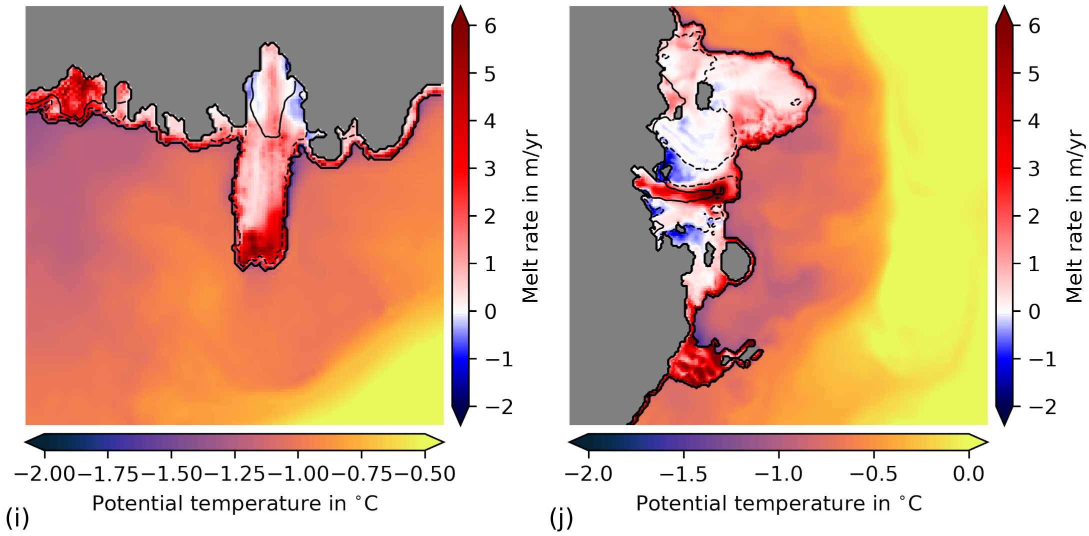

Figure H.7: Ice shelf melting and surface layer temperatures (cont.). Zoom-ins show (i) Mertz Glacier Ice Shelf and (j) Shackleton Ice Shelf.

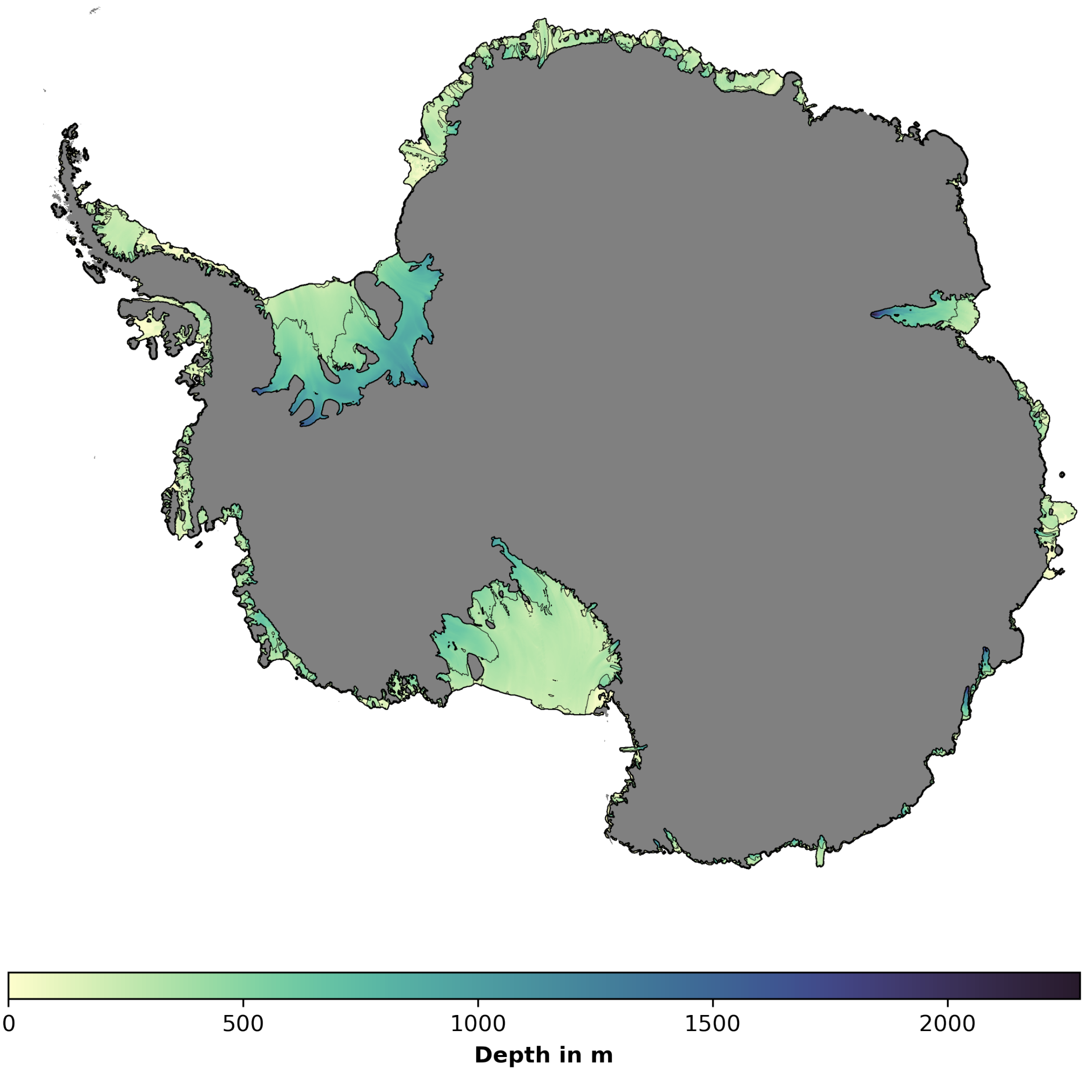

Figure H.8: Ice shelf draft used in the model. Thin black lines are 400 m and 200 m depth contours.

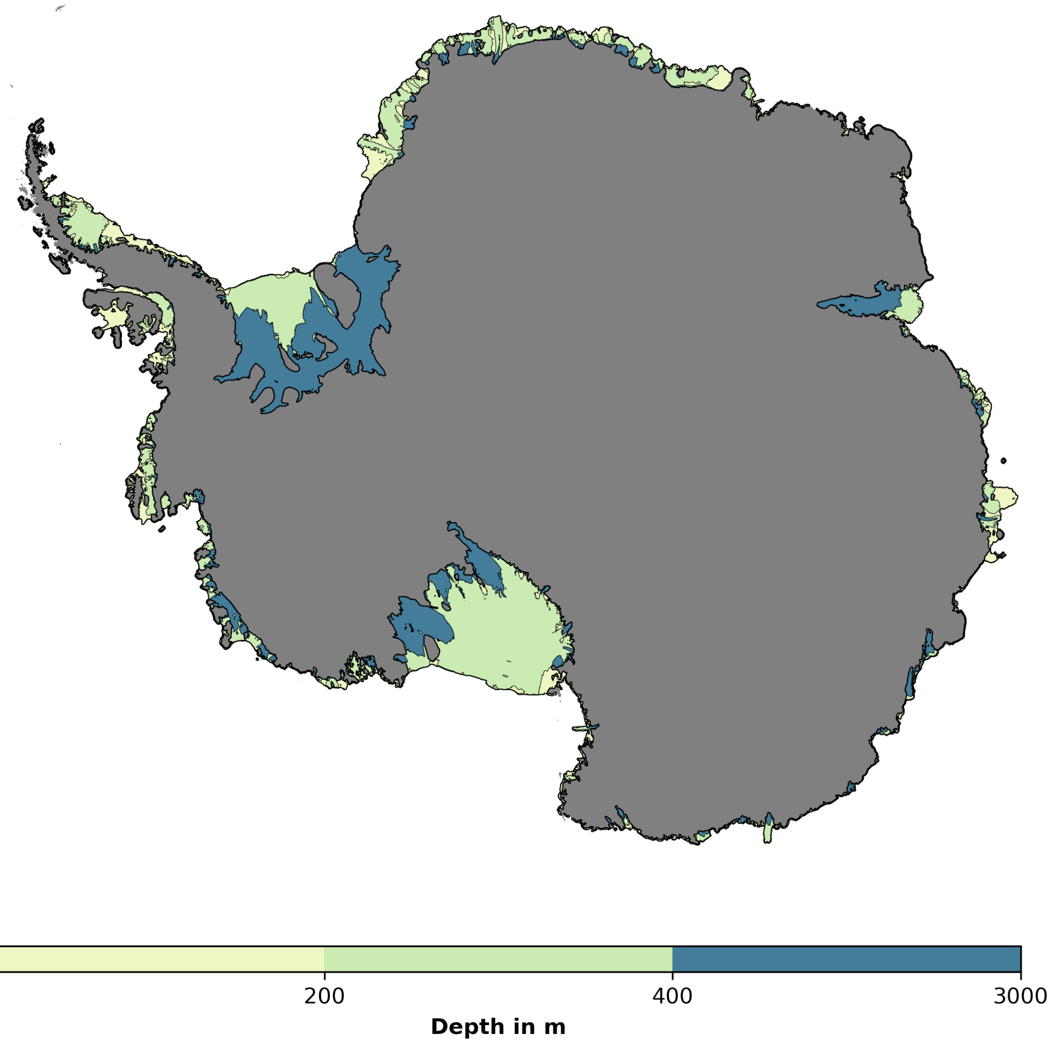

Figure H.9: Depth Ranges of ice shelf draft used to integrate mass loss quantities.

Appendix I

Ice shelf mass loss from different size classes

Table I.1: Basal mass balance of Antarctic ice shelves from different size classes. 2007 area average melt rate, area and basal mass loss for all ice in the model, ice shelves larger than 45 000 km^2 (large), between 45 000 km^2 to 5000 km^2 (medium) and smaller than 5000 km^2 (small). Also shown is the contribution from ice present in Bedmap2 (Fretwell et al., 2013), but not MEaSURES (Mouginot et al., 2016) and from within 6 km of the ice shelf front. Abbreviations are melt rate (w_b) and Basal Mass Loss (BML). The spatial distribution of the size classes is shown in Fig. B.2.

	Area (10^3km^2)	**Area fraction (%)**	w_b **(m/yr)**	**BML (Gt/yr)**	**BML fraction (%)**
Total Antarctica	1,617.62	100	0.81	1,207.04	100
Large	1,028.48	63.58	0.19	176.96	14.66
Medium	422.29	26.11	1.69	652.16	54.03
Small	72.56	4.49	2.16	143.43	11.88
Not in MEaSURES	94.29	5.83	2.72	234.49	19.43
Front	270.39	16.72	1.62	400.83	33.21

Bibliography

Årthun, M., Holland, P. R., Nicholls, K. W., and Feltham, D. L. Eddy-Driven Exchange between the Open Ocean and a Sub–Ice Shelf Cavity. *Journal of Physical Oceanography*, 43(11):2372–2387, September 2013. ISSN 0022-3670. doi: 10.1175/JPO-D-13-0137.1.

Arbic, B. K., MacAyeal, D. R., Mitrovica, J. X., and Milne, G. A. Palaeoclimate: Ocean tides and Heinrich events. *Nature*, 432(7016):460, November 2004. ISSN 1476-4687. doi: 10.1038/432460a.

Arrigo, K. R., Dijken, G. L. v., and Strong, A. L. Environmental controls of marine productivity hot spots around Antarctica. *Journal of Geophysical Research: Oceans*, 120(8):5545–5565, 2015. ISSN 2169-9291. doi: 10.1002/2015JC010888.

Arzeno, I. B., Beardsley, R. C., Limeburner, R., Owens, B., Padman, L., Springer, S. R., Stewart, C. L., and Williams, M. J. M. Ocean variability contributing to basal melt rate near the ice front of Ross Ice Shelf, Antarctica. *Journal of Geophysical Research: Oceans*, 119(7):4214–4233, July 2014. ISSN 2169-9291. doi: 10.1002/2014JC009792.

Asay-Davis, X. S., Cornford, S. L., Durand, G., Galton-Fenzi, B. K., Gladstone, R. M., Gudmundsson, G. H., Hattermann, T., Holland, D. M., Holland, D., Holland, P. R., Martin, D. F., Mathiot, P., Pattyn, F., and Seroussi, H. Experimental design for three interrelated marine ice sheet and ocean model intercomparison projects: MISMIP v. 3 (MISMIP +), ISOMIP v. 2 (ISOMIP +) and MISOMIP v. 1 (MISOMIP1). *Geoscientific Model Development*, 9(7):2471–2497, July 2016. ISSN 1991-959X. doi: 10.5194/gmd-9-2471-2016.

Asay-Davis, X. S., Jourdain, N. C., and Nakayama, Y. Developments in Simulating and Parameterizing Interactions Between the Southern Ocean and the Antarctic Ice Sheet. *Current Climate Change Reports*, 3(4):316–329, December 2017. ISSN 2198-6061. doi: 10.1007/s40641-017-0071-0.

Assmann, K. M., Jenkins, A., Shoosmith, D. R., Walker, D. P., Jacobs, S. S., and Nicholls, K. W. Variability of Circumpolar Deep Water transport onto the Amundsen Sea Continental shelf through a shelf break trough. *Journal of Geophysical Research: Oceans*, 118(12):6603–6620, 2013. ISSN 2169-9291. doi: 10.1002/2013JC008871.

Begeman, C. B., Tulaczyk, S. M., Marsh, O. J., Mikucki, J. A., Stanton, T. P., Hodson, T. O., Siegfried, M. R., Powell, R. D., Christianson, K., and King, M. A. Ocean Stratification and Low Melt Rates at the Ross Ice Shelf Grounding Zone. *Journal of Geophysical Research: Oceans*, 123(10):7438–7452, 2018. ISSN 2169-9291. doi: 10.1029/2018JC013987.

Biddle, L. C., Loose, B., and Heywood, K. J. Upper Ocean Distribution of Glacial Meltwater in the Amundsen Sea, Antarctica. *Journal of Geophysical Research: Oceans*, 124(10):6854–6870, 2019. ISSN 2169-9291.

Bronselaer, B., Winton, M., Griffies, S. M., Hurlin, W. J., Rodgers, K. B., Sergienko, O. V., Stouffer, R. J., and Russell, J. L. Change in future climate due to Antarctic meltwater. *Nature*, 564(7734):53, December 2018. ISSN 1476-4687. doi: 10.1038/s41586-018-0712-z.

Charlotte Huneke, W. G., Klocker, A., and Galton-Fenzi, B. K. Deep Bottom Mixed Layer Drives Intrinsic Variability of the Antarctic Slope Front. *Journal of Physical Oceanography*, 49(12):3163–3177, December 2019. ISSN 0022-3670. doi: 10.1175/JPO-D-19-0044.1.

Chelton, D. B., deSzoeke, R. A., Schlax, M. G., El Naggar, K., and Siwertz, N. Geographical Variability of the First Baroclinic Rossby Radius of Deformation. *Journal of Physical Oceanography*, 28(3):433–460, March 1998. ISSN 0022-3670. doi: 10.1175/1520-0485(1998)028<0433:GVOTFB>2.0.CO;2.

Colleoni, F., Santis, L. D., Siddoway, C. S., Bergamasco, A., Golledge, N. R., Lohmann, G., Passchier, S., and Siegert, M. J. Spatio-temporal variability of processes across Antarctic ice-bed–ocean interfaces. *Nature Communications*, 9(1):2289, June 2018. ISSN 2041-1723. doi: 10.1038/s41467-018-04583-0.

Cornford, S. L., Martin, D. F., Payne, A. J., Ng, E. G., Le Brocq, A. M., Gladstone, R. M., Edwards, T. L., Shannon, S. R., Agosta, C., Van Den Broeke, M. R., Hellmer, H. H., Krinner, G., Ligtenberg, S. R. M., Timmermann, R., and Vaughan, D. G. Century-scale simulations of the response of the West Antarctic Ice Sheet to a warming climate. *The Cryosphere*, August 2015. ISSN 1994-0416. doi: 10.5194/tc-9-1579-2015.

Cougnon, E. A., Galton-Fenzi, B. K., Meijers, A. J. S., and Legrésy, B. Modeling interannual dense shelf water export in the region of the Mertz Glacier Tongue (1992–2007). *Journal of Geophysical Research: Oceans*, 118(10):5858–5872, October 2013. ISSN 2169-9291. doi: 10.1002/2013JC008790.

Davis, P. E. D., Jenkins, A., Nicholls, K. W., Brennan, P. V., Abrahamsen, E. P., Heywood, K. J., Dutrieux, P., Cho, K.-H., and Kim, T.-W. Variability in Basal Melting Beneath Pine Island Ice Shelf on Weekly to Monthly Timescales. *Journal of Geophysical Research: Oceans*, 123(11):8655–8669, November 2018. ISSN 2169-9291. doi: 10.1029/2018JC014464.

Debreu, L., Marchesiello, P., Penven, P., and Cambon, G. Two-way nesting in split-explicit ocean models: Algorithms, implementation and validation. *Ocean Modelling*, 49-50:1–21, June 2012. ISSN 1463-5003. doi: 10.1016/j.ocemod.2012.03.003.

DeConto, R. M. and Pollard, D. Contribution of Antarctica to past and future sea-level rise. *Nature*, 531(7596):591–597, March 2016. ISSN 1476-4687. doi: 10.1038/nature17145.

Dee, D. P., Uppala, S. M., Simmons, A. J., Berrisford, P., Poli, P., Kobayashi, S., Andrae, U., Balmaseda, M. A., Balsamo, G., Bauer, P., Bechtold, P., Beljaars, A. C. M., Berg, L. v. d., Bidlot, J., Bormann, N., Delsol, C., Dragani, R., Fuentes, M., Geer, A. J., Haimberger, L., Healy, S. B., Hersbach, H., Hólm, E. V., Isaksen, L., Kållberg, P., Köhler, M., Matricardi, M., McNally, A. P., Monge-Sanz, B. M., Morcrette, J.-J., Park, B.-K., Peubey, C., Rosnay, P. d., Tavolato, C., Thépaut, J.-N., and Vitart, F. The ERA-Interim reanalysis: configuration and performance of the data assimilation system. *Quarterly Journal of the Royal Meteorological Society*, 137 (656):553–597, April 2011. ISSN 1477-870X. doi: 10.1002/qj.828.

Depoorter, M. A., Bamber, J. L., Griggs, J. A., Lenaerts, J. T. M., Ligtenberg, S. R. M., van den Broeke, M. R., and Moholdt, G. Calving fluxes and basal melt rates of Antarctic ice shelves. *Nature*, 502(7469):89–92, October 2013. ISSN 1476-4687. doi: 10.1038/nature12567.

Dinniman, M. S., Klinck, J. M., and Smith, W. O. Cross-shelf exchange in a model of the Ross Sea circulation and biogeochemistry. *Deep Sea Research Part II: Topical Studies in Oceanography*, 50(22):3103–3120, November 2003. ISSN 0967-0645. doi: 10.1016/j.dsr2.2003.07.011.

Dinniman, M. S., Klinck, J. M., Bai, L.-S., Bromwich, D. H., Hines, K. M., and Holland, D. M. The Effect of Atmospheric Forcing Resolution on Delivery of Ocean Heat to the Antarctic Floating Ice Shelves. *Journal of Climate*, 28(15):6067–6085, May 2015. ISSN 0894-8755. doi: 10.1175/JCLI-D-14-00374.1.

Dinniman, M. S., Asay-Davis, X. S., Galton-Fenzi, B. K., Holland, P. R., Jenkins, A., and Timmermann, R. Modeling Ice Shelf/Ocean Interaction in Antarctica: A Review. *Oceanography*, 29(4):144–153, December 2016. doi: 10.5670/oceanog.2016.106.

Dupont, T. K. and Alley, R. B. Assessment of the importance of ice-shelf buttressing to ice-sheet flow. *Geophysical Research Letters*, 32(4), 2005. ISSN 1944-8007. doi: 10.1029/2004GL022024.

Durack, P., Gleckler, P., Purkey, S., Johnson, G., Lyman, J., and Boywe, T. Ocean Warming: From the Surface to the Deep in Observations and Models. *Oceanography*, 31(2):41–51, June 2018. ISSN 1042-8275. doi: 10.5670/oceanog.2018.227.

Dutrieux, P., Vaughan, D. G., Corr, H. F. J., Jenkins, A., Holland, P. R., Joughin, I., and Fleming, A. H. Pine Island glacier ice shelf melt distributed at kilometre scales. *The Cryosphere*, 7(5):1543–1555, September 2013. ISSN 1994-0416. doi: 10.5194/tc-7-1543-2013.

Dutton, A., Carlson, A. E., Long, A. J., Milne, G. A., Clark, P. U., DeConto, R., Horton, B. P., Rahmstorf, S., and Raymo, M. E. Sea-level rise due to polar ice-sheet mass loss during past warm periods. *Science*, 349(6244), July 2015. ISSN 0036-8075, 1095-9203. doi: 10.1126/science.aaa4019.

Egbert, G. D. and Erofeeva, S. Y. Efficient Inverse Modeling of Barotropic Ocean Tides. *Journal of Atmospheric and Oceanic Technology*, 19(2):183–204, February 2002. ISSN 0739-0572. doi: 10.1175/1520-0426(2002)019<0183:EIMOBO>2.0.CO;2.

Elsner, J. B. and Tsonis, A. A. *Singular Spectrum Analysis: A New Tool in Time Series Analysis*. Springer US, 1996. ISBN 978-0-306-45472-1. doi: 10.1007/978-1-4757-2514-8.

Favier, L., Gagliardini, O., Durand, G., and Zwinger, T. A three-dimensional full Stokes model of the grounding line dynamics: effect of a pinning point beneath the ice shelf. *The Cryosphere*, 6:101–112, January 2012. doi: 10.5194/tc-6-101-2012.

Foldvik, A., Gammelsrød, T., Slotsvik, N., and Tørresen, T. Oceanographic conditions on the Weddell Sea Shelf during the German Antarctic Expedition 1979/80. *Polar Research*, 3(2):209–226, January 1985. ISSN 1751-8369. doi: 10.3402/polar.v3i2.6953.

Foldvik, A., Middleton, J. H., and Foster, T. D. The tides of the southern Weddell Sea. *Deep Sea Research Part A. Oceanographic Research Papers*, 37(8):1345–1362, August 1990. ISSN 0198-0149. doi: 10.1016/0198-0149(90)90047-Y.

Fretwell, P., Pritchard, H. D., Vaughan, D. G., Bamber, J. L., Barrand, N. E., Bell, R., Bianchi, C., Bingham, R. G., Blankenship, D. D., Casassa, G., Catania, G., Callens, D., Conway, H., Cook, A. J., Corr, H. F. J., Damaske, D., Damm, V., Ferraccioli, F., Forsberg, R., Fujita, S., Gim, Y., Gogineni, P., Griggs, J. A., Hindmarsh, R. C. A., Holmlund, P., Holt, J. W., Jacobel, R. W., Jenkins, A., Jokat, W., Jordan, T., King, E. C., Kohler, J., Krabill, W., Riger-Kusk, M., Langley, K. A., Leitchenkov, G., Leuschen, C., Luyendyk, B. P., Matsuoka, K., Mouginot, J., Nitsche, F. O., Nogi, Y., Nost, O. A., Popov, S. V., Rignot, E., Rippin, D. M., Rivera, A., Roberts, J., Ross, N., Siegert, M. J., Smith, A. M., Steinhage, D., Studinger, M., Sun, B., Tinto, B. K., Welch, B. C., Wilson, D., Young, D. A., Xiangbin, C., and Zirizzotti, A. Bedmap2: improved ice bed, surface and thickness datasets for Antarctica. *The Cryosphere*, 7 (1):375–393, February 2013. ISSN 1994-0416. doi: 10.5194/tc-7-375-2013.

Fürst, J. J., Durand, G., Gillet-Chaulet, F., Tavard, L., Rankl, M., Braun, M., and Gagliardini, O. The safety band of Antarctic ice shelves. *Nature Climate Change*, 6 (5):479–482, May 2016. ISSN 1758-678X, 1758-6798. doi: 10.1038/nclimate2912.

Gade, H. G. Melting of ice in sea water: A primitive model with application to the antarctic ice shelf and icebergs. *Journal of Physical Oceanography*, 9(1):189–198, 1979. doi: 10.1175/1520-0485(1979)009<0189:MOIISW>2.0.CO;2.

Gagliardini, O., Durand, G., Zwinger, T., Hindmarsh, R. C. A., and Meur, E. L. Coupling of ice-shelf melting and buttressing is a key process in ice-sheets dynamics. *Geophysical Research Letters*, 37(14), 2010. ISSN 1944-8007. doi: 10.1029/2010GL043334.

Galton-Fenzi, B. K., Hunter, J. R., Coleman, R., Marsland, S. J., and Warner, R. C. Modeling the basal melting and marine ice accretion of the Amery Ice Shelf. *Journal of Geophysical Research: Oceans*, 117(C9), September 2012. ISSN 2156-2202. doi: 10.1029/2012JC008214.

Galton-Fenzi, B. K., Maraldi, C., Coleman, R., and Hunter, J. The cavity under the

Amery Ice Shelf, East Antarctica. *Journal of Glaciology*, 54(188):881–887, 2008. ISSN 0022-1430, 1727-5652. doi: 10.3189/002214308787779898.

Gammelsrod, T. and Slotsvik, N. Hydrographic and Current Measurements in the Southern Weddell Sea 1979/80. *Polarforschung*, 1981.

Gayen, B., Griffiths, R. W., and Kerr, R. C. Simulation of convection at a vertical ice face dissolving into saline water. *Journal of Fluid Mechanics*, 798:284–298, July 2016. ISSN 0022-1120, 1469-7645. doi: 10.1017/jfm.2016.315.

Golledge, N. R., Keller, E. D., Gomez, N., Naughten, K. A., Bernales, J., Trusel, L. D., and Edwards, T. L. Global environmental consequences of twenty-first-century ice-sheet melt. *Nature*, 566(7742):65, February 2019. ISSN 1476-4687. doi: 10.1038/s41586-019-0889-9.

Gordon, A. L. Bottom Water Formation. In Steele, J. H., editor, *Encyclopedia of Ocean Sciences (Second Edition)*, pages 415–421. Academic Press, Oxford, January 2001. ISBN 978-0-12-374473-9. doi: 10.1016/B978-012374473-9.00006-0.

Greene, C. A., Blankenship, D. D., Gwyther, D. E., Silvano, A., and Wijk, E. v. Wind causes Totten Ice Shelf melt and acceleration. *Science Advances*, 3(11), November 2017. ISSN 2375-2548. doi: 10.1126/sciadv.1701681.

Griffies, S. M., Böning, C., Bryan, F. O., Chassignet, E. P., Gerdes, R., Hasumi, H., Hirst, A., Treguier, A.-M., and Webb, D. Developments in ocean climate modelling. *Ocean Modelling*, 2(3):123–192, January 2000. ISSN 1463-5003. doi: 10.1016/S1463-5003(00)00014-7.

Griffiths, S. D. and Peltier, W. R. Megatides in the Arctic Ocean under glacial conditions. *Geophysical Research Letters*, 35(8), April 2008. ISSN 1944-8007. doi: 10.1029/2008GL033263.

Griffiths, S. D. and Peltier, W. R. Modeling of Polar Ocean Tides at the Last Glacial Maximum: Amplification, Sensitivity, and Climatological Implications. *Journal of Climate*, 22(11):2905–2924, June 2009. ISSN 0894-8755. doi: 10.1175/2008JCLI2540.1.

Griggs, J. and Bamber, J. Antarctic ice-shelf thickness from satellite radar altimetry. *Journal of Glaciology*, 57(203):485–498, 2011. ISSN 0022-1430, 1727-5652. doi: 10.3189/002214311796905659.

Gudmundsson, G. H. Ice-shelf buttressing and the stability of marine ice sheets. *The Cryosphere*, 7(2):647–655, April 2013. ISSN 1994-0416. doi: 10.5194/tc-7-647-2013.

Gudmundsson, G. H., Krug, J., Durand, G., Favier, L., and Gagliardini, O. The stability of grounding lines on retrograde slopes. *The Cryosphere*, 6(6):1497–1505, December 2012. ISSN 1994-0424.

Guo, G., Shi, J., Gao, L., Tamura, T., and Williams, G. D. Reduced Sea Ice Production Due to Upwelled Oceanic Heat Flux in Prydz Bay, East Antarctica. *Geophysical Research Letters*, 46(9):4782–4789, 2019. ISSN 1944-8007. doi: 10.1029/2018GL081463.

Gwyther, D. E., Galton-Fenzi, B. K., Hunter, J. R., and Roberts, J. L. Simulated melt rates for the Totten and Dalton ice shelves. *Ocean Science*, 10(3):267–279, May 2014. ISSN 1812-0784. doi: 10.5194/os-10-267-2014.

Gwyther, D. E., Cougnon, E. A., Galton-Fenzi, B. K., Roberts, J. L., Hunter, J. R., and Dinniman, M. S. Modelling the response of ice shelf basal melting to different ocean cavity environmental regimes. *Annals of Glaciology*, 57(73):131–141, September 2016. ISSN 0260-3055, 1727-5644. doi: 10.1017/aog.2016.31.

Gwyther, D. E., O'Kane, T. J., Galton-Fenzi, B. K., Monselesan, D. P., and Greenbaum, J. S. Intrinsic processes drive variability in basal melting of the Totten Glacier Ice Shelf. *Nature Communications*, 9(1):3141, August 2018. ISSN 2041-1723. doi: 10.1038/s41467-018-05618-2.

Gwyther, D. E., Kusahara, K., Asay-Davis, X. S., Dinniman, M. S., and Galton-Fenzi, B. K. Vertical processes and resolution impact ice shelf basal melting: A multi-model study. *Ocean Modelling*, 147:101569, March 2020. ISSN 1463-5003. doi: 10.1016/j.ocemod.2020.101569.

Hattermann, T. Antarctic Thermocline Dynamics along a Narrow Shelf with Easterly Winds. *Journal of Physical Oceanography*, 48(10):2419–2443, September 2018. ISSN 0022-3670. doi: 10.1175/JPO-D-18-0064.1.

Hattermann, T., Nøst, O. A., Lilly, J. M., and Smedsrud, L. H. Two years of oceanic observations below the Fimbul Ice Shelf, Antarctica. *Geophysical Research Letters*, 39 (12), 2012. ISSN 1944-8007. doi: 10.1029/2012GL051012.

Hattermann, T., Smedsrud, L. H., Nøst, O. A., Lilly, J. M., and Galton-Fenzi, B. K. Eddy-resolving simulations of the Fimbul Ice Shelf cavity circulation: Basal melting and exchange with open ocean. *Ocean Modelling*, 82:28–44, October 2014. ISSN 1463-5003. doi: 10.1016/j.ocemod.2014.07.004.

Hellmer, H. H. Impact of Antarctic ice shelf basal melting on sea ice and deep ocean properties. *Geophysical Research Letters*, 31(10), May 2004. ISSN 1944-8007. doi: 10.1029/2004GL019506.

Hellmer, H. H. and Olbers, D. J. A two-dimensional model for the thermohaline circulation under an ice shelf. *Antarctic Science*, 1(4):325–336, December 1989. ISSN 1365-2079, 0954-1020. doi: 10.1017/S0954102089000490.

Hellmer, H. H., Kauker, F., Timmermann, R., Determann, J., and Rae, J. Twenty-first-century warming of a large Antarctic ice-shelf cavity by a redirected coastal current. *Nature*, 485(7397):225–228, May 2012. ISSN 1476-4687. doi: 10.1038/nature11064.

Heywood, K. J., Garabato, A. C. N., Stevens, D. P., and Muench, R. D. On the fate of the Antarctic Slope Front and the origin of the Weddell Front. *Journal of Geophysical Research: Oceans*, 109(C6), 2004. ISSN 2156-2202. doi: 10.1029/2003JC002053.

Holland, D. M. and Jenkins, A. Modeling Thermodynamic Ice–Ocean Interactions at the Base of an Ice Shelf. *Journal of Physical Oceanography*, 29(8):1787–1800, August 1999. ISSN 0022-3670. doi: 10.1175/1520-0485(1999)029<1787:MTIOIA>2.0.CO;2.

Holland, P. R. The Transient Response of Ice Shelf Melting to Ocean Change. *Journal of Physical Oceanography*, 47(8):2101–2114, June 2017. ISSN 0022-3670. doi: 10.1175/JPO-D-17-0071.1.

Holland, P. R., Feltham, D. L., and Jenkins, A. Ice Shelf Water plume flow beneath Filchner-Ronne Ice Shelf, Antarctica. *Journal of Geophysical Research*, 112(C5), May 2007. ISSN 0148-0227. doi: 10.1029/2006JC003915.

Holland, P. R., Jenkins, A., and Holland, D. M. The Response of Ice Shelf Basal Melting to Variations in Ocean Temperature. *Journal of Climate*, 21(11):2558–2572, June 2008. ISSN 0894-8755. doi: 10.1175/2007JCLI1909.1.

Holland, P. R., Corr, H. F. J., Vaughan, D. G., Jenkins, A., and Skvarca, P. Marine ice in Larsen Ice Shelf. *Geophysical Research Letters*, 36(11), June 2009. ISSN 1944-8007. doi: 10.1029/2009GL038162.

Horgan, H. J., Walker, R. T., Anandakrishnan, S., and Alley, R. B. Surface elevation changes at the front of the Ross Ice Shelf: Implications for basal melting. *Journal* *of Geophysical Research: Oceans*, 116(C2), February 2011. ISSN 2156-2202. doi: 10.1029/2010JC006192.

Hunke, E. C., Lipscomb, W. H., Turner, A. K., Jeffery, N., and Elliott, S. CICE: the Los Alamos Sea Ice Model Documentation and Software User's Manual la-cc-06-012. Technical report, Los Alamos National Laboratory, March 2015.

Jacobs, S. S. On the nature and significance of the Antarctic Slope Front. *Marine Chemistry*, 35(1):9–24, November 1991. ISSN 0304-4203. doi: 10.1016/S0304-4203(09)90005-6.

Jacobs, S. S. Bottom water production and its links with the thermohaline circulation. *Antarctic Science*, 16(4):427–437, December 2004. ISSN 1365-2079, 0954-1020. doi: 10.1017/S095410200400224X.

Jacobs, S. S. and Giulivi, C. F. Large Multidecadal Salinity Trends near the Pacific–Antarctic Continental Margin. *Journal of Climate*, 23(17):4508–4524, September 2010. ISSN 0894-8755, 1520-0442. doi: 10.1175/2010JCLI3284.1.

Jacobs, S. S., Helmer, H. H., Doake, C. S. M., Jenkins, A., and Frolich, R. M. Melting of ice shelves and the mass balance of Antarctica. *Journal of Glaciology*, 38(130): 375–387, 1992. ISSN 0022-1430, 1727-5652. doi: 10.3189/S0022143000002252.

Jacobs, S. S., Jenkins, A., Giulivi, C. F., and Dutrieux, P. Stronger ocean circulation and increased melting under Pine Island Glacier ice shelf. *Nature Geoscience*, 4(8): 519, August 2011. ISSN 1752-0908. doi: 10.1038/ngeo1188.

Jacobs, S. S., Giulivi, C. F., Dutrieux, P., Rignot, E., Nitsche, F., and Mouginot, J. Getz Ice Shelf melting response to changes in ocean forcing. *Journal of Geophysical Research: Oceans*, 118(9):4152–4168, 2013. ISSN 2169-9291. doi: 10.1002/jgrc.20298.

Jenkins, A. Convection-Driven Melting near the Grounding Lines of Ice Shelves and Tidewater Glaciers. *Journal of Physical Oceanography*, 41(12):2279–2294, July 2011. ISSN 0022-3670. doi: 10.1175/JPO-D-11-03.1.

Jenkins, A., Nicholls, K. W., and Corr, H. F. J. Observation and Parameterization of Ablation at the Base of Ronne Ice Shelf, Antarctica. *Journal of Physical Oceanography*, 40(10):2298–2312, May 2010. ISSN 0022-3670. doi: 10.1175/2010JPO4317.1.

Johnson, G. C., Purkey, S. G., and Toole, J. M. Reduced Antarctic meridional overturning circulation reaches the North Atlantic Ocean. *Geophysical Research Letters*, 35(22), 2008. ISSN 1944-8007. doi: 10.1029/2008GL035619.

Jong, L., Gladstone, R., and Galton-Fenzi, B. Coupled ice sheet-ocean modelling to investigate ocean driven melting of marine ice sheets in Antarctica. In *EGU General Assembly Conference Abstracts*, page 1573, April 2017.

Joughin, I. and Padman, L. Melting and freezing beneath Filchner-Ronne Ice Shelf, Antarctica. *Geophysical Research Letters*, 30(9), May 2003. ISSN 1944-8007. doi: 10.1029/2003GL016941.

Joughin, I., Smith, B. E., and Medley, B. Marine Ice Sheet Collapse Potentially Under Way for the Thwaites Glacier Basin, West Antarctica. *Science*, 344(6185):735–738, May 2014. ISSN 0036-8075, 1095-9203. doi: 10.1126/science.1249055.

Jourdain, N. C., Molines, J.-M., Le Sommer, J., Mathiot, P., Chanut, J., de Lavergne, C., and Madec, G. Simulating or prescribing the influence of tides on the Amundsen Sea ice shelves. *Ocean Modelling*, 133:44–55, January 2019. ISSN 1463-5003. doi: 10.1016/j.ocemod.2018.11.001.

Kimura, S., Candy, A. S., Holland, P. R., Piggott, M. D., and Jenkins, A. Adaptation of an unstructured-mesh, finite-element ocean model to the simulation of ocean circulation beneath ice shelves. *Ocean Modelling*, 67:39–51, July 2013. ISSN 1463-5003. doi: 10.1016/j.ocemod.2013.03.004.

Kimura, S., Nicholls, K. W., and Venables, E. Estimation of Ice Shelf Melt Rate in the Presence of a Thermohaline Staircase. *Journal of Physical Oceanography*, 45(1): 133–148, October 2014. ISSN 0022-3670. doi: 10.1175/JPO-D-14-0106.1.

Kimura, S., Jenkins, A., Regan, H., Holland, P. R., Assmann, K. M., Whitt, D. B., Wessem, M. V., Berg, W. J. v. d., Reijmer, C. H., and Dutrieux, P. Oceanographic Controls on the Variability of Ice-Shelf Basal Melting and Circulation of Glacial Meltwater in the Amundsen Sea Embayment, Antarctica. *Journal of Geophysical Research: Oceans*, 122(12):10131–10155, 2017. ISSN 2169-9291. doi: 10.1002/2017JC012926.

King, M. A. and Padman, L. Accuracy assessment of ocean tide models around Antarctica. *Geophysical Research Letters*, 32(23), December 2005. ISSN 1944-8007. doi: 10.1029/2005GL023901.

Kusahara, K. and Hasumi, H. Modeling Antarctic ice shelf responses to future climate changes and impacts on the ocean. *Journal of Geophysical Research: Oceans*, 118(5): 2454–2475, 2013. ISSN 2169-9291. doi: 10.1002/jgrc.20166.

Kushner, P. J., Held, I. M., and Delworth, T. L. Southern Hemisphere Atmospheric Circulation Response to Global Warming. *Journal of Climate*, 14(10):2238–2249, May 2001. ISSN 0894-8755. doi: 10.1175/1520-0442(2001)014<0001:SHACRT>2.0.CO;2.

Large, W. G., McWilliams, J. C., and Doney, S. C. Oceanic vertical mixing: A review and a model with a nonlocal boundary layer parameterization. *Reviews of Geophysics*, 32(4):363–403, 1994. ISSN 1944-9208. doi: 10.1029/94RG01872.

Lewis, E. L. and Perkin, R. G. Ice pumps and their rates. *Journal of Geophysical Research: Oceans*, 91(C10):11756–11762, October 1986. ISSN 2156-2202. doi: 10.1029/JC091iC10p11756.

Little, C. M., Gnanadesikan, A., and Oppenheimer, M. How ice shelf morphology controls basal melting. *Journal of Geophysical Research: Oceans*, 114(C12), 2009. ISSN 2156-2202. doi: 10.1029/2008JC005197.

Liu, X. Modeling the effect of Ross Ice Shelf melting on the Southern Ocean in quasi-equilibrium. *The Cryosphere*, 12(9):3033–3044, September 2018. ISSN 1994-0416. doi: 10.5194/tc-12-3033-2018.

Liu, Y., Moore, J. C., Cheng, X., Gladstone, R. M., Bassis, J. N., Liu, H., Wen, J., and Hui, F. Ocean-driven thinning enhances iceberg calving and retreat of Antarctic ice shelves. *Proceedings of the National Academy of Sciences*, 112(11):3263–3268, March 2015. ISSN 0027-8424, 1091-6490. doi: 10.1073/pnas.1415137112.

Llanillo, P. J., Aiken, C. M., Cordero, R. R., Damiani, A., Sepúlveda, E., and Fernández-Gómez, B. Oceanographic Variability induced by Tides, the Intraseasonal Cycle and Warm Subsurface Water intrusions in Maxwell Bay, King George Island (West-Antarctica). *Scientific Reports*, 9(1):1–17, December 2019. ISSN 2045-2322. doi: 10.1038/s41598-019-54875-8.

Loder, J. W. Topographic Rectification of Tidal Currents on the Sides of Georges Bank. *Journal of Physical Oceanography*, 10(9):1399–1416, September 1980. ISSN 0022-3670. doi: 10.1175/1520-0485(1980)010<1399:TROTCO>2.0.CO;2.

Losch, M. Modeling ice shelf cavities in a z coordinate ocean general circulation model. *Journal of Geophysical Research: Oceans*, 113(C8), August 2008. ISSN 2156-2202. doi: 10.1029/2007JC004368.

Lüpkes, C. and Birnbaum, G. 'Surface Drag in the Arctic Marginal Sea-ice Zone: A Comparison of Different Parameterisation Concepts'. *Boundary-Layer Meteorology*, 117(2):179–211, November 2005. ISSN 0006-8314, 1573-1472. doi: 10.1007/s10546-005-1445-8.

MacAyeal, D. R. Thermohaline circulation below the Ross Ice Shelf: A consequence of tidally induced vertical mixing and basal melting. *Journal of Geophysical Research: Oceans*, 89(C1):597–606, 1984. ISSN 2156-2202. doi: 10.1029/JC089iC01p00597.

MacAyeal, D. R. Tidal Rectification Below the Ross Ice Shelf, Antarctica. *Oceanology of the Antarctic Continental Shelf*, January 1985. ISSN 9781118665206.

Mack, S. L., Dinniman, M. S., McGillicuddy, D. J., Sedwick, P. N., and Klinck, J. M. Dissolved iron transport pathways in the Ross Sea: Influence of tides and horizontal resolution in a regional ocean model. *Journal of Marine Systems*, 166:73–86, February 2017. ISSN 0924-7963. doi: 10.1016/j.jmarsys.2016.10.008.

Mack, S. L., Dinniman, M. S., Klinck, J. M., McGillicuddy, D. J., and Padman, L. Modeling Ocean Eddies on Antarctica's Cold Water Continental Shelves and Their Effects on Ice Shelf Basal Melting. *Journal of Geophysical Research: Oceans*, 124(7): 5067–5084, 2019. ISSN 2169-9291. doi: 10.1029/2018JC014688.

Makinson, K. and Nicholls, K. W. Modeling tidal currents beneath Filchner-Ronne Ice Shelf and on the adjacent continental shelf: Their effect on mixing and transport. *Journal of Geophysical Research: Oceans*, 104(C6):13449–13465, 1999. ISSN 2156-2202. doi: 10.1029/1999JC900008.

Makinson, K., Holland, P. R., Jenkins, A., Nicholls, K. W., and Holland, D. M. Influence of tides on melting and freezing beneath Filchner-Ronne Ice Shelf, Antarctica. *Geophysical Research Letters*, 38(6), March 2011. ISSN 1944-8007. doi: 10.1029/2010GL046462.

Malyarenko, A., Robinson, N. J., Williams, M. J. M., and Langhorne, P. J. A Wedge Mechanism for Summer Surface Water Inflow Into the Ross Ice Shelf Cavity. *Journal of Geophysical Research: Oceans*, 124(2):1196–1214, 2019. ISSN 2169-9291. doi: 10.1029/2018JC014594.

Mathiot, P., Jenkins, A., Harris, C., and Madec, G. Explicit representation and parametrised impacts of under ice shelf seas in the z^* coordinate ocean model NEMO 3.6. *Geoscientific Model Development*, 10(7):2849–2874, July 2017. ISSN 1991-959X. doi: 10.5194/gmd-10-2849-2017.

Mazloff, M. R., Heimbach, P., and Wunsch, C. An Eddy-Permitting Southern Ocean State Estimate. *Journal of Physical Oceanography*, 40(5):880–899, January 2010. ISSN 0022-3670. doi: 10.1175/2009JPO4236.1.

McPhee, M. G. A time-dependent model for turbulent transfer in a stratified oceanic boundary layer. *Journal of Geophysical Research: Oceans*, 92(C7):6977–6986, June 1987. ISSN 2156-2202. doi: 10.1029/JC092iC07p06977.

Mellor, G. L., Ezer, T., and Oey, L.-Y. The Pressure Gradient Conundrum of Sigma Coordinate Ocean Models. *Journal of Atmospheric and Oceanic Technology*, 11(4):1126–1134, August 1994. ISSN 0739-0572. doi: 10.1175/1520-0426(1994)011<1126:TPGCOS>2.0.CO;2.

Mellor, G. L., Oey, L.-Y., and Ezer, T. Sigma Coordinate Pressure Gradient Errors and the Seamount Problem. *Journal of Atmospheric and Oceanic Technology*, 15(5):1122–1131, October 1998. ISSN 0739-0572, 1520-0426. doi: 10.1175/1520-0426(1998)015<1122:SCPGEA>2.0.CO;2.

Menemenlis, D., Campin, J., Heimbach, P., Hill, C., Lee, T., Nguyen, A., Schodlok, M., and Zhang, H. ECCO2: High Resolution Global Ocean and Sea Ice Data Synthesis. *AGU Fall Meeting Abstracts*, December 2008.

Mercer, J. H. West Antarctic ice sheet and CO 2 greenhouse effect: a threat of disaster. *Nature*, 271(5643):321–325, January 1978. ISSN 1476-4687. doi: 10.1038/271321a0.

Millan, R., Rignot, E., Bernier, V., Morlighem, M., and Dutrieux, P. Bathymetry of the Amundsen Sea Embayment sector of West Antarctica from Operation IceBridge gravity and other data. *Geophysical Research Letters*, 44(3):1360–1368, 2017. ISSN 1944-8007. doi: 10.1002/2016GL072071.

Mondal, M., Gayen, B., Griffiths, R. W., and Kerr, R. C. Ablation of sloping ice faces into polar seawater. *Journal of Fluid Mechanics*, 863:545–571, March 2019. ISSN 0022-1120, 1469-7645. doi: 10.1017/jfm.2018.970.

Monselesan, D. P., O'Kane, T. J., Risbey, J. S., and Church, J. Internal climate memory in observations and models. *Geophysical Research Letters*, 42(4):1232–1242, February 2015. ISSN 1944-8007. doi: 10.1002/2014GL062765.

Mouginot, J., Rignot, E., and Scheuchl, B. Sustained increase in ice discharge from the Amundsen Sea Embayment, West Antarctica, from 1973 to 2013. *Geophysical Research Letters*, 41(5):1576–1584, 2014. ISSN 1944-8007. doi: 10.1002/2013GL059069.

Mouginot, J., Rignot, E., and Scheuchl, B. MEaSURES Antarctic Boundaries for IPY 2007-2009 from Satellite Radar, Version 1. Shelves, 2016.

Mueller, R. D., Padman, L., Dinniman, M. S., Erofeeva, S. Y., Fricker, H. A., and King, M. A. Impact of tide-topography interactions on basal melting of Larsen C Ice Shelf, Antarctica. *Journal of Geophysical Research: Oceans*, 117(C5), May 2012. ISSN 2156-2202. doi: 10.1029/2011JC007263.

Mueller, R. D., Hattermann, T., Howard, S. L., and Padman, L. Tidal influences on a future evolution of the Filchner–Ronne Ice Shelf cavity in the Weddell Sea, Antarctica. *The Cryosphere*, 12(2):453–476, February 2018. ISSN 1994-0416. doi: 10.5194/tc-12-453-2018.

Nakayama, Y., Timmermann, R., Rodehacke, C. B., Schröder, M., and Hellmer, H. H. Modeling the spreading of glacial meltwater from the Amundsen and Bellingshausen Seas. *Geophysical Research Letters*, 41(22):7942–7949, 2014a. ISSN 1944-8007. doi: 10.1002/2014GL061600.

Nakayama, Y., Timmermann, R., Schröder, M., and Hellmer, H. H. On the difficulty of modeling Circumpolar Deep Water intrusions onto the Amundsen Sea continental shelf. *Ocean Modelling*, 84:26–34, December 2014b. ISSN 1463-5003. doi: 10.1016/j.ocemod.2014.09.007.

Nakayama, Y., Menemenlis, D., Schodlok, M., and Rignot, E. Amundsen and Bellingshausen Seas simulation with optimized ocean, sea ice, and thermodynamic ice shelf model parameters. *Journal of Geophysical Research: Oceans*, 122(8):6180–6195, 2017. ISSN 2169-9291. doi: 10.1002/2016JC012538.

Nash, R. International Bathymetric Chart of the Southern Ocean (IBCSO), 2019.

Naughten, K. A., Meissner, K. J., Galton-Fenzi, B. K., England, M. H., Timmermann, R., and Hellmer, H. H. Future Projections of Antarctic Ice Shelf Melting Based on

CMIP5 Scenarios. *Journal of Climate*, 31(13):5243–5261, April 2018a. ISSN 0894-8755. doi: 10.1175/JCLI-D-17-0854.1.

Naughten, K. A., Meissner, K. J., Galton-Fenzi, B. K., England, M. H., Timmermann, R., Hellmer, H. H., Hattermann, T., and Debernard, J. B. Intercomparison of Antarctic ice-shelf, ocean, and sea-ice interactions simulated by MetROMS-iceshelf and FESOM 1.4. *Geoscientific Model Development*, 11(4):1257–1292, April 2018b. ISSN 1991-959X. doi: 10.5194/gmd-11-1257-2018.

Nicholls, K. W., Østerhus, S., Makinson, K., Gammelsrød, T., and Fahrbach, E. Ice-ocean processes over the continental shelf of the southern Weddell Sea, Antarctica: A review. *Reviews of Geophysics*, 47(3), September 2009. ISSN 1944-9208. doi: 10.1029/2007RG000250.

Nøst, O. A., Biuw, M., Tverberg, V., Lydersen, C., Hattermann, T., Zhou, Q., Smedsrud, L. H., and Kovacs, K. M. Eddy overturning of the Antarctic Slope Front controls glacial melting in the Eastern Weddell Sea. *Journal of Geophysical Research: Oceans*, 116(C11), 2011. ISSN 2156-2202. doi: 10.1029/2011JC006965.

Obase, T., Abe-Ouchi, A., Kusahara, K., Hasumi, H., and Ohgaito, R. Responses of Basal Melting of Antarctic Ice Shelves to the Climatic Forcing of the Last Glacial Maximum and CO2 Doubling. *Journal of Climate*, 30(10):3473–3497, February 2017. ISSN 0894-8755. doi: 10.1175/JCLI-D-15-0908.1.

Padman, L., Howard, S. L., and Muench, R. Internal tide generation along the South Scotia Ridge. *Deep Sea Research Part II: Topical Studies in Oceanography*, 53(1): 157–171, January 2006. ISSN 0967-0645. doi: 10.1016/j.dsr2.2005.07.011.

Padman, L., Howard, S. L., Orsi, A. H., and Muench, R. D. Tides of the northwestern Ross Sea and their impact on dense outflows of Antarctic Bottom Water. *Deep Sea Research Part II: Topical Studies in Oceanography*, 56(13-14):818–834, June 2009. ISSN 0967-0645. doi: 10.1016/j.dsr2.2008.10.026.

Padman, L., Costa, D. P., Dinniman, M. S., Fricker, H. A., Goebel, M. E., Huckstadt, L. A., Humbert, A., Joughin, I., Lenaerts, J. T. M., Ligtenberg, S. R. M., Scambos, T., and Broeke, M. R. v. d. Oceanic controls on the mass balance of Wilkins Ice Shelf, Antarctica. *Journal of Geophysical Research: Oceans*, 117(C1), January 2012. ISSN 2156-2202. doi: 10.1029/2011JC007301.

Padman, L., Siegfried, M. R., and Fricker, H. A. Ocean Tide Influences on the Antarctic and Greenland Ice Sheets. *Reviews of Geophysics*, 56(1):142–184, March 2018. ISSN 1944-9208. doi: 10.1002/2016RG000546.

Paolo, F. S., Fricker, H. A., and Padman, L. Volume loss from Antarctic ice shelves is accelerating. *Science*, 348(6232):327–331, April 2015. ISSN 0036-8075, 1095-9203. doi: 10.1126/science.aaa0940.

Parkinson, C. L. A 40-y record reveals gradual Antarctic sea ice increases followed by decreases at rates far exceeding the rates seen in the Arctic. *Proceedings of the National Academy of Sciences*, 116(29):14414–14423, July 2019. ISSN 0027-8424, 1091-6490. doi: 10.1073/pnas.1906556116.

Pattyn, F., Ritz, C., Hanna, E., Asay-Davis, X. S., DeConto, R., Durand, G., Favier, L., Fettweis, X., Goelzer, H., Golledge, N. R., Kuipers Munneke, P., Lenaerts, J. T. M., Nowicki, S., Payne, A. J., Robinson, A., Seroussi, H., Trusel, L. D., and van den Broeke, M. The Greenland and Antarctic ice sheets under 1.5 °C global warming. *Nature Climate Change*, 8(12):1053–1061, December 2018. ISSN 1758-6798. doi: 10.1038/s41558-018-0305-8.

Pawlowicz, R., Beardsley, B., and Lentz, S. Classical tidal harmonic analysis including error estimates in MATLAB using T_tide. *Computers & Geosciences*, 28(8):929–937, October 2002. ISSN 0098-3004. doi: 10.1016/S0098-3004(02)00013-4.

Pellichero, V., Sallée, J.-B., Schmidtko, S., Roquet, F., and Charrassin, J.-B. The ocean mixed layer under Southern Ocean sea-ice: Seasonal cycle and forcing. *Journal of Geophysical Research: Oceans*, 122(2):1608–1633, 2017. ISSN 2169-9291. doi: 10.1002/2016JC011970.

Phillips, L. R., Carroll, G., Jonsen, I., Harcourt, R., and Roughan, M. A Water Mass Classification Approach to Tracking Variability in the East Australian Current. *Frontiers in Marine Science*, 7, 2020. ISSN 2296-7745. doi: 10.3389/fmars.2020.00365.

Pörtner, D. R., Masson-Delmotte V., Zhai, P., Tignor, M., Poloczanska, E., Mintenbeck, K., Alegría, A., Nicolai, M., Petzold, J., Rama, B., and Weyer, N.M. IPCC, 2019: Summary for Policymakers. In *IPCC Special Report on the Ocean and Cryosphere in a Changing Climate*. In press.

Pritchard, H. D., Ligtenberg, S. R. M., Fricker, H. A., Vaughan, D. G., van den Broeke, M. R., and Padman, L. Antarctic ice-sheet loss driven by basal melting of ice shelves.

Nature, 484(7395):502–505, April 2012. ISSN 0028-0836, 1476-4687. doi: 10.1038/nature10968.

Purkey, S. G. and Johnson, G. C. Antarctic Bottom Water Warming and Freshening: Contributions to Sea Level Rise, Ocean Freshwater Budgets, and Global Heat Gain. *Journal of Climate*, 26(16):6105–6122, March 2013. ISSN 0894-8755. doi: 10.1175/JCLI-D-12-00834.1.

Rasp, S., Pritchard, M. S., and Gentine, P. Deep learning to represent subgrid processes in climate models. *Proceedings of the National Academy of Sciences*, 115(39):9684–9689, 2018.

Reese, R., Gudmundsson, G. H., Levermann, A., and Winkelmann, R. The far reach of ice-shelf thinning in Antarctica. *Nature Climate Change*, 8(1):53–57, January 2018. ISSN 1758-678X, 1758-6798. doi: 10.1038/s41558-017-0020-x.

Richter, O. Whole Antarctic Ocean Model [Software]. April 2020a. doi: 10.5281/zenodo.3738985.

Richter, O. Post- and Preprocessing Tools for the Whole Antarctic Ocean Model [Software]. April 2020b. doi: 10.5281/zenodo.3738998.

Rignot, E., Jacobs, S. S., Mouginot, J., and Scheuchl, B. Ice-Shelf Melting Around Antarctica. *Science*, 341(6143):266–270, July 2013. ISSN 0036-8075, 1095-9203. doi: 10.1126/science.1235798.

Robertson, R. Modeling internal tides over Fieberling Guyot: resolution, parameterization, performance. *Ocean Dynamics*, 56(5):430–444, December 2006. ISSN 1616-7228. doi: 10.1007/s10236-006-0062-5.

Robertson, R. Tidally induced increases in melting of Amundsen Sea ice shelves. *Journal of Geophysical Research: Oceans*, 118(6):3138–3145, June 2013. ISSN 2169-9291. doi: 10.1002/jgrc.20236.

Rosier, S. H. R., Green, J. a. M., Scourse, J. D., and Winkelmann, R. Modeling Antarctic tides in response to ice shelf thinning and retreat. *Journal of Geophysical Research: Oceans*, 119(1):87–97, January 2014. ISSN 2169-9291. doi: 10.1002/2013JC009240.

Rovere, A., Raymo, M., Mitrovica, J., Hearty, P., O'Leary, M., and Inglis, J. The Mid-Pliocene sea-level conundrum: Glacial isostasy, eustasy and dynamic topography.

Earth and Planetary Science Letters, 387:27–33, February 2014. ISSN 0012-821X. doi: 10.1016/j.epsl.2013.10.030.

Royston, S. and Gudmundsson, G. H. Changes in ice-shelf buttressing following the collapse of Larsen A Ice Shelf, Antarctica, and the resulting impact on tributaries. *Journal of Glaciology*, 62(235):905–911, October 2016. ISSN 0022-1430, 1727-5652. doi: 10.1017/jog.2016.77.

Savage, A. C., Arbic, B. K., Alford, M. H., Ansong, J. K., Farrar, J. T., Menemenlis, D., O'Rourke, A. K., Richman, J. G., Shriver, J. F., Voet, G., Wallcraft, A. J., and Zamudio, L. Spectral decomposition of internal gravity wave sea surface height in global models. *Journal of Geophysical Research: Oceans*, 122(10):7803–7821, 2017. ISSN 2169-9291. doi: 10.1002/2017JC013009.

Scambos, T. A., Bohlander, J. A., Shuman, C. A., and Skvarca, P. Glacier acceleration and thinning after ice shelf collapse in the Larsen B embayment, Antarctica. *Geophysical Research Letters*, 31(18), September 2004. ISSN 1944-8007. doi: 10.1029/2004GL020670.

Schaffer, J., Timmermann, R., Arndt, J. E., Kristensen, S. S., Mayer, C., Morlighem, M., and Steinhage, D. A global, high-resolution data set of ice sheet topography, cavity geometry, and ocean bathymetry. *Earth System Science Data*, 8(2):543–557, October 2016. ISSN 1866-3508. doi: 10.5194/essd-8-543-2016.

Schmidtko, S., Heywood, K. J., Thompson, A. F., and Aoki, S. Multidecadal warming of Antarctic waters. *Science*, 346(6214):1227–1231, December 2014. ISSN 0036-8075, 1095-9203. doi: 10.1126/science.1256117.

Schnaase, F. and Timmermann, R. Representation of shallow grounding zones in an ice shelf-ocean model with terrain-following coordinates. *Ocean Modelling*, 144:101487, December 2019. ISSN 1463-5003. doi: 10.1016/j.ocemod.2019.101487.

Schodlok, M. P., Menemenlis, D., and Rignot, E. Ice shelf basal melt rates around Antarctica from simulations and observations. *Journal of Geophysical Research: Oceans*, 121(2):1085–1109, February 2016. ISSN 2169-9291. doi: 10.1002/2015JC011117.

Schoof, C. Ice sheet grounding line dynamics: Steady states, stability, and hysteresis. *Journal of Geophysical Research: Earth Surface*, 112(F3), 2007. ISSN 2156-2202. doi: 10.1029/2006JF000664.

Schoof, C. Marine ice sheet stability. *Journal of Fluid Mechanics*, 698:62–72, May 2012. doi: 10.1017/jfm.2012.43.

Seny, B., Lambrechts, J., Comblen, R., Legat, V., and Remacle, J.-F. Multirate time stepping for accelerating explicit discontinuous Galerkin computations with application to geophysical flows. *International Journal for Numerical Methods in Fluids*, 71 (1):41–64, 2013. ISSN 1097-0363. doi: 10.1002/fld.3646.

Shchepetkin, A. F. and McWilliams, J. C. The regional oceanic modeling system (ROMS): a split-explicit, free-surface, topography-following-coordinate oceanic model. *Ocean Modelling*, 9:347–404, 2005. ISSN 1463-5003. doi: 10.1016/j.ocemod.2004.08.002.

Shean, D. E., Joughin, I. R., Dutrieux, P., Smith, B. E., and Berthier, E. Ice shelf basal melt rates from a high-resolution DEM record for Pine Island Glacier, Antarctica. *The Cryosphere Discussions*, pages 1–39, October 2018. ISSN 1994-0416. doi: 10.5194/tc-2018-209.

Shepherd, A., Wingham, D., and Rignot, E. Warm ocean is eroding West Antarctic Ice Sheet. *Geophysical Research Letters*, 31(23), December 2004. ISSN 1944-8007. doi: 10.1029/2004GL021106.

Shepherd, A., Ivins, E., Rignot, E., Smith, B., van den Broeke, M., Velicogna, I., Whitehouse, P., Briggs, K., Joughin, I., Krinner, G., Nowicki, S., Payne, T., Scambos, T., Schlegel, N., Geruo, A., Agosta, C., Ahlstrøm, A., Babonis, G., Barletta, V., Blazquez, A., Bonin, J., Csatho, B., Cullather, R., Felikson, D., Fettweis, X., Forsberg, R., Gallee, H., Gardner, A., Gilbert, L., Groh, A., Gunter, B., Hanna, E., Harig, C., Helm, V., Horvath, A., Horwath, M., Khan, S., Kjeldsen, K. K., Konrad, H., Langen, P., Lecavalier, B., Loomis, B., Luthcke, S., McMillan, M., Melini, D., Mernild, S., Mohajerani, Y., Moore, P., Mouginot, J., Moyano, G., Muir, A., Nagler, T., Nield, G., Nilsson, J., Noel, B., Otosaka, I., Pattle, M. E., Peltier, W. R., Pie, N., Rietbroek, R., Rott, H., Sandberg-Sørensen, L., Sasgen, I., Save, H., Scheuchl, B., Schrama, E., Schröder, L., Seo, K.-W., Simonsen, S., Slater, T., Spada, G., Sutterley, T., Talpe, M., Tarasov, L., van de Berg, W. J., van der Wal, W., van Wessem, M., Vishwakarma, B. D., Wiese, D., Wouters, B., and team, T. I. M. B. I. E. Mass balance of the antarctic ice sheet from 1992 to 2017. *Nature*, 558(7709):219–222, 2018. ISSN 1476-4687.

Sherwood, C. R., Aretxabaleta, A. L., Harris, C. K., Rinehimer, J. P., Verney, R., and Ferré, B. Cohesive and mixed sediment in the Regional Ocean Modeling System (ROMS v3.6) implemented in the Coupled Ocean–Atmosphere–Wave–Sediment Transport Modeling System (COAWST r1234). *Geoscientific Model Development*, 11 (5):1849–1871, May 2018. ISSN 1991-959X. doi: 10.5194/gmd-11-1849-2018.

Sikirić, M. D., Janeković, I., and Kuzmić, M. A new approach to bathymetry smoothing in sigma-coordinate ocean models. *Ocean Modelling*, 29(2):128–136, January 2009. ISSN 1463-5003. doi: 10.1016/j.ocemod.2009.03.009.

Silvano, A., Rintoul, S. R., Peña-Molino, B., and Williams, G. D. Distribution of water masses and meltwater on the continental shelf near the Totten and Moscow University ice shelves. *Journal of Geophysical Research: Oceans*, 122(3):2050–2068, 2017. ISSN 2169-9291. doi: 10.1002/2016JC012115.

Silvano, A., Rintoul, S. R., Peña-Molino, B., Hobbs, W. R., Wijk, E. v., Aoki, S., Tamura, T., and Williams, G. D. Freshening by glacial meltwater enhances melting of ice shelves and reduces formation of Antarctic Bottom Water. *Science Advances*, 4 (4):eaap9467, April 2018. ISSN 2375-2548. doi: 10.1126/sciadv.aap9467.

Smith, B. E., Fricker, H. A., Joughin, I. R., and Tulaczyk, S. An inventory of active subglacial lakes in Antarctica detected by ICESat (2003–2008). *Journal of Glaciology*, 55 (192):573–595, 2009. ISSN 0022-1430, 1727-5652. doi: 10.3189/002214309789470879.

Sokolov, S. and Rintoul, S. R. Circumpolar structure and distribution of the Antarctic Circumpolar Current fronts: 1. Mean circumpolar paths. *Journal of Geophysical Research: Oceans*, 114(C11), 2009. ISSN 2156-2202. doi: 10.1029/2008JC005108.

Spence, P., Griffies, S. M., England, M. H., Hogg, A. M., Saenko, O. A., and Jourdain, N. C. Rapid subsurface warming and circulation changes of Antarctic coastal waters by poleward shifting winds. *Geophysical Research Letters*, 41(13):4601–4610, 2014. ISSN 1944-8007. doi: 10.1002/2014GL060613.

Stern, A. A., Dinniman, M. S., Zagorodnov, V., Tyler, S. W., and Holland, D. M. Intrusion of warm surface water beneath the McMurdo Ice Shelf, Antarctica. *Journal of Geophysical Research: Oceans*, 118(12):7036–7048, 2013. ISSN 2169-9291. doi: 10.1002/2013JC008842.

Stewart, A. L. and Thompson, A. F. Eddy-mediated transport of warm Circumpolar Deep Water across the Antarctic Shelf Break. *Geophysical Research Letters*, 42(2): 432–440, January 2015. ISSN 1944-8007. doi: 10.1002/2014GL062281.

Stewart, A. L., Klocker, A., and Menemenlis, D. Circum-Antarctic Shoreward Heat Transport Derived From an Eddy- and Tide-Resolving Simulation. *Geophysical Research Letters*, 45(2):834–845, January 2018. ISSN 1944-8007. doi: 10.1002/2017GL075677.

Stewart, C. L., Christoffersen, P., Nicholls, K. W., Williams, M. J. M., and Dowdeswell, J. A. Basal melting of Ross Ice Shelf from solar heat absorption in an ice-front polynya. *Nature Geoscience*, page 1, April 2019. ISSN 1752-0908.

Sverdrup, H. U. The Currents off the Coast of Queen Maud Land. *Norsk Geografisk Tidsskrift - Norwegian Journal of Geography*, 14(1-4):239–249, January 1954. ISSN 0029-1951. doi: 10.1080/00291955308542731.

Tamura, T., Ohshima, K. I., Nihashi, S., and Hasumi, H. Estimation of Surface Heat/Salt Fluxes Associated with Sea Ice Growth/Melt in the Southern Ocean. *SOLA*, 7:17–20, 2011. ISSN 1349-6476. doi: 10.2151/sola.2011-005.

Taylor, K. E., Stouffer, R. J., and Meehl, G. A. An Overview of CMIP5 and the Experiment Design. *Bulletin of the American Meteorological Society*, 93(4):485–498, October 2011. ISSN 0003-0007. doi: 10.1175/BAMS-D-11-00094.1.

Thoma, M., Jenkins, A., Holland, D. M., and Jacobs, S. S. Modelling Circumpolar Deep Water intrusions on the Amundsen Sea continental shelf, Antarctica. *Geophysical Research Letters*, 35(18), 2008. ISSN 1944-8007. doi: 10.1029/2008GL034939.

Thompson, A. F., Heywood, K. J., Thorpe, S. E., Renner, A. H. H., and Trasviña, A. Surface Circulation at the Tip of the Antarctic Peninsula from Drifters. *Journal of Physical Oceanography*, 39(1):3–26, January 2009. ISSN 0022-3670. doi: 10.1175/2008JPO3995.1.

Timmermann, R., Wang, Q., and Hellmer, H. H. Ice shelf basal melting in a global finite-element sea ice/ice shelf/ocean model. *Annals of Glaciology*, 53, 2012. ISSN 0260-3055. doi: 10.3189/2012AoG60A156.

Turner, J., Orr, A., Gudmundsson, G. H., Jenkins, A., Bingham, R. G., Hillenbrand, C.-D., and Bracegirdle, T. J. Atmosphere-ocean-ice interactions in the Amundsen Sea Embayment, West Antarctica. *Reviews of Geophysics*, 55(1):235–276, March 2017. ISSN 1944-9208. doi: 10.1002/2016RG000532.

Wessem, J. M. v., Berg, W. J. v. d., Noël, B. P. Y., Meijgaard, E. v., Amory, C., Birnbaum, G., Jakobs, C. L., Krüger, K., Lenaerts, J. T. M., Lhermitte, S., Ligtenberg,

S. R. M., Medley, B., Reijmer, C. H., Tricht, K. v., Trusel, L. D., Ulft, L. H. v., Wouters, B., Wuite, J., and Broeke, M. R. v. d. Modelling the climate and surface mass balance of polar ice sheets using RACMO2 – Part 2: Antarctica (1979–2016). *The Cryosphere*, 12(4):1479–1498, April 2018. ISSN 1994-0416. doi: 10.5194/tc-12-1479-2018.

Williams, G. D., Meijers, A. J. S., Poole, A., Mathiot, P., Tamura, T., and Klocker, A. Late winter oceanography off the Sabrina and BANZARE coast (117–128°E), East Antarctica. *Deep Sea Research Part II: Topical Studies in Oceanography*, 58(9):1194–1210, May 2011. ISSN 0967-0645. doi: 10.1016/j.dsr2.2010.10.035.

Williams, G. D., Herraiz-Borreguero, L., Roquet, F., Tamura, T., Ohshima, K. I., Fukamachi, Y., Fraser, A. D., Gao, L., Chen, H., McMahon, C. R., Harcourt, R., and Hindell, M. The suppression of Antarctic bottom water formation by melting ice shelves in Prydz Bay. *Nature Communications*, 7:12577, August 2016. ISSN 2041-1723. doi: 10.1038/ncomms12577.

Wilmes, S.-B. and Green, J. a. M. The evolution of tides and tidal dissipation over the past 21,000 years. *Journal of Geophysical Research: Oceans*, 119(7):4083–4100, July 2014. ISSN 2169-9291. doi: 10.1002/2013JC009605.

Zhou, Q., Hattermann, T., Nøst, O. A., Biuw, M., Kovacs, K. M., and Lydersen, C. Wind-driven spreading of fresh surface water beneath ice shelves in the Eastern Weddell Sea. *Journal of Geophysical Research: Oceans*, 119(6):3818–3833, June 2014. ISSN 2169-9291. doi: 10.1002/2013JC009556.